ISSN 2355-5058
e-ISSN 2622-4852

JURNAL ECOTIPE

Electronic, Control, Telecommunication, Information, and Power Engineering

https://ecotipe.ubb.ac.id/

Volume 11, Issue 2, October 2024

Accreditation by Kemdikbudristek
Decree. No.158/E/KPT/2021 (rank. SINTA 3)

Electrical Engineering Department
Bangka Belitung University

JURNAL ECOTIPE
Electronic, Control, Telecommunication, Information, and Power Engineering

Volume 11, Issue 2, October 2024
DOI : 10.33019/jurnalecotipe.v11i2

Accredited by Kemdikbudristek RI
Decree No.158/E/KPT/2021 **(rank. SINTA 3)**

ISSN 2355-5068 e-ISSN 2622-4852

Editorial Board

Publisher Address:

Electrical Engineering Department
Faculty of Science and Engineering - Bangka Belitung University
Balunijuk, Bangka Regency, Bangka Belitung Islands Province, Indonesia
Phone (0717) 4260033 ext. 2125, 2128
Website : https://journal.ubb.ac.id/index.php/ecotipe
E-mail : jurnal.ecotipe@yahoo.com / jurnalecotipe@ubb.ac.id

Preface

Jurnal Ecotipe (Electronic, Control, Telecommunication, Information, and Power Engineering) published by the Electrical Engineering Department, Bangka Belitung University currently starting Volume 7 Number 2, October 2020 to Volume 12 Number 2, October 2025 has been accredited by the Ministry of Education, Culture, Research, and Technology of the Republic of Indonesia based on Decree No. 158/E/KPT/2021 with 3rd rank (SINTA 3).

Currently, Jurnal Ecotipe volume 11 issue 2, October 2024 has been published. In this edition of the journal, the journal articles are in full English. Starting from volume 9 issue 2 October 2022, for the next editions of the articles in Jurnal Ecotipe, articles will be published using English in their writing and presentation. The articles in this edition of the journal come from academics both from within and from outside the institution.

Our highest appreciation goes to the Reviewers, Editorial Board, Authors, and all parties involved in the preparation and publication of the Jurnal Ecotipe volume 11 issue 2 October 2024. Hopefully, this journal can provide benefits and add scientific insight into the field of Electrical Engineering in particular and engineering in general. Therefore, we still hope for suggestions and constructive criticism for improvements and improvements for the progress of this journal.

Editor-in-Chief

Indexed journal on:

Volume 11, Issue 2, October 2024
DOI : 10.33019/jurnalecotipe.v11i2

JURNAL ECOTIPE
Electronic, Control, Telecommunication, Information, and Power Engineering

Accredited by Kemdikbudristek RI
Decree No.158/E/KPT/2021 **(rank. SINTA 3)**

Table of Content

JURNAL ECOTIPE
Electronic, Control, Telecommunication, Information, and Power Engineering

Volume 11, Issue 2, Oktober 2024, pp. 107-116
ISSN 2355-5068 ; e-ISSN 2622-4852
DOI: 10.33019/jurnalecotipe.v11i2.4492

Analysis of Waste Utilization of Refuse Derived Fuel (RDF) into Briquettes for Steam Power Electric Generation

Yossi Arif Rachman[1], Marhama Jelita[2]
[1,2] Department of Electrical Engineering, Sultan Syarif Kasim State Islamic University in Riau, Pekanbaru 28293, Indonesia

ARTICLE INFO

Article historys:

Received : …/…/…
Revised : …/…/…
Accepted : …/…/…

Keywords:

Ash Content; Briquette; Calorific Value; Refuse Derived Fuel; Moisture Content.

ABSTRACT

Waste in Indonesia reaches 65.2 million tons per year, dominated by organic and inorganic waste. Approximately 36% of the total waste is poorly managed, including 4K1P waste (paper, wood, fabric, rubber, and plastic), which can be quickly burned and turned into RDF briquettes through pyrolysis and paraffin adhesive. These briquettes will use three variations of raw materials: organic, inorganic, and mixed waste. The quality of these briquettes is compared based on calorific value, ash content, moisture content, and the fuel requirement for a 7.5 MW capacity power plant if used as fuel. The initial weight of the raw materials for each briquette is 2 kg, resulting in 10 pieces each of organic, inorganic, and mixed briquettes. Test results indicate that inorganic briquettes have the best quality with a calorific value of 8,075.92 cal/g, moisture content of 1.75%, and ash content of 10.84%, meeting the SNI-01-6235-2000 standard. The minimum fuel requirement for the power plant using RDF briquettes is inorganic briquettes, at 3.05 tons/hour or 26,205.6 tons/year. Inorganic briquettes are of the best quality and require the least fuel for use in power plants.

Corresponding Author:

Yossi Arif Rachman
Sultan Syarif Kasim State Islamic University in Riau, Jl. HR. Soebrantas No.Km. 15, Simpang Baru, Kota Pekanbaru, Riau 28293, Indonesia
Email: 12050513509@students.uin-suska.ac.id

1. INTRODUCTION

Waste can be defined as residue or waste from an industrial, public, institutional, or human processing process [1]. All activities related to the processing of raw materials, both food and non-food, inevitably produce useless residue which creates piles of waste [2]. Based on data from the Central Statistics Agency in 2016 alone, Indonesian people produced at least 65.2 million tons of waste/year. Waste production is increasing every year. The Ministry of Environment and Forestry released data that in 2020 there was an increase in waste production of 72 million tons of waste, with details of 9 million tons of waste or the equivalent of 36% of the total waste that had not been managed properly, including 4K1P waste (paper, wood, cloth, rubber, and plastic). This waste comes from various sectors including households, industry, agencies, and the general public [3].

Waste is divided into two groups, namely organic and inorganic. Organic waste comes from living creatures and can decompose naturally, while inorganic waste comes from synthetic materials that are difficult to decompose. In Indonesia, 69% of waste is organic, consisting of 60% food waste and 9% paper. Inorganic waste is around 23%, with plastic dominating 14%, cloth 3.5%, and rubber 5.5% [4]. Waste processing is carried out through various methods, namely waste banks, compost processing, 3R TPST (Reuse, Reduce, Recycle Integrated Waste Processing Site), and PDU (Recycling Center) which focuses on recycling. In addition, TPST (Integrated Waste Processing Site) integrates various waste management methods, and ITF (Intermediate Treatment Facility) produces energy from waste. TPA

Volume 10, Issue 2, Oktober 2024, pp. 107-116
ISSN 2355-5068 ; e-ISSN 2622-4852
DOI: 10.33019/jurnalecotipe.v11i2.4492

(Final Disposal Site) is used for final disposal of waste that cannot be processed, in order to isolate its negative impacts on the environment and health [5].

Several studies have studied the 4K1P waste problem. In research by [6], processing organic waste into RDF briquettes using the chopping method resulted in a calorific value of 4,228 kcal/kg, a water content of 6.57%, an ash content of 2.25%. The research of [7] used carbonization on PET plastic waste, coconut shells, and sawdust, producing briquettes with a calorific value of 5,608 kcal/kg, water content of 5.18% and ash content of 3.55%. In research by [8] using carbonization on mixed waste, it produced a calorific value of 5,218 kcal/kg, a water content of 1.04%, and an ash content of 17.34%. In research, [9] examined a mixture of organic and inorganic waste, resulting in a calorific value of 4,819,220 kcal/kg, water content of 5.56%, and ash content of 11.64%. In research by [10], pyrolysis was used, producing a calorific value of 8,996 kcal/kg, water content of 5.5%, ash content of 4.9%, and steam content of 15.9%. The results show that 4K1P waste can be converted into type-5 RDF, namely RDF from the combustible fraction, which is compacted into pellets, slag, briquettes, and so on, with high potential for use as an alternative fuel [9, 10, 11].

The methods commonly used in processing RDF briquettes are carbonization and pyrolysis. Several studies have examined the processing of RDF into RDF briquettes using the carbonization method, namely the research of [7] used carbonization on PET plastic bottles, shell charcoal, and wood charcoal with starch adhesive, producing a calorific value of 5,608 cal/g, water content of 5.18%, ash content of 3.55%, and carbon content of 32.49%. Research [8] also uses carbonization on organic and inorganic waste, producing a calorific value of 5,218 cal/g, water content of 1.04%, and ash content of 17.34%, according to the bio briquette standard SNI 01-6235-2000. The pyrolysis method is also used to process RDF into energy, namely in research [10] on organic waste such as dry bamboo leaves and sawdust, resulting in a calorific value of 8,996 cal/g, water content of 5.5%, ash content of 4.9%, and vapor content 15.9%. As well as research [12] using pyrolysis on organic waste, producing a calorific value of 16,201 J/g, an ash content of 6.45%, and a water content of 0.92%. A comparison of the two methods shows that carbonization produces a calorific value of 5,218 -5,608 cal/g, water content of 1.04%-5.18%, and ash content of 3.55%-17.34%. Pyrolysis produces a higher heating value of up to 8,996 cal/g, water content 0.92%-5.5%, and ash content 4.9%-6.45. %. Thus, pyrolysis is more optimal for processing RDF into energy briquettes than carbonization.

Several studies have determined the optimal adhesive for making RDF briquettes, including research [8] comparing molasses, paraffin, and starch. The best results were obtained with paraffin, producing a calorific value of 5,218 cal/g. Meanwhile, research by [6] using tapioca flour in 4K1P waste produces a calorific value of 3,645 cal/g. In conclusion, paraffin adhesive produces the best quality briquettes because the calorific value is 5,218 cal/g.

RDF is considered the newest solution in waste management in Indonesia because it can be processed into various energy sources. RDF can fuel the steam power cycle in PLTUs, producing a potential electrical power of 154 MW (thermochemical) and 1.4 MW (biochemical). If applied with a biochemical cycle in a biodigester, RDF can produce 2.1 MW of power. RDF can also be used for PLTSa, and with the gasification method, it has the potential to generate 1 MW of power [13, 14]. So, from several studies that have been carried out, RDF has become a fuel for the power cycle. Steam in PLTU has more significant potential than various other energy sources.

Based on data from the Ministry of Environment and Forestry, around 36% of Indonesia's 4K1P waste, needs to be appropriately managed. This research aims to analyze the potential for flammable 4K1P waste to become type 5 RDF, namely RDF from combustible waste fractions that are compacted into briquettes [9, 10, 11]. Several studies that examine the use of 4K1P waste in RDF briquettes still focus on mixing the composition of raw materials for briquettes from 4K1P waste so that this research will compare the quality of RDF briquettes with a variety of pure organic, pure inorganic raw materials and a mixture of the two. The pyrolysis method was chosen because it produces the highest heating value and is better than other adhesives [8, 13].The quality of the briquettes will be tested using a bomb calorimeter to produce heating value, a minimum free space oven for ash content, and an ash content test oven for water content. The research will also analyze fuel requirements for a 7.5 MW PLTU, including calculating the heating value of the boiler and estimating fuel per hour and year [15].

Volume 10, Issue 2, Oktober 2024, pp. 107-116
ISSN 2355-5068 ; e-ISSN 2622-4852
DOI: 10.33019/jurnalecotipe.v11i2.4492

2. RESEARCH METHOD

This research uses a quantitative approach to analyze the manufacture of RDF briquettes from organic and inorganic waste in Indonesia, which reaches 65.2 million tons/year, with 36% still being managed, including 4K1P waste. This waste will be processed into RDF briquettes, namely organic briquettes (wood and paper), inorganic briquettes (cloth, rubber, plastic), and mixed briquettes. The quality of RDF briquettes will be tested based on calorific value, water content, and ash content according to SNI 01-6235-2000 [8]. If the briquettes are used as fuel, then the RDF briquettes will be implemented in a PLTU with a capacity of 7.5 MW. Primary data was obtained from direct observation and secondary data from related journals. Research steps include literature study, preparation of tools and materials, burning, molding RDF briquettes (100 gr/piece), drying, and quality testing (heat test, water content, ash content). Data analysis will determine whether the briquettes meet applicable standards and calculate the PLTU's fuel requirements [15].

2.1. Raw Material

The raw materials used in this research came from 4K1P waste, namely organic and inorganic raw materials. 4K1P waste is flammable, so it has the potential to be used as RDF briquettes. So, in making RDF briquettes, the raw materials chosen are paper, wood, cloth, rubber, and plastic, with the weight of each raw material being 2 kg. The raw materials come from leftovers and waste dumped in the surrounding environment.

2.2. Carbon Charcoal Production

Refuse Derived Fuel is the fuel that comes from the process of separating solid waste between flammable waste and hard-to-combust waste. The waste used is flammable when making RDF briquettes. For briquettes, the RDF waste used is small, so cutting the waste into smaller pieces is required [14, 16]. In processing 4K1P waste into briquettes using the pyrolysis combustion method. The main product of the pyrolysis process is carbon charcoal [17]. The following is the process of processing 4K1P waste into carbon charcoal:

1. Collection of tools and materials
   In this research, the materials used were 4K1P waste (paper, wood, cloth, rubber/leather, and plastic) with respective weights as in Table 1 and paraffin adhesive. The equipment used was a 60 mesh sieve, digital scales, containers, and iron drums that have been modified by adding iron pipes as chimneys, mortars, stoves, spoons, pans, briquette molds, scissors, knives, and manual paper grinders.
2. Waste cutting
   The 4K1P waste collected has a variety of different sizes. To facilitate the process of making RDF briquettes and ensure the results meet the quality standards of raw materials with a high calorific value, cutting is carried out manually using scissors, knives, and a paper grinder. The pieces of waste are cut to a size of approximately ± 5 cm, except for wood, which is already in the form of sawdust.
3. Waste drying
   To maximize the combustion process, the water content in the raw material must be removed through an evaporation process until it is dry [18]. This means drying it under direct sunlight for 24 hours or until it is completely dry.
4. Burning
   Waste that has been dried will be burned using the pyrolysis combustion method. Pyrolysis is a method of decomposing material at high temperatures without air or with limited oxygen. The main products of the pyrolysis process are carbon charcoal, oil, and gas [17]. Here are the steps:
   a. A chimney is used as a combustion site to make a pyrolysis site. This chimney is designed to remove pyrolysis gases and steam produced during the burning process of raw materials. This removes gases containing hydrocarbons or other compounds from the pyrolysis system.
   b. The raw material is 4K1P waste, each of which weighs 2 kg and will be put into the pyrolysis site. Then, the pyrolysis vat is closed tightly to burn with no or little oxygen in the combustion. In addition, every gap in the pyrolysis container must be considered so that no smoke comes out during combustion.

Volume 10, Issue 2, Oktober 2024, pp. 107-116
ISSN 2355-5068 ; e-ISSN 2622-4852
DOI: 10.33019/jurnalecotipe.v11i2.4492

c. Burning of raw materials begins with ignition from the bottom of the pyrolysis chamber, and the combustion process continues until smoke appears from the chimney, indicating that the raw materials are starting to burn. This burning process lasts 3 hours when the raw material becomes carbon charcoal.
d. After the combustion process is complete, the resulting carbon charcoal is left for 4 hours and its weight is measured.

2.3. RDF Briquette Production

In the production of RDF briquettes, 4K1P waste has gone through a combustion process using the pyrolysis method which produces carbon charcoal. The carbon charcoal will be processed into RDF briquettes, the following are the stages in producing RDF briquettes.

1. Carbon charcoal sieving
   The carbon charcoal will be sifted using a 60-mesh sieve to separate the coarse particles still present into fine particles of the same size.
2. Mixing carbon charcoal
   Adding adhesive to the manufacture of RDF briquettes greatly influences pressure resistance, heating value, ash content, and water content. The adhesive must have high binding power so that the briquettes do not decompose quickly [18]. Carbon charcoal will be mixed with 20% paraffin adhesive. The following is a design for experimental variations of RDF briquettes with a weight of 100 grams each
   a. Briquettes 1 Organic (100 gr) = 80% organic carbon charcoal (40 gr paper carbon charcoal, 40 gr wood carbon charcoal) and 20% (20 gr) paraffin adhesive.
   b. Briquette 2 Inorganic (100 gr) = 80% inorganic carbon charcoal (26.7 gr plastic carbon charcoal, 26.7 gr cloth carbon charcoal, 26.7 gr rubber carbon charcoal) and 20% (20 grams) paraffin adhesive.
   c. Briquette 3 Mixture (100 gr) = 40% organic mixed carbon charcoal (20 gr paper carbon charcoal and 20 gr wood carbon charcoal) and 40% inorganic (13.33 gr plastic carbon charcoal, 13.33 gr cloth carbon charcoal and 13, 33 gr rubber carbon charcoal) 1:1 (50% organic carbon charcoal, 50% inorganic carbon charcoal) with 20% (20 gr) paraffin adhesive.
3. RDF briquette printing
   RDF briquettes will be molded using molding iron, with a diameter of 7 cm and a weight of 100 gr. Then, the carbon charcoal is compacted using a press to apply pressure to the briquettes so that they become solid.
4. Drying of RDF briquettes
   After the RDF briquettes are printed, the briquettes will be dried using the RDF briquette drying process for 48 hours under sunlight so that the resulting briquettes can dry thoroughly and to reduce the water content contained in the RDF briquettes. The surface of the briquettes should feel dry and not damp to the touch.

2.4. Test the Quality of RDF Briquettes

The briquettes that have been produced need to be tested to determine the quality of the briquettes according to applicable standards. Good briquette testing results will be by SNI 01-6235-2000 standards as in Table 1.

Table 1. Standard Briquette Parameters

Characteristics	Unit	Quality
Calorific Value	Kal/g	≥ 5000
Water Content	%	≤ 8
Ash Content	%	≤ 8

There are parameters used in processing waste into RDF, including calorific value, water content, and ash content. Briquette testing includes:

1. Calorific Value
   Calorific value is a quantity that describes the energy value of a material. The greater the calorific value of a material, the more easily it will burn [8]. A bomb calorimeter is used to test the energy

Volume 10, Issue 2, Oktober 2024, pp. 107-116
ISSN 2355-5068 ; e-ISSN 2622-4852
DOI: 10.33019/jurnalecotipe.v11i2.4492

value contained in a briquette. The standard value is a minimum of 5,000 cal/g based on SNI 01-6235-2000.

2. Water Content
   It is hoped that the water content in RDF briquettes will be low so that lighting them does not require a large amount of energy, which can reduce the smoke that appears when burning them. The water content test in a briquette will be measured using a Minimum Free Space oven or MFS oven. The standard value is a minimum of 8% based on SNI 01-6235-2000.
3. Ash Content
   Ash content is the residue from the combustion process, consisting of the composition of unburned briquettes. After combustion, the remaining organic mineral content determines the ash content value of the briquettes. Ash content is measured using the Ash Content Test Oven, with a minimum standard of 8% according to SNI 01-6235-2000.

2.5. Fuel Requirements at PLTU

In the process of converting water into high pressure steam (steam), the boiler requires heat from burning fuel. In calculating fuel requirements for a PLTU with a capacity of 7.5 MW, initial data was obtained from previous research [15].

Table 2. Data on PLTU Boilers

Steam Pressure	Steam Temperature	Efficiency (η) Boilers	Temp. Feed Water	Boiler Capacity
3, 2 MPa	420 °c	90 %	90 °c	32 tons/hour

The heat requirement for the boiler can be calculated by:

$$Q_{boiler} = \frac{m\,.(h_o - h_i)}{\eta} \quad (1)$$

In the equation above, the enthalpy value of the superheated steam and the enthalpy value of the feed water entering the boiler will be known from the thermodynamic periodic table of water vapor temperature and the superheated steam table. To calculate fuel requirements for a boiler, use the equation:

$$Q_{fuel} = \frac{Q_{boiler}}{calorific\ value\ of\ fuel} \quad (2)$$

The calorific value contained in different fuel types significantly affects the calculation results [15]. Then, annual fuel requirements are calculated based on usage capacity using the equation:

$$Q_{fuel} \text{ x } 24 \text{ hr x } 358 \text{ days} \quad (3)$$

In 1 year the PLTU is not fully operational, it only lasts 356 days, but there are 7 days for maintenance and repairs so the effective time for a PLTU to operate is 358 days.

3. RESULTS AND DISCUSSION

In this research, RDF briquette products were produced with 3 samples that compared the calorific value, water content, and ash content, where each RDF briquette was composed of different raw materials. The process of processing RDF briquette raw materials into carbon charcoal can be seen in Table 3 where the raw materials can produce carbon charcoal as follows.

Table 3. Carbon Charcoal

Type of Raw Material	Raw Material	Initial Raw Material Weight (Kg)	Weight of Carbon Charcoal Yield (Grams)

JURNAL ECOTIPE
Electronic, Control, Telecommunication, Information, and Power Engineering
Volume 10, Issue 2, Oktober 2024, pp. 107-116
ISSN 2355-5068 ; e-ISSN 2622-4852
DOI: 10.33019/jurnalecotipe.v11i2.4492

Organic	Paper	2	875
	Wood	2	648
Inorganic	Plastic	2	1.090
	Cloth	2	856
	Rubber	2	1.160

Table 3 shows that carbon charcoal consists of organic and inorganic raw materials and 4K1P waste raw materials. The result of burning waste in the form of carbon charcoal is that the combustion process can reduce these raw materials with a reduction percentage of paper of 57%, wood at 68%, plastic at 46%, cloth at 58%, and rubber at 42% of the total raw materials reduced.

Figure 3. RDF Briquettes

Figure 3 shows the shape of the three briquette samples that have been made. The three briquette samples consist of organic briquettes, inorganic briquettes, and mixed briquettes with a weight of 100 grams each. From the carbon charcoal results for each raw material in Table 3, more than 1 RDF briquette can be produced. The following is the number of briquettes that can be produced.

Table 4. Number of Briquettes

Types of Briquettes	Number of Briquette Pieces (100 grams/piece)
Organic	10
Inorganic	10
Mixture	10

Table 4 Number of briquettes made from raw materials that have gone through the combustion process to become carbon charcoal. Each briquette weighs 100 gr/keeping using paraffin adhesive of 20% of the total briquette weight and 80% carbon charcoal from the raw material.

3.1. Calorific Value Analysis

Calorific value analysis is carried out to determine the amount of energy contained in a briquette, which will affect the ignition of the fire [10]. The following are the results of the calorific value test:

Table 5. Results of Calorific Value of RDF Briquettes

Sample Type	Calorific Value (Cal/g)	Standard Value (Cal/g)	Reference	Information

Volume 10, Issue 2, Oktober 2024, pp. 107-116
ISSN 2355-5068 ; e-ISSN 2622-4852
DOI: 10.33019/jurnalecotipe.v11i2.4492

Organic	6448,65	≥ 5000	SNI 01-6235-2000	Standard
Inorganic	8075,92			Standard
Mixture	6994,51			Standard

Table 5 shows the results of the heating value of briquettes using a bomb calorimeter. The greater the calorific value of a material, the easier it is to burn [8]. The test results showed that the highest calorific value was in inorganic briquettes at 8075.92 cal/g, then mixed briquettes at 6994.51 cal/g, and organic briquettes at 6448.65 cal/g, which produced the lowest water content value. From the laboratory test results, the calorific value of the three types of RDF briquettes is by SNI, where the value has exceeded 5,000 cal/kg. This is due to the influence of different kinds of raw briquette materials and the composition ratios of the raw materials. With this calorific value, the results can be obtained that inorganic briquettes can generate more incredible energy than organic and mixed briquettes because the calorific value produced will affect the energy that can be formed from the briquettes.

This research shows that briquettes' calorific value is higher than previous research [8] due to differences in combustion methods, burning duration, and raw material composition. This research used the pyrolysis method with a burning duration of 3 hours, while previous research used the carbonization method without specifying the burning duration. In addition, the waste composition used in this research consisted of organic, inorganic, and mixed raw materials with 4K1P raw materials, whereas previous research used different raw materials.

3.2. Water Content Analysis

Water content values are analyzed to determine the water content in the RDF briquettes produced to measure the extent to which the briquettes can provide efficient heat during combustion [8]. The following are the results of testing the water content values:

Table 6. Results of RDF briquette water content

Sample Type	Water content (%)	Standard Value (%)	Reference	Information
Organic	1,88	≤ 8	SNI 01-6235-2000	Standard
Inorganic	1,75			Standard
Mixture	1,82			Standard

Based on the results of testing the water content of RDF briquettes in Table 6, organic briquettes have the highest water content value of 1.88%, followed by mixed briquettes at 1.82% and inorganic briquettes with the lowest value of 1.75%. All water content values are by SNI standards, which do not exceed 8%. The difference in moisture content values is caused by variations in briquette raw materials, where organic waste tends to have higher moisture than inorganic waste. Pre-treatment processes such as drying raw materials also affect the water content value by reducing the mass of water that evaporates. In addition, the finer particle size in briquettes can produce a larger surface area and denser briquettes, reducing the water content.

The water content value in this study is higher than in previous research [8] with a difference of 0.71% – 0.84%. This difference could be caused by the drying process in this study, namely for 48 hours under sunlight. In contrast, in research [8], the drying process was for 24 hours under sunlight with an additional 4 hours of drying using an oven at a temperature of 105°C. Apart from that, the composition of the waste used is also different, where this research uses a mixture of organic and inorganic raw

Volume 10, Issue 2, Oktober 2024, pp. 107-116
ISSN 2355-5068 ; e-ISSN 2622-4852
DOI: 10.33019/jurnalecotipe.v11i2.4492

materials and 4K1P waste. In contrast, previous research only used a mixture of organic and inorganic waste in specific proportions.

3.3. Ash Content Analysis

Ash content analysis was carried out to determine the residue results from the combustion process of an RDF briquette. Briquettes that do not burn completely will produce combustion residue called ash. The following are the results of testing the ash content values :

Table 7. Results of Ash Content of RDF Briquettes

Sample Type	Ash Content (%)	Standard Value (%)	Reference	Information
Organic	23,17	≤ 8	SNI 01-6235-2000	Non Standard
Inorganic	10,84			Non Standard
Mixture	18,32			Non Standard

Based on the ash content test results in Table 7, organic briquettes have the highest ash content (23.17%), followed by mixed briquettes (18.32%) and inorganic briquettes (10.84%) which have the lowest ash content. The ash content values of the three types of briquettes exceed the specified SNI standards (8%). Organic briquettes tend to have a higher ash content because the characteristics of the raw material have not been adequately carbonized, causing the presence of compounds that increase the ash content value, resulting in more significant residue in the briquettes. In addition, the ash content value is inversely proportional to the heating value, which means that the greater the ash content, the lower the heating value [19].

This research shows higher ash content than previous research [8] due to differences in waste composition, burning method, and burning duration. This research uses organic, inorganic, and mixed waste compositions with 4K1P waste as raw materials, while previous research only used a mixture of organic and inorganic waste. In addition, this study used a pyrolysis method with a burning duration of 3 hours, whereas previous research used a carbonization method without a specified burning duration. Different burning methods can affect the mineral content that does not burn completely.

3.4. Fuel Requirements at PLTU

In the process of calculating the fuel requirements for a PLTU with a capacity of 7.5 MW, use equation 1 using the initial data in Table 2, where this equation produces the heat requirements for the PLTU boiler so that you can find out the fuel requirements for the boiler which are calculated using equation 2 uses 3 variations of RDF briquettes, namely organic briquettes, inorganic briquettes, and mixed briquettes. The following are the results of the heat requirements for the boiler and the fuel consumption required for the PLTU.

Table 8. PLTU Fuel Consumption

Heat in PLTU Boiler (kCal/hour)	Sample Type	Fuel Requirements (tons/hour)	Number of Briquette Pieces (pieces/hour)	Briquette Raw Materials	Amount of Carbon Charcoal (gr/hour)	Amount of Raw Materials (gr/hour)
24.679.424	Organic	3,8	38.000	Paper	1.520.000	3.474.286
				Wood	1.520.000	4.691.358

Volume 10, Issue 2, Oktober 2024, pp. 107-116
ISSN 2355-5068 ; e-ISSN 2622-4852
DOI: 10.33019/jurnalecotipe.v11i2.4492

	Inorganic	3	30.000	Plastic	799.800	1.467.523
				Cloth	799.800	1.868.692
				Rubber	799.800	1.378.966
	Mixture	3,5	35.000	Paper	700.000	1.600.000
				Wood	700.000	2.160.494
				Plastic	466.550	856.055
				Cloth	466.550	1.090.070
				Rubber	466.550	804.397

Based on Table 8, the fuel requirement for a PLTU with inorganic briquettes is 3 tons/hour, with a briquette requirement of 30,000 pieces/hour. This requires 799,800 g/hour of plastic carbon charcoal, cloth, and rubber, with plastic raw materials 1,378,276 gr/hour, 1,868,692 gr/hour of cloth, and 1,379,310 gr/hour of rubber. This is because the calorific value of inorganic briquettes is higher than that of organic and mixed briquettes. The boiler fuel requirement for this research is better than previous research, which used palm oil waste (shells) with a requirement of 5.1 tons/hour because the calorific value is higher, namely 6,448.65 to 8,075.92 cal/kg. Different types of fuel greatly influence the calculation of PLTU fuel requirements. By knowing the fuel requirement per hour, you can calculate the fuel requirement per year.

Table 9. PLTUs Fuel Consumption Per Year

Sample Type	Fuel Requirements (ton/year)	Number of Briquette Pieces (pieces/year)	Briquette Raw Materials	Amount of Carbon Charcoal (gr/year)	Amount of Raw Materials (gr/year)
Organic	32.649,60	326.496.000	Paper	13.060	29.851
			Wood	13.060	40.308
Inorganic	25.776	257.760.000	Plastic	6.872	12.609
			Cloth	6.872	16.056
			Rubber	6.872	11.848
Mixture	30.072	300.720.000	Paper	6.014	13.747
			Wood	6.014	18.563
			Plastic	4.009	7.355
			Cloth	4.009	9.366
			Rubber	4.009	6.911

Based on Table 9, the annual fuel consumption of PLTUs using inorganic briquettes is 25,776 tons, lower than other briquettes because the calorific value is higher. This requires 6,872 tons/year of carbon from plastic, cloth, and rubber, with raw materials of 12,609 tons of plastic, 16,056 tons of cloth, and 11,848 tons of rubber. This fuel requirement is more efficient than research [15], which shows a need for 43,819.2 tonnes/year from palm oil waste, with a difference of 40.19% greater.

4. CONCLUSION

From the lab test results that have been obtained, it can be seen that the best briquettes are inorganic RDF briquettes because they have the highest heating value of 8075.92 cal/kg and the lowest water content value of 1.75% which meets the SNI 01-6235-2000 standard. The best results in calculating fuel requirements for PLTUs are inorganic RDF briquettes, namely 3.05 tonnes/hour with an annual requirement of 26,205.6 tonnes/year.

REFERENCES

[1] G. Widjaja and S. Lovianda Gunawan, "Dampak Sampah Limbah Rumah Tangga Terhadap Kesehatan Lingkungan," *Zahra J. Heal. Med. Res.*, vol. 2, no. Oktober, pp. 266–275, 2022.

[2] N. F. Herlia, "Mekanisme Teknologi Pengolahan Sampah Menjadi Sumber Energi Listrik Terbarukan," *J. Technopreneur*, vol. 10, no. 2, pp. 10–16, 2022, doi: 10.30869/jtech.v10i2.962.

Volume 10, Issue 2, Oktober 2024, pp. 107-116
ISSN 2355-5068 ; e-ISSN 2622-4852
DOI: 10.33019/jurnalecotipe.v11i2.4492

[3] D. C. Aulia *et al.*, "Peningkatan Pengetahuan dan Kesadaran Masyarakat tentang Pengelolaan Sampah dengan Pesan Jepapah," *J. Pengabdi. Kesehat. Masy.*, vol. 1, no. 1, pp. 62–70, 2021.
[4] I. Pujotomo, "Pemanfaatan Sampah Menjadi Sumber Energi," *Energi & Kelistrikan*, vol. 8, no. 2, pp. 109–113, 2016.
[5] K. L. H. dan Kehutanan, "CAPAIAN KINERJA PENGELOLAAN SAMPAH," *2020*. https://sipsn.menlhk.go.id/sipsn/
[6] Firman dkk, "Studi Eksperimental Refused Derived Fuel (RDF) dari Sampah di Tempat Pembuangan Akhir (TPA) Penujah Kabupaten Tegal Sebagai Bahan Bakar Kompor RDF," pp. 22–29, 2022.
[7] A. F. Ikhsanudin, P. H. Tjahjanti, A. Fahruddin, A. i Akbar, and R. E. Fernanda, "Pengkajian Briket dari Campuran Sampah Botol Jenis PET dan Bahan Natural Dengan Perekat Kanji," *Justek J. Sains dan Teknol.*, vol. 5, no. 2, p. 73, 2022, doi: 10.31764/justek.v5i2.9971.
[8] N. A. Anggraini and Y. S. Purnomo, "Potensi Pemanfaatan Refuse Derived Fuel (RDF) Sampah Domestik di TPST Desa Taman, Sidoarjo sebagai Briket," *ESEC Proc.*, vol. 3, no. 1, pp. 65–74, 2022.
[9] M. F. Rania, I. G. E. Lesmana, and E. Maulana, "Analisis Potensi Refuse Derived Fuel (RDF) dari Sampah pada Tempat Pembuangan Akhir (TPA) di Kabupaten," *Sintek J. J. Ilm. Tek. Mesin*, vol. 13, no. 1, pp. 51–59, 2019.
[10] L. Oktavia, U. E. K. Sari, and A. Rhamadhan, "Pemanfaatan Sampah 4k1p Dari Tpa (Tempat Pemrosesan Akhir) Sebagai Bahan Baku Briket," *Pros. Semin. Nas. Sains dan Teknol.*, pp. 13–19, 2019.
[11] S. B. Sriwijaya, "Analisa Potensi Sampah Di TPSA Cilowong Sebagai Bahan Baku Refuse Derived Fuel (RDF)," *J. Ilm. TEKNOBIZ*, vol. 6, no. 3, pp. 174–182, 2016.
[12] G. M. Saragih, M. Marhadi, and Y. Defriati, "Pengolahan Sampah Organik Menjadi Biobriket Sebagai Energi Terbarukan," *J. Daur Lingkung.*, vol. 3, no. 2, p. 58, 2020, doi: 10.33087/daurling.v3i2.55.
[13] U. Surma, A. Natio, S. Harahap, and L. O. M. Firman, "Analisa pemanfaatan sampah perkotaan untuk pembangkit listrik di tpa ciniru kabupaten kuningan," *J. Ilm. Progr. Stud. Magister Tek. Mesin*, vol. 10, no. 1, pp. 7–12, 2020, [Online]. Available: http://journal.univpancasila.ac.id/index.php/teknobiz/article/view/1355/874
[14] E. Y. I. Christanti, I. N. S. Kumara, and C. G. I. Partha, "Analisis Tekno-Ekonomi dari Refuse Derived Fuel (RDF) sebagai Waste To Energy (WTE) di TPA Pakusari Jember, Jawa Timur," *Maj. Ilm. Teknol. Elektro*, vol. 21, no. 2, p. 201, 2022, doi: 10.24843/mite.2022.v21i02.p07.
[15] A. Akhdiyatul, E. Radwitya, and Y. Chandra, "Analisis Teknis dan Ekonomis Dalam Penggunaan Bahan Bakar Biomassa Di Pusat Listrik Tenaga Uap Studi Kasus di PLTU PT. Suka Jaya Makmur," *Elkha*, vol. 10, no. 2, p. 49, 2018, doi: 10.26418/elkha.v10i2.26741.
[16] D. M. Novita and E. Damanhuri, "PERHITUNGAN NILAI KALOR BERDASARKAN KOMPOSISI DAN KARAKTERISTIK SAMPAH PERKOTAAN DI INDONESIA DALAM KONSEP WASTE TO ENERGY," *J. Teh. Lingkung.*, vol. 16, no. 2, pp. 103–115, 2010, doi: 10.5614/jtl.2010.16.2.1.
[17] K. Ridhuan, D. Irawan, Y. Zanaria, and F. Firmansyah, "Pengaruh Jenis Biomassa Pada Pembakaran Pirolisis Terhadap Karakteristik Dan Efisiensibioarang - Asap Cair Yang Dihasilkan," *Media Mesin Maj. Tek. Mesin*, vol. 20, no. 1, pp. 18–27, 2019, doi: 10.23917/mesin.v20i1.7976.
[18] J. B. Mapossa, *ANALISIS PERFORMANSI PROSES GASIFIKASI REFUSE DERIVED FUEL (RDF) LIMBAH PADAT AREN DENGAN VARIASI JENIS BAHAN PENGIKAT*, vol. 372, no. 2. 2018. [Online]. Available: http://www.ncbi.nlm.nih.gov/pubmed/7556065%0Ahttp://www.pubmedcentral.nih.gov/articlerender.fcgi?artid=PMC394507%0Ahttp://dx.doi.org/10.1016/j.humpath.2017.05.005%0Ahttps://doi.org/10.1007/s00401-018-1825-z%0Ahttp://www.ncbi.nlm.nih.gov/pubmed/27157931
[19] I. G. N. A. Atmika and G. P. Suryawan, "Pengelolaan Limbah Banten sebagai Sumber Energi Terbarukan dengan Teknologi RDF Berkualitas Tinggi," *J. Bakti Sar.*, vol. 11, no. 2, pp. 97–106, 2022.

JURNAL ECOTIPE
Electronic, Control, Telecommunication, Information, and Power Engineering

Volume 11, Issue 2, October 2024, pp. 117-124
ISSN 2355-5068 ; e-ISSN 2622-4852
DOI: 10.33019/jurnalecotipe.v11i2.4497

Evaluating the Performance of High-Gain Observer (HGO) for Accurate Level Estimation in a Continuous Stirred Tank Reactor (CSTR)

Dian Mursyitah[1], Ahmad Faizal[2], Zulfatri Aini[3]
[1]UIN Sultan Syarif Kasim Riau, Jl. HR. Soebrantas KM. 15 no. 155 Simpang Baru, 28129, Pekanbaru, Indonesia

ARTICLE INFO

Article historys:

Received : …/…/…
Revised : …/…/…
Accepted : …/…/…

Keywords:

Estimation; High Gain Observer; Level; sensitivity; robustness

ABSTRACT

This paper presents an estimation method for the level in a Continuous Stirred Tank Reactor (CSTR) system. Given the inherent non-linearity of the CSTR model, our research focuses on developing observers capable of effectively handling the non-linearity. The utilization of a High Gain Observer (HGO) for accurate and robust level estimation is proposed. The desired characteristics for the estimation approach include achieving minimal error, ensuring fast convergence time, and maintaining robustness in the face of noisy measurements. To comprehensively evaluate the effectiveness and robustness of the proposed observers, simulations are conducted. The results demonstrate that the HGO effectively estimates the level, closely following the trajectories of the true states within the CSTR system. Importantly, the estimation accuracy persists across various input conditions. The fast convergence of the estimation process is validated, achieving convergence within 0.1 seconds. Furthermore, robustness is confirmed as the estimation continues to closely follow true state trajectories even in the presence of noisy measurements.

Corresponding Author:

Dian Mursyitah
UIN Sultan Syarif Kasim Riau, Jl. HR. Soebrantas KM. 15 no. 155 Simpang Baru, 28129, Pekanbaru, Indonesia
Email: dmursyitah@uin-suska.ac.id

1. INTRODUCTION

CSTR are widely used in industries that require fluid mixing in their processes. However, their operation poses challenges due to their complex non-linear behavior and the associated costs involved in industrial setups [1, 2]. A common hurdle in CSTR operation is maintaining level control, especially amidst unstable flow rates, which can significantly delay achieving desired levels, especially when setpoints change. These unstable flow rates stem from variations in inflow, outflow, or system disturbances. Traditional approaches to level estimation often rely on sensors, which, over time, can become prone to inaccuracies, drift, or even failure. To maintain the desired level, feedback control systems employing level sensors and actuators are often implemented. However, this approach is hindered by the sensor's high cost, susceptibility to noise, incipient faults, and limited responsiveness due to the harsh operational environment [3, 4]. Moreover, sometimes the sensor's measurements do not contain enough information, and some signals are impossible to measure because the sensor is placed in a hard-to-reach area.

To address these challenges, advanced estimation techniques such as observer have gained prominence. The observer is the most effective-cost approach as it can reduce the reliance on a high-cost sensor. Additionally, observers can augment or even replace sensors [5]. There are several types of observers such as Luenberger Observer (LO), Extended Kalman Filter (EKF), High Gain Observer

JURNAL ECTIPE
Electronic, Control, Telecommunication, Information, and Power Engineering
Volume 10, Issue 2, October 2024, pp. 117-124
ISSN 2355-5068 ; e-ISSN 2622-4852
DOI: 10.33019/jurnalecotipe.v11i2.4497

(HGO), and others. LO is design for linear system, providing local convergence [6]. The EKF require the modelling error to be Gaussian white noise [7]. Graton et al. have outlined criteria for choosing an observer [8]. The criteria are sensitive to noises and robust against the noise and error model. According to [9, 10], the HGO is perform well when dealing with the non-linearity with proper gain settings. Furthermore, the HGO has higher estimation accuracy and better traceability compared with the EKF as presented by [11]. The robustness of HGO has been validated in many implementation [12-14]

Given that the mathematical model of the CSTR system is non-linear, as will be presented shortly, the observers we employ are capable of accommodating this nonlinearity in the system model. Therefore, we choose to work with HGO due to its promising ability to provide accurate estimates of system states with fast convergence [7, 15, 16]. Our focus is on evaluating the performance of HGO for level estimation in CSTR and to assess the effectiveness of HGO in accurately estimating the level under varying operating conditions, different initial condition, and disturbances. The performance analysis includes two criteria: sensitivity and robustness with respect to noisy measurements, examined through simulations. The results using Luenberger Observer (LO) will be presented as comparison.

2. RESEARCH METHOD

2.1. CSTR System Mathematical Model

CSTR incorporates two inputs, flow rate (F_1) and flow rate (F_2). The output flow (F_o), affects the level in the tank, assuming a perfect fluid in a tank stirred (see **Figure 1(a)**). The mathematical modeling of this system is derived from the law of tank equivalence, assuming the absence of material exiting in vapor form. This model is grounded in the principle that the volume entering the tank must equal the volume leaving it, accounting for any changes in volume within the tank.

The mathematical representation of the level in the CSTR is formulated as follows [17]:

$$\frac{dh}{dt} = \frac{1}{A}\left(F_1 + F_2\right) - \frac{K_c}{A}\sqrt{h} \tag{1}$$

where $h(t)$ is the level of the tank, A is the cross-section area, $F_{in} = F_1 + F_2$ is the input flowrates. K_c is the a mixer constant. We can see the CSTR system in **Figure 1(a)** with the parameter of the CSTR presented in **Table 1.**

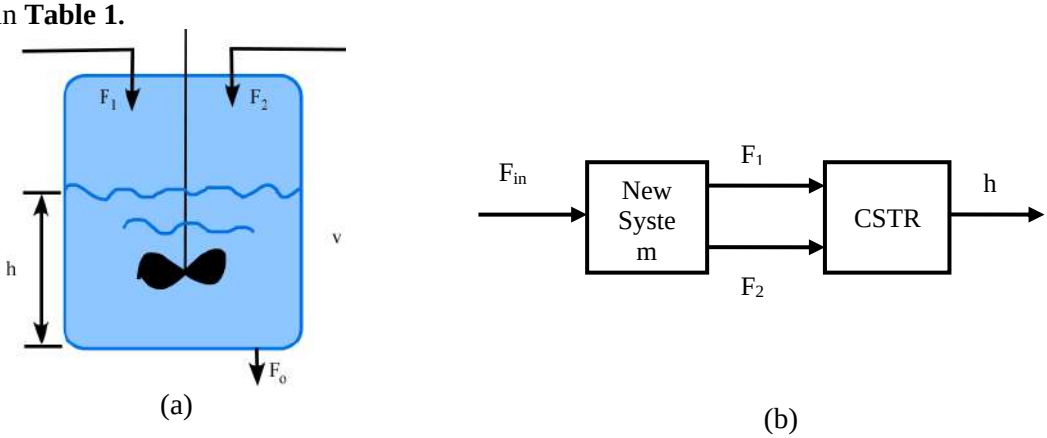

Figure 1. (a) CSTR System and decoupler (b) Decoupler design

Table 1. Parameter of CSTR System

Parameters	Units
Flow rate 1	$F_1 = 0.6m^3/sec$
Flow rate 1	$F_2 = 0.15m^3/sec$
Volume	$V = 1m^3$
Cross section	$A = 1m^2$
Mixer constant	$K_c = 0.2$ SI

The level in a CSTR is characterized by a coupled system, where disturbances introduced to one input directly influence the other output and vice versa. In such a system, changes in the first input can affect the second output, and vice versa. To mitigate this coupled effect and enable the independent

JURNAL ECOTIPE
Electronic, Control, Telecommunication, Information, and Power Engineering
Volume 10, Issue 2, October 2024, pp. 117-124
ISSN 2355-5068 ; e-ISSN 2622-4852
DOI: 10.33019/jurnalecotipe.v11i2.4497

design of observer, a decoupler is employed. The design of a decoupler ensures that disturbances in one input do not propagate to the other as shown in **Figure 1(b).**

The design of the decoupler facilitates the transformation of equation (1) into the following form:

$$\frac{dh(t)}{dt} = \frac{1}{A} F_{in}(t) - K_c \sqrt{h}(t) \tag{2}$$

where

$$F_{in}(t) = F_1(t) + F_2(t) \tag{3}$$

with this mathematical model, we proceed to design a High Gain Observer (HGO) for estimating the level in the CSTR system.

2.2. The Design of High Gain Observer (HGO)

The HGO is used for non-linear systems and is closely related to the extended Luenberger observer [18, 19]. To enhance comprehension of HGO, let us start by creating a model of CSTR system, represented by equation (4)

$$\begin{aligned} \dot{x}(t) &= f(x,u,t) \\ y(t) &= Cx(t) \end{aligned} \tag{4}$$

where $x \in \mathbf{R}^1$ is the state system, $u \in \mathbf{R}^1$ is the input signal, and $y \in \mathbf{R}^1$ is the output of the system. The non-linear function $f(\mathrm{g})$ related to state x, input signal u, and time *t*, are described below:

$$f(x,u,t) = \left[\frac{1}{A} \left(u - K_c \sqrt{x_1} \right) \right] \tag{5}$$

and the matrix *C* is presented as follows:

$$C = [1] \tag{6}$$

The HGO algorithm is presented as follows:

$$\dot{\hat{x}}(t) = A(t)\hat{x}(t) + K_H(t)\left(y(t) - C\hat{x}(t)\right) \tag{7}$$

with matrices $A(t)$ is given by:

$$A(t) = \left. \frac{\partial f(x,u,t)}{\partial x} \right|_{x=\hat{x}} = \left[\frac{K_c}{2\sqrt{x_1}} \right] \tag{8}$$

The pair of matrices *(A, C)* is observable, and observer gain is chosen as:

JURNAL ECOTIPE
Electronic, Control, Telecommunication, Information, and Power Engineering
Volume 10, Issue 2, October 2024, pp. 117-124
ISSN 2355-5068 ; e-ISSN 2622-4852
DOI: 10.33019/jurnalecotipe.v11i2.4497

$$K_{HGO}(t)=\begin{bmatrix} k_{1,1}/\theta^{1} & L & k_{1,p-1}/\theta^{1} & k_{1,p}/\theta^{1} \\ M & O & M & M \\ k_{n-1,1}/\theta^{n-1} & L & k_{n-1,p-1}/\theta^{n-1} & O \; k_{n-1,p}/\theta^{n-1} \\ k_{n,1}/\theta^{n} & L & k_{n,p-1}/\theta^{n} & k_{n,p}/\theta^{n} \end{bmatrix} \quad (9)$$

where $k_{1,1}, \ldots, k_{n,p}$ and θ are constant with $\theta = 1$ [14]. The matrix must be chosen such that $(A(t)-K_H(t)C)$ is stable. The dynamics of the error $e(t)=x(t)-\hat{x}(t)$, can be described as $\dot{e}(t)=(A(t)-K_H(t)C)e(t)$. The choice of observer gain plays a crucial role in achieving accurate and fast error reduction during the estimation process. In the next section, we presented the simulation result following with the analysis.

3. RESULTS AND DISCUSSION

3.1. System behavior

The simulation was conducted using a sampling time $T_s = 0.1$ s and a simulation duration of 25s. The input signal was set to a constant value $F_{in} = 0.75 m^3/s$. The simulation result is shown in **Figure 2**.

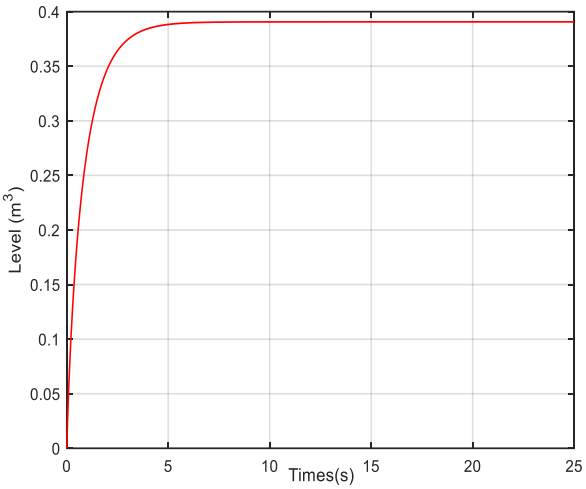

Figure 2. Output Level of CSTR System

The behaviour of the CSTR system is depicted in **Figure 2**. The input signal, denote as F_{in}, is determined by adding inputs F_1 and F_2 that has been presented in (3). It seen that when the input $F_{in} = 0.75 m^3/s$ is applied, the system output i.e., level stabilizes at $h = 0.39 m^3/s$. The estimation results obtained using HGO will be presented in the next subsection.

3.2. States estimation performance of level in CSTR system.

Based on the design in (6), the state estimation with HGO is conducted using same sampling and simulation time. The observer gain chosen for this scenario, as presented in (8) is:

$$K_{HGO} = 9.9996 \times 10^{3} \quad (10)$$

The simulation result is shown in **Figure 3**

JURNAL ECOTIPE
Electronic, Control, Telecommunication, Information, and Power Engineering
Volume 10, Issue 2, October 2024, pp. 117-124
ISSN 2355-5068 ; e-ISSN 2622-4852
DOI: 10.33019/jurnalecotipe.v11i2.4497

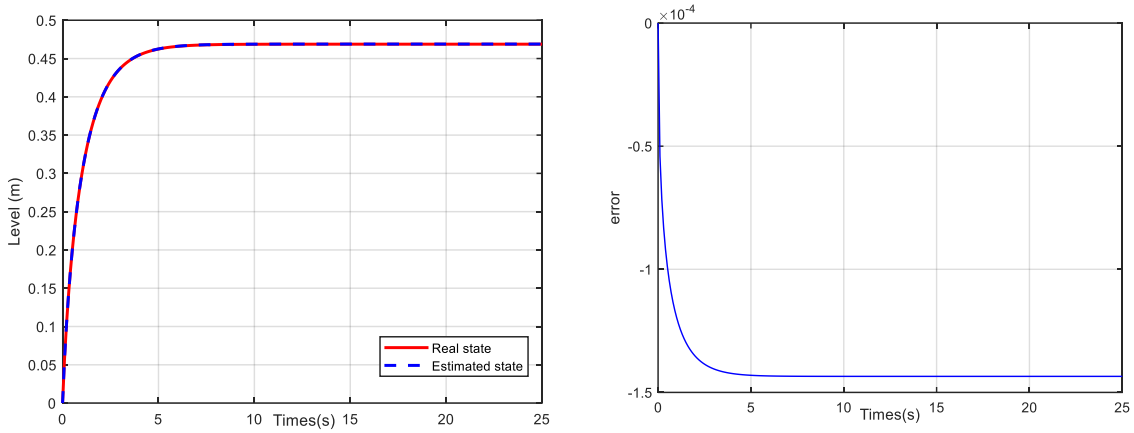

(a) (b)

Figure 3. (a) HGO State estimation of level (b) Error estimation

Based on **Figure 3(a),** the estimation of level given by HGO accurately reflects the true state i.e., level of the CSTR system. This alignment between the estimated and actual levels signifies the accuracy of the estimation process. Additionally, **Figure 3(b)** illustrates the error estimation, where it is evident that the error of estimation remains consistently at zero. This further validates the precision and reliability of the HGO in accurately estimating the system's state.

To conduct sensitivity analysis for the HGO, our next step involves modifying input signal to different operating points and adjusting the initial conditions for the HGO. This approach aims to evaluate the observer's sensitivity under varying operating conditions. By systematically testing the observer's performance against different setpoints, we aim to further validate its sensitivity of the observer in maintaining accurate estimations under different conditions. This analysis will help demonstrate the HGO's potential for real-time applications

3.3. Sensitivity Analysis

1. State estimation performance of level with different input signal

To evaluate the HGO's performance under different operating points, we create an input with different operating points, transitioning from 0s to 10s and 10s to 25s, with a step shape, as illustrated in **Figure 4(a)**. The input signal undergoes a change, transitioning from 0 to 0.75 m³/sec at 10 seconds. In the real world, we know that the flow entering the tank can vary over time and affect the level in the tank. This simulation represents real-world implementation conditions. Therefore, the simulation aims to assess the HGO's response and adaptability to different operating points in the CSTR.

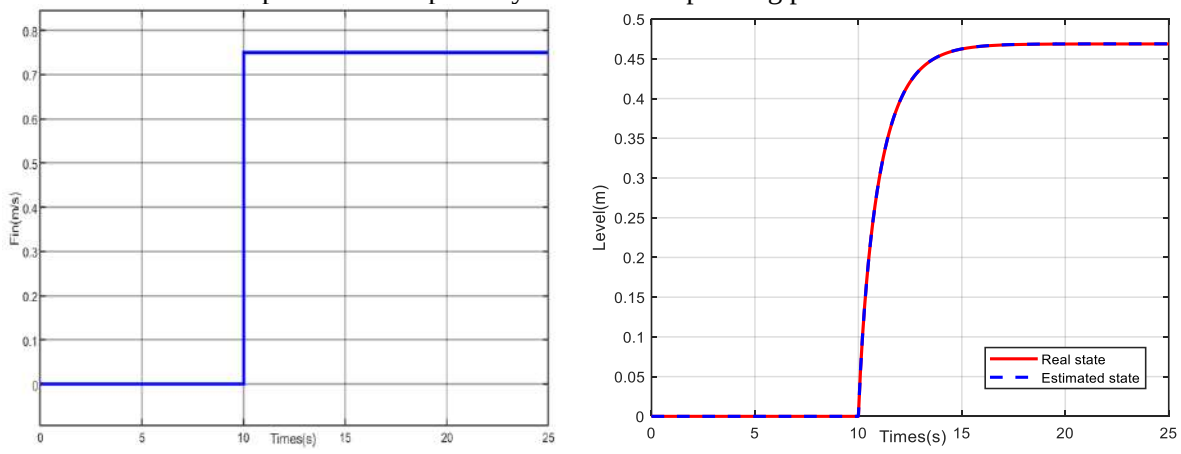

(a) (b)

Figure 4. (a) Input signal with two different operating points
(b) HGO state estimation of level in CSTR system with different operating point in input signal

Volume 10, Issue 2, October 2024, pp. 117-124
ISSN 2355-5068 ; e-ISSN 2622-4852
DOI: 10.33019/jurnalecotipe.v11i2.4497

In **Figure 4(b)**, it is evident that the HGO maintains its ability to accurately estimate the true state and track changes in the input signal with different operating point. Notably, as depicted in **Figure 4(a)**, the input is altered at 10 seconds in accordance with the scenario provided in the input signal. This proves that even with different operating points, the HGO is still capable of providing accurate estimations. The sensitivity of HGO in handling different operation point is validated. Remarkably, these results are achieved while maintaining the same initial conditions for both the system and the HGO, which are zero. With the same initial condition of both the system and observer, we next aim to understand how sensitive the HGO is when handling different initial conditions. According to [20], the initialization of observer is an important step because it sets the starting point for the estimation process. Errors in the initial conditions can propagate through the estimation process. If the initial state estimate is far from the actual state, the observer may take a long time to converge to the correct state, leading to significant estimation errors during the transient period. In some cases, an incorrect initial condition can lead to instability in the observer. This is particularly problematic in non-linear systems. The rate at which the observer converges to the true state depends on the initial condition.

In practical applications, the true initial state may not be precisely known, necessitating assumptions or approximations. This discrepancy can cause practical issues in the performance of the observer. The initial condition can be start from zero and also can be start with non-zero value. Understanding the impact of initial condition variations on the observer's performance is crucial for assessing its robustness. Therefore, in this simulation, we analyse the performance of HGO to handle the different initial condition when estimating the level in CSTR system. The initial conditions are design with two different values: the initial condition for system is at 0.6m, and the initial condition for the HGO is set at 0m. This approach seeks to assess the HGO's adaptability and performance under diverse starting conditions. The state estimation results are presented in **Figure 5**.

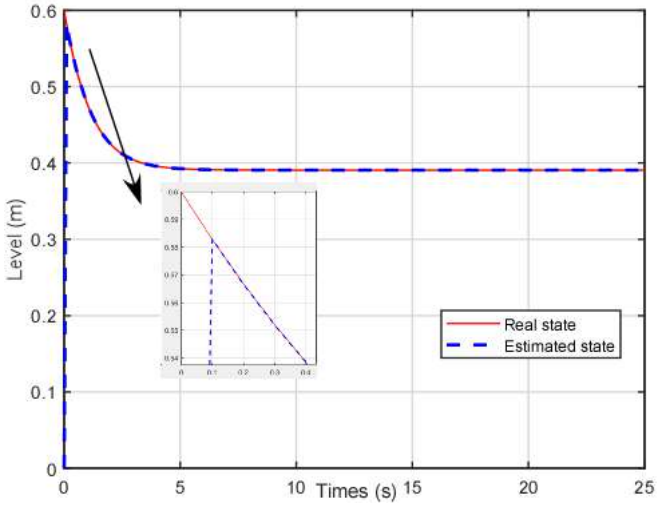

Figure 5. HGO state estimation of level in CSTR system with initial condition change

In **Figure 5**, it seen the initial condition of the system starting from 0.6m and the initial condition of HGO is from 0m. The fast convergence is validated, as shown by convergence within 0.1s. This result show that HGO is having no issues related to initial conditions, when estimating the level in the CSTR system. The estimation consistently yields favorable results, as the estimation follow trajectories the true states. To further assess the robustness of our proposed HGO, the next phase of simulation focuses on evaluating its performance with respect to measurement noise.

3.3. Robustness analysis with respect to measurement noise

In this subsection, we evaluate the performance of the HGO in handling measurement noise. The first step involves generating noise and adding it to the system. Noise is introduced into the measurements with a vector v as zero mean and variance unit. We describe the noise as $v: N\ (0,R)$, where R is presented as follows:

JURNAL ECOTIPE
Electronic, Control, Telecommunication, Information, and Power Engineering
Volume 10, Issue 2, October 2024, pp. 117-124
ISSN 2355-5068 ; e-ISSN 2622-4852
DOI: 10.33019/jurnalecotipe.v11i2.4497

$$R = 9.5367 \times 10^{-5} \quad (11)$$

The simulation result of state estimation with noisy measurement is shown in **Figure 6Figure** .

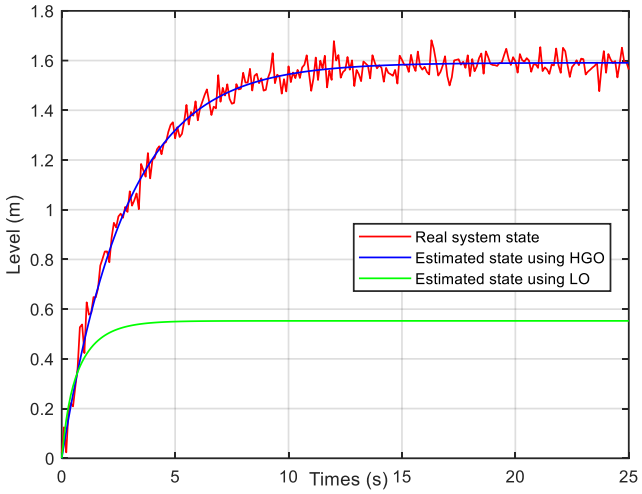

Figure 6. The HGO estimation with noisy measurements

Figure 6 show that the real system is noisy. However, the estimation still can follow the trajectory of the true state even under the presence of noise. These results indicate that the estimation performs well under these conditions. While noisy measurements introduce challenges, HGO does not encounter difficulties in estimation. For comparison, we present the estimation from the Luenberger Observer (LO), which shows that the estimation with LO is not robust with respect to measurement noise.

4. CONCLUSION

This study evaluates the performance of the HGO for accurate level estimation in a CSTR. The proposed HGO demonstrates good performance in estimating the tank level, as evidenced by **Figure 3(a)**, which shows that the HGO accurately tracks the true state with zero estimation error. Sensitivity analysis, illustrated in **Figure 4(b),** confirms that the HGO performs effectively across different operating points, indicating its robustness in handling variations in input signals. Furthermore, as depicted in **Figure 5**, the HGO exhibits notable adaptability to different initial conditions, mitigating concerns about the system's starting conditions. The fast convergence is achieved at 0.1s. The observer also maintains robust performance in the presence of measurement noise, highlighting its effectiveness in real-world scenarios where noise is a factor as shown in **Figure 6**. These results collectively affirm that the HGO is a reliable tool for accurate level estimation in CSTR systems, validating its potential for practical application.

Future works will focus on expanding the capabilities of the HGO to include fault diagnosis in the CSTR system. This extension aims to enhance the observer's functionality by enabling it to identify and respond to potential faults or anomalies within the system, contributing to a more comprehensive and versatile control framework.

REFERENCES

[1] N. Cherkasov, S. J. Adams, E. G. Bainbridge, and J. A. Thornton, "Continuous stirred tank reactors in fine chemical synthesis for efficient mixing, solids-handling, and rapid scale-up," *Reaction Chemistry & Engineering*, vol. 8, no. 2, pp. 266-277, 2023.

[2] R. Madhu Sudhanan and D. P. Poongodi, "Comparative Analysis of Various Control Strategies for a Nonlinear CSTR System," *International Journal of Nonlinear Sciences and Numerical Simulation*, vol. 18, pp. 269 - 276, 2017.

[3] D. Li, Y. Wang, J. Wang, C. Wang, and Y. Duan, "Recent advances in sensor fault diagnosis: A review," *Sensors and Actuators A: Physical*, vol. 309, p. 111990, 2020/07/01/ 2020.

Volume 10, Issue 2, October 2024, pp. 117-124
ISSN 2355-5068 ; e-ISSN 2622-4852
DOI: 10.33019/jurnalecotipe.v11i2.4497

[4] R.-X. Guo, K. Guo, and J.-K. Dong, "Fault diagnosis for sensors in a class of nonlinear systems," *IMA Journal of Mathematical Control and Information*, vol. 35, no. 2, pp. 375-391, 2018.
[5] J. Mohd Ali, N. Ha Hoang, M. A. Hussain, and D. Dochain, "Review and classification of recent observers applied in chemical process systems," *Computers & Chemical Engineering*, vol. 76, pp. 27-41, 2015/05/08/ 2015.
[6] P. Bernard and V. Andrieu, "Luenberger Observers for Nonautonomous Nonlinear Systems," *IEEE Transactions on Automatic Control*, vol. 64, no. 1, pp. 270-281, 2019.
[7] Q. Wang, X. Sun, and C. Wen, "Design Method for a Higher Order Extended Kalman Filter Based on Maximum Correlation Entropy and a Taylor Network System," *Sensors*, vol. 21, no. 17, p. 5864, 2021.
[8] G. Graton, J. Fantini, and F. Kratz, "Finite Memory Observers for linear time-varying systems. Part II: Observer and residual sensitivity," *Journal of the Franklin Institute*, vol. 351, no. 5, pp. 2860-2889, 2014.
[9] H. K. Khalil and L. Praly, "High-gain observers in nonlinear feedback control," *International Journal of Robust and Nonlinear Control*, vol. 24, no. 6, pp. 993-1015, 2014.
[10] A. Adil, I. N'Doye, and T. M. Laleg-Kirati, "High-Gain Observer Design for Nonlinear Systems with Delayed Output Measurements using Time-Varying Gains," in *2022 IEEE 61st Conference on Decision and Control (CDC)*, 2022, pp. 235-240.
[11] L. Wei, H. Zhang, C. Sun, and F. Yan, "Simultaneous estimation of ammonia injection rate and state of diesel urea-SCR system based on high gain observer," *ISA Transactions*, vol. 126, pp. 679-690, 2022/07/01/ 2022.
[12] E. Kim, S. Fan, N. Bose, and H. Nguyen, "Path Following for an Autonomous Underwater Vehicle (AUV) by Using a High-Gain Observer based on an AUV Dynamic Model," *IFAC-PapersOnLine*, vol. 52, no. 21, pp. 218-223, 2019/01/01/ 2019.
[13] L. Torres, C. Verde, G. Besançon, and O. González, "High-gain observers for leak location in subterranean pipelines of liquefied petroleum gas," *International Journal of Robust and Nonlinear Control*, vol. 24, no. 6, pp. 1127-1141, 2014.
[14] W. Rahiman, B. Wu, and Z. Ding, "Fault Detection Using High Gain Observer: Application in Pipeline System," in *Proceeding of the UKACC International Conference on Control. UK: University of Manchester*, 2008.
[15] S. Rúa, R. E. Vásquez, N. Crasta, and C. A. Zuluaga, "Observability analysis and observer design for a nonlinear three-tank system: Theory and experiments," *Sensors*, vol. 20, no. 23, p. 6738, 2020.
[16] Y. Ji, Z. Xu, J. Liu, and Y. Song, "Distributed extended high-gain observers for the generalized strict-feedback system," *International Journal of Robust and Nonlinear Control*, vol. 33, no. 13, pp. 7649-7666, 2023.
[17] D. Mursyitah, A. Faizal, and E. Ismaredah, *Level Control in Coupled Tank System Using PID-Fuzzy Tuner Controller*. 2018, pp. 293-298.
[18] J. Gauthier, H. Hammouri, and S. Othman, "A simple observer for nonlinear systems applications to bioreactors," *IEEE Transactions on automatic control*, vol. 37, no. 6, pp. 875-880, 1992.
[19] G. Besançon, D. Georges, O. Begovich, C. Verde, and C. Aldana, "Direct observer design for leak detection and estimation in pipelines," in *2007 European Control Conference (ECC)*, 2007, pp. 5666-5670: IEEE.
[20] G. Besançon, *Nonlinear observers and applications*. Springer, 2007.

JURNAL ECOTIPE
Electronic, Control, Telecommunication, Information, and Power Engineering

Volume 11, Issue 2, Oktober 2024, pp. 125-134
ISSN 2355-5068 ; e-ISSN 2622-4852
DOI: 10.33019/jurnalecotipe.v11i2.4491

Implementation OEE in Integrating Siemens S7-1200 Data with Odoo ERP

Muhammad Rafi Solakhudin[1], Muhammad Khoirul Hasin[1], Ii Munadhif[1]
[1]Automation Engineering, Faculty of Marine Electrical Engineering, Shipbuilding Institute of Polytechnic Surabaya, Surabaya 60111, Indonesia

ARTICLE INFO

Article historys:

Received : 19/Mei/2024
Revised : 14/June/2024
Accepted : …/…/…

Keywords:

API Service; ERP Odoo; Grafana; Integration IT and OT; OEE;

ABSTRACT

The integration of Operational Technology (OT) and Information Technology (IT) is crucial for enterprise-level decision-making regarding company effectiveness and productivity. This integration is achieved by developing an API service that facilitates the connection between Programmable Logic Controllers (PLCs) and Odoo Enterprise Resource Planning (ERP). This allows IT systems to synergize with OT systems, processing data obtained from industrial machine performance. The Overall Equipment Effectiveness (OEE) method was employed to monitor production outcomes. A prototype sorting system with PLC control was created as an OEE implementation. The API service acquires data from the plant and performs preliminary analysis in Odoo ERP. This analysis is conducted through the development of a manufacturing module in Odoo ERP, applying OEE method calculations to monitor effectiveness and efficiency of production process. Calculated results are monitored in real-time on Grafana. This research provided insights into the design and implementation of an integration system for the bottle sorting process, ensuring real-time monitoring through Odoo ERP and Grafana. The OEE analysis was validated against manual calculations, showing a 0% discrepancy, thereby ensuring its accuracy. Overall Equipment Effectiveness of bottle sorting machine reached 85.7%, with the three main indicators being: Availability at 96.67%, Performance at 92.53%, and Quality at 95.7%, indicating a world-class category. This research enables the production process to be optimized and provides significant benefits to the company. The findings serve as an evaluation tool at the enterprise level regarding the effectiveness and efficiency of machinery, highlighting areas for improvement and ensuring optimal production performance.

Corresponding Author:

Muhammad Rafi Solakhudin
Automation Engineering, Faculty of Marine Electrical Engineering, Shipbuilding Institute of Polytechnic Surabaya, Chemical Engineering Street, ITS Sukolilo Campus, Surabaya 60111, Indonesia
Email: rafi.solakhudin@student.ppns.ac.id

1. INTRODUCTION

The industrial automation system has rapidly evolved since the early 20th century, which required companies to enhance their production effectiveness and efficiency to keep pace with the development of the industrial era 4.0. Digital transformation has become crucial in the industry, allowing the integration of digital technologies into all of company operations in order to generate accurate and punctual data reports[1]. Nevertheless, the continued practice of manually reporting data of production results carries the potential for human error and data inconsistency between departments[2]. A decrease machine performance over time can lead to reduction in productivity and product quality. Hence, a monitoring system based on the Overall Equipment Effectiveness (OEE) method is required to monitor

JURNAL ECOTIPE
Electronic, Control, Telecommunication, Information, and Power Engineering
Volume 11, Issue 2, Oktober 2024, pp. 125-134
ISSN 2355-5068 ; e-ISSN 2622-4852
DOI: 10.33019/jurnalecotipe.v11i2.4491

machine performance in industrial automation systems[3]. To overcome these challenges, a novel integration approach is proposed that combines between Operational Technology (OT) and Information Technology (IT). OT is responsible for managing production devices such as SCADA, PLC, sensors, and induction motors, while IT oversees systems like ERP, Grafana, and other supporting applications. This integration allows direct data integration from OT to IT, eliminating the necessity for manual input thereby enhancing efficiency and productivity[4]. The implementation of OT and IT integration is facilitated through an API service that connects data from the PLC to Odoo ERP[5]. To validate the systems, a prototype was designed for bottle sorting system to monitor the volume of bottle liquid and analyze machine operation time[6]. Data from the prototype is transmitted to Odoo ERP for examination using the OEE method and subsequently monitored on Grafana, enabling companies to make more effective and efficient decisions to improve both the quality and quantity of its production[7]. The integration of OT and IT represents an effective solution for enhancing production monitoring, which has previously been conducted manually. By this integration, companies can ensure optimal production quality and quantity in the industrial era 4.0.

2. RESEARCH METHOD

In this research, the Overall Equipment Effectiveness (OEE) method is implemented on a bottle sorting plant that has been established. Subsequently, the data results from the bottle sorting plant will be transmitted through an API service by integrating data from the Programmable Logic Controller (PLC) with the Odoo Enterprise Resource Planning (ERP) system. Once the OEE calculation indicators is obtained, users can automatically determine the category of machine effectiveness and efficiency based on the OEE assessment standards[8].

2.1. The Overall System Design

In general, this research consists of four components: hardware, API Service, Odoo ERP, and Grafana. The hardware includes a bottle sorting plant and a control panel containing PLC and Arduino. Figure 1 illustrates the data input and output originating from sensors and actuators integrated into a bottle sorting plant, which is controlled by a Siemens PLC. Subsequently, data from the plant is acquired by the API Service and transmitted to the ERP Odoo. After the data has been processed, the results are displayed on Grafana.

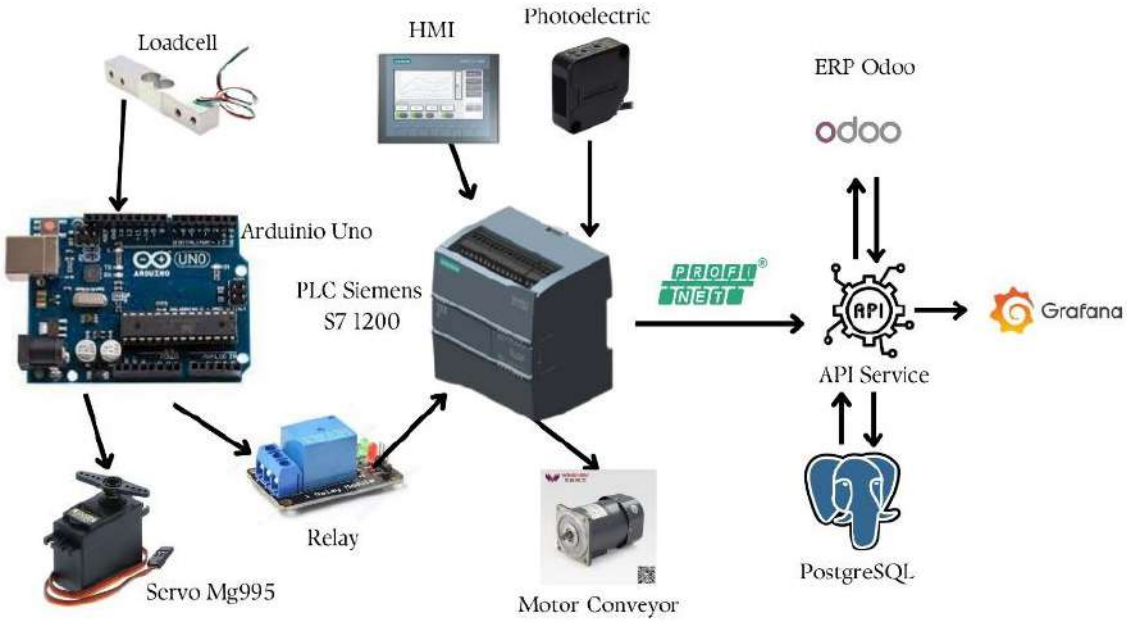

Figure 1. Block Diagram System

JURNAL ECTIPE
Electronic, Control, Telecommunication, Information, and Power Engineering
Volume 11, Issue 2, Oktober 2024, pp. 125-134
ISSN 2355-5068 ; e-ISSN 2622-4852
DOI: 10.33019/jurnalecotipe.v11i2.4491

2.2. Overall Equipment Effectiveness

Overall Equipment Effectiveness (OEE) is a method used to assess the extent to which equipment or machines are effectively utilized. OEE is calculated based on three elements Availability, Performance, and Quality Rate[9]. The systematic formula for OEE can be expressed as follows:

$$\text{Availability (\%)} = \frac{Operating\ Time}{Loading\ Time} \text{ x } 100\% \quad (1)$$

$$\text{Performance (\%)} = \frac{Cycle\ Time\ x\ Actual\ Output}{Operating\ Time} \text{ x } 100\% \quad (2)$$

$$\text{Quality (\%)} = \frac{Good\ Product}{Actual\ Output} \text{ x } 100\% \quad (3)$$

From the calculation of these three elements, a formula for overall equipment effectiveness is obtained:

(Overall Equipment Effectiveness (OEE) = Availability x Performance x Quality x 100%)

Overall Equipment Effectiveness (OEE) indicators in a company can be categorized into several assessment standards which can be seen in the table[10].

Table 1. Overall Equipment Effectiveness Category

Value OEE	Category
40% - 59%	Low
60% - 84%	Currently
85% - 99%	World Class
100%	Perfect

2.3. Hardware Design

The hardware in this study consists of a bottle sorting plant and a controller panel as depicted in Figures 2 and 3. The bottle sorting plant is comprised of two controllers: a PLC and an Arduino. On the PLC side, a photoelectric sensor is responsible to trigger the conveyor stop, calculate the time cycle, and determine the total number of products. Meanwhile, on the Arduino side, a load cell sensor is used to distinguish the weight of good and bad products, along with an MG995 servo actuator to reject bad products. Data transmission for good and bad products data, a relay is used, which is connected to the PLC's digital input pins. The plant is also equipped with an HMI to control the conveyor's operation and monitor the value read by the sensors. Bottles with a volume of 150ml are indicated as good products, while bottles with a volume less than 100ml are classified as bad products[11]. The workflow of the bottle sorting plant is depicted in Figure 3.

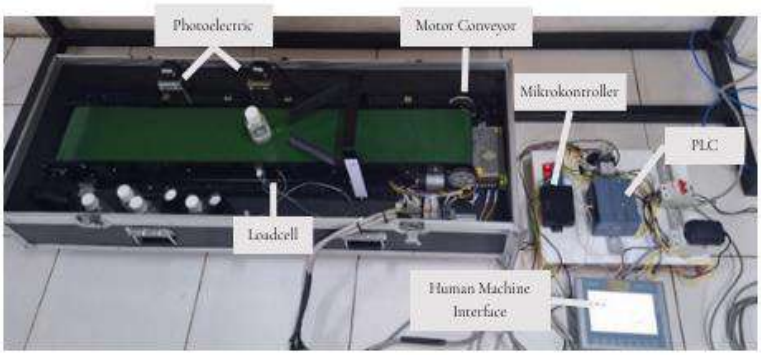

Figure 2. Bottle Sorting Plant and Control Panel

JURNAL ECOTIPE
Electronic, Control, Telecommunication, Information, and Power Engineering
Volume 11, Issue 2, Oktober 2024, pp. 125-134
ISSN 2355-5068 ; e-ISSN 2622-4852
DOI: 10.33019/jurnalecotipe.v11i2.4491

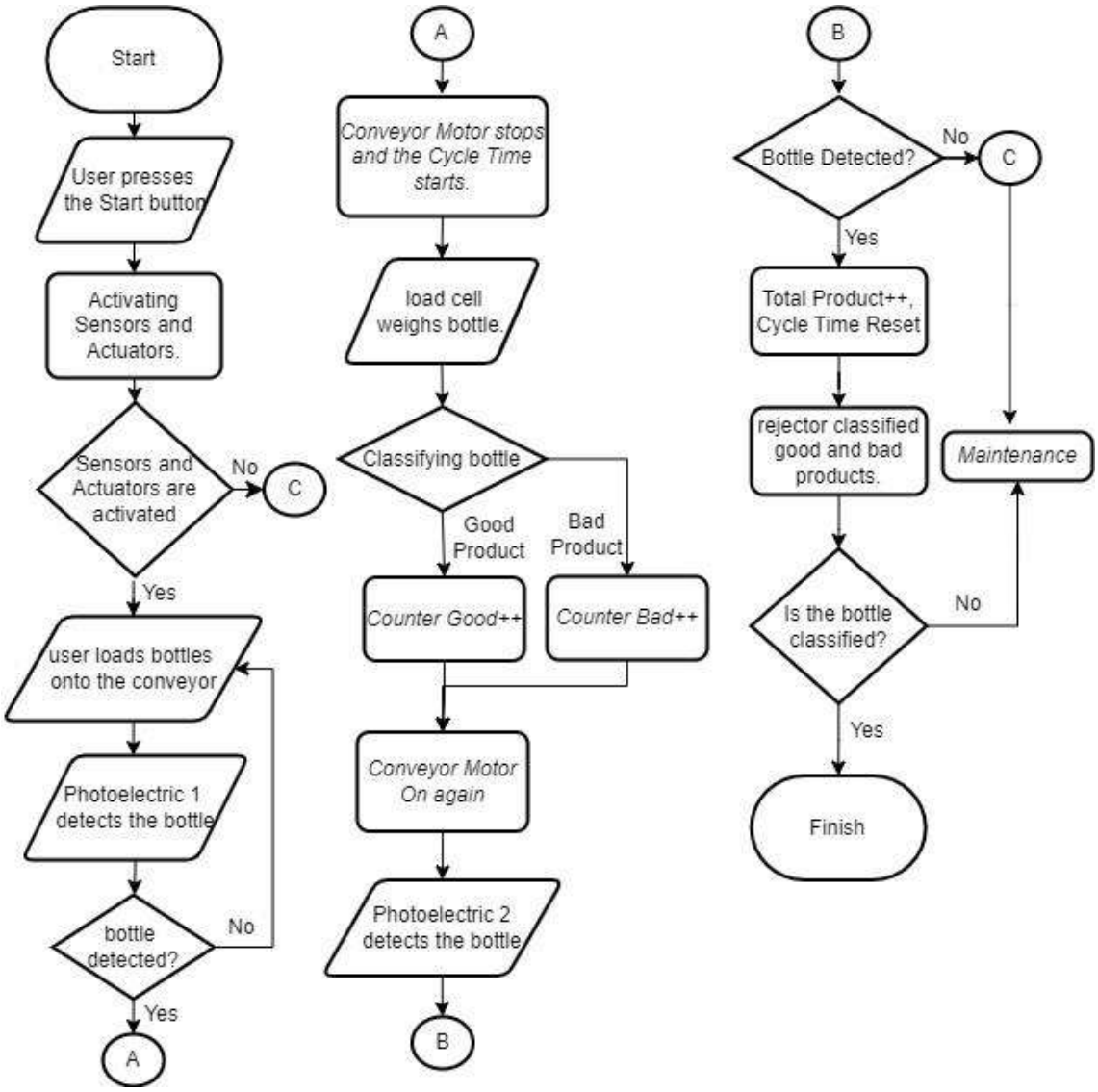

Figure 3. Workflow of the bottle sorting plant

2.4. Software Design

In this research, there are three main components of the software: API Service, ERP Odoo, and Grafana. The API service was developed using the VS Code as debugger and the Node.js programming language to acquire values from the Siemens PLC using the Profinet protocol. The acquired values are then sent to PostgreSQL as the database for ERP Odoo. In ERP Odoo, an analysis of the bottle production results is performed using the OEE method[12]. To enable monitoring, data from PostgreSQL is sent to Grafana for visualization using graphs, bar charts, and pie charts, displaying the three main OEE assessment indicators: Availability Ratio, Performance Rate, and Rate of Quality[13].

JURNAL ECTIPE
Electronic, Control, Telecommunication, Information, and Power Engineering
Volume 11, Issue 2, Oktober 2024, pp. 125-134
ISSN 2355-5068 ; e-ISSN 2622-4852
DOI: 10.33019/jurnalecotipe.v11i2.4491

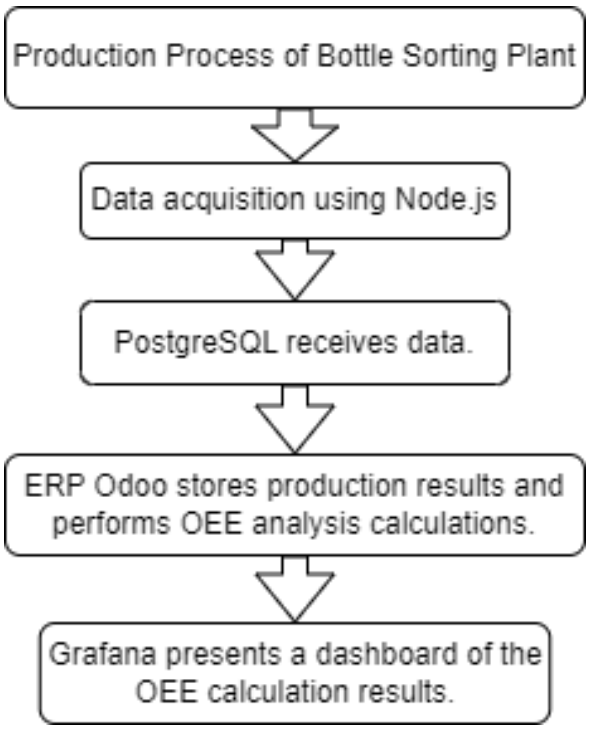

Figure 4. Use Case Software Process

3. RESULTS AND DISCUSSION

This chapter will discuss the results of the research and testing that has been conducted. The testing includes hardware, API Service, ERP Odoo and Grafana.

3.1. Hardware Testing

The hardware testing was carried out to assess the success of integrating the PLC, Arduino, and the bottle sorting plant. The Arduino was programmed to process reading the data from photoelectric and load cell sensors to detect incoming products and activate an actuators to dispose any defect items. The sensor data readings by Arduino was transmitted using relays through the digital inputs available on the PLC. The success of this integration was confirmed by the bottle status readings displayed on the HMI, as shown in Figure 5.

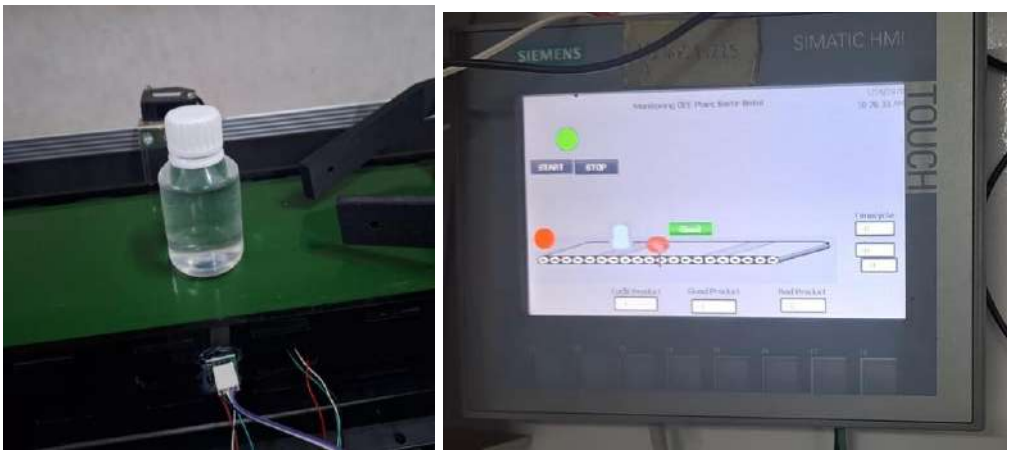

Figure 5. Integration of PLC, Arduino, and bottle sorting plant

In the bottle sorting plant, there are several sensors to support the acquisition of values needed for OEE analysis. The following table shows the relationship between components with their functions and purposes:

JURNAL ECOTIPE
Electronic, Control, Telecommunication, Information, and Power Engineering
Volume 11, Issue 2, Oktober 2024, pp. 125-134
ISSN 2355-5068 ; e-ISSN 2622-4852
DOI: 10.33019/jurnalecotipe.v11i2.4491

Table 2. Relationship between components and their functions

No.	Sensor	Pembacaan
1.	Photoelectric Sensor	Cycle time dan total produksi
2.	Loadcell Sensor	*Bad product* atau *good product*
3.	Button on HMI	Downtime

Once the contributions of each sensor has been established, the PLC address that will be used can be determined. A list of PLC addresses to will be used can be found in the following table:

Table 3. I/O List PLC Siemens

No.	PLC	Hardware	Address
1	DI 0	Sensor Photoelectric belakang	%I0.0
2	DI 1	Sensor Photoelectric depan	%I0.1
3	DI 2	Relay Good Product	%I0.2
4	DI 3	Relay Bad Product	%I0.3
5	DO 0	Motor Conveyor	%Q0.0
6	DO 1	Lampu ON	%Q0.1
7	DO 3	Lampu OFF	%Q0.3

Table 4. Memory List PLC Siemens

No.	Memory Address	Explanation
1.	%M0.5	Clock 1 Hz
2.	%M1.4	Stop
3.	%M1.7	Start

Table 5. Data Block Memory PLC Siemens

No.	Address	Explanation
1.	%DB1	Count Total Product
2.	%DB3	Count Bad Product
3.	%DB4	Count Good Product
4.	%DB12	Timer Get Quality
5.	%DB9	Timer Motor Conveyor Stop
6.	%DB5	Time Cycle Second
7.	%DB7	Time Cycle Minute

3.2. API Service Testing

The testing of the API Service software involves embedding the node.js logic into an executable (.exe) file. During the acquisition process, configuration of the PLC's IP Address, port, rack and slot used in the Profinet protocol is required. The .exe file will execute its logic by retrieving values from the PLC. Parameters that are read on the PLC including the actual output, good product, bad product, planned time, and downtime are used for OEE analysis. The acquired values will then be stored in a PostgreSQL database and processed through ERP Odoo. The following is display of the PLC data acquisition. In addition, it is necessary to configure the data transmission trigger, which can be based on time intervals or sent when only there is incoming data[14].

JURNAL ECOTIPE
Electronic, Control, Telecommunication, Information, and Power Engineering
Volume 11, Issue 2, Oktober 2024, pp. 125-134
ISSN 2355-5068 ; e-ISSN 2622-4852
DOI: 10.33019/jurnalecotipe.v11i2.4491

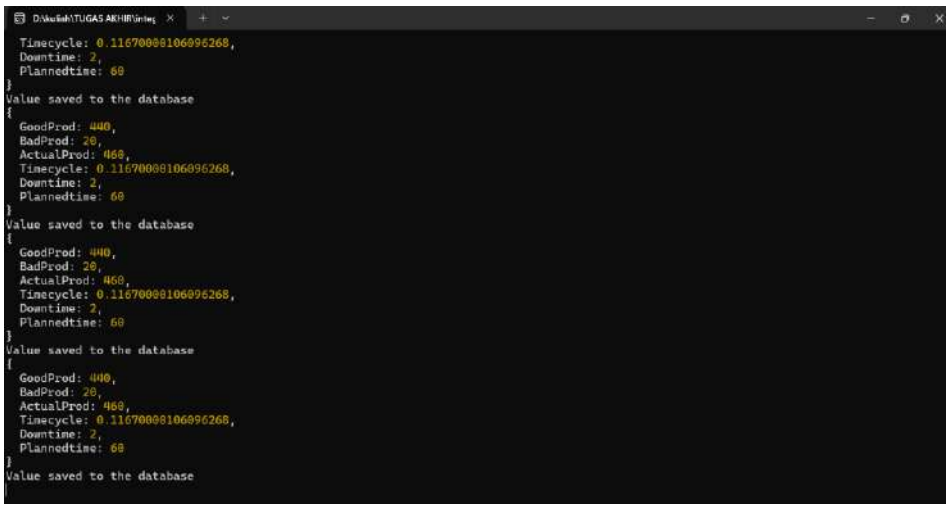

Figure 6. Value of Data Acquisition API Service using node.js

3.3 ERP Odoo Testing

The ERP Odoo, OEE analysis will be performed on the bottle sorting plant. The testing process is conducted by accessing the database utilized by Odoo itself, namely PostgreSQL. The data sent from the Siemens PLC will be obtained by the API Service. After that, the data will be stored in the database. Furthermore, it will be processed in the Odoo backend using the OEE calculation formula. This backend data will then be displayed in Grafana in the form of tables and charts.

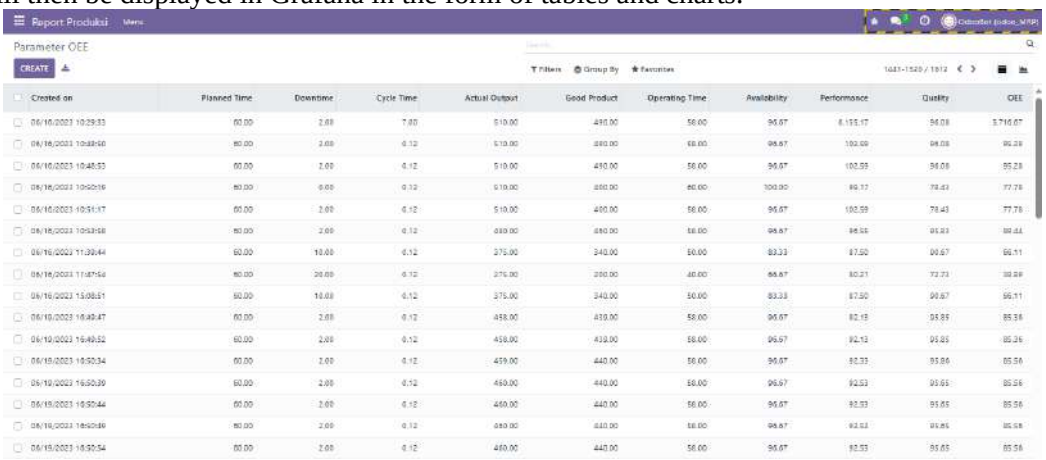

Figure 7. results of OEE analysis calculations

The image above shows the Odoo interface displaying real-time production data, including planned time, downtime, actual output, good product, and cycle time. Moreover, the results of the OEE analysis will be displayed, based on the data that has been received. These OEE data include Availability, Performance, Quality, and the total OEE.

3.4 Grafana Testing

In order to facilitate the process of monitoring the OEE analysis results, a dashboard is created as shown in the image. The dashboard displayed a gauge chart and a bar chart of the OEE calculation results, making it easier to monitor OEE based on real-time data and shift data.

JURNAL ECOTIPE
Electronic, Control, Telecommunication, Information, and Power Engineering
Volume 11, Issue 2, Oktober 2024, pp. 125-134
ISSN 2355-5068 ; e-ISSN 2622-4852
DOI: 10.33019/jurnalecotipe.v11i2.4491

Figure 8. OEE dashboard results on Grafana

3.5 Result of OEE analysis

Data collection from the bottle sorting plant is carried out every 1 hour, which represents data collection in the industry periodically every shift. The collected data from the plant includes the number of good products produced, the number of bad products, the downtime duration, the loading time, and the cycle time. Production results can be seen in the table 5[15].

Table 6. Production Outcome Data for OEE Calculation

No.	Data				
	Loading Time(Menit)	**Cycle Time(Menit)**	**Downtime(Menit)**	**Good Product**	**Actual Output**
1	60	0,116666667	2	440	460

Here are the manual calculation results of the production outcomes presented in Table 6

$$\text{Availability (\%)} = \frac{Operating\ Timw}{Loading\ Time} \text{ x } 100\ \%$$
$$= \frac{60-2}{60} \text{ x } 100\ \%$$
$$= 96{,}67\%$$

$$\text{Performance (\%)} = \frac{\text{Cycle Time x Actual Output}}{Operating\ Time} \text{ x } 100\ \%$$
$$= \frac{0{,}116666667 \text{ x } 460}{60-2} \text{ x } 100\ \%$$
$$= 92{,}53\ \%$$

$$\text{Quality (\%)} = \frac{\text{Good Product}}{Actual\ Output} \text{ x } 100\ \%$$
$$= \frac{440}{460} \text{ x } 100\ \%$$
$$= 95{,}65\ \%$$

Once the final results for the three OEE variables, Availability, Performance, and Quality, are known, the OEE value based on this data is:

OEE (%) = Availability x Performance x Quality
= 0,9667 x 0,9253 x 0,9565
= 0,8556
= 85,56 %

3.6 Comparison of Manual OEE Analysis ~~dan~~ and ERP Odoo

In order to demonstrate the successful integration of the system, a comparison is made between the OEE analysis results in the Odoo ERP, as shown in Figure 7 and the manual calculations performed. The results of this comparison are presented in Table 7.

Table 7. Comparison Results of Manual OEE with ERP Odoo

Volume 11, Issue 2, Oktober 2024, pp. 125-134
ISSN 2355-5068 ; e-ISSN 2622-4852
DOI: 10.33019/jurnalecotipe.v11i2.4491

No	OEE (Manual) (%)	OEE (ERP Odoo) (%)	Error (%)
1	85,56 %	85,56%	0%

The results of the comparison in Table 6 demonstrate that the overall OEE calculations in the Odoo ERP are accurate and function well. This is evidenced by the fact that the percentage error obtained from the overall OEE calculation comparison between the manual calculation and the system calculation is only 0%.

4. CONCLUSION

Based on the results of the testing conducted, it can be concluded that:

1. The integration system between IT (Information Technology) and OT (Operational Technology) is achieved through the development of a bottle sorting prototype controlled by a Siemens PLC using the Profinet protocol. The production results from this prototype are acquired by the API Service, sent to the ERP Odoo for OEE analysis, and displayed on the Grafana dashboard. Furthermore, the results of OEE can be displayed in the form of graphs and dashboards. The real-time data transmission from the PLC to ERP Odoo will facilitate improvements in efficiency and productivity, ensuring that production runs smoothly and product quality is maintained. To ascertain the efficacy of the API Service in acquiring data from the Siemens PLC and performing OEE analysis, a comparison was conducted with manual calculations. The absence of any discrepancy between the manual calculations and those performed by ERP Odoo, with a 0% error rate, indicates that the integration system between IT and OT has been successfully implemented.
2. Data acquisition from the PLC to the API Service is done by inputting the IP address and Port configuration of the PLC. Subsequently, it is necessary to configure the addresses from which data will be acquired and the PostgreSQL database configuration to which the data will be sent. In this study, the API Service successfully acquired data from the Siemens PLC using the Profinet protocol.

REFERENCES

[1] R. E. Wulansari, A. F. Khasanah, M. Djunaidi, J. T. Industri, F. Teknik, dan U. M. Surakarta, "Prosiding IENACO 2020 Teknik Industri UMS (18 Maret 2020) 185," hal. 185–193, 2020.

[2] Muhammad Naufal 'Izzudin, "Mesin Sag-Mill Menggunakan Support Vector Regression," 2023, [Daring]. Tersedia pada: https://repository.its.ac.id/104344/.

[3] N. Niland *et al.*, "Analisis Pengukuran Overall Equipment Effectiveness (OEE) dan Overall Labour Effectiveness (OLE) Sebagai Rekomendasi Untuk Peningkatan Produktivitas Fall Board," *Glob. Heal.*, vol. 167, no. 1, hal. 1–5, 2020, [Daring]. Tersedia pada: https://www.e-ir.info/2018/01/14/securitisation-theory-an-introduction/.

[4] F. N. Asita, M. K. Hasin, Z. Maulana, dan A. Putra, "Pengiriman Data Realtime PLC ke ERP Odoo dengan Dilengkapi Analisa OEE," vol. 15, no. x, hal. 1–13, 2023.

[5] Tri Baswara Ari Aji, Hamidillah Ajie, dan Murien Nugraheni, "Pengembangan Web Service Aplikasi Manajemen Aset Upt Tik Universitas Negeri Jakarta," *PINTER J. Pendidik. Tek. Inform. dan Komput.*, vol. 6, no. 2, hal. 69–75, 2022, doi: 10.21009/pinter.6.2.9.

[6] R. Riyandar, M. Wildan, A. Goeritno, dan J. Irawan, "Pengembangan Embedded Device Berbasis PLC untuk Simulator Rejection System dengan Penambahan Human Machine Interface," *J. RESTI (Rekayasa Sist. dan Teknol. Informasi)*, vol. 5, no. 6, hal. 1171–1181, 2021, doi: 10.29207/resti.v5i6.3641.

[7] R. T. Darmawan, "Implementasi Grafana untuk Auto-Scaling pada NGINX Web-Server di Lingkungan Docker Container," *Pengemb. Teknol. Inf. dan Ilmu Komput.*, vol. 7, no. 7, hal. 3163–3167, 2023.

Volume 11, Issue 2, Oktober 2024, pp. 125-134
ISSN 2355-5068 ; e-ISSN 2622-4852
DOI: 10.33019/jurnalecotipe.v11i2.4491

[8] L. Lukmandono, E. Sulistyowati, dan ..., "Pendekatan Overall Equipment Effectiveness Dan Response Surface Methodology Dengan Pertimbangan Root Cause Failure Analysis Untuk Meminimalkan Six Big …," *Katalog Buku Karya …*, hal. 70–112, 2020, [Daring]. Tersedia pada: http://ejurnal.itats.ac.id/buku/article/view/1439/0.

[9] M. H. A. Soliman, "Overall Equipment Effectiveness Simplified: Analyzing OEE to Find the Improvement Opportunities," no. September, 2020, doi: 10.5281/zenodo.4274026.

[10] M. Dipa, F. D. Lestari, M. Faisal, dan M. Fauzi, "Analisis Overall Equipment Effectiveness (Oee) Dan Six Big Losses Pada Mesin Washing Vial Di Pt. Xyz," *J. Bayesian J. Ilm. Stat. dan Ekon.*, vol. 2, no. 1, hal. 61–74, 2022, doi: 10.46306/bay.v2i1.29.

[11] M. Yusri, A. Maulana, A. Fitriati, dan M. Nur, "Rancang Bangun Sistem Sortir Ikan Berdasarkan Berat Berbasis Plc," *MAPLE Mechatronics J. Prof. Enterp.*, vol. 4, no. 2, hal. 48–53, 2022, [Daring]. Tersedia pada: https://jurnal.politeknikbosowa.ac.id.

[12] P. P. and N. C. S. Pichidtienthum, "Developing Module Generation for Odoo Using Concept of Low-Code Development Platform and Automation Systems," *Int. Conf. Ind. Eng. Appl.*, hal. 529–533, 2021.

[13] B. M. Ridwan, "Penerapan Enterprise Architecture Pada Perusahaan Manufaktur Baja di Era Industri 4.0," *JATISI (Jurnal Tek. Inform. dan Sist. Informasi)*, vol. 9, no. 3, hal. 2652–2663, 2022, doi: 10.35957/jatisi.v9i3.2000.

[14] I. V. Nițulescu dan A. Korodi, "Supervisory Control and Data Acquisition Approach in Node-RED: Application and Discussions," *Internet of Things*, vol. 1, no. 1, hal. 76–91, 2020, doi: 10.3390/iot1010005.

[15] E. K. Karmilawati, K. M. Mulyono, dan S. N. Nugroho, "Pendekatan OEE (Overall Equipment Effectiveness) Untuk Mengurangi Losses Pada Mesin Moulding Cerex," *J. Optimasi Tek. Ind.*, vol. 3, no. 2, hal. 46, 2021, doi: 10.30998/joti.v3i2.8576.

JURNAL ECOTIPE
Electronic, Control, Telecommunication, Information, and Power Engineering

Volume 11, Issue 2, October 2024, pp. 135-143
ISSN 2355-5068 ; e-ISSN 2622-4852
DOI: 10.33019/jurnalecotipe.v11i2.4499

Testing Smoker Detection Using Google Cloud Services and Infrastructure

Muhammad Mustajib[1], Sri Gunawan[2], Aldo Lovely Arief Suyoso[3], Hendro Margono[4], Muhammad Rafi Solakhudin[5]
[1,2,3,4]Universitas Airlangga, Surabaya 60115, Indonesia
[5]Politeknik Perkapalan Negeri Surabaya (PPNS), Surabaya, Indonesia

ARTICLE INFO

Article historys:

Received :…/…/…
Revised :…/…/…
Accepted :…/…/…

Keywords:

Cloud Computing, Deep Learning, Google Cloud Vision API, Image Processing, Smoker Detection

ABSTRACT

Smoking remains a significant public health challenge globally, contributing to a wide range of detrimental health outcomes, including cardiovascular diseases, cancer, and respiratory disorders. Despite concerted efforts to curb smoking rates through policy interventions, effective monitoring and enforcement remain complex and resource-intensive tasks for health authorities and organizations. Innovative approaches leveraging advanced technologies, such as visual detection systems powered by deep learning, offer promising solutions to enhance smoking behavior detection and monitoring. Integrating the Google Cloud Vision API enables real-time identification of smoking indicators and discrimination from complex visual backgrounds. This capability supports proactive health monitoring and strengthens the enforcement of public health policies aimed at reducing smoking prevalence. The research methodology utilizes a dataset of 600 images sourced from the Kaggle platform, encompassing diverse scenarios to optimize model training. Techniques such as image segmentation, feature extraction, and machine learning-based classification are employed to achieve high levels of precision and recall in identifying smokers and cigarette smoke. The model achieved a precision of 96% and a recall of 96%, indicating its high accuracy in identifying smokers. However, the study acknowledges challenges such as bandwidth constraints and security risks associated with handling sensitive health data. Nevertheless, technological innovations in visual detection systems and cloud services are pivotal in mitigating the health impacts of smoking and advancing public health initiatives.

Corresponding Author:

Muhammad Mustajib
Airlangga University, Surabaya 60115, Indonesia
Email: ajibmustajib14@gmail.com

1. INTRODUCTION

The presence of cigarettes has become a complex and controversial topic with significant impacts on public well-being. While smoking is legal, its effects extend beyond individual smokers. Cigarette smoke, whether in open spaces or enclosed environments like workplaces, restaurants, or public transportation, poses discomfort and health risks to those exposed. Long-term effects include increased risks of serious illnesses such as lung cancer, heart disease, and respiratory disorders.

Previous research has shown that technology offers promising solutions to address these health impacts. For example, a study by Kahendra explored factors affecting the implementation of smoke-free area policies and highlighted the need for effective monitoring systems to support these policies[1]. Another study by Gojali and Tjiong developed an application using the YOLOv3 algorithm to detect

Volume 10, Issue 2, October 2024, pp. 135-143
ISSN 2355-5068 ; e-ISSN 2622-4852
DOI: 10.33019/jurnalecotipe.v11i2.4499

smoking activities, demonstrating the potential of visual detection systems in identifying smokers and cigarette smoke in various settings[2].

In line with these findings, visual detection systems using cameras and image processing algorithms can swiftly and accurately identify smokers and cigarette smoke. These algorithms, powered by deep learning, enable cameras to recognize smoking behaviors and distinguish cigarette smoke from the visual background. Integrated with health monitoring systems or public alert mechanisms, such technology provides real-time, precise information on cigarette presence in public spaces, aiding in enforcing health policies related to smoking and mitigating associated health risks effectively.

For instance, Google Cloud leverages image processing technology for smoker detection. The Google Cloud Vision API detects text in images, which can be adapted to recognize smoker indicators. This enhances health monitoring by ensuring more accurate and efficient data management using Cloud Storage for data storage and Cloud Functions for automated monitoring processes. Google Cloud thus facilitates effective health monitoring through these integrated services[3].

In conclusion, technological innovations like visual detection systems and cloud services play a crucial role in combating the public health impacts of smoking. They provide advanced tools for monitoring and enforcing health regulations, ultimately contributing to a healthier environment for all.

2. RESEARCH METHOD

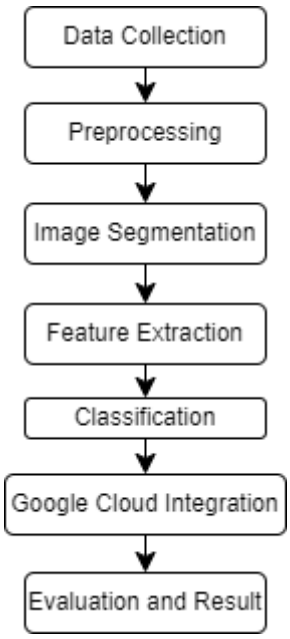

Figure 1. Thinking Framework Picture

Smoker detection using Google Cloud services and infrastructure involves a segmentation process to identify relevant areas of images, followed by feature extraction to distinguish the presence of smoking behavior. Classification algorithms use machine learning models to predict image classes as smoker or non-smoker. Services like AutoML Vision or Cloud Vision API accelerate this process by providing pre-trained classification algorithms or enabling custom model training. Integrating image processing methods with Google Cloud allows rapid and efficient processing of large-scale image data, supporting public health monitoring and innovative technological solutions for complex health issues[4].

2.1. Dataset

The dataset used consists of images downloaded from the Kaggle platform, specifically curated for image analysis and detection. It comprises a total of 600 images, with 250 training images depicting smokers and 250 non-smokers, along with 100 test images—50 each of smokers and non-smokers. The dataset includes diverse images of smokers, coughing individuals, people using inhalers, talking on the

JURNAL ECOTIPE
Electronic, Control, Telecommunication, Information, and Power Engineering
Volume 10, Issue 2, October 2024, pp. 135-143
ISSN 2355-5068 ; e-ISSN 2622-4852
DOI: 10.33019/jurnalecotipe.v11i2.4499

phone, and drinking. Researchers aimed to ensure diversity in both classes to enhance model training by inducing a certain level of class confusion. Varied conditions and positions in the images can bolster the analytical capabilities on Google Cloud.

According to Zha [5], the primary goal of this dataset is to develop and test a smoker detection model. The training data is utilized to train machine learning or artificial intelligence models, while the test data is used to evaluate the model's performance post-training. The dataset is split into 80% for training and 20% for testing. This dataset serves the purpose of developing and evaluating smoker detection models effectively. The following is an example of an image of a person smoking from Kaggle.

Figure 2. Smoker Images from Kaggle

2.2. Image Segmentation

The image segmentation process employs the K-means clustering algorithm, which divides an image into several segments based on color and texture similarities. This algorithm clusters pixels that share similar characteristics, forming homogeneous segments. To evaluate the quality of the segmentation, we use the Intersection over Union (IoU) metric, which measures the overlap between the predicted segmentation and the ground truth. Additionally, the Dice coefficient is used to assess the similarity between two samples, effectively evaluating the true positive rate of the segmentation.

2.3. Feature Extraction

During the feature extraction stage, techniques such as Scale-Invariant Feature Transform (SIFT) and Histogram of Oriented Gradients (HOG) are used to extract significant features from the segmented images. SIFT is employed to detect and describe local features in the images, while HOG identifies the orientation of gradients or edges within the images. This process also includes edge detection using the Canny method to identify significant edges, as well as texture analysis to evaluate texture patterns in the images. These techniques aim to identify unique characteristics that can distinguish between smokers and non-smokers.

2.4. Classification

Once the features are extracted, the next step involves classification using Support Vector Machine (SVM) and Neural Networks. SVM is utilized to find the optimal hyperplane that separates the smoker and non-smoker classes in the feature space, while neural networks provide a more complex and deep approach to data classification. The performance of the classification models is evaluated using various metrics, including accuracy, which measures the proportion of correctly classified instances out of the total instances. Precision evaluates the ratio of true positive predictions to the total positive predictions, recall measures the ratio of true positive predictions to the actual positive instances, and the F1 score, which is the harmonic mean of precision and recall, provides a single metric to evaluate the overall performance of the model.

2.5. Image Processing on Google Cloud

Image processing on Google Cloud involves uploading images to Google Cloud Storage, where they can be preprocessed for quality and format. The Cloud Vision API then analyzes these images, performing tasks like object detection, text extraction, and facial recognition. Advanced users can utilize machine learning tools such as AutoML Vision or custom TensorFlow models for specialized image

JURNAL ECTIPE
Electronic, Control, Telecommunication, Information, and Power Engineering
Volume 10, Issue 2, October 2024, pp. 135-143
ISSN 2355-5068 ; e-ISSN 2622-4852
DOI: 10.33019/jurnalecotipe.v11i2.4499

classification and analysis. Results can be integrated with other Google Cloud services for scalable and efficient data processing, making it a versatile platform for a wide range of image-related tasks from basic analysis to sophisticated machine learning applications[6][7].

2.6. Image Data Analysis Testing

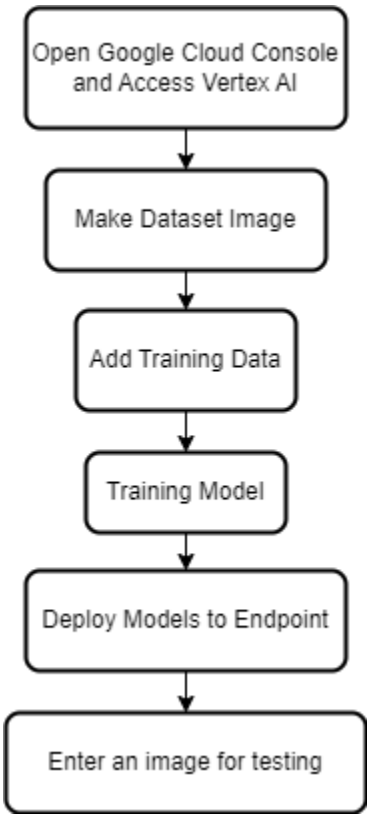

Figure 3. Workflow of the Smoker Detection

The technical explanation for using Google Cloud for image analysis to detect smokers begins with the initial step of open a web browser and navigate to the Google Cloud console at console.cloud.google.com then click on the search menu and type and select "Vertex AI".Creating a dataset begins by selecting the "Create a dataset" option at the bottom. Choose "Image" as the dataset type since the researcher is working with images. Next, provide a relevant name for the dataset. For image classification, select single label because the object being studied has only one label, which is smoking or non-smoking. After successfully creating the dataset, the next step is to access it by clicking on the name of the newly created dataset. Training data can then be added by clicking the "Select File" button. Researchers can upload relevant training images for the analysis project. Ensure to provide appropriate labels for each image so that the model can learn the correct class or category of each image. This process ensures that your dataset is ready for training an image classification model. After finishing adding training data to the dataset, the next step is to train the model. Click the "Start Training" button to initiate this process. Researchers will be given the option to either create a new model from scratch or use an existing one. Next, select the training configuration that suits your project needs, such as the algorithm to be used, hyperparameters, and allocation of computing resources. This process will train the model based on the prepared data, enabling researchers to produce a model ready for image classification. After the model training process is complete, the next step is to return to the model dashboard. Select the trained model by clicking on it, then click the "Deploy Model" option. Researchers will be directed to the configuration page to deploy the model. At this stage, researchers can specify endpoint configurations, including location, endpoint name, and the resources to be used. Once the configuration is set up, click the "Deploy" button to initiate the model deployment process. By following these steps, researchers will successfully deploy the model, making it accessible through the created

JURNAL ECOTIPE
Electronic, Control, Telecommunication, Information, and Power Engineering
Volume 10, Issue 2, October 2024, pp. 135-143
ISSN 2355-5068 ; e-ISSN 2622-4852
DOI: 10.33019/jurnalecotipe.v11i2.4499

endpoint. Final steps click "Upload Image" and upload the test image data to evaluate the model's accuracy. After that, the results will appear.

3. RESULTS AND DISCUSSION

This chapter will discuss the results of the research and testing that has been conducted. The Testing involves conducting Smoker Detection using Google Cloud Services and Infrastructure.

3.1. Impact of Cloud Computing on Image Processing

Cloud computing offers significant advantages for image processing tasks. Scalability allows users to adjust computing resources as needed, enhancing efficiency for intensive analyses. Cloud services provide robust infrastructure, significantly boosting image processing speeds. High availability ensures uninterrupted access, crucial for continuous or real-time image processing applications. Cloud computing facilitates seamless team collaboration and provides monitoring tools for efficient image processing workflows[8].

While cloud computing has revolutionized image processing, challenges exist. Bandwidth limitations can slow down data transfer between users and the cloud, potentially delaying overall processing. Security risks include data leakage or theft during image data transfer or storage in the cloud, despite providers offering multiple security layers[9]. Issues with cloud computing resource availability may disrupt image processing, impacting real-time applications [10].

3.2. Detailed Evaluation

All labels

Average precision	0.995
Precision	96%
Recall	96%
Created	Apr 2, 2024, 9:21:25 AM
Total images	500
Training images	400
Validation images	50
Test images	50

Figure 4. Detail Evaluation

Figure 4 shows a precision result of 96%, indicating that the majority of cases predicted as positive by the model are indeed positive. In the context of smoker detection, this high precision demonstrates the model's ability to accurately identify images containing smokers[11]. A recall of 96% indicates the model's capability to retrieve most of the actual smoker cases present in the dataset. The model tends to miss very few actual smoker cases. According to Lestari[12], high precision and recall rates suggest that the model performs well with minimal false positives and a low number of missed smoker cases.

JURNAL ECTIPE
Electronic, Control, Telecommunication, Information, and Power Engineering
Volume 10, Issue 2, October 2024, pp. 135-143
ISSN 2355-5068 ; e-ISSN 2622-4852
DOI: 10.33019/jurnalecotipe.v11i2.4499

3.3 Precision-recall Threshold

Figure 5. Precision-Recall and Threshold

Figure 5 displays the Precision-Recall (PR) curve, a useful visualization tool for evaluating classification model performance, particularly in scenarios where minority classes or positive cases are rare. The PR curve illustrates the relationship between precision and recall at various threshold values used by the model to classify instances. Precision measures the proportion of correctly predicted positives out of all predicted positives, while recall measures the proportion of correctly predicted positives out of all actual positive instances [13].A Precision-Recall Curve at 100% and a Precision-Recall Threshold also at 100% can refer to two distinct situations. A Precision-Recall Curve at 100% may indicate that the model achieves 100% precision across all observed recall ranges on the PR curve. This signifies that the model provides completely accurate positive predictions for all detected positive cases, without any false positive results. A Precision-Recall Threshold at 100% indicates that the threshold used by the model to classify instances as positive or negative has been set to 100%. The model will only make positive predictions if it is completely confident that the instance is truly positive. While this can result in high precision, it may also reduce recall as some actual positive cases might be missed[14]. Both a Precision-Recall Curve at 100% and a Precision-Recall Threshold at 100% indicate excellent model performance in classifying positive cases, with perfect precision.

3.4 Confusion matrix of label predictions

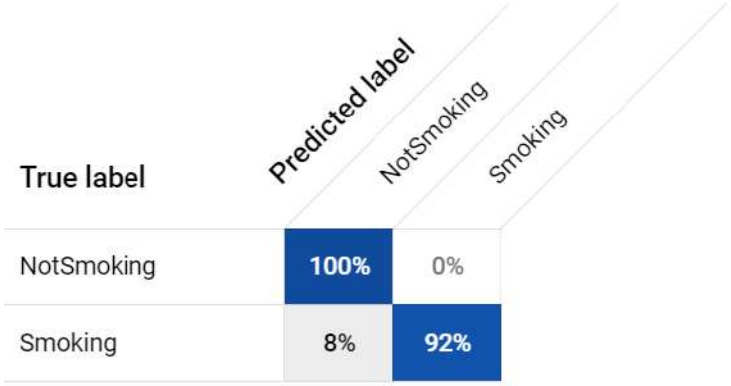

Figure 6. Confusion matrix of label predictions

Figure 6 illustrates a confusion matrix. In the first scenario, the model accurately predicts the "notsmoking" label with 100% precision. This means all predictions made by the model for "notsmoking" are correct. However, despite the high precision of 100% for "notsmoking" predictions, there is a small portion (8%) of cases that should have been "notsmoking" but were incorrectly predicted as "smoking". In the second scenario, the model does not make any predictions for the "smoking" label in cases that should be "notsmoking". This results in a 0% precision for "smoking" predictions in "notsmoking" cases. However, when the model predicts the "smoking" label in cases that are actually "smoking", it achieves a precision of 92%. This indicates that 92% of all "smoking" predictions are correct.Overall, these results show that the model performs well in identifying the "notsmoking" class with high precision but makes some errors in predicting "smoking" in cases that should be "notsmoking". On the other hand, the model has high precision in predicting "smoking" when the class occurs, while not making "smoking" predictions for cases that should be "notsmoking".

Volume 10, Issue 2, October 2024, pp. 135-143
ISSN 2355-5068 ; e-ISSN 2622-4852
DOI: 10.33019/jurnalecotipe.v11i2.4499

3.5 Confusion matrix calculates label predictions.

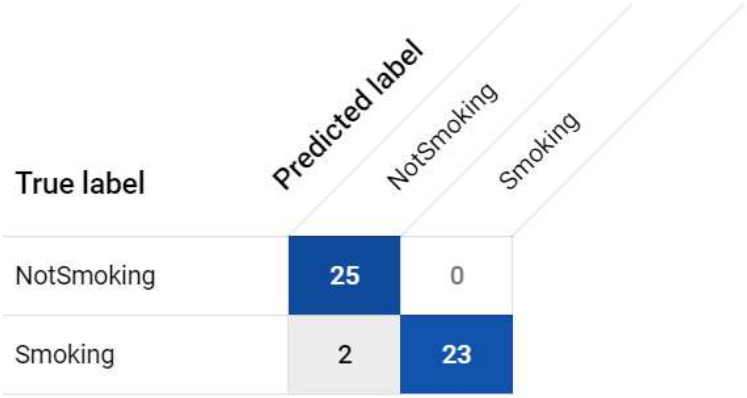

Figure 7. Confusion matrix calculates label predictions.

Figure 7 depicts the model predicting the "notsmoking" label, with 25 correct predictions. This means that most of the cases that should be "notsmoking" were correctly predicted as "notsmoking". However, despite the high precision of 100% for "notsmoking" predictions, there are 2 cases that were incorrectly predicted as "smoking" out of the total number of "notsmoking" predictions. In the second situation, the model does not make any "smoking" predictions for cases that should be "notsmoking", resulting in all "smoking" predictions in "notsmoking" cases being correct negatives. However, when the model predicts the "smoking" label, it correctly predicts 23 cases. Overall, the model demonstrates a high level of precision in predicting the "notsmoking" label, with 100% correct predictions. However, there are some errors in predicting "smoking" in cases that should be "notsmoking". On the other hand, the model does not make "smoking" predictions at all for cases that should be "notsmoking" and shows good precision in predicting "smoking" in cases that should be "smoking".

3.6 Accurate predictions of non-smokers and smokers in the test images

Figure 8. Correct Prediction of Non-Smokers

This figure demonstrates the machine learning model's capability to accurately identify non-smokers. The individuals shown are coughing, and the model successfully distinguishes this as a non-smoking activity. This accurate prediction showcases the model's effectiveness in differentiating between smoking and non-smoking actions based on subtle cues.

JURNAL ECTIPE
Electronic, Control, Telecommunication, Information, and Power Engineering
Volume 10, Issue 2, October 2024, pp. 135-143
ISSN 2355-5068 ; e-ISSN 2622-4852
DOI: 10.33019/jurnalecotipe.v11i2.4499

Figure 9. Correct Prediction of Smokers

Figure 9 illustrates the model's precision in identifying smokers. The individuals using cigarettes are correctly labeled as smokers. This accuracy highlights the model's ability to detect smoking activities, leveraging visual cues associated with cigarette usage to make correct predictions.

Figure 10. Incorrect Prediction Due to Mistaken Cues

Figure 10 presents an example of a misprediction by the model. The image contains mist that resembles cigarette smoke due to cold air, or a woman's hair that might be detected as cigarette smoke. These elements cause the model to incorrectly identify the situation as smoking, emphasizing the challenges in distinguishing between similar visual patterns.

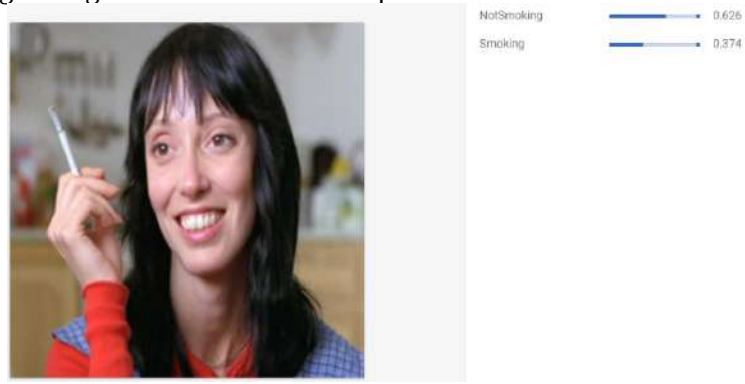

Figure 11. Incorrect Prediction Due to Unclear Cigarette Image

Figure 11 shows another instance of misprediction. The image contains an unclear object that resembles a cigarette, such as a pen, and lacks smoke. This ambiguity leads the model to fail in detecting the cigarette image accurately. This example highlights the limitations of the model when dealing with unclear or ambiguous visual inputs.

JURNAL ECOTIPE
Electronic, Control, Telecommunication, Information, and Power Engineering
Volume 10, Issue 2, October 2024, pp. 135-143
ISSN 2355-5068 ; e-ISSN 2622-4852
DOI: 10.33019/jurnalecotipe.v11i2.4499

4. CONCLUSION

Cloud computing offers significant advantages for image processing tasks. Scalability allows users to adjust computing resources as needed, enhancing efficiency for intensive analyses. Cloud services provide robust infrastructure, significantly boosting image processing speeds. High availability ensures uninterrupted access, crucial for continuous or real-time image processing applications. Cloud computing facilitates seamless team collaboration and provides monitoring tools for efficient image processing workflows[15].

While cloud computing has revolutionized image processing, challenges exist. Bandwidth limitations can slow down data transfer between users and the cloud, potentially delaying overall processing. Security risks include data leakage or theft during image data transfer or storage in the cloud, despite providers offering multiple security layers. Issues with cloud computing resource availability may disrupt image processing, impacting real-time applications.

REFERENCES

[1] Fariz Kahendra, Bagoes Widjanarko, dan Farid Agushybana, "Faktor-Faktor yang Mempengaruhi Implementasi Kebijakan Kawasan Tanpa Rokok : Literature Review," *Media Publ. Promosi Kesehat. Indones.*, vol. 6, no. 3, hal. 430–435, 2023, doi: 10.56338/mppki.v6i3.3284.

[2] M. I. Gojali dan E. L. Tjiong, "Pengembangan Aplikasi Deteksi Objek Rokok Dan Kegiatan Merokok Menggunakan Algoritma YOLOv3," *KALBISCIENTIA J. Sains dan Teknol.*, vol. 10, no. 02, hal. 201–208, 2023, doi: 10.53008/kalbiscientia.v10i02.3108.

[3] P. Baker dan L. Collins, "Creating and analysing a multimodal corpus of news texts with Google Cloud Vision's automatic image tagger," *Appl. Corpus Linguist.*, vol. 3, no. 1, hal. 100043, 2023, doi: 10.1016/j.acorp.2023.100043.

[4] J. Valentino dan Y. A. Susetyo, "Analisis Perbandingan Optical Character Recognition Google Vision dengan Microsoft Computer Vision pada Pembacaan KTP-el," *J. JTIK (Jurnal Teknol. Inf. dan Komunikasi)*, vol. 7, no. 4, hal. 552–561, 2023, doi: 10.35870/jtik.v7i4.1046.

[5] D. Zha, Z. P. Bhat, K. H. Lai, F. Yang, dan X. Hu, "Data-centric AI: Perspectives and Challenges," *2023 SIAM Int. Conf. Data Mining, SDM 2023*, hal. 945–948, 2023, doi: 10.1137/1.9781611977653.ch106.

[6] A. Ravikumar dan H. Sriraman, "Acceleration of image processing and computer vision algorithms," *Handb. Res. Comput. Vis. Image Process. Deep Learn. Era*, hal. 1–18, 2022, doi: 10.4018/978-1-7998-8892-5.ch001.

[7] A. Amrullah, A. Nugroho, dan Z. Ramadhan, "Perbandingan Kinerja Web Server Pada Penyedia Layanan Cloud Microsoft Azure Dan Amazon Web Services," *J. Inform. Teknol. dan Sains*, vol. 5, no. 1, hal. 92–97, 2023, doi: 10.51401/jinteks.v5i1.2487.

[8] M. I. P. Nasution, "TEKNIK PELESTARIAN PRIVASI DATA DI DATABASE CLOUD Raisida Salwa, Muhammad Irwan Padli Nasution Fakultas Ekonomi Dan Bisnis Islam Universitas Islam Negeri Sumatera Utara," vol. 3, no. 7, 2024.

[9] Ferryanto dan N. Chandra, "Analisis Ancaman Keamanan Data Dalam Cloud Computing," *JCOME (Journal Comput. Multimed. Enginering)*, vol. 1, hal. 1–5, 2023.

[10] B. R. Allo, N. Mardiana, O. Soleh, dan V. Lazinu, "Peran Teknologi Cloud Computing Dalam Transformasi Infrastruktur Ti Perusahaan: Studi Analisis Implementasi Di Industri Manufaktur," *J. Cahaya Mandalika*, vol. 18, hal. 1408–1414, 2018.

[11] F. R. Tarigan, R. Andrian, dan R. Safe'i, "Klasifikasi Skala Kerapatan dan Transparansi Tajuk Jenis Daun Jarum dengan VGG16," *MALCOM Indones. J. Mach. Learn. Comput. Sci.*, vol. 3, no. 2, hal. 253–263, 2023, doi: 10.57152/malcom.v3i2.940.

Volume 10, Issue 2, October 2024, pp. 135-143
ISSN 2355-5068 ; e-ISSN 2622-4852
DOI: 10.33019/jurnalecotipe.v11i2.4499

[12] F. Lestari, E. D. Putra, A. Sonita, dan Y. Darnita, "Human Object Counter Tracking Using Connected Component Labelling On Digital Image Processing," *J. Komputer, Inf. dan Teknol.*, vol. 3, no. 2, hal. 251–258, 2023, doi: 10.53697/jkomitek.v3i2.1218.

[13] R. F. Putra dan D. I. Mulyana, "Optimasi Deteksi Objek Dengan Segmentasi dan Data Augmentasi Pada Hewan Siput Beracun Menggunakan Algoritma You Only Look Once (YOLO)," *J. JTIK (Jurnal Teknol. Inf. dan Komunikasi)*, vol. 8, no. 1, hal. 93–103, 2024, doi: 10.35870/jtik.v8i1.1391.

[14] J. Alfred Daniel, C. Chandru Vignesh, B. A. Muthu, R. Senthil Kumar, C. B. Sivaparthipan, dan C. E. M. Marin, "Fully convolutional neural networks for LIDAR–camera fusion for pedestrian detection in autonomous vehicle," *Multimed. Tools Appl.*, vol. 82, no. 16, hal. 25107–25130, 2023, doi: 10.1007/s11042-023-14417-x.

[15] D. He dan S. Xiong, "Image Processing Design and Algorithm Research Based on Cloud Computing," *J. Sensors*, vol. 2021, 2021, doi: 10.1155/2021/9198884.

JURNAL ECOTIPE
Electronic, Control, Telecommunication, Information, and Power Engineering

Volume 11, Issue 2, October 2024, pp. 144-152
ISSN 2355-5068 ; e-ISSN 2622-4852
DOI: 10.33019/jurnalecotipe.v11i2.4495

Design Of LPG Leakage Detection Device Using MQ-2 Sensor Equipped with Hazard Warning System

Fadila Maiza[1], Suratun Nafisah[1], Khansa Salsabila Suhaimi[1],Ahmad Fahri Fahrezi[1]
[1]Department of Electrical Engineering, Faculty of Industrial Technology, Institut Teknologi Sumatera, Jl. Terusan Ryacudu, Way Huwi, Jati Agung, Lampung Selatan, 35365, Indonesia

ARTICLE INFO

Article historys:

Received : …/…/…
Revised : …/…/…
Accepted : …/…/…

Keywords:

Buzzer, Light Emitting Diode, Liquefied Petroleum Gas, MQ-2 Sensor

ABSTRACT

The use of liquefied petroleum gas (LPG) as household fuel in Indonesia has increased because it has greater heating power and equipment efficiency than other fuels. LPG is flammable and can explode if a leakage occurs and is exposed to a fire source. Therefore, explosions can be anticipated by installing a gas leakage detector equipped with a danger warning feature called Tor-G (LPG Detector) based on the NodeMCU ESP8266 microcontroller using an MQ-2 sensor with a buzzer and LED as a danger warning feature. Tor-G can detect when a gas leakage occurs and provides a danger signal in the form of a sound from a buzzer which can be heard several meters away by the homeowner so that an explosion can be anticipated quickly. This research carried out four tests: the sensor accuracy test, the sensor responsiveness test, the distance between the sensor and the leakage source test, and the responsiveness of the buzzer and LED test. The results of the tests show that the sensor only detects the LPG. The sensor readings are accurate since the value of Rs/Ro on the Tor-G is not much different from that of Rs/Ro on the datasheet, thus producing an error value in the 0% -0.08% range. The ideal installation position of the Tor-G is 75 cm from the gas cylinder and the danger warning system from the buzzer and red LED lights up within 18.88 seconds.

Corresponding Author:

Suratun Nafisah
Department of Electrical Engineering, Faculty of Industrial Technology, Institut Teknologi Sumatera, Jl. Terusan Ryacudu, Way Huwi, Jati Agung, Lampung Selatan, 35365, Indonesia
Email: suratun.nafisah@el.itera.ac.id

1. INTRODUCTION

In this progressive era, there is a shift from the use of conventional fuels to environmentally friendly fuels, one such environmentally friendly fuel is LPG (Liquefied Petroleum Gas) [1] [2]. LPG is a hydrocarbon gas consisting of propane and butane liquefied under pressure for easy storage [3]. Apart from being composed of these two main components, LPG gas also consists of small amounts of propylene and butylene, as well as the addition of a small amount of a pungent gas mixture such as Ethanethiol which serves to make it easier for the gas to be smelled when a gas leak occurs [4]. Several sizes of LPG circulating on the market, namely 3 kg, 5 kg and 12 kg, but 3 kg LPG is generally used in households. Based on data from the Ministry of Energy and Mineral Resources, the use of LPG as household fuel in Indonesia will reach 8.2 million tons in 2022 [5]. This is in line with the presentation by the Central Statistics Agency (BPS) regarding the comparison of household fuel use in 2021, which consists of LPG at around 82%, firewood at 11%, kerosene 2%, electric stove 0.7%, gas network/ biogas 0.5% and briquettes/charcoal 0.08% [6]. The increase in the use of LPG as a household fuel is due to greater heating power and equipment efficiency than other fuels. Using LPG as household fuel can also support the government program switching kerosene fuel to LPG.

Volume 10, Issue 2, October 2024, pp. 144-152
ISSN 2355-5068 ; e-ISSN 2622-4852
DOI: 10.33019/jurnalecotipe.v11i2.4495

While LPG has many advantages as a household fuel, it has disadvantages, including being flammable and having the potential to explode if leakage occurs and exposure to a fire source [7]. Explosions due to LPG leakages can happen when the gas level is between the Lower Explosion Threshold (ALB) and the Upper Explosion Threshold (ALA). This is because, in this situation, the levels of LPG and oxygen in the air are of balanced composition (between 1.95% and 8.95% in the air), which causes an explosion. If the leakage ed gas level is below the Lower Explosion Threshold (ALB), it is still safe and will not cause an explosion because, in this condition, the oxygen level is higher than the leakage ed gas level [8]. This also happens in ALA conditions because the leaked gas levels are higher than the oxygen levels in the air, so it does not cause an explosion but can cause health problems for users exposed to the leakage. Reporting from kompas.com, in the 2018-2022 period, there were 3,208 cases of fires in Indonesia involving household fires and 859 cases caused by LPG leakages. Data from the Bandar Lampung Regional Disaster Management Agency (BPBD) as of 2022 recorded 60 cases of fires due to LPG leakages [9]. The cause of LPG leakages in households are caused by several problems with the main components, such as hoses, regulators, stoves and gas cylinders, that do not meet the specified safety standards [10]. Apart from that, can identify other factors that could cause an explosion, namely negligence and the presence of inappropriate gas cylinders [11].

One effort that can be made to prevent and overcome gas leakage fires is by installing an LPG leakage detection device equipped with a danger warning when a gas leakage occurs [12] [13]. Therefore, the author developed and designed an LPG leakage detection tool based on the NodeMCU ESP8266 microcontroller using an MQ-2 sensor as a gas leakage level detector, a buzzer and an LED as a danger warning feature when the owner is at home.

2. COMPONENTS AND METHODS

The components used in the LPG leakage detection device are as follows:

a. MQ-2 Sensor

The MQ-2 sensor is used to detect gases such as LPG, carbon monoxide, and hydrogen in the air. This sensor can detect within a temperature range of -20°C to 50°C and can use a current of no more than 150 mA at 5 V [14]. The specifications of the MQ-2 sensor include pins for 5 V VCC, ground, digital output, and analogue output. The output from the MQ-2 sensor is a resistance value that must be converted into parts per million (ppm) units to be used as input for the microcontroller [15]. The MQ-2 sensor can detect not only LPG but also other gases and smoke. To accurately detect LPG without interference from other gases, the sensor needs to be calibrated.

b. NodeMCU ESP8266

The NodeMCU ESP8266 is an IoT-based component that is open source. This device uses the ESP8266 system on a chip, which can perform microcontroller functions and provide internet connectivity. NodeMCU refers to the firmware that can be used on the development kit. The advancement of NodeMCU technology allows for features like microcontroller access with Wi-Fi and a Universal Serial Bus (USB) to serial communication chip, simplifying the user experience without needing wiring techniques or USB to serial modules to download a program. This feature makes it possible to program the NodeMCU ESP8266 using a USB data cable, similar to a smartphone data or charging cable.

c. Adaptor

An adapter or power supply is an important component used in electronic devices that provides DC voltage for powering the device. The main function of the adapter is to control the voltage to prevent overheating and to convert Alternating Current (AC) electricity into Direct Current (DC).

d. Buzzer

JURNAL ECOTIPE
Electronic, Control, Telecommunication, Information, and Power Engineering
Volume 10, Issue 2, October 2024, pp. 144-152
ISSN 2355-5068 ; e-ISSN 2622-4852
DOI: 10.33019/jurnalecotipe.v11i2.4495

A buzzer is an electronic component that produces sound from electrical vibration changes. Its operating principle is that when a current flows, the coil acts as an electromagnet, attracting and repelling the diaphragm, causing air to vibrate and produce sound. Buzzers are often used as warning indicators when a device encounters an error.

e. LED

A light-emitting diode or LED is an electronic component that indicates the state of an electronic device through coloured light. LEDs have different characteristics based on the colour used. When a high current flows, the indicator light will shine very brightly. The current used in LEDs is around 10 mA-20 mA, and if the current exceeds this standard, the light may burn out. To prevent such issues, resistors are used to limit the current.

f. LCD

A liquid crystal display or LCD is an electronic component used to provide information or an indicator derived from a microcontroller.

The diagram block of the LPG leakage detection device using the MQ-2 sensor is shown in Figure 1. The MQ-2 sensor is used because it can detect LPG within a concentration range of 200 parts per million (ppm) to 10,000 ppm. Additionally, the microcontroller is utilized as an open-source program storage device. LPG leakage monitoring is performed by connecting the microcontroller to a Direct Current (DC) adapter powered by electricity. The data is then presented via a liquid crystal display (LCD), Light Emitting Diode (LED), and buzzer for close-range notification.

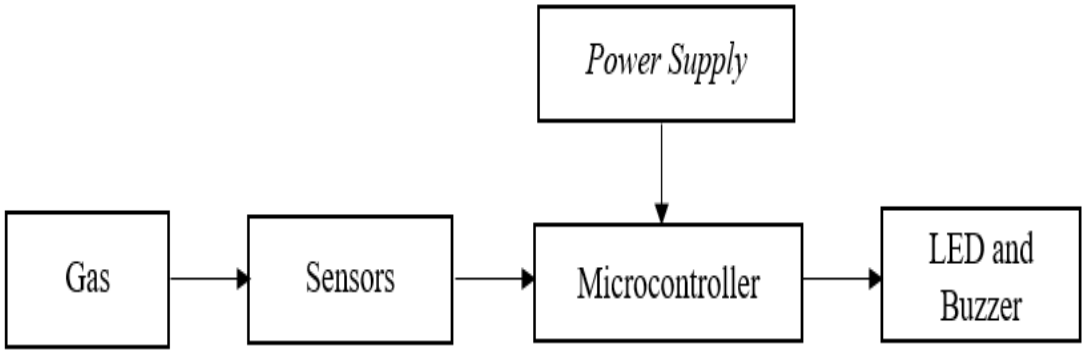

Figure 1. Diagram block of the LPG leakage detection device

The methodology for developing the LPG leakage detection device begins with the design of the electrical circuit and product layout. This initial stage involves creating a schematic diagram that includes all necessary components such as the MQ-2 sensor, NodeMCU ESP8266, buzzer, LED, LCD, and power supply. Additionally, a physical layout is planned to ensure efficient and functional placement of these components within the device.

Following the layout design, the focus shifts to software development. Using the Arduino IDE, the required software is coded to meet the system's functional requirements. This code enables the system to interface with the MQ-2 sensor for gas detection, process the data received, and appropriately trigger alarms or indicators through the buzzer, LED, and LCD. The software also facilitates communication with the NodeMCU ESP8266, allowing for data transmission and remote monitoring capabilities.

The final stage is the product assembly, where the designed circuit is physically assembled on a Printed Circuit Board (PCB). This involves soldering the components securely to ensure proper electrical connections and structural stability. After assembling the hardware, the developed software is

JURNAL ECTIPE
Electronic, Control, Telecommunication, Information, and Power Engineering
Volume 10, Issue 2, October 2024, pp. 144-152
ISSN 2355-5068 ; e-ISSN 2622-4852
DOI: 10.33019/jurnalecotipe.v11i2.4495

uploaded to the NodeMCU ESP8266, completing the process and ensuring that the device operates according to the intended design specifications.

3. RESULTS AND DISCUSSION

In its implementation, all components, including the MQ-2 sensor, buzzer, and LED, are connected to the microcontroller. The MQ-2 sensor is the component that interacts directly with the gas and serves as the input for the ESP8266. The input data is processed and then sent to the buzzer and LED, which act as the final outputs in this subsystem according to the conditions set on the ESP8266. The pin configuration for each component with the NodeMCU ESP8266 is provided in Table 1, and the implementation of these components is shown in Figure 2.

Table 1. Configuration of components pin with NodeMCU ESP8266 pin

Component	Pin on component	Pin on NodeMCU ESP8266	Implementation
MQ-2 Sensor	VCC Pin	15 (VCC) Pin	
	GND Pin	14 (GND) Pin	
	AO Pin	1 (A0) Pin	
Buzzer	VCC Pin	22 (D6) Pin	
	GND Pin	2 (GND) Pin	
Red LED	VCC Pin	21 (D7) Pin	
	GND Pin	14 (GND) Pin	
Green LED	VCC Pin	20 (D8) Pin	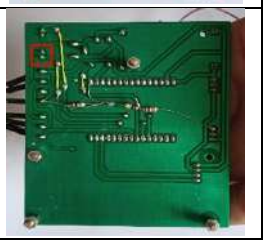
	GND Pin	14 (GND) Pin	

JURNAL ECTIPE
Electronic, Control, Telecommunication, Information, and Power Engineering
Volume 10, Issue 2, October 2024, pp. 144-152
ISSN 2355-5068 ; e-ISSN 2622-4852
DOI: 10.33019/jurnalecotipe.v11i2.4495

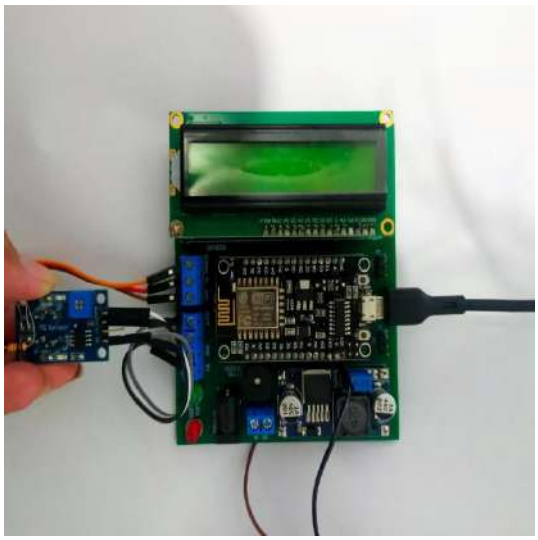

Figure 2. Implementation of components in the LPG leakage detection device

There are 4 tests in this project, namely sensor accuracy testing, testing the sensor's responsiveness, testing the sensor's distance to the source of the LPG leakage and testing the responsiveness of the buzzer and LED. Testing is carried out on the sensor to determine that the sensor, buzzer and LED are working according to the expected device design. Each test on the Tor-G sensing subsystem is explained in detail in the following sub-section.

3.1. Sensor Accuracy Testing

Sensor accuracy testing is carried out to determine the accuracy of sensor readings. To obtain accurate data from sensor readings regarding LPG levels, data on the ratio of the resistance of LPG levels to the reference resistance in the form of air (Rs/Ro) from the value on the sensor datasheet with sensor test data is carried out. This test was carried out in a room measuring 4 m × 4.5 m at room temperature. A comparison graph of the datasheet ratio with the test ratio can be seen in Figure 3.

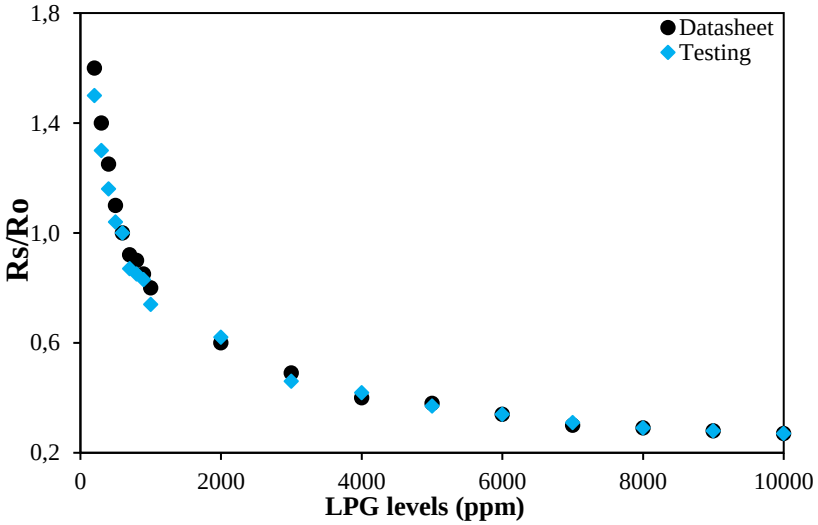

Figure 3. Graph Of Sensor Accuracy Testing Results

From testing the accuracy of the MQ-2 sensor which was carried out by comparing the ratio values from the tool readings with the ratio values on the sensor datasheet, data was obtained in the form of datasheet ratio values, test ratios and error values. The error value aims to see that the data read is accurate. The ratio value comparison is taken from 200 ppm to 10,000 ppm according to the detection range of the MQ-2 sensor for LPG. From the data that has been presented, it can be seen that the ratio value from the tool reading results is not much different from the ratio value on the sensor datasheet, resulting in an error value in the range of 0% -0.08%. The resulting error value shows that the tool

JURNAL ECOTIPE
Electronic, Control, Telecommunication, Information, and Power Engineering
Volume 10, Issue 2, October 2024, pp. 144-152
ISSN 2355-5068 ; e-ISSN 2622-4852
DOI: 10.33019/jurnalecotipe.v11i2.4495

reading for LPG is accurate because the resulting error value does not exceed the error tolerance value of 10%.

3.2 Sensor Responsiveness Testing

Sensor responsiveness testing is carried out to determine the relationship between the level of leakage gas and the sensor readings. Apart from that, this test also determines how quickly the sensor responds in detecting LPG leakages. The test was carried out using LPG installed with a high-pressure regulator as a source of gas leakages. There are 3 variations of lever rotation data as the leakage level used in this test, namely at rotation positions 1, 2 and 4. The distance between the leakage source and the tool is 30 cm, and it is carried out in a room measuring 4 m × 4.5 m at room temperature. This test was carried out 5 times each at each rotation point. The following data from the MQ-2 sensor responsiveness testing results can be seen in Figure 3.

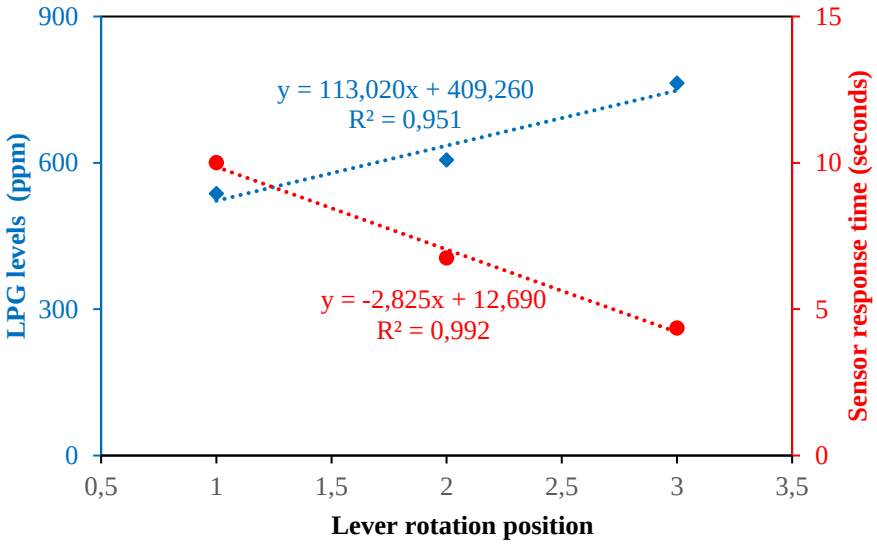

Figure 4. Graph Of Sensor Responsiveness Testing Results

From the graphic analysis, it can be concluded that the amount of gas detected by the sensor is directly proportional to the amount of rotation of the head on the regulator. This can happen because the more significant the rotation of the regulator on the gas cylinder, the greater the pressure received by the gas cylinder so the greater the level of gas that comes out. The greater the level of gas that comes out, the faster the sensor can detect a leakage. This can be seen in Figure 3, there is a relationship between the rotation of the regulator head and the detected gas level and the time measured is directly proportional. Apart from that, in this test, it can be seen that the test result data for gas levels is linear for each rotation of the regulator head.

3.3 Testing Sensor Distance from LPG Leakage Source

Testing the distance of the sensor from the source of the LPG leakage is a test carried out to determine the proportional position of the device. Apart from that, this test also determines how far the sensor can detect LPG leakages. The test was carried out using LPG installed with a high-pressure regulator as a source of gas leakages. There are 4 distances used in this test, namely at 25 cm, 50 cm, 75 cm and 100 cm. This test was carried out and carried out in a room measuring 4 meters by 4.5 meters at room temperature. This test was carried out 5 times each at each distance variation. The following graph shows the relationship between changes in the rotation of the regulator lever with rate and time, which can be seen in Figure 4.

JURNAL ECTIPE
Electronic, Control, Telecommunication, Information, and Power Engineering
Volume 10, Issue 2, October 2024, pp. 144-152
ISSN 2355-5068 ; e-ISSN 2622-4852
DOI: 10.33019/jurnalecotipe.v11i2.4495

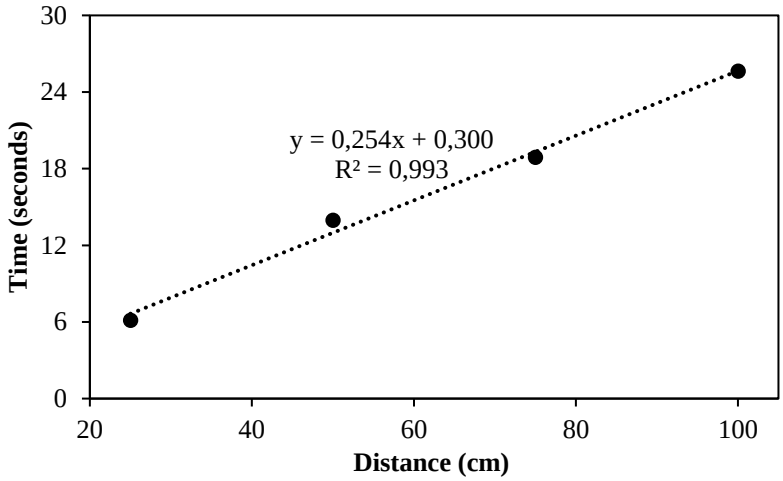

Figure 5. Graph Of Sensor Distance from LPG Leakage Source Testing Result

Test data on the distance between the sensor and the source of the LPG leakage can be seen in Figure 4. The test was carried out at four different distances (25 cm, 50 cm, 75 cm and 100 cm), each with five tests. The graph shows that the relationship between sensor distance and gas levels and response time decreases the detected gas levels as the distance increases. In addition, the sensor response time also increases with distance. This shows that distance dramatically influences the performance of the MQ-2 sensor in detecting gas levels, where the sensor is more responsive at closer distances. Distance has a significant influence on the performance of the MQ-2 sensor. The sensor detects higher gas levels at closer distances and responds more quickly. Conversely, the detected gas levels are lower at longer distances, and the response time is longer. This must be considered when setting the sensor distance, which requires accurate and fast gas detection.

3.4 Buzzer and LED Responsiveness Testing

Testing the responsiveness of the buzzer and LED is carried out by bringing the gas cylinder with the high-pressure regulator installed close to the rotation position at point 1 at a distance of 75 cm. Distance selection in this test is done by finding the median value of the time data obtained in the previous distance test. This is done after knowing the proportional distance from the installation of the tool to the source of the leakage. The following data from the buzzer and LED responsiveness testing results can be seen in Table 1.

Table 2. Data From Buzzer and LED Responsiveness Testing Results

Testing To-	Distance (cm)	Rate (ppm)	LED response	Buzzer Response	Time (seconds)
1	75	593,10	The red LED is on	On	18,47
2		555,40	The red LED is on	On	19,50
3		585,30	The red LED is on	On	18,52
4		548,00	The red LED is on	On	18,67
5		570,10	The red LED is on	On	18,98
Average		**570,38**	The red LED is on	On	**18,88**

Testing the responsiveness of the buzzer and LED is carried out by providing a gas leakage with a high-pressure regulator installed in the rotation position at point 1 at a distance of 75 cm. The selection of this distance is based on the value of the time data obtained in the previous distance test, which aims to determine the proportional distance from the installation of the device to the source of the gas leakage. An average gas content value of 570.38 ppm indicates that the MQ-2 sensor is quite sensitive in detecting gas levels at this distance. The red LED and buzzer that light up on each trial suggest that the sensor can

Volume 10, Issue 2, October 2024, pp. 144-152
ISSN 2355-5068 ; e-ISSN 2622-4852
DOI: 10.33019/jurnalecotipe.v11i2.4495

detect gas levels in the alert condition to trigger an alarm, and consistency in this response indicates that the warning system is working correctly. The average response time of 18.88 seconds means the sensor takes approximately 19 seconds to detect gas levels and activate the warning device. From the results of the data analysis in Table 4.1, it can be concluded that the MQ-2 sensor at a distance of 75 cm has good capabilities in detecting gas levels and providing a warning response via a red LED and buzzer. The detected gas levels were pretty consistent, and the warning device functioned well whenever the alert condition was reached.

4. CONCLUSION

LPG leakage detection device using the MQ-2 sensor equipped with a danger warning system or Tor-G can detect LPG leakages in 3 levels of conditions, namely safe conditions for leakage levels of 200 ppm-500 ppm, alert conditions at levels above 500 ppm - 1000 ppm and dangerous conditions for levels above 1000 ppm. From the tests related to sensor accuracy that have been carried out, data for safe conditions was obtained, and the error value from the comparison of the ratio values on the datasheet with the test data was 0.26%. In alert conditions, the error value is 0.21%; in dangerous conditions, the error value is 0.02%. From the three errors data, it can be concluded that the sensor readings in detecting LPG are accurate because the error value does not exceed the error tolerance limit. These three conditions have preventive measures to prevent explosions due to LPG leakages. Tor-G is equipped with an early warning system in the form of a sound from a buzzer and a red LED, which will be active when the system detects leakageing gas levels above 500 ppm-1000 ppm or in standby condition. From tests carried out on the buzzer and LED responses, which were carried out 5 times, it was found that both warning systems succeeded in providing information in the form of sound and visual signals within 18.88 seconds so that users at home could take preventive action in the form of opening windows as air ventilation. Even though an LPG leakage detection device using the MQ-2 sensor shows accurate results, ensuring reliable detection at lower concentrations of LPG could involve integrating additional sensors or developing advanced algorithms for data processing. Additionally, investigating the use of alternative power sources, such as solar power, could enhance the device's sustainability and make it more versatile and valuable for broader applications in residential, industrial, or commercial settings.

ACKNOWLEDGEMENTS

This work is fully funded by the Institut Teknologi Sumatera (Itera), Republic of Indonesia, through the “Penelitian Mahasiswa” research scheme. The authors would like to thank the Faculty of Industrial Technology, Itera, for assistance in the publication of this work in the national journal.

REFERENCES

[1] G. T. Hashem and M. Al-Dawidy, "Use of LPG in SI Engine- A Review Study," *Al-Qadisyah Journal For Engineering Sciences*, vol. XIV, no. 1, pp. 51-58, 2021.

[2] J. P. Nshimiyiman, M. C. Mukeshimana and E. Nshimyimana, "Tracking The Progress Towards Adopting LPG As A Clean Cooking Fuel In Rwanda: User's Perspective," *Energy For Sustainable Development*, vol. 80, no. 1, pp. 101-141, 2024.

[3] E. Fatkhiyah, D. Persada and D. Andayati, "Early Detection of Leaks on Gas Cylinders Using Arduino Based MQ-6 Sensors," IOP Publishing, Bandung, 2019.

[4] V. Valencia, L. P. Purnama, C. Tjong and J. Liman, "Rancang Bangun Alat Pendeteksi Kebocoran Gas LPG Berbasis Internet of Things Dengan Katup Regulator Otomatis," *Jurnal Ilmiah Elektronika*, vol. XXI, no. 2, pp. 225-242, 2022.

[5] Kementrian ESDM, "Statistik Minyak dan Gas Bumi," Kementrian ESDM, Jakarta, 2022.

[6] Badan Pusat Statistik, "Distribusi Persentase Rumah Tangga dan Bahan Bakar Utama untuk Memasak," Badan Pusat Statisktik, Jakarta, 2022.

Volume 10, Issue 2, October 2024, pp. 144-152
ISSN 2355-5068 ; e-ISSN 2622-4852
DOI: 10.33019/jurnalecotipe.v11i2.4495

[7] M. H. Beheshti, S. F. Deghan, R. Hajizadeh, S. M. Jafari and A. K. paei, "Modelling the Consequences of Explosion, Fire and Gas Leakage in Domestic Cylinders Containing LPG," *Annls of Medical and Health Sciences Research,* vol. VIII, no. 1, pp. 83-88, 2019.

[8] F. Shaik, "An Experimental Investigationand Analysis of Proposed Gas Leakage System," *Helix,* vol. XI, no. 1, pp. 23-30, 2021.

[9] L. Huda, "Ada 8.004 Kebakaran Terjadi Sepanjang 2018-2022," Kompas, Jakarta, 2022.

[10] M. R. A. Rassyid, K. B. Adam and M. Ramdhani, "LPG Gas Leak Detection Based Interner of Things," *e-Proceeding of Engineering,* vol. VII, no. 3, pp. 1-8, 2020.

[11] M. S. Sonwani, N. Ateriya, A. Kumar and A. Kohli, "Two deaths due to explosion of cylinders of Liquid Petroleum Gas," *Egyptian Journal of Forensic Sciences,* vol. XI, no. 6, pp. 1-5, 2021.

[12] M. M. Khan, "Sensor-Based Gas Leakage Detector System," *Engineering Poceedings,* vol. 28, no. 2, pp. 1-6, 2020.

[13] B. Jena, S. K. Pradhan, R. Jha, S. Goel and R. Sharma, "LPG Gas Leakage Detection System Using IoT," *Poceedings,* vol. 74, no. 4, pp. 795-800, 2023.

[14] B. Rahman, F. Pernando and N. Indriawan, "Sistem Monitoring Kebocoran Gas dan Api Menggunakan Sensor MQ-2 dan Flame Sensor Berbasis Android," *Journal Sensi*, vol. VIII, no. 2, pp. 209-222, 2022.

[15] B. Kommey, D. Opoku, J. Lartey, K. Kumah and M. Tantuo, "A Simple, Low-cost, Efficent and Smart Consumer Gas Leakage Detection System," *International Journal of Informatics Information System and Computer Engineering,* vol. III, no. 1, pp. 105-123, 2022.

JURNAL ECOTIPE
Electronic, Control, Telecommunication, Information, and Power Engineering

Volume 11, Issue 2, October 2024, pp. 153-158
ISSN 2355-5068 ; e-ISSN 2622-4852
DOI: 10.33019/jurnalecotipe.v11i2.4496

Design and Implementation of LPG Leakage Detection System using IoT-based Regulator Lever Automation on a Household Scale

Lusiana Sinaga, Suratun Nafisah, Khansa Salsabila Suhaimi, and Muhammad Akmal Shani
Department of Electrical Engineering, Faculty of Industrial Technology, Institut Teknologi Sumatera, Jl. Terusan Ryacudu, Way Huwi, Jati Agung, Lampung Selatan, 35365, Indonesia

ARTICLE INFO

Article history:

Received : …/…/…
Revised : …/…/…
Accepted : …/…/…

Keywords:

LPG Leakage, Servo motor, NodeMCU ESP8266, PWM

ABSTRACT

Liquefied Petroleum (LPG) is very common in daily cooking activities. Therefore, preventive measures must be taken to reduce the risk of fire and explosion due to LPG leakages. One action that can be taken is to install a regulator lever that can open automatically when a leakage is detected. In this research, Pulse Width Modulation (PWM) is used to control the rotational speed of the servo motor on the regulator lever, which aims to implement an automatic control system that is responsive when an LPG leakage is detected. Using servo motor control to automatically open the regulator lever can reduce the impact of accidents or losses due to LPG leakages. The test results show that the regulator lever can be opened effectively with a pulse value of 0.55 ms at a rotation angle of 0° in 0 seconds, while it can be closed with a pulse value of 2.45 ms at an angle rotation of 180° in 1.66 seconds. This shows that the regulator responds appropriately to the level of danger detected and is precise in adjusting position. The use of PWM on servo motors in the regulator control system has proven effective in increasing responsiveness to LPG leakages, as seen from the fast response (0 to 1.66 seconds) and accuracy (100% success percentage for 15 trials). This shows that using PWM can respond to emergencies quickly and precisely.

Corresponding Author:

Suratun Nafisah
Departemen of Electrical Engineering, Faculty of Industrial Technology, Institut Teknologi Sumatera, Jl. Terusan Ryacudu, Way Huwi, Jati Agung, Lampung Selatan, 35365, Indonesia
Email: suratun.nafisah@el.itera.ac.id

1. INTRODUCTION

With the continued development of technology, information and industry, Indonesia's energy needs are increasingly becoming important in people's daily lives. The role of natural resources, especially fossil energy such as petroleum, in people's livelihoods shows that availability is increasingly limited [1]. Therefore, reducing dependence on fossil energy is necessary by switching to more sustainable natural resources such as natural gas [2]. Since 2007, the Indonesian government has implemented a kerosene to Liquefied Petroleum Gas (LPG) conversion program to convert subsidised kerosene users, especially those from economically disadvantaged groups, into LPG users as part of energy transformation efforts [3].

LPG is a hydrocarbon gas produced from oil refineries and gas refineries [4]. The main components are Propane and Butane gas, packaged in tubes [5]. LPG has a variety of applications, with its primary use as a cooking fuel[6]. Apart from that, LPG is also used as fuel in the food, glass, and ceramics industries and as fuel for forklifts [7]. LPG is flammable and can explode when a leakage occurs and is exposed to a fire source [8]. In the initial phase of converting to LPG, new users must adapt to cooking

JURNAL ECOTIPE
Electronic, Control, Telecommunication, Information, and Power Engineering
Volume 11, Issue 2, October 2024, pp. 153-158
ISSN 2355-5068 ; e-ISSN 2622-4852
DOI: 10.33019/jurnalecotipe.v11i2.4496

devices such as stoves, hoses and regulators [9]. Data from the National Consumer Protection Agency recorded incidents of LPG explosion accidents in 2007, 2008 and 2009 as 5, 27 and 30. Until 2017, reports of LPG-related accidents still occur frequently, highlighting the urgency of attention to the safety of LPG use [10].

To reduce the risk of accidents that LPG leakages can cause, the increasing use of LPG as an energy source in households creates a need to improve security and leakage detection systems [11]. The safety aspect of LPG is essential, considering the potential risks that could arise from gas leakages [12]. Therefore, the existence of an LPG Detector (Tor-G) is a very relevant and essential step in efforts to design and implement an LPG leakage detection system with the Internet of Things (IoT)-based regulator lever automation on a household scale [13].

2. RESEARCH METHOD

This research was conducted to evaluate the performance of servo motors in opening and closing the regulator lever with a focus on operational reliability. Meanwhile, assessing the speed of servo motor response to LPG leakage detection is designed to measure the system's effectiveness in responding to emergencies [14]. This research focuses on the Regulator Automation subsystem. The methodological flow diagram of this research can be seen in Figure 1.

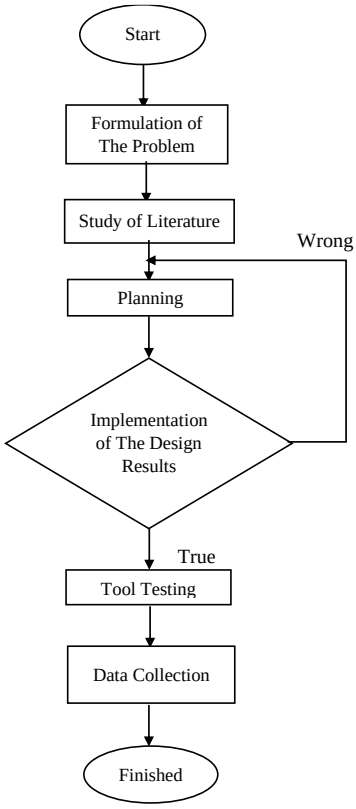

Figure 1. Flowchart of Research Methodology

This research began by formulating problems related to the regulator automation subsystem. After developing the problem, the author conducted a literature study to gain an in-depth understanding of the problem to be solved. Determining the literature study involves several stages until finalisation, including specification of tool requirements, design, implementation and testing.

The determination of tool specifications is based on the results of literature studies and is the focus of the Final Project research on the regulator automation subsystem. After obtaining the specifications for tool requirements, the author carried out a design, which was then implemented and tested. If the test is inappropriate, the author returns to the design stage. On the other hand, if the tools are suitable, the author continues his research.

JURNAL ECOTIPE
Electronic, Control, Telecommunication, Information, and Power Engineering
Volume 11, Issue 2, October 2024, pp. 153-158
ISSN 2355-5068 ; e-ISSN 2622-4852
DOI: 10.33019/jurnalecotipe.v11i2.4496

2.1. Regulator Automation Testing Methods

Next are the steps taken in regulator automation testing:

1. Make sure the NodeMCU ESP8266 is connected to the internet according to the initialisation in the source code and verify the success of sending gas sensor data. Ensure the gas sensor data is successfully detected and the servo motor automatically opens and closes the regulator lever according to the desired command.
2. Prepare a program on the Arduino IDE to set the servo motor angle and a protractor to compare the set angle with the measured angle.
3. Make sure the program on the NodeMCU ESP8266 can send PWM signals with a duty cycle and carry out tests by varying the duty cycle.

3. RESULTS AND DISCUSSION

The following are the results of tests carried out for regulator automation. Table 1 shows the regulator's response to LPG levels detected by the MQ-2 sensor. This table includes various gas concentrations in units (ppm), conditions and regulator responses, with each condition being taken 5 times [15].

Table 1. Regulatory response

Gas concentration (ppm)	Condition	Regulator response
6,61	Safe	Closed
12,94	Safe	Closed
74,71	Safe	Closed
88,89	Safe	Closed
93,97	Safe	Closed
678,70	Standby	Closed
688,10	Standby	Closed
697,60	Standby	Closed
748,00	Standby	Closed
758,70	Standby	Closed
1019,00	Danger	Open
1119,00	Danger	Open
1155,00	Danger	Open
1232,00	Danger	Open
2314,00	Danger	Open

Angular responsiveness testing is carried out to assess the servo motor's ability to rotate according to the desired angle. This test involves comparing the angle set on the servo motor and the angle measured using a protractor. This test was performed 9 times at various angles, as in Table 2.

Table 2. Angular responsiveness results

Set the Angle on the servo motor (°)	The angle on a protractor (°)
0	0
30	30
45	45
60	60
90	90
120	120
135	135

JURNAL ECOTIPE
Electronic, Control, Telecommunication, Information, and Power Engineering
Volume 11, Issue 2, October 2024, pp. 153-158
ISSN 2355-5068 ; e-ISSN 2622-4852
DOI: 10.33019/jurnalecotipe.v11i2.4496

Set the Angle on the servo motor (°)	The angle on a protractor (°)
150	150
180	180

The data results above showed that each experimental angle matched the angle set on the servo motor and the angle measured using a protractor. This data will then be processed using Microsoft Excel to produce a graph showing the relationship between the servo motor angle and the protractor angle, as shown in Figure 2.

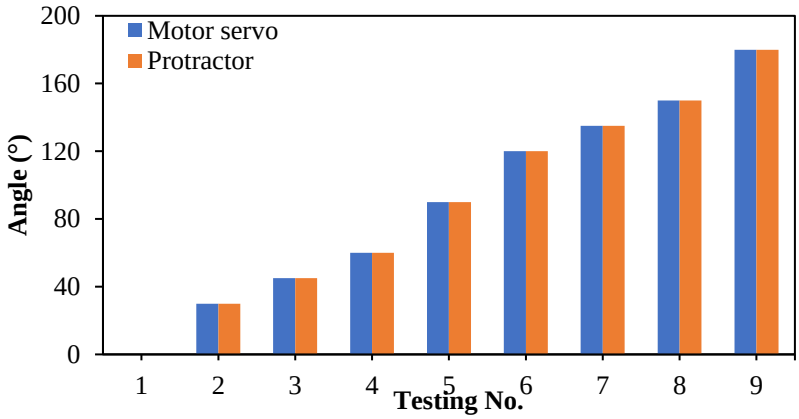

Figure 2. Servo angle responsiveness graph

This test is carried out by varying the pulse value from 0.55 milliseconds to 2.45 milliseconds to determine the shape of the pulse and the speed at which the servo motor moves according to the desired angle.

Table 3. Time responsiveness results

Pulse (ms)	Pulse Form (%)	The angle on the servo motor (°)	Time (s)
0,55		0	0,00
0,80		30	1,23
1,05		45	1,26
1,25		60	1,27
1,50		90	1,32
1,75		120	1,36

JURNAL ECTIPE
Electronic, Control, Telecommunication, Information, and Power Engineering
Volume 11, Issue 2, October 2024, pp. 153-158
ISSN 2355-5068 ; e-ISSN 2622-4852
DOI: 10.33019/jurnalecotipe.v11i2.4496

Pulse (ms)	Pulse Form (%)	The angle on the servo motor (°)	Time (s)
1,95		135	1,39
2,20		150	1,49
2,45		180	1,66

Based on the data obtained, it is known that each pulse value produces a different pulse shape and time. This data is then processed using Microsoft Excel to create a graph showing the relationship between the pulse and the angle of the servo motor and the time required as shown in Figure 3.

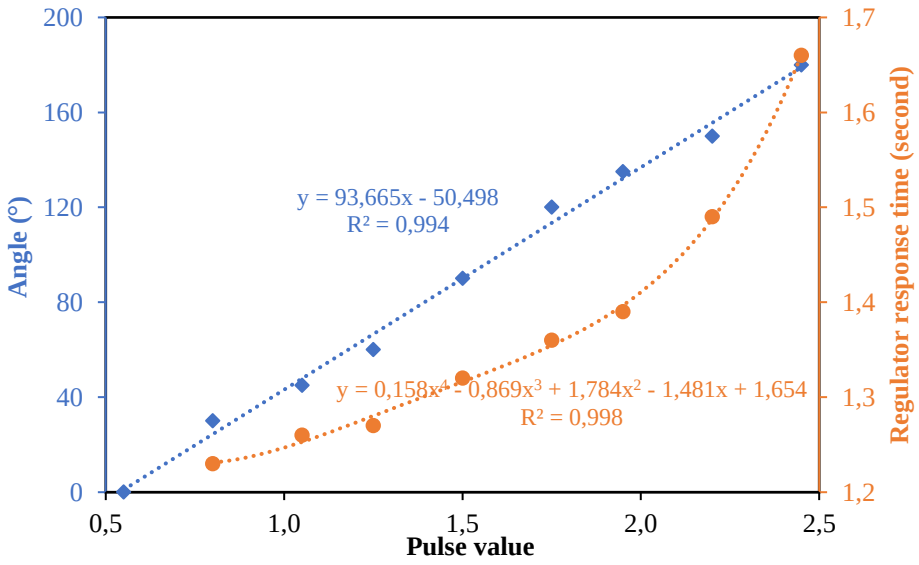

Figure 3. Time responsiveness graph

4. CONCLUSION

The servo motor shows excellent and optimal performance in opening and closing the regulator lever. In 5 experiments carried out in each condition, the results showed that when in a safe and alert condition, the regulator lever remained closed. However, when in a dangerous condition, the regulator lever will open. The servo motor has proven to be effective in responding to LPG leakage detection which is read on the MQ-2 sensor. With high speed and consistency in emergency situations, servo motors demonstrate reliable adaptability and effective response in the face of dangerous conditions. To open the regulator lever automatically, the effective angle is 0° with a pulse value of 0.55 ms and the response time is 0 seconds. Meanwhile, to close the regulator lever, the effective angle is 180° with a pulse value of 2.45 ms with a response time of 1.66 seconds.

ACKNOWLEDGEMENTS

Volume 11, Issue 2, October 2024, pp. 153-158
ISSN 2355-5068 ; e-ISSN 2622-4852
DOI: 10.33019/jurnalecotipe.v11i2.4496

This work is funded by Institut Teknologi Sumatera (Itera) through the 2024 Itera Student Research Grant scheme. The authors would like to thank the Faculty of Industrial Technology, Itera, for assistance in the publication of this work in the national journal.

REFERENCES

[1] E. A, S. Berberoglu, T. Nagano, and S. Kapur, *The Bioeconomy Approach*. 2020.
[2] A. E. Setyono and B. F. T. Kiono, "Dari Energi Fosil Menuju Energi Terbarukan: Potret Kondisi Minyak dan Gas Bumi Indonesia Tahun 2020 – 2050," *Jurnal Energi Baru dan Terbarukan*, vol. 2, no. 3, pp. 154–162, Oct. 2021, doi: 10.14710/jebt.2021.11157.
[3] M. Izul Maulana, "161010084 (1)," *Skripsi*, pp. 1–99, Mar. 2021.
[4] T. Kivevele, T. Raja, V. Pirouzfar, B. Waluyo, and M. Setiyo, "LPG-Fueled Vehicles: An Overview of Technology and Market Trend," *Jurnal Unimma Automotive Experiences*, vol. 3, no. 1, pp. 6–19, 2020, doi: 10.31603/ae.v3i1.3334.
[5] M. Amer *et al.*, "Low Carbon strategies for Sustainable Bio-Alkane Gas Production and Renewable Energy," *Energy Environ Sci*, vol. 13, no. 6, pp. 1818–1831, Jun. 2020, doi: 10.1039/d0ee00095g.
[6] J. P Nshimiyimana, M. C. Mukeshimana, and Evariste Nshimyimana, "Tracking the progress towards adopting LPG as a clean cooking fuel in Rwanda: User's perspective," *Elsevier*, vol. 80, Jun. 2024.
[7] Y. A. Hasan, "Sistem Pendeteksi Kebocoran Tabung Gas LPG Otomatis Berbasis Arduino Uno Menggunakan Metode Prototype," *Skripsi*, pp. 1–51, Jun. 2022.
[8] F. Shaik, "An Experimental Investigation and Analysis of Proposed Gas Leakage System," *Helix The Scientific Explorer*, vol. 11, no. 1, pp. 23–30, Feb. 2021, doi: 10.29042/2021-11-1-23-30.
[9] C. F. Gould and J. Urpelainen, "The Gendered Nature of Liquefied Petroleum Gas Stove Adoption and Use in Rural India," *Journal of Development Studies*, vol. 56, no. 7, pp. 1309–1329, Jul. 2020, doi: 10.1080/00220388.2019.1657571.
[10] A. Mutaqin and E. Sitompul, "Perancangan Detektor Kebocoran Gas LPG Berbasis Arduino yang Terhubung dengan Smartphone," *Journal of Electrical and Electronics Engineering*, vol. 3, no. 1, pp. 65–71, 2019.
[11] Z. Tasnim, S. Das, R. Islam, J. Biswas, F. M. J. M. Shamrat, and A. Khater, "Sensor based Smart Automated Gas Leakage Detection and Prevention System," in *International Conference on Trends in Electronics and Informatics*, Institute of Electrical and Electronics Engineers Inc., 2022, pp. 460–466. doi: 10.1109/ICOEI53556.2022.9777130.
[12] B. Dharaskar, A. Gaigawali, S. Meshram, A. Tembhurne, A. Gautam, and A. Nanhe, "LPG Gas Leakage Detection and Alert System," *International Journal for Research in Applied Science and Engineering Technology* , vol. 11, no. 4, pp. 3302–3305, Apr. 2023, doi: 10.22214/ijraset.2023.50964.
[13] B. B. Sharma *et al.*, "Arduino based LPG Leakage Detection and Prevention System," *IEEE Xplore*, pp. 161–166, 2021.
[14] J. Tj, L. EA, and S. Chakraborty, "Alexa Enabled LPG Regulator Knob Control Over Mobile Phone Using AWS IoT, Lambda, ESP Module, And C#," *International Research Journal of Modernization in Engineering Technology and Science*, vol. 5, no. 12, Dec. 2023, doi: 10.56726/irjmets47497.
[15] V. Valencia, L. Putra Purnama, C. Tjong, and J. Liman, "Design of Internet of Things Based LPG Gas Leak Detection Device with Automatic Regulator Valve," *Ilmiah Elektronika Techne*, vol. 21, pp. 225–242, 2022.

JURNAL ECOTIPE
Electronic, Control, Telecommunication, Information, and Power Engineering

Volume 11, Issue 2, October 2024, pp. 159-169
ISSN 2355-5068 ; e-ISSN 2622-4852
DOI: 10.33019/jurnalecotipe.v11i2.4506

Implementation of Natural Language Processing for Bullying Complaints with Voice to Text Conversion

Miftahul Ilmi[1], Dasril Aldo[2], Sapta Eka Putra[3], Adanti Wido Paramadini[4], Yohani Setiya Rafika Nur[5]

[1]Institut Teknologi dan Bisnis Indobaru Nasional, Batam, 29444, Indonesia
[2,4,5]Institut Teknologi Telkom Purwokerto, Jl. Panjaitan, Purwokerto, 53147, Indonesia
[3]Universitas Tamansisw, Jl. Tamansiswa, Padang, 25171, Indonesia

ARTICLE INFO

Article historys:

Received : …/…/…
Revised : …/…/…
Accepted : …/…/…

Keywords:

Bullying, Natural Language Processing (NLP), Support Vector Machine (SVM), Mobile Application, Anonymous Reporting.

ABSTRACT

Bullying in high school is frequent and negatively affects students' psychological well-being. The lack of effective reporting mechanisms makes students hesitant to report bullying cases for fear of their identity being exposed, which can lead to stigma or retaliation. The lack of data on bullying incidents also hampers prevention and intervention measures. The study designed and implemented a mobile application that uses natural language processing (NLP) for speech-to-text conversion, enabling anonymous and convenient reporting of bullying cases. The app ensures the anonymity of whistleblowers and facilitates the collection of accurate data on bullying incidents, helping schools respond with appropriate preventive measures. Software engineering methodologies are used with a focus on requirements analysis, system design, implementation, and application testing. NLP technology is used to interpret verbal instructions into text, with the Support Vector Machine (SVM) method for text classification, ensuring high accuracy in detecting bullying incidents. The trial application in several high schools showed the relevance and effectiveness of the application. Ethical and security considerations are top priorities, with an emphasis on whistleblower identity protection and data security. The test results showed that the application achieved 92% accuracy, 90% precision, and 88% recall, demonstrating its effectiveness in collecting bullying reports anonymously and accurately.

Corresponding Author:

Dasril Aldo
Institut Teknologi Telkom Purwokerto, Jl. Panjaitan, Purwokerto, 53147, Indonesia
Email: dasril@ittelkom-pwt.ac.id

1. INTRODUCTION

One form of adolescent violence that often appears is bullying behavior [1]. Many in high school, bullying has become a persistent problem that negatively impacts students' psychological well-being. Deviant treatment that can have a bad effect on others. The high incidence of bullying in schools shows that this educational institution has become a common location for this behavior. Of the number of students recorded, 18.5% had been victims of bullying, 29.4% had faced acts of physical violence, and 3.1% had experienced sexual harassment. This phenomenon interferes with the learning process and can lead to long-term consequences for the victim. Although its existence has long been recognized, efforts to address bullying are often hampered by the lack of effective and reliable reporting mechanisms. Concerns about identity disclosure have discouraged many students from reporting bullying cases, which in turn perpetuates a cycle of violence and insecurity [2, 3].

Volume 11, Issue 2, October 2024, pp. 159-169
ISSN 2355-5068 ; e-ISSN 2622-4852
DOI: 10.33019/jurnalecotipe.v11i2.4506

Advances in information system-based technology [4] and integrated with AI, can be combined in the field of Natural Language Processing (NLP) [5] and a voice-to-text conversion system [6, 7], the ability of NLP to convert speech to text and text to speech [8] offers the opportunity to develop innovative solutions that can facilitate anonymous reporting of bullying. Mobile applications that utilize this technology can be an important tool to collect accurate data about bullying incidents, schools can respond with appropriate prevention and intervention measures. By ensuring the anonymity of the reporter, the app can reduce students' fear of the negative impact of reporting a bullying case, such as stigma or retaliation.

This research is important to overcome bullying that has an impact on student welfare. The app, developed using NLP and speech-to-text conversion, aims to facilitate anonymous reporting of bullying, increase the number of reports and enable more appropriate school actions. The study will also examine the effectiveness of technology in changing reporting mechanisms, contributing to a safer learning environment.

To address the problem of bullying in high school, this study will adopt several strategies. The approach to solving problem formulation involves the integration of advanced technology by applying Natural Language Processing (NLP) to support verbal reports into text. It provides an intuitive method and is similar to speaking directly, but with maintained privacy. Data analytics will be used for proactive response, where data from the app will be analyzed for bullying patterns, assisting schools in planning prevention and data-driven interventions. In addition, the development of private and secure applications is a priority, with a focus on anonymity and data security, as well as reducing psychological barriers through user-friendly design.

A problem-solving strategy includes several steps. First, the development of an application with advanced NLP algorithms will be carried out, simplifying the reporting process through speech-to-text conversion. Second, data optimization for schools will be carried out by utilizing data to facilitate prevention and intervention measures, as well as improving the accuracy and availability of data through efficient reporting features. Finally, the design of the app will focus on users with the implementation of features that support the anonymity of the complainant, as well as training and education for the safe use of the app. This strategy is expected to facilitate bullying reporting, increase the number of reports received, and allow for more appropriate preventive measures and interventions from the school, thereby creating a safer school environment.

This study will improve previous research by focusing on bullying complaint applications using NLP technology and speech-to-text conversion. Previous research, such as voice sentiment analysis [9], a voice-to-text app for police [10], increasing the resilience of NLP systems to ASR errors [11], the development of virtual bots with human-like conversations [12], and a voice-to-text conversion system in Ukrainian [13], despite making a significant contribution, did not specifically handle bullying complaints. The study offers a more precise solution by integrating the latest technology for accurate and efficient speech-to-text conversion, specifically designed to help individuals report bullying cases in real-time, thereby improving the response and handling of bullying cases.

2. RESEARCH METHOD

In facing the challenges of bullying in high school, this research is directed to develop innovative technology-based solutions. This flowchart presents a comprehensive view of the planned research methodology, from pre-research to final output. The focus is on creating mobile applications that leverage advances in Natural Language Processing (NLP) to simplify and improve the bullying reporting process.

JURNAL ECOTIPE
Electronic, Control, Telecommunication, Information, and Power Engineering
Volume 11, Issue 2, October 2024, pp. 159-169
ISSN 2355-5068 ; e-ISSN 2622-4852
DOI: 10.33019/jurnalecotipe.v11i2.4506

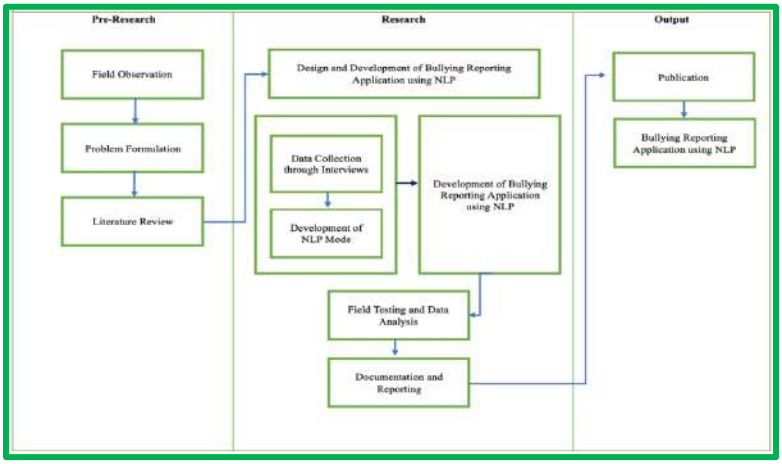

Figure 1. Research Methodology

Based on the flow chart shown in Figure 1, the research methodology can be explained by the following steps:

2.1 Pre-Research

At this stage the researcher conducts a series of initial activities before application development.

1. Field Observation: The researcher will conduct observations in the high school environment to understand the context and dynamics of bullying that occurs. This helps in identifying the specifications needed for the application.
2. Problem Formulation: Based on field observations, researchers formulate specific problems that the application will address, such as the lack of efficient and safe reporting mechanisms for students.
3. Literature Review: Before starting development, researchers will conduct a literature study to understand existing research on bullying, reporting applications, and NLP technology. This study will provide a theoretical and practical foundation for application development.

2.2 The core phase of the research includes the development of NLP-based applications.

1. Bullying and NLP Reporting Application Design and Design: Designing the application architecture and interface. The researcher will determine the main features based on the results of observations and literature reviews.
2. Interview Data Collection: Conduct interviews with stakeholders (students, teachers, and school administration) to collect data to be used in the creation of NLP models and to ensure the application meets the needs of users.
3. NLP Model Creation: Develop an NLP model that will be used to analyze and interpret spoken bullying reports. This model will be tested and adjusted for accuracy in recognizing bullying terminology and context. Shown food Figure 2.

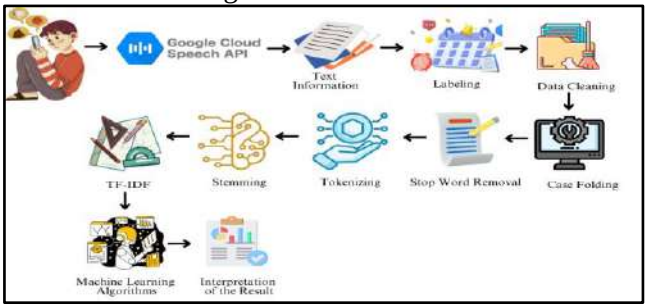

Figure 2. NLP Process

From Figure 2. The following is an explanation of the stages of the NLP process in this study based on figure 2 given:

Volume 11, Issue 2, October 2024, pp. 159-169
ISSN 2355-5068 ; e-ISSN 2622-4852
DOI: 10.33019/jurnalecotipe.v11i2.4506

a. Voice Input from Users: Users, in this case victims or witnesses of bullying, use mobile devices to record their complaints in the form of voice.
b. Voice to Text Conversion: Voices recorded by users are sent to the Google Cloud Speech API to be converted into text. The Google Cloud Speech API uses speech recognition technology to convert speech to text with high accuracy.
c. Text Information Collection: is the stage where the text of the voice conversion is collected and stored in a structured format for further analysis [14]. At this stage, the text is given additional labels such as bullying categories, locations, and other relevant information to organize the data properly. This stage ensures that the data is ready for the cleaning process and subsequent analysis.
d. Labeling: Each generated text is labeled accordingly [15], such as the bullying category (0 = not bullying, 1 = verbal, 2 = physical, 3 = social, 4 = emotional, 5 = online).
e. Data Cleanup:
    i. Case Folding: Lowercase all letters in text for consistency [16].
    ii. Stop Word Removal: Removes common words that do not have significant meaning in the analysis (such as "and", "or", "which") [17].
    iii. Tokenization: Breaking down text into small units called tokens (usually individual words) [18].
    iv. Stemming: Reducing words to their basic form (e.g., "hit" to "hit") to unify variants of the same word [19].
f. TF-IDF: After preprocessing the text, including case folding, stopword removal, tokenization, and stemming, we implement TF-IDF (Term Frequency-Inverse Document Frequency) to convert the text into numerical features [20].
g. Machine Learning Algorithm Application: The cleaned and processed data is used to train a machine learning algorithm that will help in detecting bullying patterns from the generated text. These algorithms can be either classification or clustering models depending on the needs of the analysis.
h. Interpretation of Results: The results of machine learning algorithms are interpreted to gain insights and information regarding the incidence of bullying. This includes identifying the types of bullying that often occur, locations prone to bullying, and profiles of perpetrators and victims.

4. Field Testing and Data Analysis: Once the app is developed, field testing will be conducted to see how well the app performs in a real environment. Data from these tests will be analyzed to see how effective the app is.
5. Documentation and Reporting: Create complete documentation of the application development process and test results. This will include reporting on the effectiveness of the app, usage in the field, and feedback from users.

2.3 Output

The final results of this study include two main aspects.

1. Publications: Researchers will write and publish research results in accredited journals or conferences to share knowledge and findings with the wider community.
2. NLP-based Bullying Reporting Application: The end product is a fully functional application that allows anonymous and secure reporting of bullying, ready for adoption by schools participating in the study.

This methodology emphasizes a systematic and iterative approach, which ensures that the developed application is tailored to the needs of the user and has a strong foundation in best practices from the existing literature as well as input from the user.

3. RESULTS AND DISCUSSION

3.1 Input Voice Data from User

JURNAL ECOTIPE
Electronic, Control, Telecommunication, Information, and Power Engineering
Volume 11, Issue 2, October 2024, pp. 159-169
ISSN 2355-5068 ; e-ISSN 2622-4852
DOI: 10.33019/jurnalecotipe.v11i2.4506

In this study, the recorded data of bullying complaints received will be presented in Table 1. The data contains reports in Indonesian made by victims or witnesses of bullying. Once the data is recorded, the next step is to translate it into english. The results of the voice data input are shown in Table 1.

Table 1. Voice Input

No	Name	Sound Visualization
1	File14.wav	
2	file13.mp3	
3	file10.mp3	
…	…	…
1000	File1000.mp3	

3.2 Google Cloud Speech API

Voice recordings are converted to text using the Google Cloud Speech API. This technology converts voice into text information that can be further processed. The number of data displayed is only 5 data out of 1000 data obtained, shown in Table 2.

Table 2. Conversion Results

No	Teks
1	They spread lies about me, saying I did things I didn't do. Now everyone believes them and avoids me. It's destroying my social life.
2	Every time there is a music lesson, I am always laughed at by my classmates. They call me names and say I'm useless. It's really affecting my self-esteem. I feel so worthless.
3	Every time I make a mistake, they point it out and laugh. They say I'm a failure and that I'll never succeed. It's crushing my confidence. I feel so hopeless.
4	I used to have a group of friends, but now they ignore me. They act like I'm not there and talk behind my back. It's so painful.
5	I get shoved into lockers almost every day. They say it's just a joke, but it hurts. I have bruises from it. I want it to stop but I'm afraid to say anything.

3.3 Text Information

From the data in Table 2 is the stage where the text of the voice conversion is collected and stored in a structured format for further analysis. At this stage, the text is given additional labels such as bullying categories and other relevant information to organize the data well. This stage ensures that the data is ready for the cleaning process and subsequent analysis.

```
df = pd.read_excel('latif.xlsx', sheet_name='DATA')
df.head()
```

	No	Filename	Bullying text	Category
0	959	file959.mp3	They spread lies about me, saying I did things...	Social Bullying
1	176	file176.mp3	Every time there is a music lesson, I am alway...	Verbal Bullying
2	686	file686.mp3	Every time I make a mistake, they point it out...	Emotional Bullying
3	927	file927.mp3	I used to have a group of friends, but now the...	Social Bullying
4	618	file618.mp3	I get shoved into lockers almost every day. Th...	Physical Bullying

Figure 3. Results of Ketogori Administration

Figure 3 shows how bullying data is loaded using Python from an Excel file named 'latif.xlsx'. The pd.read_excel command is used to read data from a sheet named 'DATA', and df.head() displays the first five rows of the loaded DataFrame. The data consists of the 'No' column which contains the serial number of each entry, 'Filename' which contains the name of the audio file of the bullying complaint recording, 'Bullying text' which contains the text of the transcription from the voice recording, and 'Category' which contains bullying categories such as 'Social Bullying', 'Verbal Bullying', 'Emotional Bullying', and 'Physical Bullying'. By loading and displaying this data, we can understand the structure

JURNAL ECOTIPE
Electronic, Control, Telecommunication, Information, and Power Engineering
Volume 11, Issue 2, October 2024, pp. 159-169
ISSN 2355-5068 ; e-ISSN 2622-4852
DOI: 10.33019/jurnalecotipe.v11i2.4506

and content of bullying reports, which is an important first step before conducting further text analysis or applying machine learning techniques.

3.4 Labeling

Labeling bullying data is an important process for classifying the types of bullying detected in the text of the voice conversion. Each bullying text that has been collected is numerically labeled based on its category. This label aids in further analysis, especially in the application of machine learning algorithms to detect bullying patterns.

	No	Filename	Bullying text	Category	Label
0	959	file959.mp3	They spread lies about me, saying I did things...	Social Bullying	3
1	176	file176.mp3	Every time there is a music lesson, I am alway...	Verbal Bullying	1
2	686	file686.mp3	Every time I make a mistake, they point it out...	Emotional Bullying	4
3	927	file927.mp3	I used to have a group of friends, but now the...	Social Bullying	3
4	618	file618.mp3	I get shoved into lockers almost every day. Th...	Physical Bullying	2

Figure 4. Labeling Results

Figure 5 shows bullying data that has been given numerical labels for each bullying category, consisting of 'No', 'Filename', 'Bullying text', 'Category', and 'Label' columns. The folder function of Pandas is used to change the bullying category to numeric labels, such as 'Social Bullying' to 3, 'Verbal Bullying' to 1, and so on. This process is essential for converting qualitative data into quantitative, facilitating further analysis and application of machine learning algorithms. With numerical labeling, bullying data becomes more structured and ready to be used in machine learning models to detect text-based bullying patterns.

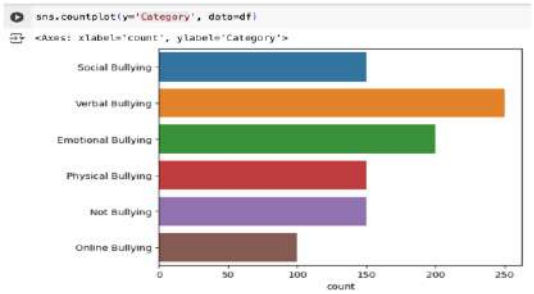

Figure 5. Results of Count Against Category

Figure 5 shows a bar chart created using Seaborn to visualize the distribution of bullying categories in a dataset. The 'sns.countplot' function is used to generate this graph, with the parameter 'y='Category'' indicating that the bullying category is displayed on the y-axis, and the parameter 'data=df' indicating that the data is retrieved from a DataFrame named 'df'. Analysis of this graph shows that 'Verbal Bullying' has the highest number of incidences among other bullying categories, followed by 'Social Bullying' and 'Emotional Bullying'. The 'Online Bullying' category has the fewest number of incidences. This distribution provides an overview of the prevalence of each type of bullying in the dataset, which can help in determining the focus of interventions and more effective prevention strategies.

3.5 Data Cleaning

Data cleansing involves several steps to ensure that the data used is clean and ready for further analysis. The process is shown in figure 6.

data.head()

	Bullying text	Label
0	they spread lies about me, saying i did things...	3
1	every time there is a music lesson, i am alway...	1
2	every time i make a mistake, they point it out...	4
3	i used to have a group of friends, but now the...	3
4	i get shoved into lockers almost every day. th...	2

(a)

data.head()

	Teks Bullying	Label
0	spread lies saying things didnt everyone belie...	3
1	every time music lesson always laughed classma...	1
2	every time make mistake point laugh say im fai...	4
3	used group friends ignore act like im talk beh...	3
4	get shoved lockers almost every day say joke h...	2

(b)

data.head()

	Teks Bullying	Label
0	[spread, lies, saying, things, didnt, everyone...	3
1	[every, time, music, lesson, always, laughed, ...	1
2	[every, time, make, mistake, point, laugh, say...	4
3	[used, group, friends, ignore, act, like, im, ...	3
4	[get, shoved, lockers, almost, every, day, say...	2

(c)

Figure 6. Case Folding Results (a), Stop Word Results (b), Tokenization Results (c)

JURNAL ECOTIPE
Electronic, Control, Telecommunication, Information, and Power Engineering
Volume 11, Issue 2, October 2024, pp. 159-169
ISSN 2355-5068 ; e-ISSN 2622-4852
DOI: 10.33019/jurnalecotipe.v11i2.4506

Figure 6 (a) shows bullying data that has undergone a case folding process, which is displayed using the data.head() function. The casefolding function is used to convert text to lowercase, which ensures consistency in the text and helps to reduce variations caused by differences in case and lowercase. The implementation of this function uses the .lower() method on the text identified as a string. In the DataFrame data, the 'Text Bullying' column is casefolded for each text entry. This case folding process is important in text preprocessing because it allows machine learning algorithms to perceive words like "Bullying" and "bullying" as the same entity, improving the accuracy and efficiency of subsequent text analysis. These results ensure that all bullying texts in the dataset are lowercase, ready for the next step of data cleaning and analysis.

Figure 6 (b) shows the results of bullying text after going through the stop word cleaning stage using the clean function. This function cleans up the text by removing various irrelevant elements such as @mentions, hashtags, URLs, numbers, single characters, punctuation, emojis, HTML entities, and non-ASCII characters. In addition, this function also lowercase all letters, remove certain phrases such as "translated by Google", and combine some spaces into one. This cleanup process results in cleaner and more consistent text, making it easier for further analysis or use in machine learning models. The end result is a more structured bullying text that is free of bullying elements, thus improving the accuracy of text analysis.

Figure 6 (c) shows the results of bullying text after going through the tokenization stage using the tokenize function. This function converts the text into a list of tokens (individual words) using word_tokenize from the NLTK library. Each bullying text in the 'Bullying Text' column is tokenized function, which generates a list of words from each text. Tokenization breaks down each sentence or phrase into individual words, making it easier to further analyze such as word frequency, n-grams, and the application of machine learning algorithms. For example, the text "They spread lies about me saying I did things I didn't do. Now everyone believes them and avoids me." is changed to [spread, lies, saying, things, didn't, everyone]. This process ensures that the text is more structured and ready for subsequent preprocessing steps or more in-depth analysis.

```
data.head()
```

	Bullying text	Label
0	[spread, lies, saying, things, didnt, everyone...	3
1	[every, time, music, lesson, always, laughed, ...	1
2	[every, time, make, mistake, point, laugh, say...	4
3	[used, group, friends, ignore, act, like, im, ...	3
4	[get, shoved, lockers, almost, every, day, say...	2

Figure 8. Stemming Results

Figure 8 shows the results of the bullying text after going through the stemming stage using the stemming function, which uses the Porter Stemmer of the NLTK library to convert each word into its basic form. This function checks if the input is a string, then breaks the text into tokens and applies stemming to each token. The result is more consistent and simple text, with words like "running" becoming "run" and "saying" becoming "say". This word normalization helps to reduce word variation, improve the accuracy of text analysis, and reduce the number of unique features in the text, making it easier to further analyze and apply machine learning models for bullying detection and classification.

3.6 TF-IDF

The TF-IDF (Term Frequency-Inverse Document Frequency) process will be applied to convert bullying text into a numerical feature that reflects the importance of the words in the document relative to all other documents. The steps to be taken include: initialization of TF-IDF Vectorizer, transformation of bullying text into TF-IDF features, and conversion of TF-IDF matrices into DataFrames for further analysis shown in Figure 10.

JURNAL ECOTIPE
Electronic, Control, Telecommunication, Information, and Power Engineering
Volume 11, Issue 2, October 2024, pp. 159-169
ISSN 2355-5068 ; e-ISSN 2622-4852
DOI: 10.33019/jurnalecotipe.v11i2.4506

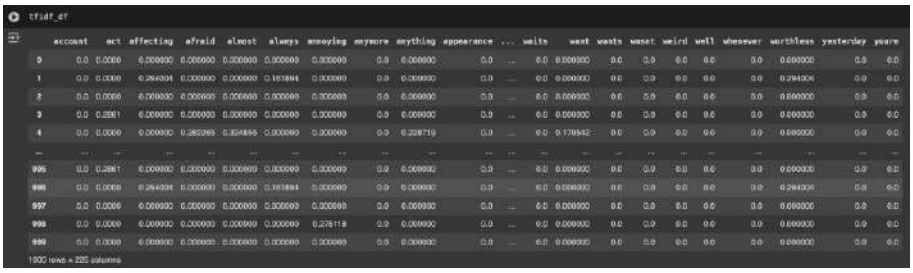

Figure 10. TF-IDF Results

Figure 10 shows the TF-IDF matrix of the processed bullying text. Each row in this matrix represents a single document or text entry of bullying, while each column represents a unique word contained in the entire document set. The values in the matrix show the TF-IDF score for each word in each document. This score reflects the importance of the word in a particular document, taking into account how often it appears and how common the word is throughout the document. For example, the word "affecting" in the second line has a high TF-IDF score, indicating that the word is significant in the document. Next, the results of WordCloud are displayed in Figure 11.

Figure 11. Word Cloud

Figure 11 shows a visualization of the words that most often appear in the processed bullying text, with the word size reflecting their relative TF-IDF score. Words such as "say", "i'm", "feel", "names", "group", "always", "want", "every", and "make" appear larger, indicating that they appear frequently and have a high TF-IDF score, so they are considered important in bullying texts. These words reflect different aspects and contexts of bullying, such as ridicule or name-calling ("names", "called"), feelings of the victim ("feel", "hurt", "isolated"), and the social context in which bullying occurs ("group", "always", "everyone"). This Word Cloud helps in identifying common keywords and themes in bullying texts, provides a quick and easy-to-understand visual overview of the most significant words, and facilitates initial data exploration and further analysis.

3.7 Machine Learning Algorithm Applications:

Support Vector Machine (SVM) is a highly effective machine learning algorithm for classification tasks, including in natural language processing (NLP). SVM works by looking for hyperplanes that separate data from different classes by maximum margin, and is particularly effective for high-dimensional data that is often found in text. In the context of NLP, SVM can be used for tasks such as text classification, sentiment analysis, and spam detection. These algorithms can handle non-linear data through the use of kernel functions, which transform the data into higher dimensions where it can be separated linearly.

For SVM implementations in NLP, text is usually converted into numerical features using methods such as TF-IDF before being applied to SVMs. After that, the data was divided into training data and testing data with a ratio of 75% for training and 25% for testing. The SVM model is initialized with SVC(), trained using data training (X_train and y_train) with svm.fit(X_train, y_train), and used to predict the results on the test data with svm.predict(X_test). The model performance evaluation is carried out using metrics such as accuracy, precision, recall, and f1-score generated from classification_report(y_test, y_pred), to ensure the model performs well on the given NLP task. Furthermore, an evaluation was carried out on the model with the results as shown in Figure 12.

JURNAL ECOTIPE
Electronic, Control, Telecommunication, Information, and Power Engineering
Volume 11, Issue 2, October 2024, pp. 159-169
ISSN 2355-5068 ; e-ISSN 2622-4852
DOI: 10.33019/jurnalecotipe.v11i2.4506

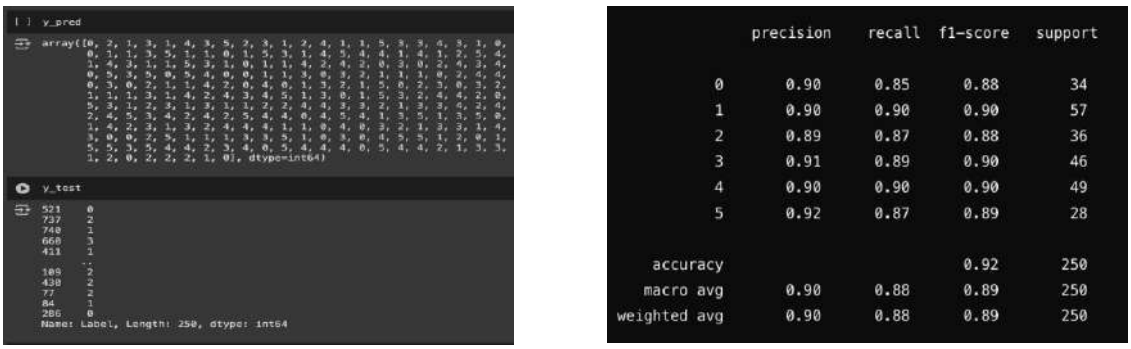

(a) (b)

Figure 12. Prediction Results (a) Evaluation Results (b)

Figure 12 (a) shows the prediction results (y_pred) and actual values (y_test) of the SVM model for bullying data. y_pred contains the model's predicted labels, while y_test contains the actual labels. Correct predictions occur when both values match; differences indicate errors. Classes include 0, 1, 2, 3, 4, and 5. Analyzing these differences helps calculate accuracy and identify error patterns. Figure 12 (b) presents the SVM model evaluation using a classification report with precision, recall, f1-score, and support metrics from scikit-learn's classification_report function. Precision ranges from 0.89 to 0.92, recall from 0.85 to 0.90, and F1-score from 0.88 to 0.90. Support shows instance counts, such as 34 for class 0 and 57 for class 1. The overall accuracy is 0.92. Macro and weighted average precision, recall, and f1-score are 0.90, 0.88, and 0.89. This report highlights the model's high accuracy and balanced precision and recall across classes.

3.8 Interpretation of Results

The final stage in our process is the "Interpretation of Results". This involves analyzing the output generated by the machine learning algorithms to derive meaningful insights and conclusions regarding the instances of bullying reported through the application.

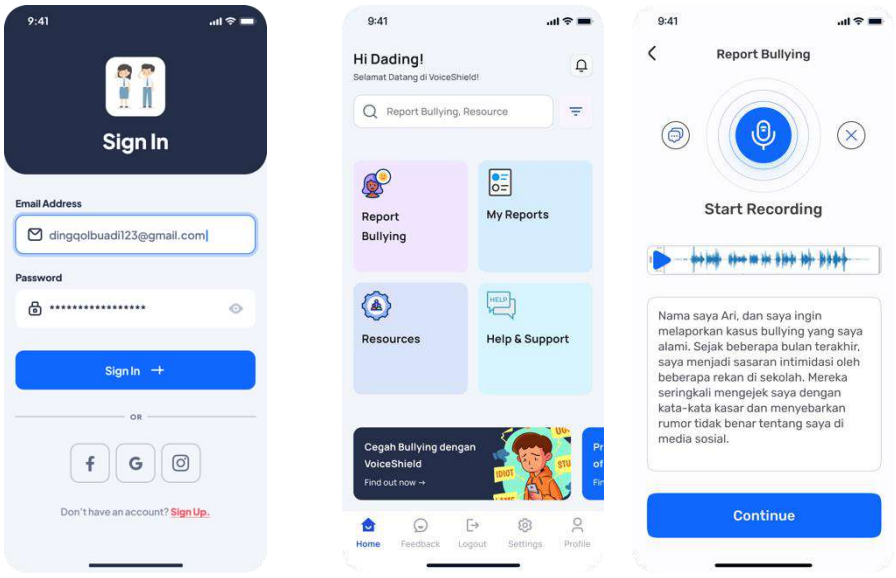

Figure 13. VoiceShield Application Implementation Results

The mobile app "VoiceShield: Bullying Protector App with NLP" is designed to help high school students report bullying incidents and get support. The login page of this application displays a high school student icon above the login form, giving a special impression for high school students. After logging in, users are redirected to the home page which contains menus such as Home, Report Bullying, My Reports, Resources, Help & Support, Profile, Settings, Feedback, and Logout. On the complaints page, users can record their complaints using the voice recorder button, and the results of the recording

Volume 11, Issue 2, October 2024, pp. 159-169
ISSN 2355-5068 ; e-ISSN 2622-4852
DOI: 10.33019/jurnalecotipe.v11i2.4506

and transcription of the complaint are displayed for review. For example, the transcription shown in the image depicts the bullying incidents experienced by users in the field. In addition, there is an admin page that contains a list of incoming complaints with a "play" action button to process the complaint. With this application, users are expected to be able to report bullying incidents more easily and get the necessary support.

4. CONCLUSION

The "VoiceShield: Bullying Protector App with NLP" app is designed to help high school students report bullying incidents effectively and get the support they need. The app has several important features, including a login page, a main page with important menus, a complaints page that allows users to record and transcribe their complaints, and an admin page to process complaints. The main process in this application is the conversion of speech to text using Natural Language Processing (NLP), which is then further analyzed. The results of the performance evaluation of the SVM model applied in the application show very satisfactory results, with an accuracy rate of 92%, precision of 90%, recall of 88%, and F1-score of 89%. This evaluation shows that the SVM model is able to classify bullying-related texts with a high degree of accuracy, as well as a balance between precision and recall. As such, the app not only provides users with useful tools for reporting bullying cases, but also ensures that the generated reports can be processed and analyzed with high accuracy, providing more effective support for bullying victims.

ACKNOWLEDGMENTS

We would like to express our deepest gratitude to the Directorate of Research and Community Service (DRTPM) for providing research funds that make this research possible. Financial support from DRTPM was instrumental in the development and implementation of "VoiceShield: Bullying Protection App with NLP". We would also like to thank all the speakers who have shared their experiences and insights, being a valuable source of information and inspiration for this research.

REFERENCES

[1] A. Y. Azhari, D. L. N. Janah, F. E. Meyliana, and B. Setiawan, "The Influence of the Development of Character Education in Overcoming the Problem of Bullying in Indonesia," *Sinar Dunia J. Ris. Sos. Hum. and educator knowledge.*, vol. 2, no. 4, hlm. 257–271, Nov 2023, doi: 10.58192/sidu.v2i4.1588.

[2] N. Aristiani, M. Kanzunnudin, and N. Fajrie, "Bullying Behavior in Elementary School Children in Gribig Village, Kudus," *J. type pedagog.*, vol. 4, no. 2, Des 2021, doi: 10.24176/jpp.v4i2.5989.

[3] Y. Siswati and M. Saputra, "The Role of the School Anti-Bullying Task Force in Overcoming the Phenomenon of Bullying in Senior High Schools," *Cive J. Researcher. Educators. Pancasila and Citizenship*, vol. 3, no. 7, hlm. 216–225, Jul 2023, doi: 10.56393/decive.v3i7.1656.

[4] M. Ilmi, D. R. Habibie, and Y. Arifin, "Analysis and Design of the Monitoring Information System for Street Vendor Students at SMK Permata Harapan," *JOINS J. Inf. Syst.*, vol. 8, no. 2, hlm. 177–187, Nov 2023, doi: 10.33633/joins.v8i2.9233.

[5] M. Furqan, S. Sriani, and M. N. Shidqi, "Telegram Chatbot Using Natural Language Processing," *Walisongo J. Inf. Technol.*, vol. 5, no. 1, HLM. 15–26, Jun 2023, doi: 10.21580/wjit.2023.5.1.14793.

[6] R. M. Suryadi, "Design and Build Glasses to Convert Voice to Text," *J. Tek. Machine Learning*, Vol. 4, No. 1, HLM. 53, Jul 2021, doi: 10.17977/um054v4i1p53-61.

[7] M. P. R, M. Anu, dan D. S, "Building A Voice Based Image Caption Generator with Deep Learning," dalam *2021 5th International Conference on Intelligent Computing and Control Systems (ICICCS)*, Madurai, India: IEEE, Mei 2021, hlm. 943–948. doi: 10.1109/ICICCS51141.2021.9432091.

[8] A. Anand, A. A. Rastogi, R. A. Chadichal, A. Surana, Dr. S. G, dan Dr. L. N. R, "Handwritten Text Recognition and Conversion to Speech," *Int. J. Res. Appl. Sci. Eng. Technol.*, vol. 11, no. 6, hlm. 3904–3914, Jun 2023, doi: 10.22214/ijraset.2023.54317.

Volume 11, Issue 2, October 2024, pp. 159-169
ISSN 2355-5068 ; e-ISSN 2622-4852
DOI: 10.33019/jurnalecotipe.v11i2.4506

[9] A. Apturkar, A. I. Iliev, A. Anand, A. Oli, S. Reddy Siddenki, dan V. Reddy Meka, "Sentiment Analysis of Speech with Application to Various Languages," *Digit. Present. Preserv. Cult. Sci. Herit.*, vol. 10, pp. 103–118, Sep 2020, doi: 10.55630/dipp.2020.10.6.

[10] R. A. K, T. Triveni, V. N R, V. K, dan R. B M, "Speech to Text App Customized for Police Functioning in Different Languages," dalam *2023 4th International Conference for Emerging Technology (INCET)*, Belgaum, India: IEEE, May 2023, hlm. 1–4. doi: 10.1109/INCET57972.2023.10170687.

[11] T. Cui, J. Xiao, L. Li, X. Jiang, dan Q. Liu, "An Approach to Improve Robustness of NLP Systems against ASR Errors." arXiv, 25 Maret 2021. Diakses: 12 Juli 2024. [Daring]. Tersedia pada: http://arxiv.org/abs/2103.13610

[12] Lviv Polytechnic National University, Y. Tyshchuk, V. Vysotska, Lviv Polytechnic National University, O. Vlasenko, dan Zhytomyr Ivan Franko State University, "Information system for converting audio in Ukrainian language into its textual representation using nlp methods and machine learning," *Vìsn. The National University of L'vìvì Polìhnìka serìiâ ìformation sist. Ta Merezì*, vol. 12, HLM. 23–51, As of 2022, doi: 10.23939/sisn2022.12.023.

[13] G. P. Ashok, "Virtual Bot Powered by Machine Learning and NLP Technologies: Emulating Human-Like Conversations through Speech-to-Text Conversions," *INTERANTIONAL J. Sci. Res. Eng. Manag.*, vol. 07, no. 07, Jul 2023, doi: 10.55041/IJSREM24835.

[14] A. Mishra, A. Sahay, M. A. Pandey, dan S. S. Routaray, "News text Analysis using Text Summarization and Sentiment Analysis based on NLP," dalam *2023 3rd International Conference on Smart Data Intelligence (ICSMDI)*, Trichy, India: IEEE, Mar 2023, hlm. 28–31. doi: 10.1109/ICSMDI57622.2023.00014.

[15] L. Cui, Y. Li, dan Y. Zhang, "Label Attention Network for Structured Prediction," *IEEEACM Trans. Audio Speech Lang. Process.*, vol. 30, HLM. 1235–1248, 2022, doi: 10.1109/TASLP.2022.3145311.

[16] R. P. Dias, C. S. L. Vidanapathirana, R. Weerasinghe, A. Manupiya, R. M. S. J. Bandara, dan Y. P. H. W. Ranasinghe, "Automated use case diagram generator using NLP and ML." arXiv, 2023. doi: 10.48550/ARXIV.2306.06962.

[17] F. Liu, H. Huang, Z. Yang, Z. Hao, dan J. Wang, "Search-Based Algorithm With Scatter Search Strategy for Automated Test Case Generation of NLP Toolkit," *IEEE Trans. Emerg. Top. Comput. Intell.*, vol. 5, no. 3, HLM. 491–503, Jun 2021, doi: 10.1109/TETCI.2019.2914280.

[18] A. M. Maatuk dan E. A. Abdelnabi, "Generating UML Use Case and Activity Diagrams Using NLP Techniques and Heuristics Rules," dalam *International Conference on Data Science, E-learning and Information Systems 2021*, Ma'an Jordan: ACM, Apr 2021, hlm. 271–277. doi: 10.1145/3460620.3460768.

JURNAL ECOTIPE
Electronic, Control, Telecommunication, Information, and Power Engineering

Volume 11, Issue 2, October 2024, pp. 170-177
ISSN 2355-5068 ; e-ISSN 2622-4852
DOI: 10.33019/jurnalecotipe.v11i2.4505

Reliability Analysis of Coal Feeder Instrumentation Using Failure Mode and Effect Analysis (FMEA) at PT. PLN Nusantara Power UP Tenayan

Aulia Rahmadana[1], Jufrizel[2], Hilman Zarory[3], Putut Son Maria[4]
[1,2,3,4] Department of Electrical Engineering, Universitas Islam Negeri Sultan Syarif Kasim Riau, Jl. HR. Soebrantas No. Km 15, Riau, 28923

ARTICLE INFO

Article historys:

Received : …/…/…
Revised : …/…/…
Accepted : …/…/…

Keywords:

Instrumentation Components, Failure Mode and Effect Analysis, Risk Priority Number.

ABSTRACT

PT. PLN Nusantara Power UP Tenayan is a coal-fired power plant supplying electricity to the Riau region with a capacity of 2 x 110 MW. Operating 24/7, the plant faces frequent failures, particularly in the instrumentation components of the coal feeder. This research employs the Failure Mode and Effect Analysis (FMEA) method to identify and analyze these failures. The Risk Priority Number (RPN), calculated by multiplying severity, occurrence, and detection ratings, helps determine the failure level. Research stages include a preliminary study, problem identification, observations and interviews, data collection and processing, FMEA analysis, and conclusion drawing. The results indicate that the instrumentation components are generally reliable, with RPN values below the critical threshold of 200. The speed sensor, with the highest RPN value of 160, is still categorized as reliable. Failures in these components can lead to operational failures, suboptimal coal feeder performance, and monitoring difficulties. The study recommends preventive maintenance every six months to enhance reliability and minimize disruptions.

Corresponding Author:

Jufrizel
Universitas Islam Negeri Sultan Syarif Kasim Riau,28129, Pekanbaru
Email: jufrizel@uin-suska.ac.id

1. INTRODUCTION

Electric energy is a renewable energy source that plays a very important role in the life and economy of a country. In several industries, including power plants, instrumentation systems have a crucial role in maintaining the performance and reliability of equipment. These instrumentation systems regulate critical parameters such as temperature, pressure, and vibration. Their function is to maintain the continuity of power plant operations by monitoring and controlling their conditions [1].

The Tenayan Steam Power Plant (PLTU Tenayan) is one of the main power plants that supply electricity needs in the Riau region and its surroundings. This company operates 24 hours a day by operating electricity with a capacity of 2 x 110 MW, organized by the government, and functions to distribute electricity needs in the Riau area [2].

PT. PLN Nusantara Power UP Tenayan operates through a complex process, utilizing various equipment and machinery. However, the production process does not always run smoothly due to frequent issues or failures in the machine components used. This results in disruptions in electricity production. Among the various machines used, one of the main components that experience failure is

JURNAL ECOTIPE
Electronic, Control, Telecommunication, Information, and Power Engineering
Volume 11, Issue 2, October 2024, pp. 170-177
ISSN 2355-5068 ; e-ISSN 2622-4852
DOI: 10.33019/jurnalecotipe.v11i2.4505

the coal feeder. As a coal-fired power plant, PLTU Tenayan has a Coal Feeder system that functions to deliver coal from the bunker to the boiler. The boiler is equipment that can supply the energy needs designed to meet the company's electricity requirements. The Coal Feeder is a critical component in the electricity generation process because a disruption in the coal feeder can cause interruptions in the coal supply to the boiler, leading to disruptions in the overall power generation process. Therefore, more intensive maintenance is required to maintain its performance to work as desired [3].

Based on direct observations and interviews with the instrumentation and control team leader at PT. PLN Nusantara Power UP Tenayan, it was explained that failures in instrumentation components can have wide-ranging impacts. Several problems that occur in the coal feeder instrumentation are prone to failures that can cause performance disruptions in the coal feeder. Coal feeder instrumentation failures can be caused by factors such as component damage, installation errors, extreme environmental conditions, and others.

One of the parameters that can be used to measure the performance reliability of the coal feeder instrumentation is by improving its reliability using the Failure Mode and Effect Analysis (FMEA) method. Failure Mode and Effect Analysis (FMEA) is a common approach used to analyze the risk of failure and to identify the causes of future failures [4]. Failure Mode and Effect Analysis (FMEA) qualitatively assesses the severity, occurrence, and detection of each activity for both the operational process and the equipment or components of a specific system. The three components that receive the highest Risk Priority Numbers (RPN) will be proposed for risk reduction strategies [5].

Previous research on reliability analysis was conducted by [6] with the title “Reliability Analysis of Instrumentation in the Central Mechanical Electrical Unit Using the Failure Mode and Effect Analysis (FMEA) Method.” The method used in their research was the failure mode and effect analysis method by identifying failure modes from a cause of failure and the impact of each component's failure on a system. The analysis results showed that the devices in PT. Telkom Area Network Riau Daratan Pekanbaru are reliable, with an RPN percentage not exceeding 200 [7].

In the research conducted by [8], the RPN values were calculated for the temperature sensor, steam flowmeter, control valve, white liquor flowmeter, gamma ray level, pressure transmitter, and kappa number, with all instrumentation exceeding the standard RPN limit of 200. Therefore, actions need to be taken on these instruments by recommending preventive maintenance, which is safe and reliable to use. In the research conducted by [3], the results significantly contributed to the implementation of water level and temperature data processing technology through RPN value calculation simulation using the FMEA method implemented in MPSA. The medium-risk values obtained from the RPN calculation ranged from 4 to 23.

Research conducted by [9] based on the FMEA results identified components with a Risk Priority Number (RPN) > 300, namely the Dise Knife and bolt nuts. If the operator detects symptoms indicating problematic components, they fill out a damage form and send it to the mechanical department, which then performs a series of maintenance procedures to repair the components.

By conducting Failure Mode and Effect Analysis (FMEA) on the coal feeder instrumentation at PLTU Tenayan, it is expected to obtain comprehensive information regarding potential failure modes, causes, and impacts, as well as recommendations for actions needed to improve system reliability. The results of this analysis can be used as a basis for making improvements and optimizations to the coal feeder instrumentation system, thereby enhancing the reliability and performance of the coal feeder and ultimately supporting a more efficient and reliable electricity generation process at PLTU Tenayan [10].

This study aims to analyze the reliability of coal feeder instrumentation using the Failure Mode and Effect Analysis (FMEA) method at PT PLN Nusantara Power UP Tenayan. By identifying potential failures and their impacts, as well as formulating appropriate preventive actions, it is expected that the reliability of the coal feeder system can be improved, ensuring a sustainable coal supply and reducing the risk of disruptions or failures in the electricity production process.

2. RESEARCH METHOD

Failure Mode and Effects Analysis (FMEA) is a systematic method for identifying and preventing potential problems in a product or process before they occur. This research was conducted at PT. PLN

Volume 11, Issue 2, October 2024, pp. 170-177
ISSN 2355-5068 ; e-ISSN 2622-4852
DOI: 10.33019/jurnalecotipe.v11i2.4505

Nusantara Power UP Tenayan, Pekanbaru. In the context of analyzing the reliability of coal feeder instrumentation, the FMEA method can be used to analyze potential failure modes in the coal feeder instrumentation components, as well as the effects of these failures.

2.1. Research Design

To facilitate the research process, the researcher created a flowchart to clearly outline each stage. The flowchart of the research process can be seen in Figure 1 as follows.

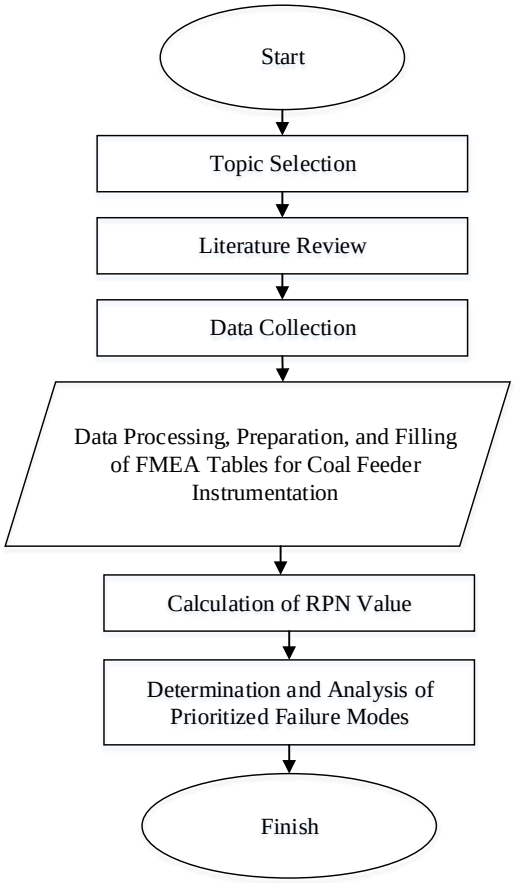

Figure 1. Research Flowchart

2.2. FMEA Analysis

The initial step in conducting research is called a preliminary study. This preliminary study involves gathering initial reviews through written sources such as journals, articles, and books. After conducting the preliminary study, the researcher collects data by identifying issues through interviews and field observations. Through interviews and observations, data is gathered regarding the failures of instrumentation components, their causes, and the effects of these failures using the FMEA method.

Failure Mode and Effect Analysis (FMEA) is a method implemented to determine the failure levels at a specific system level and to reduce a system to minimize the likelihood of critical issues in system components [11]. FMEA is a cyclical risk analysis technique used to identify the consequences arising from a failed piece of equipment, facility, or system [12].

The main objective of FMEA is to determine the level of failure based on the Risk Priority Number (RPN). The RPN value is obtained from the multiplication of severity, occurrence, and detection, and can be written using the following formula:

$$\text{RPN} = Severity \times Occurence \times Detection \quad (1)$$

JURNAL ECOTIPE
Electronic, Control, Telecommunication, Information, and Power Engineering
Volume 11, Issue 2, October 2024, pp. 170-177
ISSN 2355-5068 ; e-ISSN 2622-4852
DOI: 10.33019/jurnalecotipe.v11i2.4505

Description:

- RPN : Risk Priority Number
- Severity (Sev) : Severity Level
- Occurrence (OCC) : Frequency of Failure
- Detection (Det) : Detection of Failure Causes

Severity represents the severity or effects inflicted on the entire machine by a failure mode. Occurrence refers to the frequency of failure or damage. Detection is the control system used to detect the causes or modes of failure [13]. A higher RPN value indicates a higher level of criticality or problem within the system. Conversely, a lower RPN value indicates a lower level of criticality [14].

3. RESULTS AND DISCUSSION

3.1. Failure Mode and Effects Analysis

Failure Mode Effect and Analysis is used to identify the coal feeder instrumentation components that are most vulnerable to failure during the electricity production process. The FMEA worksheet aims to assess severity, occurrence, and detection based on the potential impact of failures, their causes, and the control actions taken, resulting in a Risk Priority Number (RPN). The FMEA table can be seen in Table 1 below:

Table 1. FMEA Worksheet for Coal Feeder Instrumentation at PT. PLN Nusantara Power UP Tenayan

Component	function	Potential Failure Mode	Potential Effect Failure	SEV	Potential Of Failure	OCC	Current Control	DET	RPN	Recommended Action
Load Cell	Measures the weight of coal used	Load cell position is unbalanced	Cannot read the load normally	6	Uneven load cell mounting surface	4	Checking the voltage at the sensor cable connection terminals	4	96	Create a strong sensor support and perform maintenance every 6 months
Sensor Speed	Measures the speed of the coal feeder mechanism	Measured speed is erratic	Equipment operational failure	8	Sensor overheats and fails to stop	5	Speed readings per second on the display module are unstable	4	160	Perform sensor maintenance every 1 month
Pressure Transmitter	Measures air or gas pressure for coal flow to furnace	Discrepancy between local and DCS readings	Uncontrolled coal flow to the boiler	5	Corrosion at cable terminals	4	Readings in the CCR do not match those in the local area	5	80	Perform maintenance every 6 months
Belt Sway	Detects if the belt conveyor stays on track	Belt sway switch failure	Conveyor belt breakage	7	Corrosion at switch terminal due to coal dust	4	Belt sway sensor cannot cut off or stop the conveyor belt during jogging	4	112	Perform maintenance on sensor terminal connections every 6 months
Level Transmitter	Measures the coal level in the bunker	Sensor cannot accurately read coal level	Equipment cannot operate normally	8	Rusted cable terminals	4	Display on the DCS is not accurate	3	96	Perform zero calibration every 6 months

JURNAL ECTIPE
Electronic, Control, Telecommunication, Information, and Power Engineering
Volume 11, Issue 2, October 2024, pp. 170-177
ISSN 2355-5068 ; e-ISSN 2622-4852
DOI: 10.33019/jurnalecotipe.v11i2.4505

Flow transmitter.	Measures the rate of coal flow into the furnace	Sensor fails to read coal flow	Inaccuracy in measuring coal flow	4	Rusted sensor	7	Visual inspection in the local area	4	112	Perform calibration every 6 months
Temperature Indicator	Reads local temperature	Temperature reading error	Operator cannot control effectively	5	Weak spring	5	Temperature readings are not accurate	3	75	Verify sensor every 6 months

The data on the instrumentation components of the coal feeder is as follows:

1. Load Cell

   This component measures the weight or load of the coal to be used. The failure occurring is that the load cell position is unbalanced, preventing it from reading the load normally due to an uneven load cell mounting surface. This can be observed when checking the voltage at the sensor cable connection terminals. The team leader for instruments and control assigned a severity score of 6, an occurrence score of 4 due to the low likelihood of failure, and a detection score of 4 because the failure can be detected. Therefore, the RPN value for the component is 96.

2. Sensor Speed

   This component measures the speed of the coal feeder mechanism. The failure observed is that the measured speed is erratic, leading to operational failures because the sensor overheats and fails to stop working. This can be seen from the unstable speed readings per second on the display module. The team leader for instruments and control assigned a severity score of 8, an occurrence score of 5, and a detection score of 4. Therefore, the RPN value for the speed sensor is 160.

3. Pressure Transmitter

   This component measures the air or gas pressure used to convey coal to the furnace. There is a discrepancy between readings in the local area and those in the Distributed Control System (DCS), resulting in uncontrolled coal flow to the boiler due to corrosion at the cable terminals. This discrepancy can be observed from the readings in the Central Control Room (CCR) not matching those in the local area. The team leader for instruments and control assigned a severity score of 5, an occurrence score of 4 due to the very low likelihood of failure, and a detection score of 5. Therefore, the RPN value for the component is 80.

4. Belt Sway

   This sensor is used to detect if the belt conveyor stays on its track. The failure occurring is that the switch on the belt sway sensor is broken, leading to a conveyor belt breakage due to corrosion at the switch terminal caused by frequent coal dust ingress. This can be observed when the belt sway sensor fails to stop or shut off during jogging of the conveyor belt. The team leader for instruments and control assigned a severity score of 7, an occurrence score of 4 due to the very low likelihood of failure, and a detection score of 4. Therefore, the RPN value for the component is 112.

5. Level Transmitter

   This component measures the height or level of coal in the bunker. The failure occurring is that the sensor cannot accurately read the coal level, preventing normal operation of the equipment due to rusted cable terminals. This is evident from the display on the DCS not reflecting the actual level. The team leader for instruments and control assigned a severity score of 8, an occurrence score of 4 due to the very low likelihood of failure, and a detection score of 3. Therefore, the RPN value for the component is 96.

6. Flow Transmitter

JURNAL ECTIPE
Electronic, Control, Telecommunication, Information, and Power Engineering
Volume 11, Issue 2, October 2024, pp. 170-177
ISSN 2355-5068 ; e-ISSN 2622-4852
DOI: 10.33019/jurnalecotipe.v11i2.4505

This component measures the rate of coal flow into the furnace. The failure occurring is that the sensor fails to accurately read the flow, leading to inaccurate measurements of coal due to sensor rust. This is evident from visual inspections in the local area. The team leader for instruments and control assigned a severity score of 4, an occurrence score of 7 due to the sensor being corroded, and a detection score of 4. Therefore, the RPN value for the component is 112.

7. Temperature Indicator

This component is used to read the local temperature. The failure occurring is temperature reading errors, making it difficult for the operator to control effectively due to a weak spring. This can be observed from the temperature readings not being accurate. The team leader for instruments and control assigned a severity score of 5 because damage to the temperature indicator prevents the operator from controlling it effectively, an occurrence score of 5 due to the very low likelihood of failure, and a detection score of 5. Therefore, the RPN value for the component is 75.

Based on the Risk Priority Number (RPN) analysis using the Failure Mode and Effects Analysis (FMEA) method, it can be concluded that the instrumentation components of the coal feeder at PT. PLN Nusantara Power UP Tenayan exhibit very good performance. The RPN values for each component are below the standard threshold of 200. According to the literature, a high RPN value indicates a more urgent need for maintenance, while a low RPN value, below 200, suggests that the components are still in good condition and do not require immediate maintenance. [13].
There is a Pareto chart of the Risk Priority Number (RPN) values as follows:

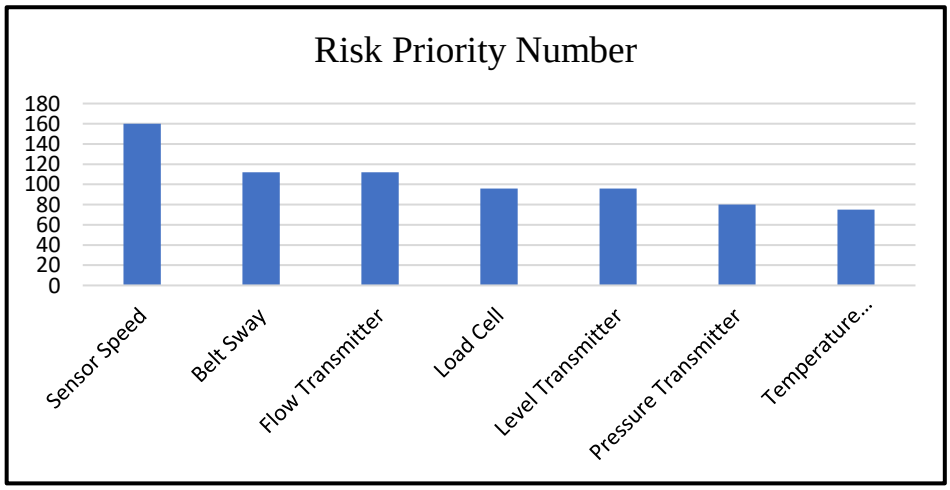

Figure 2. Pareto Diagram

From the Pareto diagram above, it is evident that the component with the highest RPN value is the speed sensor, which functions to measure the speed of the coal feeder mechanism. This component significantly impacts the continuity of electricity production, with an RPN of 160, indicating that this sensor frequently experiences failures, such as inaccuracies in speed measurement due to the sensor overheating. Conversely, the Temperature Indicator is a tool used to read local temperature and is the component with the least damage, having an RPN of 75. All these components are interdependent, so a failure in one component can cause the entire system to malfunction or trip until the damaged component is repaired and returns to normal operation. The Pareto chart is used to address major problems before minor ones and to identify failure points with significant contributions, allowing for optimal improvements by prioritizing resources for corrective actions [15].

4. CONCLUSION

From the reliability analysis of the coal feeder instrumentation at PT. PLN Nusantara Power Up Tenayan, Pekanbaru, using the Failure Mode and Effect Analysis (FMEA) method, several

Volume 11, Issue 2, October 2024, pp. 170-177
ISSN 2355-5068 ; e-ISSN 2622-4852
DOI: 10.33019/jurnalecotipe.v11i2.4505

conclusions can be drawn. Firstly, the analysis identified various failure modes in the coal feeder, including discrepancies between local area and DCS readings, switch failures, and speed measurement issues caused by overheating sensors. Secondly, despite the high Risk Priority Number (RPN) of 160 for the sensor speed, it is still categorized as reliable because it does not exceed the standard RPN threshold of 200. Finally, the ranking of instrumentation components based on their RPN values, from highest to lowest, is as follows: Sensor Speed (160), Belt Sway (112), Flow Transmitter (112), Load Cell (96), Level Transmitter (96), Pressure Transmitter (80), and Temperature Indicator (75). The effects of these failures include operational disruptions, suboptimal performance of the coal feeder, and challenges in monitoring the system effectively.

REFERENCES

[1] I. Pangerang, A. Dengen, A. A. Akbar, R. P. Siwi, and M. Aswin, "Analysis of Coal Feeder Operation on Power Plant Performance at PT. PLN (Persero) PLTU Punagaya 2× 100 MW," Journal of Science and Technology, pp. 1-9, 2023.

[2] Prasetyo, Japri, Sunaryo, "Application of Reliability Centered Maintenance on Ship Unloader Equipment at PLTU Tenayan 2 X 110 MW," Journal of Integrated Industrial Engineering (Jutin), Vol. 3, No. 2, pp. 1-15, November. 2020.

[3] F. S. Nevada, E. B. Utomo, Z. Darojah, and E. Kusumawati, "Risk Priority Number Calculation Using Failure Mode and Effect Analysis Method on Modular Production System," Proceedings of the National Seminar on Electrical Engineering, Information Systems, and Informatics Engineering (SNESTIK), Vol. 1, No. 1, pp. 434-440, June. 2024.

[4] Y. A. A. Sadewa, P. P. Sl, and N. E. Mayangsari, "Analysis of Protective Coating on Coal Feeder and Coal Mill at Fertilizer Company," Conference On Safety Engineering And Its Application, Vol. 2, No. 1, pp. 847-852, December. 2018.

[5] I. Pamungkas and H. T. Irawan, "Risk Reduction Strategy for Critical Boiler Components in the Power Generation Industry," Journal of Optimization, Vol. 6, No. 1, pp. 86-95, 2020.

[6] A. Faizal and S. Arifin, "Reliability Analysis of Instrumentation in Central Mechanical Electrical Unit Using Failure Mode and Effect Analysis (FMEA) Method (Case Study PT. Telkom Area Network Riau Daratan Pekanbaru)," National Seminar on Information and Communication Technology and Industry, pp. 360-366, 2017.

[7] T. J. Wibowo, T. S. Hidayatullah, and A. Nalhadi, "Maintenance Analysis on Lathe Machine Using Reliability Centered Maintenance (RCM) Approach," Journal of Industrial Engineering (JRI), Vol. 3, No. 2, pp. 110-120, 2021.

[8] F. P. Pradana, "Reliability Analysis of Continuous Digester Instrumentation Using Reliability Centered Maintenance (RCM) Method in Pulp Making 8 PT. Indah Kiat Pulp And Paper Perawang Riau," Doctoral Dissertation, Sultan Syarif Kasim State Islamic University Riau, 2022.

[9] A. R. Hidayat, "Optimization Time Analysis for CNC Milling Machine Maintenance Using Value Stream Mapping Approach and Improvement with Failure Mode and Effect Analysis on CNC Milling Machine," Journal of Mechanical Engineering, Vol. 18, No. 3, pp. 345-354, 2023.

[10] D. Ramadhani and G. Putra, "Optimization Analysis of Coal Feeder Machine Using Reliability Centered Maintenance (RCM) Method at PT PLN (Persero) UPK Nagan Raya," Sitekin: Journal of Science, Technology and Industry, Vol. 19, No. 2, pp. 257-265.

[11] S. Andriyan, "Reliability Analysis of Instrumentation in Lime Kiln Unit Using Reliability Centered Maintenance (RCM) Method at PT. Indah Kiat Pulp And Paper Perawang," Doctoral Dissertation, Sultan Syarif Kasim State Islamic University Riau, 2024.

Volume 11, Issue 2, October 2024, pp. 170-177
ISSN 2355-5068 ; e-ISSN 2622-4852
DOI: 10.33019/jurnalecotipe.v11i2.4505

[12] Saputri, S. N., et al. "Application of FMEA Method in Risk Management Assessment of Hospital Information Systems," Journal of Inovtek Polbeng Informatics Series, vol. 9, no. 1, 2024.
[13] Alijoyo, B. Wijaya, and I. Jacob, "Failure Mode and Effect Analysis: Failure Mode and Impact Risk Assessment Based on ISO 31010," CRMS Indonesia, 2016.
[14] M. Rinoza, J. Junaidi, and F. A. Kurniawan, "RPN (Risk Priority Number) Analysis on Double Screw Compressor Machine Component Reliability Using FMEA Method at PT. XYZ Cement Plant," Main Engineering Bulletin, Vol. 17, No. 1, pp. 34-40, 2021.
[15] V. Dofantara, A. Subekti, and H. N. Amrullah, "Component Failure Identification on Container Crane Using Failure Mode Effects and Criticality Analysis (FMECA) and Fault Tree Analysis (FTA)," Conference on Safety Engineering and Its Application, Vol. 7, No. 1, pp. 169-178, October. 2023.

JURNAL ECOTIPE
Electronic, Control, Telecommunication, Information, and Power Engineering

Volume 11, Issue 2, October 2024, pp. 178-186
ISSN 2355-5068 ; e-ISSN 2622-4852
DOI: 10.33019/jurnalecotipe.v11i2.4522

The Characterization of a Thermoelectric Generator Type TEC1-12706 Hybridized on 50 W Polycrystalline PV

Arif Rahman Hakim[1], Mustofa[1], Rustan Hatib[1], Yuli Asmi Rahman[2], Zuryati Djafar[3], Wahyu Haryadi Piarah[3]

[1]Department of Mechanical Engineering, Universitas Tadulako, Palu 9418, Indonesia
[2]Department of Electrical Engineering, Universitas Tadulako, Palu 94148, Indonesia
[3]Department of Mechanical Engineering, Universitas Hasanuddin, Gowa 92171, Indonesia

ARTICLE INFO

Article historys:

Received : …/…/…
Revised : …/…/…
Accepted : …/…/…

Keywords:

Hybrid PV-TEG; Shear resistance; Potentiometer; Thingspeak platform; Thermoelectric generator

ABSTRACT

The capability of solar energy to produce electricity using Thermoelectric Generators (TEG) and Photovoltaic (PV) technology is significant. Therefore, it is important to understand how the technology works. This study aims to characterize the electrical generation of 12 TEG modules type TEC1-12706 hybridized with 2 PV panels. One PV panel is left without a TEG module as a comparison. Meanwhile, on the cold side of the TEG attached to the PV, a heatsink with 3 fins is placed. The left and right fins are air allowed to flow naturally, while the middle fin flows with cold water fluid through a 0.01 m diameter water hose with 2 flow rates; 0.02 and 0.05 m/s. The study showed that the fluid flow rate 0.02 presented a better TEG performance effect than 0.05 m / s at an irradiance of 450 W/m^2. Different things are shown by PV solar panels, where the power generation and efficiency are better in TEG at a flow rate of 0.05 m/s compared to 0.02 m/s for the same irradiance. Overall, the performance of PV-TEG is better at a TEG cooling fluid flow rate of 0.05 m/s.

Corresponding Author:

Mustofa
Department of Mechanical Engineering, Universitas Tadulako, Palu 94148, Indonesia
Email: mustofauntad@gmail.com

1. INTRODUCTION

The study of electrical energy conversion is always interesting if it uses renewable energy as its source, such as solar energy. The abundant, non-polluting and available solar energy potential can be used as energy input for solar panel technology and thermoelectric generator (TEG) modules to generate electrical energy. Photon light emitted to the surface of the PV semiconductor will be converted into electrical energy. In contrast, solar thermal energy transmitted to the surface of the panel will affect the temperature difference on both sides of the TEG as the Seebeck effect is attached to the bottom surface of the PV, thus generating a difference in electrical voltage at both poles of the TEG. The electrical energy output of PV and TEG becomes a broad topic for researchers if combined into PV-TEG. Although the form of energy output is the same, the performance characteristics of the two technologies are different. Many researchers focus on the characteristics of PV cooled with various cooling modes, such as PCM [1-3] and thermoelectric [4-6].

Both PV and TEG use photon and thermal energy sources from the sun and other energy sources including light bulbs. However, light bulbs that have a spectrum similar to solar energy are only Halogen, Xenon, and Mercury as proposed by Doolittle [7]. This encourages researchers to test other types of bulbs including LEDs [8-12]. Although these types of bulbs have the visible light wavelength spectrum (300-700 nm) needed by PV and the near-infrared spectrum between 700 and 900 nm for

JURNAL ECOTIPE
Electronic, Control, Telecommunication, Information, and Power Engineering
Volume 11, Issue 2, October 2024, pp. 178-186
ISSN 2355-5068 ; e-ISSN 2622-4852
DOI: 10.33019/jurnalecotipe.v11i2.4522

TEG needs, the ability of visible light waves in bulbs is relatively low to release covalent bonds of electrons in the valence band to the conduction band in semiconductor materials which produces very small electric currents [9]. Modification of PV and TEG materials is needed to increase their output power if they continue to use these bulbs.

The main reason for combining PV and TEG is to maintain the PV surface temperature below the critical temperature between 60 till 80°C, both experimentally [13-17] and numerically [18,19]. Increasing the PV surface temperature beyond the critical limit will reduce its performance [20]. Therefore, to achieve this effort, a good understanding of the characteristics and performance of not only the PV panel but also the TEG module is required. Siregar [21] characterized the TEC1-12706 type thermoelectric. Unfortunately, the characterization was limited to knowing the open circuit voltage (V_{oc}) of two thermoelectric modules connected in series based on the temperature difference between the two sides of the module, without describing the P-V and I-V characterization in detail. Jaziri et al., [22] provided complete information about the fabrication technology and its implementation which can be used as a benchmark to see the performance of the Peltier module based on its operating conditions.

Based on the above research gap phenomenon, this study aims to characterize the output power and performance of TEG attached to the bottom surface of PV solar panels separately, so that the effects of photon light and solar thermal energy on the PV-TEG system can be widely seen.

2. RESEARCH METHOD

Figure 1 shows the flow diagram of the TEG characteristic testing on PV compared to PV without TEG. There are 3 stages carried out starting from the experimental setup, temperature monitoring with the IoT platform using ThingSpeak application combined with digital multimeters for current and voltage. The last stage is data analysis and conclusion.

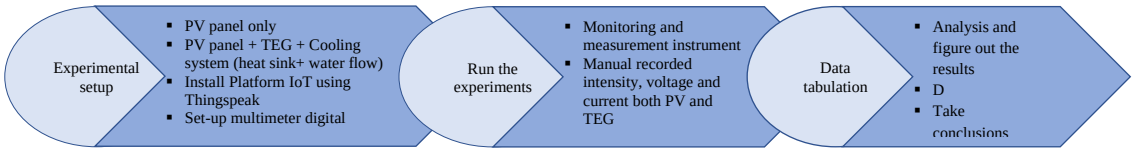

Figure 1. Experimental flow-chart

2.1. TEG and PV module specifications

In general, the main materials used in producing TEG modules are Bi2Te3, $PbSe_{0.5}Te_{0.5}$, $Bi_{0.3}Sb_{1.7}Te_3$, and Zn_4Sb_3, as well as AIN [23]. Our research selected 12 TEG modules based on Bismuth Telluride (Bi2Te3) TEC1-12706 with an operating temperature of -30 to 70°C in white. For PV, three panels of 50 W polycrystalline were used as seen in Figure 2. Two TEG combined PV panels and one PV panel without TEG combined as a comparison. The specifications of the PV used are as in Table 1.

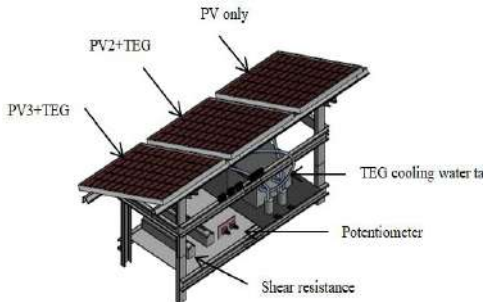

Figure 2. Experimental set-up

JURNAL ECOTIPE
Electronic, Control, Telecommunication, Information, and Power Engineering
Volume 11, Issue 2, October 2024, pp. 178-186
ISSN 2355-5068 ; e-ISSN 2622-4852
DOI: 10.33019/jurnalecotipe.v11i2.4522

Table 1. Specification of PV Polycrystalline 50 W

Rate maximum power (P_{max})	5.0 Wp
Voltage at maximum power (V_{mp})	17.6 V
Current at maximum power (I_{mp})	2.86 A
Open circuit voltage (V_{oc})	21 V
Short circuit current (I_{sc})	3.2 A
Maximum system voltage	1000 V

Twelve TEG modules are connected in series and form a circle configuration as shown in Figure 3. The cold side of the module is attached to an aluminum heat sink that has three fins, where the left and right paths are permitted to have natural airflow, while the middle fin flows with cold water fluid with a flow rate of 0.02 m/s at PV2 and 0.05 m/s at PV3 which aims to maintain the constant temperature of the cold side of the TEG, as well as to obtain a greater temperature difference with the hot side. The greater the temperature difference on both sides of the module, the better its performance [23-25].

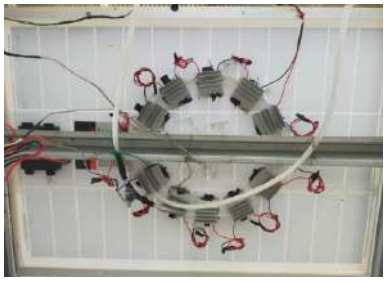

Figure 3. Configuration of 12 TEG modules on the bottom surface of the PV

2.2 Monitoring and measurement instrument

During testing, sensors powered by IoT technology with the Thingspeak application were used to measure the upper and lower surface temperatures of the PV and the cold side temperature of the TEG, which can be monitored live at https://monitoring-pv-mustofa.blogspot.com. The Pasco SF-9569A Digital Voltmeter and Ampere Meter are used to measure the output voltage and current of the PV and TEG, and the Solar Power Meter SM206-SOLAR is for sunlight irradiance. Furthermore, to obtain the characteristics of power (P) - voltage (V) and current (I) - V on the PV, the YOKOGAWA 2791 shear resistor is used with a nominal resistance of 4.7Ω/10Ω, while the 10Ω potentiometer is used as a load on the TEG circuit module.

3. RESULTS AND DISCUSSION

3.1. PV1 characterization

To examine the characteristics of the solar panel, the test was carried out on two irradiance points; a minimum of around 445 W/m^2 and a maximum irradiance of minimum of about 1200 W/m^2 at the time of observation. Figure 4 shows the I-V characteristics of PV1 without TEG at minimum and maximum irradiance. For the PV, the efficiency value is determined as the fraction of incident power that is converted to electricity and is defined as.

$$P_{\max} = V_{OC} I_{SC} FF \tag{1}$$

$$\eta_{PV} = \frac{V_{OC} I_{SC} FF}{P_{in}} \tag{2}$$

$$P_{in} = AG \tag{3}$$

V_{OC} is the open-circuit voltage, I_{SC} is the short-circuit current, FF is the fill factor, A is the area of PV (0.41 m^2) and G is the solar irradiance (W/m^2). In this test, PV-TEG characterization was carried out using three shear resistors on the PV and two potentiometers for the TEG.

JURNAL ECOTIPE
Electronic, Control, Telecommunication, Information, and Power Engineering
Volume 11, Issue 2, October 2024, pp. 178-186
ISSN 2355-5068 ; e-ISSN 2622-4852
DOI: 10.33019/jurnalecotipe.v11i2.4522

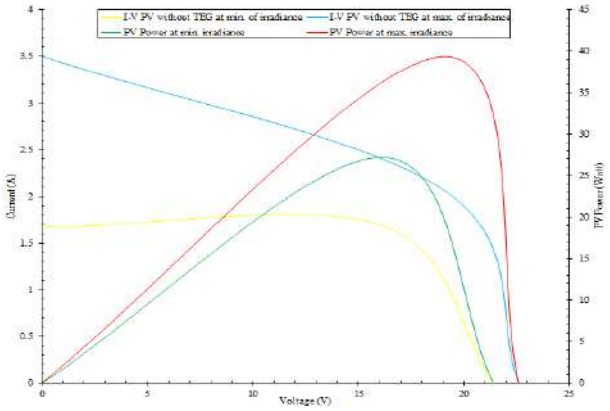

Figure 4. I-V and P-V characteristics of PV without TEG

Figure 4 shows the parameters for determining the results as in Table 2. It can be seen that 14.91% is at the minimum irradiance of 445 W/m^2 and 7.99% is at the maximum irradiance of 1200 W/m^2.

Table 2. Characteristic parameters of PV without TEG for two irradiance points

PV1 without TEG at minimum irradiance of 445 W/m^2				
V_{OC} (V)	I_{SC} (A)	P (W)	FF	η_{PV} (%)
21.4	0	0	0.76	14.91
16.1	1.69	27.21		
0	1.67	0		
PV1 without TEG at maximum irradiance of 1200 W/m^2				
22.6	0	0	0.49	7.99
19.1	2.06	39.35		
0	3.5	0		

3.2. PV2 characterization

The I-V characteristics of PV2 combined with TEG decreased in power at the beginning of the observation but increased by 4.67 Watts during the day compared to PV1 (Figure 2). Similarly, the solar panel performance value increased by 0.96% at maximum irradiance, as shown in Table 3. This suggests that attaching the TEG module to PV has begun to take effect.

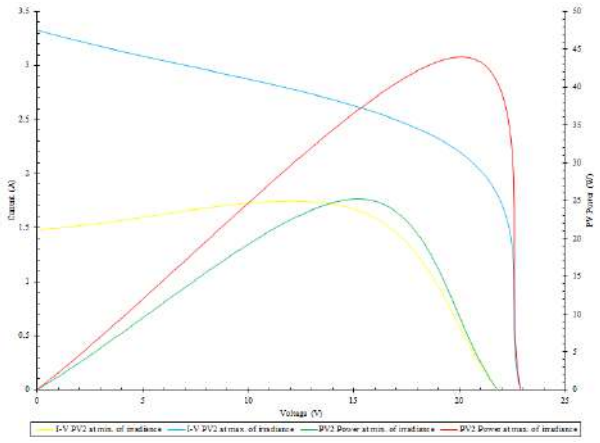

Figure 5. I-V and P-V characteristics of PV2 with TEG1

Table 3. Characteristic parameters of PV2 with TEG1 (TEG cooling fluid flow rate 0.02 m/s)

PV2 combined with TEG at minimum irradiance of 445 W/m^2				
V_{OC} (V)	I_{SC} (A)	P (W)	FF	η_{PV} (%)

JURNAL ECTIPE
Electronic, Control, Telecommunication, Information, and Power Engineering
Volume 11, Issue 2, October 2024, pp. 178-186
ISSN 2355-5068 ; e-ISSN 2622-4852
DOI: 10.33019/jurnalecotipe.v11i2.4522

21.8	0	0	0.78	13.83
15.2	1.66	25.232		
0	1.48	0		
PV2 combined with TEG at maximum irradiance of 1200 W/m^2				
22.9	0	0	0.58	8.95
20.1	2.19	44.02		
0	3.33	0		

3.3. PV3 characterization

Unlike the 2 PVs above, PV3 in Figure 6 and Table 4 shows the effect of the TEG combination on PV in terms of increasing actual power and efficiency when compared to PV without a waste heat absorption module. Power and efficiency characteristics increase simultaneously in PV. In PV without TEG from 27.21 W to 28.181 W in PV with TEG and from PV efficiency of 14.91% to 15.54% under the same conditions at minimum irradiance. Meanwhile, in the maximum irradiance conditions, the power increases from 39.35 W to 45.70 W and from 7.99% to 9.29%. One of the factors is that the flow rate of the cooling fluid on the cold side of the TEG significantly increases the ΔT of the TEG module and the PV surface.

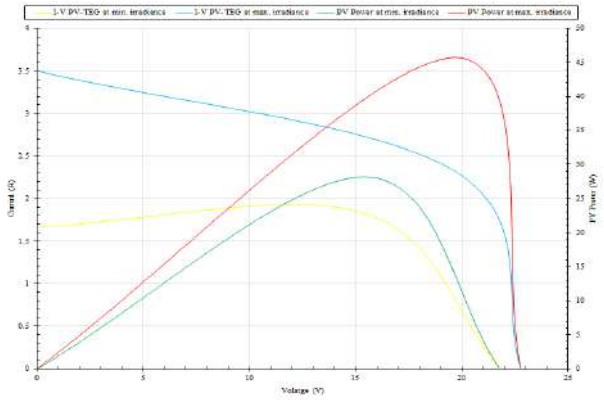

Figure 6. I-V and P-V characteristics of PV3 with TEG2

Table 4. Characteristic parameters of PV3 with TEG2 (TEG cooling fluid flow rate 0.05 m/s)

PV3 combined with TEG at minimum irradiance of 445 W/m^2				
V_{OC} (V)	I_{SC} (A)	P (W)	FF	η_{PV} (%)
21.8	0	0	0.78	15.45
15.4	1.83	28.182		
0	1.67	0		
PV3 combined with TEG at maximum irradiance of 1200 W/m^2				
22.	0	0	0.57	9.29
19.7	2.32	45.70		
0	3.5	0		

The figure and table above indicate that the efficiency and power of PV hybridized with TEG module circular configuration are better at a cooling fluid flow rate of 0.05 m/s compared to 0.02 m/s and with PV without TEG. This is also seen in the electrical power of the type of PV hybridized with a rectangular TEG module configuration [24]. One of the parameters that cause this to happen is the difference in PV surface temperature, where the upper surface temperature of PV2+TEG1 water cooling rate 0.02 m/s is higher than PV3+TEG2 with TEG water cooling rate 0.05 m/s (43.75°C> 40.75°C at minimum irradiance and 60.125°C>47°C at maximum irradiance). Therefore, the combination of TEG modules and their cooling types provides good recommendations for improving the performance of the PV-TEG system.

3.4. TEG1 and TEG2 characterization

The characteristics of TEG1 are different from PV2 even though they both produce electrical energy. The formulation used to calculate the efficiency of the TEG module is based on the maximum

JURNAL ECOTIPE
Electronic, Control, Telecommunication, Information, and Power Engineering
Volume 11, Issue 2, October 2024, pp. 178-186
ISSN 2355-5068 ; e-ISSN 2622-4852
DOI: 10.33019/jurnalecotipe.v11i2.4522

conversion efficiency that could be expressed in the function of the Carnot efficiency ($(T_h-T_c)/T_h$) and the dimensionless figure of merit factor of the materials used as [26] with a ZT value of 0.7 or 1 for the type of TEG material used in this study [22][27].

$$\eta_{TEG1\max} = \frac{T_h - T_c}{T_h} \frac{(\sqrt{1+ZT}-1)}{\sqrt{1+ZT}+{}^{T_C}\!/_{T_h}} \tag{4}$$

Where T_h and T_c are TEG hot side and cold side temperatures, simultaneously. Using equation (4) based on test data, the value of $\eta TEG1_{max}$ at PV2 is 8.7% at ΔT 6°C. Furthermore, Figure 7 shows the general characteristics of the TEG module, where moderate increase in electric power accompanies the sharp decrease in TEG electric current. The increase in power continues until the maximum power point and decreases sharply after the peak until the voltage approaches the maximum. The figure also shows the magnitude of the equivalent power with the magnitude of the temperature difference between the two sides of the module. At ΔT 8°C, the TEG1 power is 0.006 W compared to 0.003 W at ΔT 6°C.

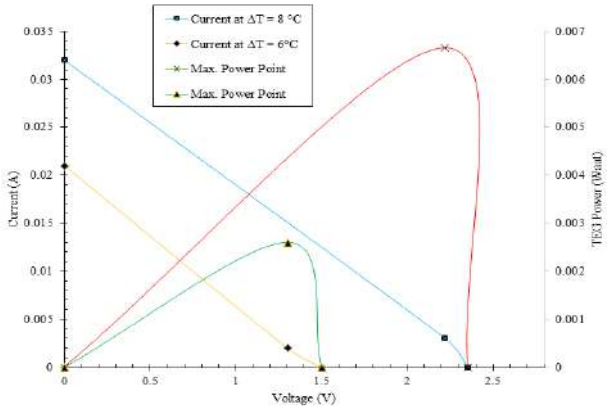

Figure 7. I-V and P-V characteristics of TEG1 attached to PV2

In contrast, Figure 8 shows the difference in characterization of TEG2 on PV3 with TEG1 on PV2. The output power of TEG2 increased by 0.0033 W/m^2 or more than 50% compared to the generated power on TEG1 in maximum solar thermal radiation (1200 W/m^2). Interestingly, at the beginning of the observation, the output power of TEG1 was actually greater than TEG2 (0.0026 > 0.0013 W). This is likely due to the rate of water cooling on the cold side of the TEG which began to have an effect when the sun's intensity increased.

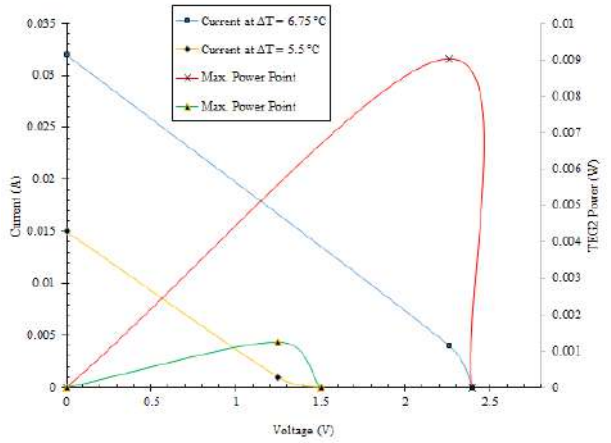

Figure 8. I-V and P-V characteristics of TEG2 attached to PV3

JURNAL ECTIPE
Electronic, Control, Telecommunication, Information, and Power Engineering
Volume 11, Issue 2, October 2024, pp. 178-186
ISSN 2355-5068 ; e-ISSN 2622-4852
DOI: 10.33019/jurnalecotipe.v11i2.4522

Regarding the module's performance, TEG1 is better than TEG2 (8.07>6.71%) at minimum irradiance. The same thing happens at maximum irradiance (10.09>8.09%). The characteristics of TEG that occurred in this study are akin to the research results conducted by Piarah *et al*., [9], the difference lies in the thermal energy source used from a Halogen bulb with a power of only about 1 µW.

In this research, the characteristics of TEG are visible where the increase in electrical voltage (V) is accompanied by a sharp decrease in current (I), while the output power increases to a peak point and decreases thereafter. Unlike TEG, the characteristics of PV show that the position of the electrical current tends to be flat when the voltage and electrical power increase. The decrease in current occurs when it reaches the maximum power point (MPP).

4. CONCLUSION

The characterization analysis of the thermoelectric generator type TEC1-12706 made from Bismuth Telluride (Bi2Te3) shows that the I-V and P-V generation are increasingly different from PV. The number and configuration of TEG modules attached to the bottom surface of the PV also have a major influence on PV performance. The more TEG modules with even circulation of cooling fluid on the cold side of the module, the better the effect on PV performance. This research also proves that using the Thingspeak platform as an IoT application is very accurate in helping to provide temperature data for the PV-TEG hybrid system.

ACKNOWLEDGMENTS

Our highest gratitude to all parties who helped experimental set up of this research and writes the scientific paper, both in mechanical and electrical engineering UNTAD and mechanical engineering UNHAS.

REFERENCES

[1] A. N. Al-shamani, “Using Hybrid System Photovoltaic Thermal / Phase Change Materials / Thermoelectric (PVT / PCM / TE): A Review,” vol. 2022, no. 1365, pp. 1365–1400, 2022.

[2] A. Makki, S. Omer, and H. Sabir, “Advancements in hybrid photovoltaic systems for enhanced solar cells performance,” *Renew. Sustain. Energy Rev.*, vol. 41, pp. 658–684, 2015, doi: 10.1016/j.rser.2014.08.069.

[3] G. Muthu, S. Thulasi, V. Dhinakaran, and T. Mothilal, “Performance of solar parabolic dish thermoelectric generator with PCM,” *Mater. Today Proc.*, vol. 37, no. Part 2, pp. 929–933, 2020, doi: 10.1016/j.matpr.2020.06.123.

[4] S. U. A and S. A. Jumaat, “The Hybrid Photovoltaic-Thermoelectric Generator Configurations for Energy Performance Improvement,” *Int. J. Integr. Eng.*, vol. 14, no. 3, 2022, doi: 10.30880/ijie.2022.14.03.001.

[5] Mustofa *et al.*, “Low Sun spectrum on simulation of a thin film photovoltaic, heat absorber, and thermoelectric generator system,” *Nihon Enerugi Gakkaishi/Journal Japan Inst. Energy*, vol. 99, no. 8, 2020, doi: 10.3775/jie.99.88.

[6] R. E. Rachmanita, C. N. Karimah, and N. Azizah, “Experimental investigations on the performance of thermoelectric generator as energy conversion system,” *IOP Conf. Ser. Earth Environ. Sci.*, vol. 672, no. 1, 2021, doi: 10.1088/1755-1315/672/1/012103.

[7] A. Doolittle, “Lecture 2 : The Nature of Light Reading Assignment – Chapter 2 of PVCDROM The Nature of Light,” *Nat. Light. Read. Assign.*, p. Chapter 2, 2007, [Online]. Available: http://users.ece.gatech.edu/~alan/ECE4833/Lectures/Lecture2_PropertiesOfSunlight.pdf

[8] Mustofa, Z. Djafar, W. H. Piarah, and Syafaruddin, “A New Hybrid of Photovoltaic-thermoelectric Generator with Hot Mirror as Spectrum Splitter,” *J. Phys. Sci.*, vol. 29, pp. 63–75, 2018.

[9] W. H. Piarah, Z. Djafar, Syafaruddin, and Mustofa, “The characterization of a spectrum splitter of Techspec AOI 50.0mm square hot and cold mirrors using a halogen light for a photovoltaic-thermoelectric generator hybrid,” *Energies*, 2019, doi: 10.3390/en12030353.

Volume 11, Issue 2, October 2024, pp. 178-186
ISSN 2355-5068 ; e-ISSN 2622-4852
DOI: 10.33019/jurnalecotipe.v11i2.4522

[10] Mustofa, Basri, and Y. A. Rahman, "Experimental investigation from different focal length of Fresnel lens on thermoelectric generators performance," in *IOP Conf. Series: Earth and Environmental Science 175 (2018) 012004*, IOP Conference Series: Earth and Environmental Science, 2018.

[11] Mustofa, Iskandar, Muchsin, S. Suluh, and T. M. Kamaludin, "The effectiveness of a mini photovoltaic cell by using light LED bulbs as a source of photon energy," *IOP Conf. Ser. Earth Environ. Sci.*, vol. 926, no. 1, 2021, doi: 10.1088/1755-1315/926/1/012090.

[12] Mustofa, S. P. Krisnawan, R. Hatib, Iskandar, Asmeati, and Hariyanto, "Harvesting of Photon Energy through PV on Building Envelope and Windows Canopy," *IOP Conf. Ser. Earth Environ. Sci.*, vol. 1157, no. 1, 2023, doi: 10.1088/1755-1315/1157/1/012036.

[13] A. Abdo, M. Ahmed, and S. Ookawara, "Efficient Operation of Hybrid Photovoltaic-Thermoelectric System Combined With Micro-," *16th Int. Conf. Clean Energy*, no. May, pp. 9–11, 2018.

[14] D. Kraemer, L. Hu, A. Muto, X. Chen, G. Chen, and M. Chiesa, "Photovoltaic-thermoelectric hybrid systems: A general optimization methodology," *Appl. Phys. Lett.*, vol. 92, no. 24, 2008, doi: 10.1063/1.2947591.

[15] H. Demir, "Application of Thermal Energy Harvesting from Photovoltaic Panels," *Energies*, vol. 15, no. 21, 2022, doi: 10.3390/en15218211.

[16] M. A. Qasim, V. I. Velkin, S. E. Shcheklein, S. A. Salih, B. A. Aljashaami, and A. A. Sammour, "Conversion of Heat Generated During Normal PV Panel Operation into Useful Energy via a Hybrid PV-TEG Connection," *Int. J. Renew. Energy Res.*, vol. 12, no. 4, pp. 1779–1786, 2022, doi: 10.20508/ijrer.v12i4.13471.g8603.

[17] M. A. Qasim, V. I. Velkin, and S. E. Shcheklein, "Experimental study on hybridization of a PV–TEG system for electrical performance enhancement using heat exchangers, energy, exergy and economic levelized cost of energy (LCOE) analysis," *Clean Energy*, vol. 7, no. 4, pp. 808–823, 2023, doi: 10.1093/ce/zkad023.

[18] J. Islam, "Numerically Performance Analyses of a PV-TEG System under Climate Condition of Chittagong ICMERE2023-PI-082 Numerically Performance Analyses of a PV-TEG System under Climate Condition of Chittagong," no. January, 2024.

[19] A. Das and S. Datta Peu, "Modeling of PV cell, PV Module, PV array and PV IV characteristics analysis using MATLAB/SIMULINK," no. x, 2022, doi: 10.20944/preprints202209.0304.v1.

[20] R. P. Dewi and S. Rahmat, "Feasibility Analysis of the Implementation of a Photovoltaic Water Cooling System," *J. Ecotipe (Electronic, Control. Telecommun. Information, Power Eng.*, vol. 11, no. 1, pp. 19–28, 2024, doi: 10.33019/jurnalecotipe.v11i1.4442.

[21] A. R. Siregar, "Analisis Pengaruh Karakteristik Termoelektrik Generator Seabagi Peubah Energi Panas," *J. Pendidik. Sains dan Komput.*, vol. 2, no. 02, pp. 235–241, 2022, doi: 10.47709/jpsk.v2i02.1530.

[22] N. Jaziri, A. Boughamoura, J. Müller, B. Mezghani, and F. Tounsi, "A comprehensive review of Thermoelectric Generators : Technologies and common applications," *Energy Reports*, vol. 6, pp. 264–287, 2020, doi: 10.1016/j.egyr.2019.12.011.

[23] P. L. Alluri, D. R. Alli, and D. V. R. K. Reddy, "Studies on the TEG with changes in temperature difference and material properties," *Int. J. Innov. Res. Sci. Stud.*, vol. 7, no. 1, pp. 63–72, 2024, doi: 10.53894/ijirss.v7i1.2439.

[24] Y. A. Rahman, M. Masarrang, K. Malvino, and T. Sau, "Enhanced of PV-TEG Performance and Water Cooling on TEG with Serial Different Configurations," 2024.

[25] T. Muhtar Kamaludin, S. Awal Syahrani, W. Danny Syamsu, Basri, and Mustofa, "Experimental study of cascaded thermoelectric generators with differences in focal length using LED lights energy radiation," *IOP Conf. Ser. Mater. Sci. Eng.*, vol. 909, no. 1, 2020, doi: 10.1088/1757-899X/909/1/012023.

[26] H. S. Kim, W. Liu, G. Chen, C. W. Chu, and Z. Ren, "Relationship between thermoelectric figure of merit and energy conversion efficiency," *Proc. Natl. Acad. Sci. U. S. A.*, vol. 112, no. 27, pp. 8205–8210, 2015, doi: 10.1073/pnas.1510231112.

Volume 11, Issue 2, October 2024, pp. 178-186
ISSN 2355-5068 ; e-ISSN 2622-4852
DOI: 10.33019/jurnalecotipe.v11i2.4522

[27] B. Beltrán-Pitarch, J. Prado-Gonjal, A. V. Powell, P. Ziolkowski, and J. García-Cañadas, "Thermal conductivity, electrical resistivity, and dimensionless figure of merit (ZT) determination of thermoelectric materials by impedance spectroscopy up to 250 °C," *J. Appl. Phys.*, vol. 124, no. 2, 2018, doi: 10.1063/1.5036937.

JURNAL ECOTIPE
Electronic, Control, Telecommunication, Information, and Power Engineering

Volume 11, Issue 2, October 2024, pp. 187-194
ISSN 2355-5068 ; e-ISSN 2622-4852
DOI: 10.33019/jurnalecotipe.v11i2. 4504

Reliability Analysis of Steam Turbine Instrumentation Using the Failure Mode and Effect Analysis (FMEA) Method at PT. PLN Nusantara Power UP Tenayan

Anzhar Devalma[1], Jufrizel[2], Aulia Ulah[3], Ahmad Faizal[4]
[1,2,3,4] Sultan Syarif Kasim Riau State Islamic University, Jl. HR. Soebrantas No. Km 15, Riau, 28923

ARTICLE INFO

Article history:

Received : …/…/…
Revised : …/…/…
Accepted : …/…/…

Keywords:

Failure mode and effect analysis, Realiability, Steam turbine.

ABSTRACT

PT. PLN Nusantara Power Unit Generation Tenayan is a company operating in the Steam Power Plant sector in Pekanbaru, Indonesia. One of the main components of a steam power plant (PLTU) is a steam turbine. A steam turbine is a machine that functions to convert kinetic energy into electrical current. Operational failures are often caused by less than optimal instrumentation in the steam turbine. This research uses the failure mode and effect analysis (FMEA) method with the aim of identifying the type of failure, the cause of the failure, the effect of the failure, and determining the RPN value. The analysis results from this research show that the turbine instrumentation components still meet performance standards because the risk priority number (RPN) value is less than 200. The conclusion from this research is that errors in steam turbine instrumentation are inaccurate sensor readings, switches cannot deactivate the equipment, and readings control room does not match local readings, the instrumentation component with the highest risk priority number (RPN) is the solenoid valve with a value of 140, and the instrumentation component with the lowest risk priority number (RPN) is the pressure indicator with a value of 30. The component given top priority in action The recommendation is for the solenoid valve component, namely to carry out maintenance every 6 months and add an overspeed protection system.

Corresponding Author :

Jufrizel
Sultan Syarif Kasim Riau State Islamic University, 28129, Pekanbaru
Email: jufrizel@uin-suska.ac.id

1. INTRODUCTION

The type of secondary energy most commonly used by humans is electrical energy, electrical energy is produced from the conversion of primary energy sources such as water, wind, petroleum, coal, sunlight, gas, and others [1] . Electrical energy can be easily converted into various forms of energy and easily transferred from one form to another [2] . Therefore, electrical energy is mandatory for the production process to take place, both for large and small industries [3] .

The need for electrical energy in Indonesia is increasing every year, one of which is Riau province. From data from the Central Statistics Agency, Riau province has an area of 87,023.66 km2 with a population in 2016 of 6,500,971 people, in 2017 of 6,657,911 people, in 2018 of 6,814,909 people, and in 2019 of 6,971,745 soul. This increasing population growth causes a very large need for electrical energy [4] . Therefore, PT. PLN Nusantara Power UP Tenayan built PLTU Tenayan Raya to overcome the electrical energy crisis that occurred in Riau (Fadilla et al., 2023). Steam power plants

JURNAL ECTIPE
Electronic, Control, Telecommunication, Information, and Power Engineering
Volume 11, Issue 2, October 2024, pp. 187-194
ISSN 2355-5068 ; e-ISSN 2622-4852
DOI: 10.33019/jurnalecotipe.v11i2. 4504

(PLTU) are plants that rely on kinetic energy from steam to produce electrical energy [1] . PLTU Tenayan has a capacity of 2 × 110 Mega Watt [5] .

In carrying out the process, the Tenayan Steam Power Plant (PLTU) involves a series of complex stages, supported by various kinds of equipment and machines. However, the production process of Steam Power Plants (PLTU) is often hampered. This is caused by a failure in the instrumentation components on the machine used, which results in disruption of the electrical energy production process. One machine that often fails is the steam turbine.

One of the main components in a steam power plant is a turbine [6] . A steam turbine is a machine that functions to convert kinetic energy into electrical current [7] . A simple steam turbine has one moving part called a rotor. When fluid flows into the turbine, the blades rotate, producing the energy needed to move the rotor [8] . In a steam turbine there are several instrumentation components such as temperature indicators, vibration sensors, resistance temperature detection, pressure indicators, temperature indicator switches, solenoid valves, limit switches, pressure transmitters.

From the results of interviews and observations carried out directly with the instrumentation and control team leader at PT. PLN Nusantara Power UP Tenayan, it is known that failures that occur in steam turbine instrumentation components can cause damage to other components, and result in the performance of the steam turbine not being optimal. In order to ensure that the components in the steam turbine run well, it is necessary to prevent failure to identify potential causes of failure that will occur. One maintenance method that is able to identify failures is the Failure Mode and Effect Analysis (FMEA) method [9] . In the FMEA analysis process, there are three variables used to determine the problem, including severity, frequency and detection level [10] .

In research [11] discussed the damage that occurred on the Al Pin 350 lathe machine, and succeeded in proving that the machine was still in the reliable category and was proven by calculating the risk priority number (RPN) value using the failure mode effect and analysis (FMEA) method, even though the machine there is damage with the highest RPN but it is still in the reliable category. Research [12] Analysis that was carried out using the Failure Mode and Effect Analysis (FMEA) method succeeded in obtaining important components in lubricant system failures that require high priority for maintenance activities in the lubrication system on ships.

In research conducted by [13] using the failure mode and effect analysis (FMEA) method, it succeeded in identifying the failure mode and the failure effects resulting from the failure, and was able to provide recommendations for actions that the company should take to reduce the effects of failure. It was discovered that failures had an RPN value. The highest is still in the low category, but the frequency of damage occurs frequently and cannot be ignored.

Another study [14] also discussed the reliability of thresher machine components using the FMEA method. The researchers succeeded in getting availability values for machine components and knowing which equipment required special maintenance. In another study [15] also analyzed the RPN value of double screw compressor machine components using the FMEA method, and it can be seen that the FMEA method is able to identify failures and analyze the RPN value on double screw compressor machines by getting the highest RPN value and getting the lowest availability of components. double screw compressor machine.

Based on several related studies above, the FMEA method is able to identify failures and reduce the occurrence of failures by providing suggestions for preventive or maintenance actions for machine components that have the highest RPN values. The author is interested in conducting research which aims to determine the RPN value and analyze failures that occur in steam turbine instrumentation at PT. PLN Nusatara Power UP Tenayan using the failure mode and effect analysis (FMEA) method.

2. RESEARCH METHOD

2.1. Research Design

This research is illustrated in a flow diagram which aims to explain the steps in conducting research, the research diagram is shown in Figure 1 Research flowchart.

JURNAL ECTIPE
Electronic, Control, Telecommunication, Information, and Power Engineering
Volume 11, Issue 2, October 2024, pp. 187-194
ISSN 2355-5068 ; e-ISSN 2622-4852
DOI: 10.33019/jurnalecotipe.v11i2. 4504

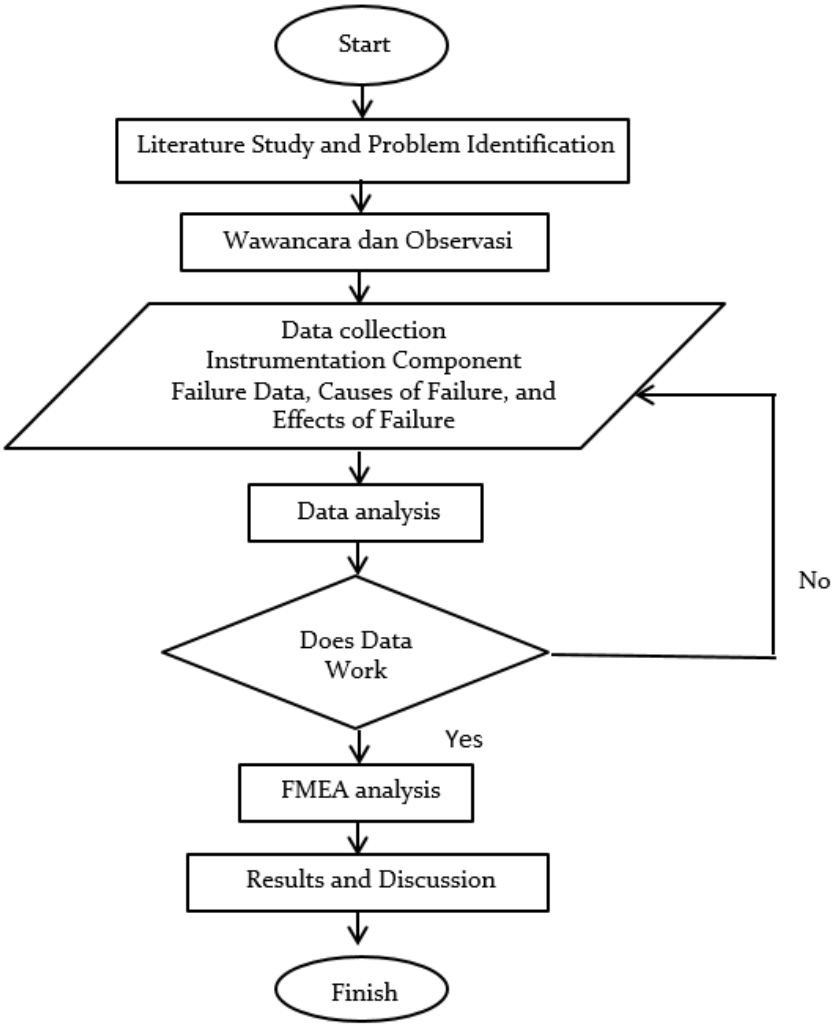

Figure 1. Research Flowchart

2.2. FMEA analysis

Failure Mode and Effect Analysis (FMEA) is a method that can be used to identify and eliminate defects or failures in products during the production process. FMEA can be used to define the consequences of failure at each stage, then create priorities related to prevention and improvement efforts, with the aim that the products produced in the next production process can be in accordance with customer wishes. In the FMEA analysis process, there are three variables used to determine the problem, including severity, frequency and detection level [10] .

In the FMEA method, the risk priority number (RPN) is calculated to determine the highest level of failure risk, by connecting three criteria, namely severity, occurrence and detection. The higher the RPN value, the lower the level of reliability of a system's components [15]. To determine the level of risk of failure, it can be written using the following equation

$$RPN = Sev \times Occ \times Det \quad (1)$$

Information
RPN = risk priority number
Sev = severity (level of damage)
Occ = occurrence (frequency)
Det = detection (detection level)

JURNAL ECOTIPE
Electronic, Control, Telecommunication, Information, and Power Engineering
Volume 11, Issue 2, October 2024, pp. 187-194
ISSN 2355-5068 ; e-ISSN 2622-4852
DOI: 10.33019/jurnalecotipe.v11i2. 4504

3. RESULTS AND DISCUSSION

3.1. Failure Mode Effect And Analysis

Failure mode effect and analysis is used to see the steam turbine instrumentation components that most often fail during the electricity production process. FMEA worksheet table which functions to provide severity, occurrence and detection values based on potential failure effects, causes of failure and control processes carried out, thus producing a risk priority number (RPN) value. The FMEA worksheet can be seen in table 1 below:

Table 1. FMEA Worksheet

No	Component	*function*	*Potential Failure Mode*	*Potential Effect Failure*	SEV	*Potential Of Failure*	OCC	*Current Control*	DET	RPN	*Recommended Action*
1	Pressure transmitters	Measuring pressure and carrying out monitoring	Error sensor reading	Damage to other components	5	The sensor is infected with dirt or dust	4	Readings on DCS do not match local	4	80	Carry out preventive maintenance every 6 months and provide special protection so that it is not easily infected by dirt
2	Temperature indicator	Temperature measurement in steam turbines	Function failure	The performance of the steam turbine is not optimal	4	High temperature	5	The temperature indicator indication is not accurate	3	60	Carry out preventive maintenance every 6 months and add a temperature protection system
3	Temperature indicator switch	Controls the temperature on the turbine	The switch failed to turn off the equipment	Trip units	8	Age of use	2	The equipment remains active at elevated temperatures	7	112	Carry out checks and maintenance every 6 months
4	Vibraton sensor	Measuring vibrations in steam turbines	Sensor readings are inaccurate	Trip units	8	Corrosion sensor connector cable	4	The reading in the control room is unreadable	3	128	Carry out preventative maintenance every 6 months and provide a protection system to prevent excessive vibration
5	Resistance temperature detector	Detect and monitor temperature changes	Overheating or excessive temperature in the turbine	Damage to other devices	5	Improper calibration	5	Readings in the control room are local	4	100	Recalibrate the sensor every 6 months and add a protection system for overheating
6	Solenoid valve	Controls fluid flow automatically	Failure to control fluid flow to the turbine	Fluid entering the turbine is excessive (overspeed)	7	Damaged or disconnected connection cable	5	Computers in the control room	4	140	Carry out maintenance every 6 months and add an overspeed protection system
7	Pressure indicator	Pressure gauge on steam turbine	The reading on the pressure indicator is inaccurate	damage to other related devices	5	Long service life	2	Readings on local indicators are inaccurate	3	30	Carry out preventative maintenance once every 1 year

JURNAL ECOTIPE
Electronic, Control, Telecommunication, Information, and Power Engineering
Volume 11, Issue 2, October 2024, pp. 187-194
ISSN 2355-5068 ; e-ISSN 2622-4852
DOI: 10.33019/jurnalecotipe.v11i2. 4504

1. Pressure transmitter

This instrumentation component functions to measure pressure and carry out monitoring by sending electrical signals to the controller. Failure occurs when the reading from the sensor is inaccurate, causing damage to other components because the sensor is contaminated by dirt or dust. This can be seen from the reading on the DCS not matching the local reading. The instrument and control team leader gave a score of 5 for severity, gave a score of 4 for frequency of occurrence, and gave a score of 4 for level of detection. So the RPN value is 80.

2. Temperature indicator

This instrumentation component functions as a temperature measurement in the steam turbine. The failure that occurred was an error in the temperature sensor reading. So it can result in high temperatures and have an effect on non-optimal steam turbine performance. This can be seen from the inaccurate indication of the temperature indicator. The instrument and control team leader gave a score of 4 for severity, gave a score of 5 for frequency of occurrence, and gave a score of 3 for detection level. So the RPN value is 60.

3. Temperature indicator switch

This instrumentation component functions as a device that automatically activates or deactivates based on the temperature detected in the steam turbine. The failure that occurs in this component is that the switch fails to turn off the equipment when overheating occurs due to the lifetime of the temperature sensor, resulting in the unit tripping. This can be seen from the device remaining active at increasing temperatures. The instrument and control team leader gave a score of 8 for severity, gave a score of 2 for frequency of occurrence, and gave a score of 7 for detection level. So the RPN value is 112.

4. Vibration sensor

This instrumentation component functions as a vibration measurement in the steam turbine. Failure occurs because the sensor readings are inaccurate, which can result in excessive vibration and the effect of the unit shutting down. This is caused by corrosion of the cable or connector and can be seen from the CCR (central control room) being unreadable. The instrument and control team leader gave a score of 8 for severity, gave a score of 4 for frequency of occurrence, and gave a score of 3 for detection level. So the RPN value is 128.

5. Resistance temperature detector

This instrumentation component functions to detect changes and monitor temperature changes and can be monitored from the DCS (distributed control system) room. Failure is overheating or excessive temperature in the turbine which occurs because the readings on the DCS do not match the local readings. This can result in damage to the related equipment and it not being able to work properly, which is caused by improper cable calibration and can be seen from the readings in the control room. The instrument and control team leader gave a score of 5 for severity, gave a score of 5 for frequency of occurrence, and gave a score of 4 for detection level. So the RPN value is 100.

6. Solenoid valve

This instrumentation component functions to control fluid flow automatically. The failure that occurs is the inability to control the fluid flow due to damaged or disconnected cables or connections, causing the fluid entering the turbine to be uncontrolled, in other words, it can cause overspeed. This can be seen from the computer in the control room where the rotation of the turbine increases due to uncontrolled fluid flow entering the turbine. The instrument and control team leader gave a score of 7 for severity, gave a score of 5 for frequency of occurrence, and gave a score of 4 for level of detection. So the RPN value is 140.

7. Pressure indicator

This instrumentation component functions as a pressure gauge in the steam turbine. The failure that occurs is that the pressure reading on the pressure indicator is inaccurate due to the age of the sensor, this can cause damage to other devices because the pressure exceeds the safe limit. This can be

JURNAL ECOTIPE
Electronic, Control, Telecommunication, Information, and Power Engineering
Volume 11, Issue 2, October 2024, pp. 187-194
ISSN 2355-5068 ; e-ISSN 2622-4852
DOI: 10.33019/jurnalecotipe.v11i2. 4504

seen from the indication on the pressure indicator which is not actual.sentence. The instrument and control team leader gave a score of 5 for severity, gave a score of 2 for frequency of occurrence, and gave a score of 3 for detection level. So the RPN value is 30.

From the analysis carried out on the steam turbine instrumentation components at PT. PLN Nusantara Power Up Tenayan using the failure mode and effect analysis (FMEA) method has produced a risk priority number (RPN) value for the steam turbine instrumentation, and it can be seen from the FMEA worksheet table above, it can be summarized from highest to lowest as follows in table 2 below. The results of identifying the RPN value on steam turbine instrumentation show that all components of the steam turbine instrumentation have an RPN value below 200. Based on the literature, an RPN value that has a value range of less than 200 means that the risk of this condition is considered low, and the instrumentation can be categorized as reliable [16] .

Table 2. Risk Priority Number Steam Turbine

NO	Component	Risk Priority Number (RPN)
1	Pressure transmitters	80
2	Temperature indicator	60
3	Temperature Indicator Switch	112
4	Vibration sensor	128
5	Resistance temperature detector	100
6	Solenoid valve	140
7	Pressure Indicator	30

Based on the results of reliability analysis carried out using the qualitative FMEA method. So it is found that the instrumentation components have risk priority number (RPN) values from highest to lowest, namely solenoid valve 140, vibration sensor 128, temperature indicator switch 112, resistance temperature detector 100, pressure transmitter 80, temperature indicator 60, and pressure indicator 30. The following is a form of Pareto diagram that makes it easier for readers to briefly identify the components that have the highest RPN values and the components that have the lowest RPN values.

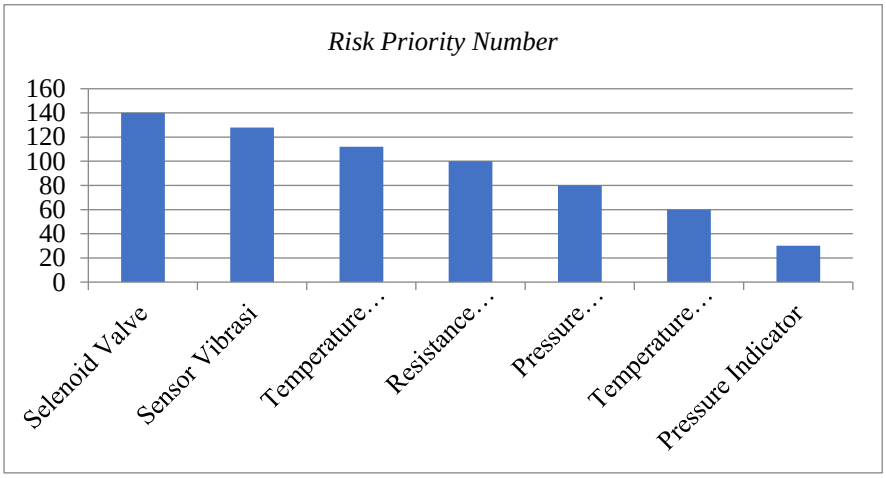

Figures 2. Steam Turbine Pareto Diagram

From the Pareto diagram above, it shows that the largest RPN value lies in the solenoid valve component which is useful for controlling fluid flow automatically. This component is very influential in the continuity of electricity production with an RPN value of 140, which means that this component often experiences failures such as failure to control fluid flow to the turbine. Meanwhile, the pressure indicator component is an instrumentation tool that is useful for measuring pressure in steam turbines, which is the component that experiences the least damage with an RPN of 30. All of these components depend on other components, because if one component is damaged then the system cannot run or can be said to trip until the damaged component can return to normal operation.

Volume 11, Issue 2, October 2024, pp. 187-194
ISSN 2355-5068 ; e-ISSN 2622-4852
DOI: 10.33019/jurnalecotipe.v11i2. 4504

4. CONCLUSION

Based on the results of the reliability analysis of the instrumentation system on the PT steam turbine. PLN Nusantara Power UP Tenayan Pekanbaru, using the faiure mode and effect analysis (FMEA) method, it can be concluded that.

1. After analyzing the instrumentation system on the steam turbine using the failure mode and effect analysis (FMEA) method, it can be seen that the instrumentation component on the steam turbine that has the highest RPN value is the solenoid valve with a value of 140, even though the solenoid valve component has the highest value but still in the reliable category.
2. The results of identifying the type of failure that occurred in the steam turbine were that the readings from the sensors were inaccurate, the switch failed to turn off the equipment, and the readings in the control room did not match local conditions.
3. The causes of failure are sensors contaminated by dirt, age, improper calibration, and corroded or disconnected connection cables.
4. The effects of failure caused by failure of instrumentation components are damage to other related components, the performance of the steam turbine is not optimal, excessive speed occurs and the unit shuts down.

REFERENCES

[1] R. Apriandi and A. Mursadin, “Steam Turbine Performance Analysis Based on Performance Test of Pt Pt. Indocement P-12 Tarjun,” *Sci. J. Mech. Eng. Kinemat.* , vol. 1, no. 1, pp. 37–46, 2016, doi: 10.20527/sjmekinetika.v1i1.26.

[2] A. Rahman Hafiz, A. Nuramal, and N. Iman Supardi, "ANALYSIS OF ELECTRICITY PRODUCTION IN MINIHYDRO POWER PLANT (PLTM) Analysis of Electricity Production in Mini Hydro Power Plants (PLTM)," *J. Rekayasa Mek.* , vol. 6, no. 1, p. 2022, 2022.

[3] PRH Marpaung, H. Eteruddin, and D. Setiawan, "Study of Load Changes on AVR Performance on Synchronous Generator Unit 2 of PT Steam Power Plant (PLTU). Ubjom Tenayan Raya,” *Semin. Nas. Science Works. Multidisciplinarity* , vol. 1, no. 1, pp. 96–109, 2021.

[4] E. Team, “20. JT, Vol.14, No.2, Transient Analysis of the Riau 150 kV Transmission System After the Operation of PLTU Tenayan Raya, AiO”.

[5] rahayu deny danar and alvi furwanti Alwie, AB Prasetio, R. Andespa, PN Lhokseumawe, and K. Introduction, "Final Assignment Final Project," *J. Ekon. Vol. 18, Number 1 March 201* , vol. 2, no. 1, pp. 41–49, 2020.

[6] R. Djafar, B. Liputo, and Y. Djamalu, "Determining Energy Losses in Main Components of PLTU Using Cylcle Tempo Simulation," *J. Teknol. Pertan. Gorontalo* , vol. 7, no. 1, pp. 36–40, 2022, doi: 10.30869/jtpg.v7i1.911.

[7] J. Permana and I. Kurniawan, “Calculation analysis of generated turbine power and steam turbine efficiency in Unit 1 and Unit 2 at Pt. Indonesia Power Uboh Ujp Banten 3 Lontar," *Mot. Burn J. Tech. Machines* , vol. 1, no. 2, pp. 1–8, 2017, doi: 10.31000/mbjtm.v1i2.731.

[8] H. Santoso, "Optimization to Produce Ideal Efficiency of Steam Turbines for Biomass Power Plants with a Capacity of 20 MW," *STRING (Unit for Research and Innovation Technology* , vol. 3, no. 2, p. 181, 2018, doi : 10.30998/string.v3i2.3044.

[9] D. Reza and G. Ramayanti, "DAMAGE ANALYSIS OF MANDREL TENSION REEL MACHINE USING THE FAILURE MODE AND EFFECT ANALYSIS (FMEA) METHOD," no. November, pp. 190–195, 2017.

[10] Suseno and SI Kalid, "Quality Control of Leather Bag Product Defects Using Failure Mode and Effect Analysis (Fmea) and Fault Tree Analysis (Fta) Methods at Pt Mandiri Jogja Internasional," *J. Cakrawala Ilm.* , vol. 1, no. 6, pp. 1307–1320, 2022, doi: 10.53625/jcijurnalcakrawalailmiah.v1i6.1131.

[11] I. Nurdiansah, Marno, and A. Santosa, "Damage Analysis of the Al Pin 350 Lathe Machine Using the Failure Mode and Effect Analysis (FMEA) Method," *J. Ilm. Educator's Ride.* , vol.

JURNAL ECTIPE
Electronic, Control, Telecommunication, Information, and Power Engineering
Volume 11, Issue 2, October 2024, pp. 187-194
ISSN 2355-5068 ; e-ISSN 2622-4852
DOI: 10.33019/jurnalecotipe.v11i2. 4504

8, no. 1, pp. 704–708, 2022, doi: 10.5281/zenodo.5921782.

[12] SH Al Hakiki and D. Dwisetiono, "Analysis of Lubricating Systems Using the FMEA Method to Determine System Failures," *Zo. Sea J. Inov. Science and Technology. To the sea.* , vol. 2, no. 3, pp. 99–105, 2021, doi: 10.62012/zl.v2i3.18594.

[13] W. Amalia, D. Ramadian, and SN Hidayat, "Damage Analysis of Palm Oil Mill Sterilizer Machines Using Failure Modes and Effect Analysis (FMEA)," *J. Tek. Ind. J. Has. Researcher. and Science Works. in Bid. Tech. Ind.* , vol. 8, no. 2, p. 369, 2022, doi: 10.24014/jti.v8i2.19179.

[14] SB Marpaung, DAA Ritonga, and A. Irwan, "Analysis of Risk Priority Number (Rpn) on the Reliability of Thresher Machine Components Using the Fmea Method at Pt . 9, no. 2, pp. 74–81, 2021, doi: 10.35447/jitekh.v9i2.427.

[15] M. Rinoza and F. Ahmad Kurniawan, "Rpn (Risk Priority Number) Analysis of the Reliability of Double Screw Compressor Machine Components Using the Fmea Method at the Pt Cement Factory. Xyz," *Print) Bul. Main Tech.* , vol. 17, no. 1, pp. 1410–4520, 2021.

[16] TJ Wibowo, TS Hidayatullah, and A. Nalhadi, "Maintenance Analysis on Lathes Using the Reliability Centered Maintenance (RCM) Approach," *J. Rekayasa Ind.* , vol. 3, no. 2, pp. 110–120, 2021, doi: 10.37631/jri.v3i2.485.

JURNAL ECOTIPE
Electronic, Control, Telecommunication, Information, and Power Engineering

Volume 11, Issue 2, October 2024, pp. 195-206
ISSN 2355-5068 ; e-ISSN 2622-4852
DOI: 10.33019/jurnalecotipe.v11i2.4511

Implementation of Natural Language Processing in the Reporting and Handling System of Sexual Violence Cases on Campus

Ilwan Syafrinal[1], Sapta Eka Putra[2], Mahazam Afrad[3]
[1]Universitas Universal, Sungai Panas, Kec. Batam, Batam 29444, Indonesia
[2]Universitas Tamansiswa, Jl. Taman Siswa, Padang 25171, Indonesia
[3]Institut Teknologi Telkom Purwokerto, Jl. DI Panjaitan No.12, Purwokerto 53147, Indonesia

ARTICLE INFO

Article historys:

Received :.../.../...
Revised :.../.../...
Accepted :.../.../...

Keywords: NLP, Sexual Violence, Reporting Systems, SVM.

ABSTRACT

Sexual violence in the campus environment is a serious problem that requires an effective reporting and handling system. This research aims to develop a Natural Language Processing (NLP)-based system that can improve the process of reporting and handling cases of sexual violence on campus. The methodology used includes the application of NLP techniques such as sentiment analysis and entity recognition to automate the identification and handling of reports. The Support Vector Machines (SVM) algorithm is used for the classification of text in this system. The data is collected from various sources, pre-processed, and used to train NLP models. The results of the study show that the system developed has an accuracy level of 91%, precision of 93%, and recall of 87%, which illustrates its effectiveness in collecting reports of sexual violence anonymously and accurately. Feedback from early adopters shows that the system improves the efficiency and accuracy of the reporting process. The conclusion of this study is that the implementation of NLP can significantly improve the reporting and handling system of sexual violence on campus. Further research is suggested to expand the scope of the system and improve its analysis capabilities.

Corresponding Author:
Ilwan Syafrinal
Universitas Tamansiswa, Jl. Taman Siswa, Padang and 25171, Indonesia
Email: ilwansynl@gmail.com

1. INTRODUCTION

This research is motivated by the fact that sexual violence in the educational environment [1-3], especially on campus, has become one of the major sins that threatens the integrity and safety of educational institutions [4]. This problem not only violates human rights but also creates an unsafe environment, hindering the learning process and personal growth of students. Although many cases occur, most go unreported due to the lack of an accessible, anonymous, and sensitive reporting facility to the needs of victims [5]. Therefore, the purpose of this research is to develop a more effective reporting system that addresses these gaps by providing a platform that ensures anonymity and sensitivity to the victim's needs. This research seeks to fill the gap by focusing on the development of reporting mechanisms in educational institutions, particularly in higher education, which have not been adequately addressed in previous studies.

Sexual violence in the campus environment is a serious problem that has a significant impact on the mental and physical health of the victim, and can damage the reputation of educational institutions [6]. According to data from https://databoks.katadata.co.id/There were many cases of sexual violence, namely 13,156 in 2023. Victims of sexual violence are reluctant to report such incidents due to fear,

JURNAL ECOTIPE
Electronic, Control, Telecommunication, Information, and Power Engineering
Volume 11, Issue 2, October 2024, pp. 195-206
ISSN 2355-5068 ; e-ISSN 2622-4852
DOI: 10.33019/jurnalecotipe.v11i2.4511

social stigma, and distrust of the existing reporting system [7]. This situation demands a more efficient and reliable reporting system to ensure that all cases of sexual violence are handled appropriately.

Current sexual violence reporting systems are often less effective in identifying and following up on reports [8]. Limitations in analyzing report data quickly and accurately lead to many cases that are not handled properly, leaving victims without adequate support. Therefore, a new approach is needed that can improve accuracy and efficiency in handling reports of sexual violence.

Various studies have been conducted to overcome this problem with various technological approaches, including using text mining techniques to analyze reports of sexual violence, but facing obstacles in handling large volumes of data [9]. Developed a mobile application for reporting sexual violence, but still faced problems in validating report data [10]. Applied the Naive Bayes algorithm for text classification, but the results were less accurate in the context of sexual violence reports [11]. Using Random Forests to improve classification accuracy, but this model still faces challenges in interpreting the results [12]. Lastly, applying deep learning for sentiment analysis, but it requires high computing and is difficult to implement on a large scale [13]. While these approaches make a significant contribution, they still lack accuracy and scalability. This research offers a new approach by combining Natural Language Processing (NLP) and Support Vector Machines (SVM) algorithms to automate the process of reporting and handling cases of sexual violence on campus. SVM was chosen because of its strong ability to handle text classification with high accuracy and good interpretability [14]. This approach is expected to overcome the limitations of previous research and provide a more effective and efficient solution.

The main purpose of this study is to develop and implement a reporting and handling system for sexual violence cases based on NLP and SVM in the campus environment. In addition, the study aims to increase the reporting rate of sexual violence cases, reduce social stigma, and provide better support for victims. This research makes a significant contribution to science by providing a new approach to dealing with sexual violence on campus through NLP and SVM technology. In addition, this research also opens up opportunities for further development in a more sophisticated and user-friendly sexual violence reporting system. Thus, this research is expected to be an important reference for researchers and practitioners in the field of campus security and information technology.

This research seeks to fill the gap by focusing on the development of reporting mechanisms in educational institutions, particularly in higher education, which have not been adequately addressed in previous studies. The problem addressed in this research is the lack of a robust reporting system that can ensure both accessibility and protection for victims, which has led to underreporting and ineffective handling of sexual violence cases. The objective is to create a solution that improves the accuracy and efficiency of reporting, while fostering a safer environment for students. tranlateka

2. RESEARCH METHOD

Sexual violence on campus is a serious problem that requires special attention. To effectively address this problem, this study uses methodologies based on Natural Language Processing (NLP) and Support Vector Machines (SVM) in developing a system for reporting and handling sexual violence. The diagram below explains the stages of the methodology used in this study. Each stage is designed to ensure that the data is processed correctly and produce an accurate and reliable model.

JURNAL ECOTIPE
Electronic, Control, Telecommunication, Information, and Power Engineering
Volume 11, Issue 2, October 2024, pp. 195-206
ISSN 2355-5068 ; e-ISSN 2622-4852
DOI: 10.33019/jurnalecotipe.v11i2.4511

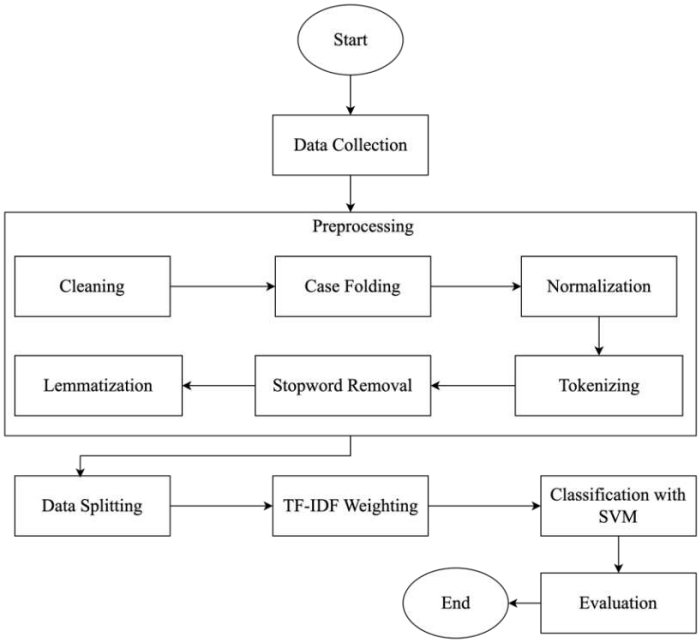

Figure 1. Research Methodology

The methodology of this research consists of several systematic stages, ranging from data collection to model evaluation. Each stage has an important role in the process of developing a system for reporting and handling sexual violence. Here is a detailed explanation of each stage:

1. Start, this stage marks the beginning of the research process, where the research objectives and framework are established.
2. Data Collection, Data collection on sexual violence reports is carried out through various sources, such as surveys, anonymous reports, or data from related institutions. The data collected must include the different types of sexual violence that occur on campus to get a comprehensive picture.
3. Preprocessing
    a. Cleaning, the data cleaning process is carried out to remove irrelevant information or noise from the raw data. This includes the removal of unnecessary special characters, numbers, and punctuation.
    b. Case Folding, all text is converted to lowercase letters to ensure consistency in data processing. For example, the words "Violence" and "violence" are considered the same after case folding.
    c. Normalization, Text normalization is done by changing words into standard or standard forms. This can involve replacing abbreviations with full forms or changing non-standard word forms to standard forms.
    d. Tokenizing, the process of tokenization breaks down text into smaller units, such as words or phrases. These tokens are then used in the next stage of analysis.
    e. Stopword Removal, Common words that do not provide significant information (stopwords) such as "and", "which", "with", are removed from the text to reduce noise.
    f. Lemmatization, Lematization transforms words into their basic form or lemma. For example, the words "run," "run," and "run" are all changed to "run."
4. Data Splitting, the processed data was then divided into two sets: a training set of 80% data or 3368 data and a testing set of 20% or 842 data. The training set is used to train the model, while the test set is used to evaluate the model's performance.
5. TF-IDF Weighting, TF-IDF (Term Frequency-Inverse Document Frequency) It is used to give weight to words in text based on their frequency in the document and their relative frequency throughout the document. This weight helps in identifying the most relevant words in the classification.

JURNAL ECOTIPE
Electronic, Control, Telecommunication, Information, and Power Engineering
Volume 11, Issue 2, October 2024, pp. 195-206
ISSN 2355-5068 ; e-ISSN 2622-4852
DOI: 10.33019/jurnalecotipe.v11i2.4511

6. Classification with SVM, Algoritma Support Vector Machines (SVM) used to classify text into appropriate categories. SVM was chosen because of its strong ability to handle text classification problems with high accuracy.

Table 1. Kernel Formula In SVM[15]

Karnel	Formula
Polynomial[16]	k(x, y) = (x. y + c) ^{d}
Sigmoid[17]	$k(x, y)$ = tanh($\gamma x. y + c$)
Linear[18]	$k(x, y) = x. y + c$v
Radial Basis Function (RBF)[19]	$k(x, y)$ = exp $(-\gamma \|\|x - y\|\| 2)$

The SVM, as shown in Table 1, employs various kernel functions (Polynomial, Sigmoid, Linear, and RBF) to convert input data into a higher-dimensional feature space, facilitating the identification of a hyperplane separator. The choice of kernel function and its parameters is influenced by the nature of the data, as each kernel has its own strengths and weaknesses. For instance, the Polynomial kernel elevates a dot product to a specified power and adds a constant, the Sigmoid kernel utilizes a hyperbolic tangent function, the Linear kernel carries out a dot product operation, and the RBF kernel assesses distances using the Gaussian function.

7. Evaluation, the evaluation stage is carried out to assess the performance of the classification model. Evaluation metrics such as accuracy, precision, recall, and F1-score are used to measure how well the model can identify and classify reports of sexual violence.
   a. Akurasi

   $$Accuracy = \frac{\text{TP+FP+TN+FN}}{\text{TP+TN}} \quad (1)$$

   In equation (1) it can be explained that, TP (True Positive) is the number of correct positive predictions, TN (True Negative) is the number of correct negative predictions, FP (False Positive) is the number of false positive predictions, FN (False Negative) is the number of false negative predictions. Accuracy provides an overview of how often classification models give correct predictions, but can be misleading if there is a class imbalance[20].
   b. Precision

   $$Precision = \frac{TP}{TP+FN} \quad (2)$$

   In equation (2) it can be explained that, TP (True Positive) is the number of correct positive predictions, FP (False Positive) is the number of false positive predictions, Precision shows the proportion of correct positive predictions of all positive predictions made. High precision means that the model rarely makes positive mistakes [21].
   c. Recall

   $$Recall = \frac{TP}{TP+FN} \quad (3)$$

   In equation (3) it can be explained that, TP (True Positive) is the number of correct positive predictions, FN (False Negative) is the number of false negative predictions. The recall shows the proportion of correct positive predictions of all instances that are actually positive. High recall means that the model successfully captures most positive instances[22].
   d. F-1 Score

   $$F-1\ Score = 2 * \frac{Precision\ x\ Recall}{Precision + Recall} \quad (4)$$

   F1-Score achieves its best score of 1 and worst at 0, providing a balance between precision and recall, especially useful in cases with an unbalanced class distribution [23].
8. End, The final stage of the research process where the results of analysis and evaluation are collected and interpreted to make conclusions and recommendations.

JURNAL ECOTIPE
Electronic, Control, Telecommunication, Information, and Power Engineering
Volume 11, Issue 2, October 2024, pp. 195-206
ISSN 2355-5068 ; e-ISSN 2622-4852
DOI: 10.33019/jurnalecotipe.v11i2.4511

With this structured methodology, the research is expected to produce a more effective, efficient, and accurate reporting and handling system for sexual violence in the campus environment.

3. RESULTS AND DISCUSSION

The results of the study will be discussed in depth to understand the implications of the findings, as well as to compare them with previous relevant studies. The analysis will include evaluation metrics such as accuracy, precision, recall, and F1-score to assess the performance of the classification model that has been developed.

3.1. Data Collections

The study used 3000 reports covering different types of sexual and non-sexual violence. The data is categorized into three main types: Non-Sexual Violence Data, Physical Sexual Violence Data, and Non-Physical Sexual Violence Data. Non-Sexual Violence data includes reports such as lost items or non-violent incidents. Physical Sexual Violence data involves reports of physical contact, such as physical harassment and rape. Meanwhile, Non-Physical Sexual Violence Data includes reports such as verbal, visual, and online harassment. Data collection is carried out through surveys, anonymous reports, and data from related institutions. Each report is anonymized to protect the privacy of the reporter and is processed through various stages of preprocessing before being used for training and evaluation of the classification model. The goal is to provide a representative dataset to train an SVM-based classification model that is effective in identifying and handling reports of sexual violence on campus. An example of the data used is shown in Figure 2.

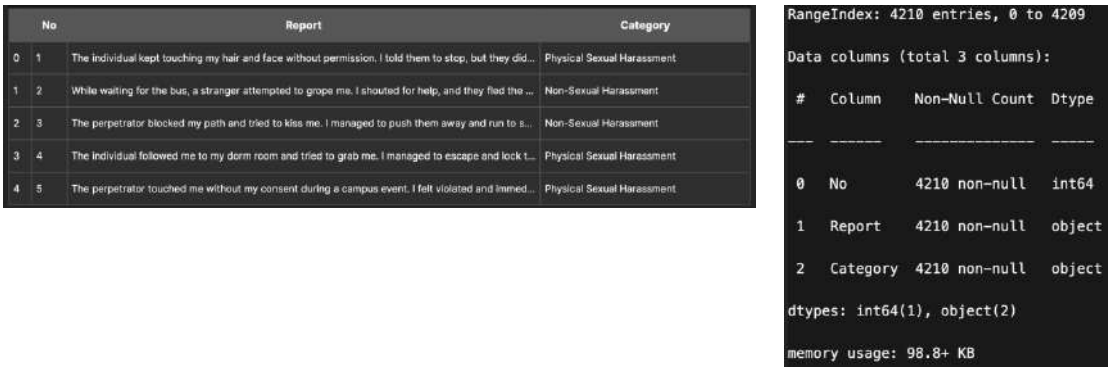

	No	Report	Category
0	1	The individual kept touching my hair and face without permission. I told them to stop, but they did...	Physical Sexual Harassment
1	2	While waiting for the bus, a stranger attempted to grope me. I shouted for help, and they fled the ...	Non-Sexual Harassment
2	3	The perpetrator blocked my path and tried to kiss me. I managed to push them away and run to s...	Non-Sexual Harassment
3	4	The individual followed me to my dorm room and tried to grab me. I managed to escape and lock t...	Physical Sexual Harassment
4	5	The perpetrator touched me without my consent during a campus event. I felt violated and immed...	Physical Sexual Harassment

```
RangeIndex: 4210 entries, 0 to 4209
Data columns (total 3 columns):
 #   Column    Non-Null Count  Dtype
---  ------    --------------  -----
 0   No        4210 non-null   int64
 1   Report    4210 non-null   object
 2   Category  4210 non-null   object
dtypes: int64(1), object(2)
memory usage: 98.8+ KB
```

Figure 2. Data Collection Results

This DataFrame contains 4,210 entries with three columns, namely "No", "Report", and "Category". The "No" column has an integer data type (int64) that serves as the sequence number or index for each entry. The "Report" column contains a description of the report, while the "Category" column contains the category or label associated with each report. There are no blank values in these three columns, so all entries are complete. The size of the memory used by this DataFrame is about 98.8 KB, indicating that this dataset is light to process.

3.2. Preprocesing

Pre-processing is an important step in data analysis or machine learning workflows, especially when working with text data. The main purpose of pre-processing is to convert the raw data into a clean, structured format that is suitable for analysis. This step involves a series of operations that help improve data quality, reduce noise, and ensure that the resulting features are informative and representative of the underlying patterns in the data.

JURNAL ECOTIPE
Electronic, Control, Telecommunication, Information, and Power Engineering
Volume 11, Issue 2, October 2024, pp. 195-206
ISSN 2355-5068 ; e-ISSN 2622-4852
DOI: 10.33019/jurnalecotipe.v11i2.4511

Original 'Report' column:

	Report
0	The individual kept touching my hair and face without permission. I told them to stop, but they didn't listen.
1	While waiting for the bus, a stranger attempted to grope me. I shouted for help, and they fled the scene.
2	The perpetrator blocked my path and tried to kiss me. I managed to push them away and run to safety.
3	The individual followed me to my dorm room and tried to grab me. I managed to escape and lock the door.
4	The perpetrator touched me without my consent during a campus event. I felt violated and immediately reported it to security.

Cleaned 'Report' column:

	Cleaned_Report
0	The individual kept touching my hair and face without permission I told them to stop but they didnt listen
1	While waiting for the bus a stranger attempted to grope me I shouted for help and they fled the scene
2	The perpetrator blocked my path and tried to kiss me I managed to push them away and run to safety
3	The individual followed me to my dorm room and tried to grab me I managed to escape and lock the door
4	The perpetrator touched me without my consent during a campus event I felt violated and immediately reported it to security

Figure 3. Data Cleaning

Cleaned 'Report' column before casefolding:

	Cleaned_Report
0	The individual kept touching my hair and face without permission I told them to stop but they didnt listen
1	While waiting for the bus a stranger attempted to grope me I shouted for help and they fled the scene
2	The perpetrator blocked my path and tried to kiss me I managed to push them away and run to safety
3	The individual followed me to my dorm room and tried to grab me I managed to escape and lock the door
4	The perpetrator touched me without my consent during a campus event I felt violated and immediately reported it to security

Sesudah Casefolding:

Cleaned 'Report' column after casefolding:

	Casefolded_Report
0	the individual kept touching my hair and face without permission i told them to stop but they didnt listen
1	while waiting for the bus a stranger attempted to grope me i shouted for help and they fled the scene
2	the perpetrator blocked my path and tried to kiss me i managed to push them away and run to safety
3	the individual followed me to my dorm room and tried to grab me i managed to escape and lock the door
4	the perpetrator touched me without my consent during a campus event i felt violated and immediately reported it to security

Figure 4. Case Folding

Casefolded 'Report' column after normalisasi:

	Casefolded_Report
0	the individual kept touching my hair and face without permission i told them to stop but they didnt listen
1	while waiting for the bus a stranger attempted to grope me i shouted for help and they fled the scene
2	the perpetrator blocked my path and tried to kiss me i managed to push them away and run to safety
3	the individual followed me to my dorm room and tried to grab me i managed to escape and lock the door
4	the perpetrator touched me without my consent during a campus event i felt violated and immediately reported it to security

Casefolded 'Report' column before normalisasi:

	Normalized_Report
0	the individual kept touching my hair and face without permission i told them to stop but they did not listen
1	while waiting for the bus a stranger attempted to grope me i shouted for help and they fled the scene
2	the perpetrator blocked my path and tried to kiss me i managed to push them away and run to safety
3	the individual followed me to my dorm room and tried to grab me i managed to escape and lock the door
4	the perpetrator touched me without my consent during a campus event i felt violated and i ammediately reported it to security

Figure 5. Normalization

JURNAL ECOTIPE
Electronic, Control, Telecommunication, Information, and Power Engineering
Volume 11, Issue 2, October 2024, pp. 195-206
ISSN 2355-5068 ; e-ISSN 2622-4852
DOI: 10.33019/jurnalecotipe.v11i2.4511

Normalized 'Report' column before tokenization:

	Normalized_Report
0	the individual kept touching my hair and face without permission i told them to stop but they did not listen
1	while waiting for the bus a stranger attempted to grope me i shouted for help and they fled the scene
2	the perpetrator blocked my path and tried to kiss me i managed to push them away and run to safety
3	the individual followed me to my dorm room and tried to grab me i managed to escape and lock the door
4	the perpetrator touched me without my consent during a campus event i felt violated and i ammediately reported it to security

After Tokenization:

Normalized 'Report' column after tokenization:

	Tokenized_Report
0	[the, individual, kept, touching, my, hair, and, face, without, permission, i, told, them, to, stop, but, they, did, not, listen]
1	[while, waiting, for, the, bus, a, stranger, attempted, to, grope, me, i, shouted, for, help, and, they, fled, the, scene]
2	[the, perpetrator, blocked, my, path, and, tried, to, kiss, me, i, managed, to, push, them, away, and, run, to, safety]
3	[the, individual, followed, me, to, my, dorm, room, and, tried, to, grab, me, i, managed, to, escape, and, lock, the, door]
4	[the, perpetrator, touched, me, without, my, consent, during, a, campus, event, i, felt, violated, and, i, ammediately, reported, it, to, security]

Figure 6. Tokenizing

Before Stopword Removal:

Tokenized 'Report' column before stopword removal:

	Tokenized_Report
0	[the, individual, kept, touching, my, hair, and, face, without, permission, i, told, them, to, stop, but, they, did, not, listen]
1	[while, waiting, for, the, bus, a, stranger, attempted, to, grope, me, i, shouted, for, help, and, they, fled, the, scene]
2	[the, perpetrator, blocked, my, path, and, tried, to, kiss, me, i, managed, to, push, them, away, and, run, to, safety]
3	[the, individual, followed, me, to, my, dorm, room, and, tried, to, grab, me, i, managed, to, escape, and, lock, the, door]
4	[the, perpetrator, touched, me, without, my, consent, during, a, campus, event, i, felt, violated, and, i, ammediately, reported, it, to, security]

After Stopword Removal:

Tokenized 'Report' column after stopword removal:

	Stopword_Removed_Report
0	[individual, kept, touching, hair, face, without, permission, told, stop, listen]
1	[waiting, bus, stranger, attempted, grope, shouted, help, fled, scene]
2	[perpetrator, blocked, path, tried, kiss, managed, push, away, run, safety]
3	[individual, followed, dorm, room, tried, grab, managed, escape, lock, door]
4	[perpetrator, touched, without, consent, campus, event, felt, violated, ammediately, reported, security]

Figure 7. Stopword Removal

Stopword Removed 'Report' column before lemmatization:

	Stopword_Removed_Report
0	[individual, kept, touching, hair, face, without, permission, told, stop, listen]
1	[waiting, bus, stranger, attempted, grope, shouted, help, fled, scene]
2	[perpetrator, blocked, path, tried, kiss, managed, push, away, run, safety]
3	[individual, followed, dorm, room, tried, grab, managed, escape, lock, door]
4	[perpetrator, touched, without, consent, campus, event, felt, violated, immediately, reported, security]

After Lemmatization:

Stopword Removed 'Report' column after lemmatization:

	Lemmatized_Report
0	[individual, kept, touch, hair, face, without, permission, told, stop, listen]
1	[wait, bus, stranger, attempt, grope, shout, help, flee, scene]
2	[perpetrator, block, path, try, kiss, manage, push, away, run, safety]
3	[individual, follow, dorm, room, try, grab, manage, escape, lock, door]
4	[perpetrator, touch, without, consent, campus, event, felt, violate, immediately, report, security]

Figure 8. Lemmatization

JURNAL ECOTIPE
Electronic, Control, Telecommunication, Information, and Power Engineering
Volume 11, Issue 2, October 2024, pp. 195-206
ISSN 2355-5068 ; e-ISSN 2622-4852
DOI: 10.33019/jurnalecotipe.v11i2.4511

The image shows the steps in the text cleaning and processing process in Natural Language Processing (NLP):

1. Figure 3: Data Cleanup – Remove punctuation, contraction, and lower capital letters to get cleaner text.
2. Figure 4: Case Folding – Lowercase all text for consistency.
3. Figure 5: Normalization - Correcting spelling errors, removing unimportant words, and word duplication.
4. Figure 6: Tokenizing - Breaks down the text into word units (tokens) for more detailed analysis.
5. Figure 7: Stopword Removal - Removes common words that do not have significant informational value.
6. Figure 8: Lemmatization – Converting a word to its basic form for consistency and reducing word variation.

This process ensures that the text becomes cleaner and ready for further analysis in NLP applications.

3.3. Data Splitting

Data splitting is an important step in data analysis and machine learning that aims to separate the dataset into two main parts: training and testing. This data sharing ensures that the built model can be evaluated objectively and has good generalization capabilities against new data. Training sets are used to train models, where the model learns patterns and relationships from that data. The test set is used to evaluate the performance of a model after it has been trained, with the goal of measuring how well the model performs on data that has never been seen before. By dividing the data into training and testing sets, we can avoid overfitting and ensure a more robust and reliable model.

3.4. TF-IDF Weighting

TF-IDF (Term Frequency-Inverse Document Frequency) is a statistical method used to evaluate how important a word is in the context of a document relative to the document set (corpus). It helps in identifying keywords that have significant meaning in the text.

	accidentally	account	activity	advance	almost	annoyed	another	anxious
count	3368	3368	3368	3368	3368	3368	3368	3368
mean	0.0094312517	0.0052885365	0.0047927277	0.015868244	0.0049096861	0.0034802996	0.0034802996	0.0039670765
std	0.054041494	0.0454526182	0.0411913616	0.0682104348	0.0453672864	0.0344686643	0.0344686643	0.0387185154
min	0	0	0	0	0	0	0	0
25%	0	0	0	0	0	0	0	0
50%	0	0	0	0	0	0	0	0
75%	0	0	0	0	0	0	0	0
max	0.3429979625	0.395817578	0.3587090384	0.3295720732	0.423995455	0.3447543839	0.3447543839	0.3817461074

Figure 9. TF-IDF Results

Figure 9 shows a basic statistical table for some of the words in the dataset, including mean, standard deviation, minimum, maximum, and specific percentiles for the TF-IDF values of each word. For example, the word "accidentally" has a TF-IDF mean value of 0.0049 and a standard deviation (std) of 0.0540.

JURNAL ECTIPE
Electronic, Control, Telecommunication, Information, and Power Engineering
Volume 11, Issue 2, October 2024, pp. 195-206
ISSN 2355-5068 ; e-ISSN 2622-4852
DOI: 10.33019/jurnalecotipe.v11i2.4511

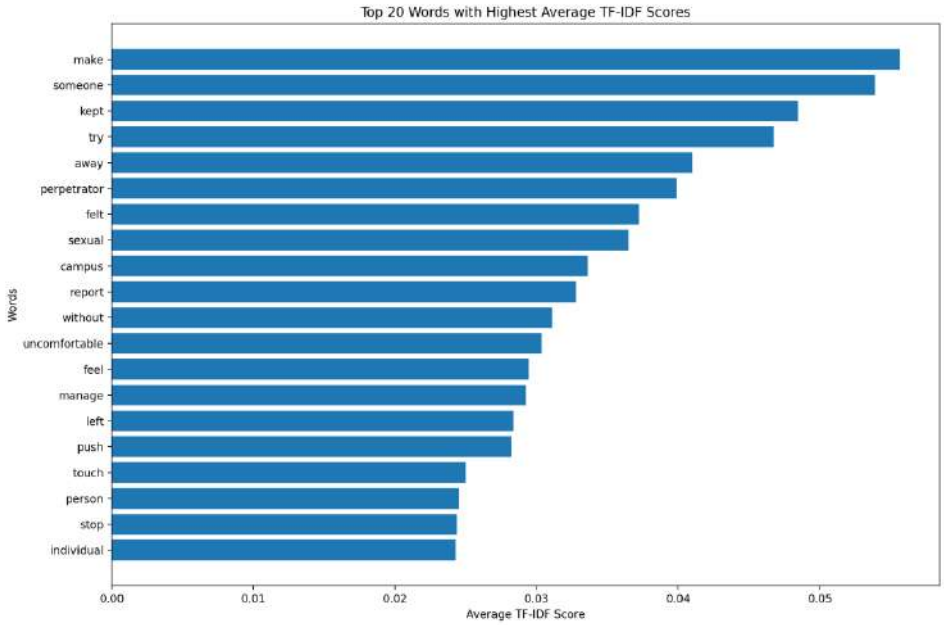

Figure 10. Words with the highest average TF-IDF value in Corpus

Figure 10. shows a bar graph showing 20 words with the highest average TF-IDF value in the corpus. These words include "make", "someone", "kept", "try", and others. The length of each bar represents the average TF-IDF value of the word, with the word "make" having the highest value. These graphs help in identifying the most significant words in the document set and provide insight into the keywords that may be relevant in further analysis.

3.5. Classification with SVM

After the data was divided into train and test data, TFIDF weighting was carried out and continued with classification using the Support Vector Machine (SVM) method. This study uses four SVM kernels: linear, polynomial, sigmoid, and RBF. The four kernels will be tuned to determine the best parameter value on each kernel using the Grid Search method by entering the hyperparameter value as the input. The Grid Search process will generate the best parameter values for each kernel. The parameter input values were processed and tested on the training data using grid search to obtain the optimal combination of parameter values. The best hyperparameters generated from each kernel are presented in Table 2. After determining the optimal parameter values for each kernel, the performance of each kernel is evaluated in terms of accuracy, precision, recall, and F1-Score. The RBF kernel achieved the highest accuracy, precision, recall, and F1-Score, with values of 0.90 0.89 0.88 0.885 respectively.

3.6. Evaluasi

After training the SVM (Support Vector Machine) model with various kernels, the next step is to evaluate the model's performance using several evaluation metrics such as accuracy, precision, recall, and F1-score. These metrics provide a variety of perspectives on the model's performance. Additionally, the confusion matrix is used to provide a more detailed picture of the correct and false predictions made by the model. The confusion matrix helps in identifying the types of errors made by the model, such as false positives and false negatives. Figure 11 will display the results of the confusion matrix for the SVM model.

JURNAL ECOTIPE
Electronic, Control, Telecommunication, Information, and Power Engineering
Volume 11, Issue 2, October 2024, pp. 195-206
ISSN 2355-5068 ; e-ISSN 2622-4852
DOI: 10.33019/jurnalecotipe.v11i2.4511

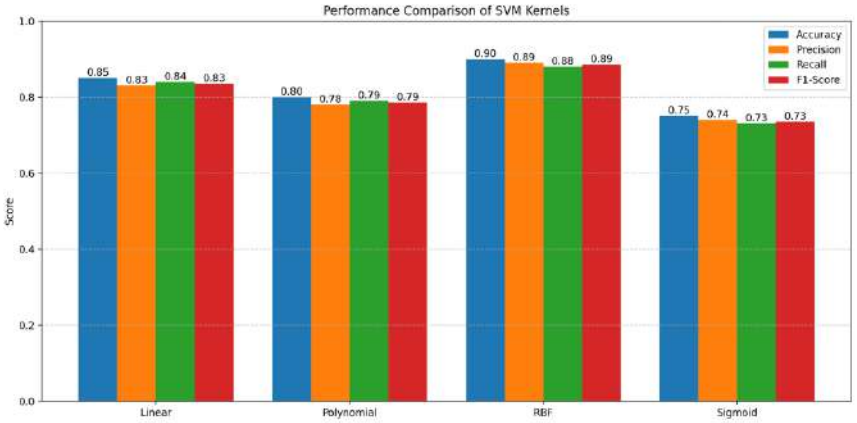

Figure 11. Results of the Confusion Matrix of the Karnel Baningan

Figure 11 shows a comparison of the performance of the SVM (Support Vector Machine) model using different kernel types: Linear, Polynomial, RBF (Radial Base Function), and Sigmoid. The evaluation was carried out based on the main metrics, namely accuracy, precision, recall, and F1-score. The RBF kernel showed the best performance with an accuracy value of 0.90, precision of 0.89, recall of 0.88, and F1-score of 0.89. This kernel is very effective in handling non-linear data. The Linear Kernel also performs quite well with almost balanced metric values, slightly below the RBF. Meanwhile, the Polynomial and Sigmoid kernels showed lower performance with all metrics being around 0.78 to 0.80 for Polynomial and 0.73 to 0.75 for Sigmoid. From the results of this evaluation, it can be seen that the RBF kernel is the best choice for this scenario, as it provides the most accurate and consistent prediction and classification results among all the kernels tested.

The novelty of this research lies in several key aspects that distinguish it from previous studies. First, this research combines Support Vector Machines (SVM) with Natural Language Processing (NLP) to handle sexual violence report data, an approach that has not been widely explored in earlier studies. This integration of technologies offers a more accurate solution for report classification while maintaining the anonymity of victims, which is a sensitive issue in this context. Second, this research conducts a comprehensive analysis of various SVM kernels (Linear, Polynomial, RBF, and Sigmoid) using several evaluation metrics such as accuracy, precision, recall, and F1-score. The findings demonstrate that the RBF kernel provides the best performance in handling non-linear data, with higher accuracy and consistency compared to other kernels. Third, this research offers real-world applications by developing a practical and scalable reporting system for educational institutions. Unlike previous studies, which tend to be theoretical, this study provides a concrete solution that can be implemented to more effectively address sexual violence cases. Finally, this research introduces data-driven improvements, where the use of the RBF kernel in the SVM model has proven to enhance the accuracy and efficiency of classification compared to traditional methods, offering a new contribution in handling sexual violence reports within the campus environment.

4. CONCLUSION

This research aims to develop a Natural Language Processing (NLP)-based system to improve the This research successfully developed a Natural Language Processing (NLP)-based system combined with the Support Vector Machines (SVM) algorithm to improve the reporting and handling of sexual violence cases on campus. The RBF kernel outperformed other kernels with an accuracy of 0.90, precision of 0.89, recall of 0.88, and an F1-score of 0.89, demonstrating its effectiveness in handling non-linear data. The model was trained on 3,000 reports, divided into 80% training and 20% testing data, ensuring that the system could generalize well.

However, this study has several limitations. First, the dataset size was relatively small, and future research should include larger, more diverse data to ensure better generalization. Second, the scope was limited to textual reports, while future studies should consider incorporating multimedia elements such as images or videos for a more comprehensive analysis. Additionally, this research did not specifically

Volume 11, Issue 2, October 2024, pp. 195-206
ISSN 2355-5068 ; e-ISSN 2622-4852
DOI: 10.33019/jurnalecotipe.v11i2.4511

address the issue of imbalanced data, which may skew results in categories with fewer occurrences. Addressing this issue with techniques like oversampling or undersampling could improve the model's performance. Lastly, the computational resources required for deep learning models like this one are considerable, and future research should focus on optimizing the model for greater efficiency and scalability. Despite these limitations, this study provides a solid foundation for improving sexual violence reporting systems on campus, offering better support for victims while ensuring accurate and efficient classification of reports.

ACKNOWLEDGMENTS

We would like to express our sincere gratitude to the Directorate of Research, Technology, and Community Service (DRTPM) for their invaluable support and guidance during this research. We would also like to thank the Institute for Research and Community Service (LPPM) of Universal University for providing the necessary resources and facilities. The administrative support and enthusiasm provided by LPPM greatly helps the progress and quality of our research. Thank you to all faculty members, staff, and colleagues who have helped directly or indirectly in this research. Our award is also given to participants and respondents whose contributions are critical to the study. Without the support of all the parties mentioned above, this research would not have been possible.

REFERENCES

[1] Raineka Faturani, "Kekerasan Seksual di Lingkungan Perguruan Tinggi," Sep 2022, doi: 10.5281/ZENODO.7052155.

[2] S. Sopyandi dan S. Sujarwo, "Kekerasan Seksual di Lingkungan Pendidikan dan Pencegahannya," *J. Pendidik. Ilmu Pengetah. Sos.*, vol. 15, no. 1, hlm. 19–25, Mei 2023, doi: 10.37304/jpips.v15i1.9448.

[3] A. Y. Susilowati, "Kampus Ramah Mahasiswa dari Kekerasan Seksual: Analisis Tingkat Pengetahuan Mahasiswa Terkait Pencegahan dan Penanganan Kekerasan Seksual," *Empower J. Pengemb. Masy. Islam*, vol. 7, no. 2, hlm. 233, Des 2022, doi: 10.24235/empower.v7i2.11516.

[4] D. S. Yunina *dkk.*, "SOSIALISASI 3 DOSA BESAR DALAM PENDIDIKAN UNTUK MENANAMKAN NILAI KARAKTER PESERTA DIDIK DI SDN BANJAR KEMUNING," vol. 05, no. 02, 2023.

[5] Franciscus Xaverius Wartoyo dan Yuni Priskila Ginting, "Kekerasan Seksual Pada Lingkungan Perguruan Tinggi Ditinjau Dari Nilai Pancasila," *J. Lemhannas RI*, vol. 11, no. 1, hlm. 29–46, Mei 2023, doi: 10.55960/jlri.v11i1.423.

[6] F. Bentivegna dan P. Patalay, "The impact of sexual violence in mid-adolescence on mental health: a UK population-based longitudinal study," *Lancet Psychiatry*, vol. 9, no. 11, hlm. 874–883, Nov 2022, doi: 10.1016/S2215-0366(22)00271-1.

[7] L. M. Orchowski, L. Grocott, K. W. Bogen, A. Ilegbusi, A. B. Amstadter, dan N. R. Nugent, "Barriers to Reporting Sexual Violence: A Qualitative Analysis of #WhyIDidntReport," *Violence Women*, vol. 28, no. 14, hlm. 3530–3553, Nov 2022, doi: 10.1177/10778012221092479.

[8] K. Parti dan R. A. Robinson, "What Hinders Victims from Reporting Sexual Violence: A Qualitative Study with Police Officers, Prosecutors, and Judges in Hungary," *Int. J. Crime Justice Soc. Democr.*, vol. 10, no. 2, Jun 2021, doi: 10.5204/ijcjsd.1851.

[9] C. Peersman, M. Edwards, E. Williams, dan A. Rashid, "A Survey of Relevant Text Mining Technology," 2022, *arXiv*. doi: 10.48550/ARXIV.2211.15784.

[10] F. Balahadia, Z. J. Astoveza, G. Jamolin, dan N. E. A. Astoveza, "Development and Implementation of Violence against Women and their Children Report System Mobile Application," *Int. J. Sci. Technol. Eng. Math.*, vol. 2, no. 3, hlm. 17–42, Sep 2022, doi: 10.53378/352906.

[11] Q. Zeng *dkk.*, "Improved Naive Bayes with Mislabeled Data," 2023, *arXiv*. doi: 10.48550/ARXIV.2304.06292.

[12] S. Etzler, F. D. Schönbrodt, F. Pargent, R. Eher, dan M. Rettenberger, "Machine Learning and Risk Assessment: Random Forest Does Not Outperform Logistic Regression in the Prediction of

Volume 11, Issue 2, October 2024, pp. 195-206
ISSN 2355-5068 ; e-ISSN 2622-4852
DOI: 10.33019/jurnalecotipe.v11i2.4511

Sexual Recidivism," *Assessment*, vol. 31, no. 2, hlm. 460–481, Mar 2024, doi: 10.1177/10731911231164624.
[13] K. L. Tan, C. P. Lee, K. M. Lim, dan K. S. M. Anbananthen, "Sentiment Analysis With Ensemble Hybrid Deep Learning Model," *IEEE Access*, vol. 10, hlm. 103694–103704, 2022, doi: 10.1109/ACCESS.2022.3210182.
[14] D. Mustafa Abdullah dan A. Mohsin Abdulazeez, "Machine Learning Applications based on SVM Classification A Review," *Qubahan Acad. J.*, vol. 1, no. 2, hlm. 81–90, Apr 2021, doi: 10.48161/qaj.v1n2a50.
[15] A. O. Kuyoro, S. Alimi, dan O. Awodele, "Comparative Analysis of the Performance of Various Support Vector Machine kernels," dalam *2022 5th Information Technology for Education and Development (ITED)*, Abuja, Nigeria: IEEE, Nov 2022, hlm. 1–7. doi: 10.1109/ITED56637.2022.10051564.
[16] B. A. Kindhi, N. Susanto, W. Handayani, S. V. Kurniasari, dan A. P. Pratama, "Prediction of the Tuberculosis Patients Who Can Recover Normally Using a Support Vector Machine with Radial and Polynomial Kernels," dalam *2021 3rd East Indonesia Conference on Computer and Information Technology (EIConCIT)*, Surabaya, Indonesia: IEEE, Apr 2021, hlm. 365–368. doi: 10.1109/EIConCIT50028.2021.9431878.
[17] S. Saha, M. Das, B. S. Mondal, S. Sarkar, dan J. Maiti, "D $_i$ PSVM: A Polynomial Kernel-free Support Vector Machine," dalam *2021 International Conference on Data Analytics for Business and Industry (ICDABI)*, Sakheer, Bahrain: IEEE, Okt 2021, hlm. 448–452. doi: 10.1109/ICDABI53623.2021.9655976.
[18] R. Chahar, A. K. Dubey, dan S. K. Narang, "A Mental Health Performance Assessment using Support Vector Machine," dalam *2023 3rd International Conference on Intelligent Technologies (CONIT)*, Hubli, India: IEEE, Jun 2023, hlm. 1–7. doi: 10.1109/CONIT59222.2023.10205772.
[19] S. Jueyendah, M. Lezgy-Nazargah, H. Eskandari-Naddaf, dan S. A. Emamian, "Predicting the mechanical properties of cement mortar using the support vector machine approach," *Constr. Build. Mater.*, vol. 291, hlm. 123396, Jul 2021, doi: 10.1016/j.conbuildmat.2021.123396.
[20] L. Fischer dan P. Wollstadt, "Precision and Recall Reject Curves for Classification," 2023, *arXiv*. doi: 10.48550/ARXIV.2308.08381.
[21] R. Yusof, N. Hashim, N. Abdul Rahman, S. Y. Mohd Yunus, dan N. A. Aziz Fadzillah, "Academic Performance Prediction Model Using Classification Algorithms: Exploring the Potential Factors," *Int. J. Acad. Res. Progress. Educ. Dev.*, vol. 11, no. 3, hlm. Pages 706-724, Agu 2022, doi: 10.6007/IJARPED/v11-i3/14753.
[22] Z. Tian, Y. Li, Z. Li, dan S. Li, "Recall Network: A Simple Brain-Inspired Algorithm for Classification," *Comput. Intell. Neurosci.*, vol. 2022, hlm. 1–52, Agu 2022, doi: 10.1155/2022/9374946.
[23] A. Humphrey *dkk.*, "Machine-learning classification of astronomical sources: estimating F1-score in the absence of ground truth," *Mon. Not. R. Astron. Soc. Lett.*, vol. 517, no. 1, hlm. L116–L120, Okt 2022, doi: 10.1093/mnrasl/slac120.

JURNAL ECOTIPE
Electronic, Control, Telecommunication, Information, and Power Engineering

Volume 11, Issue 2, October 2024, pp. 207-215
ISSN 2355-5068 ; e-ISSN 2622-4852
DOI: 10.33019/jurnalecotipe.v11i2.4514

Application of K-Nearest Neighbor Algorithm for Consumer Behaviour Identification and Product Personalisation Based on Big Data Analysis

Sapta Eka Putra[1], Miftahul Ilmi[2]
[1]Universitas Tamansiswa, Jl. Taman Siswa, Padang 25171, Indonesia
[2]Sistem Informasi, Institut Teknologi dan Bisnis Indobaru Nasional, Batam 29461, Indonesia

ARTICLE INFO

Article historys:

Received : …/…/…
Revised : …/…/…
Accepted : …/…/…

Keywords:

Consumer Behavior, Big Data, K-Nearest Neighbor, Product Personalization, Retail Industry

ABSTRACT

The rapid digital transformation has fundamentally altered the retail industry, presenting challenges such as shifting consumer behavior and intensified market competition. This research explores the application of the K-Nearest Neighbor (KNN) algorithm for identifying consumer behavior and developing product personalization systems based on big data insights. Utilizing a dataset comprising 10,000 transaction records from January to December 2023 and 5,302 product types, we implemented the KNN algorithm to predict consumer purchases. The data was processed into 89,908 distinct transaction records. Our evaluation, using 5-fold cross-validation, demonstrated that the optimal performance of the KNN model was achieved with k=10, yielding a precision of 0.8319, recall of 0.8311, and an F1-score of 0.8312. These findings highlight the effectiveness of KNN in enhancing consumer satisfaction through precise product recommendations. This study provides strategic insights for modern retailers aiming to leverage AI and big data to remain competitive and meet evolving consumer expectations.

Corresponding Author:

Sapta Eka Putra
Universitas Tamansiswa, Jl. Taman Siswa, Padang 25171, Indonesia
Email:saptaeka54putra@gmail.com

1. INTRODUCTION

The digital era has fundamentally changed the landscape of the retail industry, with rapid changes in consumer behavior and increasingly fierce market competition being the two main challenges [1-3]. Modern consumers want a more personalized, fast, and convenient shopping experience, triggering the need for continuous adaptation of retail businesses [4,5]. In this context, the use of Artificial Intelligence (AI) and big data analysis has become very relevant. These technologies offer the ability to understand and respond to consumer behavior more accurately and in a timely manner, enabling personalization of products and services that can improve the shopping experience and customer satisfaction [6-8]. This research aims to explore the potential of AI in identifying consumer behavior and developing a dynamic product personalization system based on big data insights. The urgency of this research lies in the urgent need of the retail industry to adapt to the rapid changes in consumer behavior and the intensification of market competition [9-11]. Without the use of technologies such as AI and big data, modern retail struggles to meet evolving consumer expectations, potentially losing market share and relevance [12,13].

JURNAL ECOTIPE
Electronic, Control, Telecommunication, Information, and Power Engineering
Volume 11, Issue 2, October 2024, pp. 207-215
ISSN 2355-5068 ; e-ISSN 2622-4852
DOI: 10.33019/jurnalecotipe.v11i2.4514

Some of the main problems that need to be addressed in the modern retail industry include a lack of understanding of consumer behavior, limited product personalization, inefficient data processing, and fierce market competition. Previous research has shown that the use of AI and big data in the retail sector can provide various significant benefits. For example, research by Sathyanarayana (2023) shows that big data analysis can improve understanding of consumer spending patterns and predict future needs [14]. Meanwhile, research by Krishnareddy et al. (2022) highlights how the implementation of AI in product personalization can improve customer satisfaction and loyalty levels [15].

This research is expected to provide strategic insights and practical solutions for the retail industry in utilizing technology to improve consumer satisfaction, as well as optimizing operations and marketing strategies. The development of innovative AI models and effective personalization systems is the main focus of this research. Using the K-Nearest Neighbors (KNN) method, this study offers a new approach in identifying consumer behavior that is more accurate and responsive to changes in shopping patterns. The advantages of this research include the use of the KNN method which is known for its high classification ability and flexibility in various types of data, a big data approach that provides deeper and more accurate insights into consumer behavior, innovations in product personalization that can be adjusted to specific consumer needs in real-time, and industry relevance that provides practical solutions that can be implemented by retail business actors to increasing competitiveness and sustainable growth in the digital era. Thus, this research is expected to help the modern retail sector in facing the challenges of the digital era, strengthening competitiveness, and encouraging sustainable growth.

2. RESEARCH METHOD

The development of a recommendation system requires several important stages to ensure that the data can provide accurate prediction results. This process includes data collection and processing, as well as the application of machine learning algorithms. The following is a flow chart that illustrates the stages of this research from raw data input to evaluation of prediction results. Shown in Figure 1.

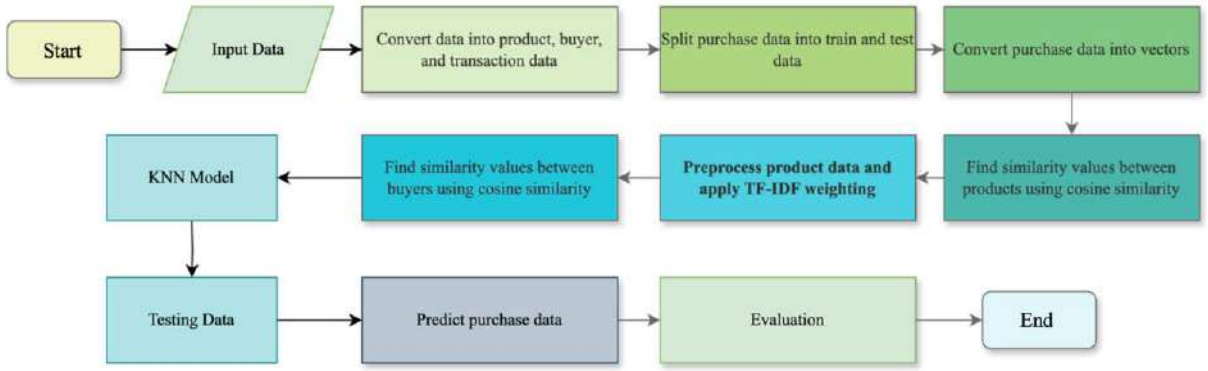

Figure 1. Research Methodology

Here is a detailed explanation in paragraph form for each stage:

1. Start: This process begins by marking the beginning of the entire procedure.
2. Data Input: Raw data from purchase transactions is entered into the system. This data includes various important attributes such as IDTransis that uniquely identify each transaction, Transaction Date and TimeTransaction which records when the transaction was made, IDProde and Product Name that identifies the product purchased, Amount that indicates the quantity of the product, Discount given, Payment Method used, Subscriber ID that identifies the customer, AgeCustomer, GenderCustomer, LocationCustomer, Loyalty Points that the customer has, CouponsUsed in transactions, RatingFeedback from customers, and Total Spend that reflect the total value of spending in the transaction.
3. Transform data into product, buyer, and transaction data: At this stage, the raw data that has been collected is broken down into several separate entities. Product data contains detailed information about each product such as Product ID, Product Name, and other attributes. Buyer

JURNAL ECTIPE
Electronic, Control, Telecommunication, Information, and Power Engineering
Volume 11, Issue 2, October 2024, pp. 207-215
ISSN 2355-5068 ; e-ISSN 2622-4852
DOI: 10.33019/jurnalecotipe.v11i2.4514

data contains information about each buyer such as Subscriber ID, Customer's Age, Customer's Gender, and Customer's Location. Transaction data records what products are purchased by each buyer in each transaction. At this stage, data that originally combined many products in a single transaction is broken down into a more structured format.

4. Split purchase data into train and test data: Purchase data that has been split is then divided into two parts: training data and test data. This division is carried out in a certain proportion, for example 80% for training data and 20% for test data. The purpose of this division is to ensure that the model to be built can be tested for performance after being trained with training data.
5. Convert purchase data to vectors: Transaction data that has been broken down is converted into vector representations. This involves the formation of a product-buyer matrix where the rows represent the buyer and the columns represent the product, with the values within the matrix indicating whether the buyer bought a particular product and how much. Each buyer and product is represented as a vector within a higher feature space, allowing for further mathematical analysis and the application of machine learning algorithms.
6. Finding the similarity value with cosine similarity: At this stage, the similarity value between the products is calculated using the cosine similarity method. Cosine similarity measures the similarity between two vectors by calculating the cosine of the angle between them. It helps in identifying products that are often purchased together by buyers.
7. KNN Model: The KNN (K-Nearest Neighbors) model is then built using processed data. The model is trained with training data to understand patterns in the data. The K-NN algorithm is used to make predictions based on similarities between buyer vectors, by using the K-values of the nearest neighbor to determine the prediction result.
8. Testing Data: The testing data is used to test the KNN model that has been built. The model is tested with test data to assess its performance. The goal is to examine how well the model can predict the correct outcome based on data that has never been seen before.
9. Prediction of purchase data: The KNN model predicts new purchase data based on test data. The model predicts what products a buyer is likely to buy based on patterns that have been learned from the training data, using similarities between buyer vectors to determine which products are most likely to be purchased.
10. Evaluation: The evaluation stage is conducted to assess the performance of the model. Metrics such as accuracy, precision, recall, and F1-score are used to evaluate the prediction results. The prediction results are compared with actual data to measure how well the model performs predictions, and this evaluation provides insight into the model's strengths and weaknesses.
11. Completed: This stage marks the end of the overall process. The results of the evaluation are used to make further improvements to the model if needed, ensuring that the model is continuously improved to provide more accurate and reliable results.

3. RESULTS AND DISCUSSION

3.1 Analysis

This section discusses the results obtained from the research as well as the analysis and interpretation of existing findings. The latest input data is from 10,000 transaction data made at retail from January to December 2023, and product data of 5302 types of products. A sample of the data is shown in Figure 2.

JURNAL ECOTIPE
Electronic, Control, Telecommunication, Information, and Power Engineering
Volume 11, Issue 2, October 2024, pp. 207-215
ISSN 2355-5068 ; e-ISSN 2622-4852
DOI: 10.33019/jurnalecotipe.v11i2.4514

	IDTransaksi	TanggalTransaksi	WaktuTransaksi	IDProduk
0	4761191	2023-07-31	18:57:04	BDBPK-4273,P-6566,K-8901
1	4761192	2023-03-25	19:49:00	M-7532,BDBPK-0854,P-4906,P-8034,P-0145,P-1099,P-1752,P-...
2	4761193	2023-08-25	14:28:56	P-2132,P-4177,P-1056,P-1517,P-0789
3	4761194	2023-10-27	10:18:19	P-3415,P-1729,P-9632,BBM-1373,P-8478
4	4761195	2023-10-20	10:24:21	P-3401,P-6553,S-5621,BGG-8940,P-3000,P-9077,P-2999,B-67...

Figure 2. Raw Data

From the raw data input, data extraction will be carried out so that it can be broken down into several parts based on each product so that the data becomes 89,908 data as shown in Figure 3.

	IDTransaksi	TanggalTransaksi	WaktuTransaksi	IDProduk	Jumlah	Diskon	MetodePembayaran	IDPelanggan	PoinLoyalit
0	4761191	2023-12-03	16:16:53	PMB-2992	8	11111.1111111111	E-Wallet	SRHJUY-6447002	99
1	4761191	2023-12-03	16:16:53	P-3477	9	11111.1111111111	E-Wallet	SRHJUY-6447002	99
2	4761191	2023-12-03	16:16:53	P-2282	8	11111.1111111111	E-Wallet	SRHJUY-6447002	99
3	4761191	2023-12-03	16:16:53	BDBPK-2493	10	11111.1111111111	E-Wallet	SRHJUY-6447002	99
4	4761191	2023-12-03	16:16:53	P-0177	10	11111.1111111111	E-Wallet	SRHJUY-6447002	99

Figure 3. Transaction Breakdown Data

This step uses the scikit-learn library in Python, from the results of splitting the data by using the Interaction command on the train data: 390926.6666666667 (79.68%) and Interaction on the test data: 99678.66666666666 (20.32%). Displays information about the user-product matrix, displays the number of features (unique products): 4876. For example, we display the first five products: ['0000' '0002' '0012' '0016' '0017'], then the result is as shown in figure 4.

	0000	0002	0012	0016	0017	0019	0020	0023	0024	0026	0029	0032	0033	0036	0037	0039
SRHJUY-6447000	0	0	0	0	0	0	0	0	0	0	0	0	0	0	0	0
SRHJUY-6447001	0	0	0	0	0	0	0	0	0	0.087253529	0	0	0	0	0	0
SRHJUY-6447002	0	0	0	0	0	0	0	0	0	0	0	0	0	0.084050319	0	0
SRHJUY-6447003	0	0	0	0	0	0	0	0	0	0	0	0	0	0	0	0
SRHJUY-6447004	0.1017943386	0	0	0	0	0	0	0	0	0	0	0	0	0	0	0

Figure 4. The first five lines of the user-product matrix

Figure 4 displays the first five rows of a user-product matrix, representing the relationship between users and products. Each row, labeled with codes like "SRHJUY-6447000" to "SRHJUY-6447004," corresponds to a unique user within the system. The columns, labeled with numbers such as 0000, 0002, 0012, up to 0039, represent specific products. The values in the table indicate the level of interaction or rating by users for each product. A value of 0 signifies that the user has not interacted with or rated the

JURNAL ECOTIPE
Electronic, Control, Telecommunication, Information, and Power Engineering
Volume 11, Issue 2, October 2024, pp. 207-215
ISSN 2355-5068 ; e-ISSN 2622-4852
DOI: 10.33019/jurnalecotipe.v11i2.4514

product, while non-zero values, such as 0.087253529 or 0.084050319, indicate that the user has interacted with or provided a rating or preference for the product. This matrix offers a clear representation of user-product interactions and is typically utilized in recommendation systems to predict products that users might prefer based on their previous behaviors.

	0000	0002	0012	0016	0017	0019	0020	0023	0024
count	1000	1000	1000	1000	1000	1000	1000	1000	1000
mean	0.0020336365	0.0016333185	0.001355434	0.0014161004	0.0022482338	0.0014271753	0.0014121701	0.0020415675	0.0033306701
std	0.014797568	0.0130339025	0.012861569	0.0120516599	0.0155026302	0.0126686061	0.0124706961	0.0146041334	0.0173262765
min	0	0	0	0	0	0	0	0	0
25%	0	0	0	0	0	0	0	0	0
50%	0	0	0	0	0	0	0	0	0
75%	0	0	0	0	0	0	0	0	0
max	0.2050914404	0.1405194602	0.2188048801	0.1265554707	0.1783403836	0.1616308002	0.1523845708	0.162045992	0.1331272132

Figure 5. Matrix Statistics

In this stage, the purchase data has been converted into a vector representation using TF-IDF (*Term Frequency-Inverse Document Frequency*). The result is a user-product matrix with dimensions of 1000 x 4876, where each row represents a customer and each column represents a product. The values in the matrix show how important a product is to a customer based on the frequency of purchases and the uniqueness of the product among all customers. This matrix has a high level of sparsity (97.95%), which means that most of the values in the matrix are zero. This is a common characteristic in recommendation data, where most customers only buy a small fraction of the total available products. This vector representation allows us to perform further mathematical analysis and apply various machine learning algorithms to the recommendation system.

Furthermore, the KNN algorithm with the Collaborative Filtering, Content-Based, or Hybrid method is run to find top-n recommendations to a buyer. The Collaborative Filtering method uses similarities between buyers as the basis for recommendations. The Content-Based method uses similarities between products as the basis for recommendations. Meanwhile, the Hybrid method combines the results of Collaborative Filtering and Content-Based as the basis for recommendations. The test data from the 5-fold cross-validation process is used as input to make predictions. The results of the prediction are then calculated with precision, recall, and F-measure values to determine the performance of the method used in product personalization.

The KNN model predicts new purchase data based on test data. The model predicts what products shoppers are likely to buy based on patterns learned from training data, using similarities between buyer vectors to determine which products are most likely to be purchased." With data:

'UsiaPelanggan': 20,
'JenisKelaminPelanggan': "F,
'LokasiPelanggan': 'Bukittinggi',
'PoinLoyalitas': 10,
'MetodePembayaran': 'Tunai',
'KuponDigunakan' '1',.

Based on the analysis of the nearest neighbors in the KNN model, here are the recommended products for these new customers:

1. GREEN LEAF CETAKAN AGAR AGAR 0966 DORI
2. AMSAFE BLUE PISAU CUKUR
3. PERASAN JERUK PLASTIK LEMON SQUEEZER
4. NAGATA SIKAT BOTOL 336
5. ENFAGROW A+ 3 PLAIN 400GR

JURNAL ECOTIPE Electronic, Control, Telecommunication, Information, and Power Engineering
Volume 11, Issue 2, October 2024, pp. 207-215
ISSN 2355-5068 ; e-ISSN 2622-4852
DOI: 10.33019/jurnalecotipe.v11i2.4514

3.2 Recommendations

1. Product Variety: Recommendations cover a wide range of product categories, including kitchenware, personal care, and baby products. This shows that customers with similar profiles have diverse interests.
2. Customer Preferences:
   a. Kitchenware: GREEN LEAF CETAKAN AGAR AGAR 0966 DORI and PERASAN JERUK PLASTIK LEMON SQUEEZER show interest in kitchen appliances.
   b. Personal Care: AMSAFE BLUE PISAU CUKUR Demonstrate interest in personal care products.
   c. Baby Products: ENFAGROW A+ 3 PLAIN 400GR show interest in baby products.
3. Marketing Strategy:
   a. Bundling: Consider creating a product package that combines multiple items from a recommended list, such as a kitchenware package or a personal care package.
   b. Targeted Promotion: Focus your promotion on the product categories that appear in the recommendations, especially kitchen appliances and baby products.
   c. Personalization: Use this information to personalize marketing offers and communications to customers.
4. Improved Customer Experience:
   Given the high rating predictions (5), the main focus should be on maintaining a high level of customer satisfaction:
   a. Customer Service: Maintain a high quality of customer service to ensure a satisfying shopping experience.
   b. Product Education: Provide detailed information about the benefits and how to use the product, especially for kitchen and baby products.
   c. Loyalty Program: Leverage customer loyalty points (10 points) to provide special offers or discounts.
5. Location Analysis:
   The customer is from Bukittinggi. Consider tailoring product recommendations to local preferences or trends in the area.
6. Payment Methods:
   Customers use the Cash payment method. Consider offering incentives if using digital payment methods to improve transaction efficiency.
7. Coupon Usage:
   Customers use coupons (KuponDigunakan: '1'). This shows that customers are responsive to promotions. Consider offering additional coupons or discount programs to increase loyalty and value of shopping.

Taking all these factors into account, the main focus should be on maintaining a high level of customer satisfaction and offering products that match the preferences seen from the recommendations.

3.3 Evaluation

The test was carried out to evaluate the performance of the Collaborative Filtering method, this test was carried out by calculating the precision, recall, and F-measure values of each method. The testing process uses the 5-fold Cross-Validation method, which divides the data into five parts. In each iteration, one part is used as test data and the other four parts are used as training data. This process is repeated five times so that each piece of data is used as test data once. The percentage of data used in this study is 80% for training data and 20% for test data. In this study, there were 10,000 transactions that were processed and extracted into 89,908 transaction data. The test was carried out using k parameters, namely 10, 30, 50, 80, 100.

The following are the results of the evaluation of the KNN model with various k values (10, 30, 50, 80, 100) using the Collaborative Filtering method:

1. k=10: Precision=0.8319, Recall=0.8311, F1-measure=0.8312
2. k=30: Precision=0.5330, Recall=0.5326, F1-measure=0.5325
3. k=50: Precision=0.4437, Recall=0.4437, F1-measure=0.4436
4. k=80: Precision=0.3833, Recall=0.3831, F1-measure=0.3831

JURNAL ECOTIPE
Electronic, Control, Telecommunication, Information, and Power Engineering
Volume 11, Issue 2, October 2024, pp. 207-215
ISSN 2355-5068 ; e-ISSN 2622-4852
DOI: 10.33019/jurnalecotipe.v11i2.4514

5. k=100: Precision=0.3684, Recall=0.3683, F1-measure=0.3683

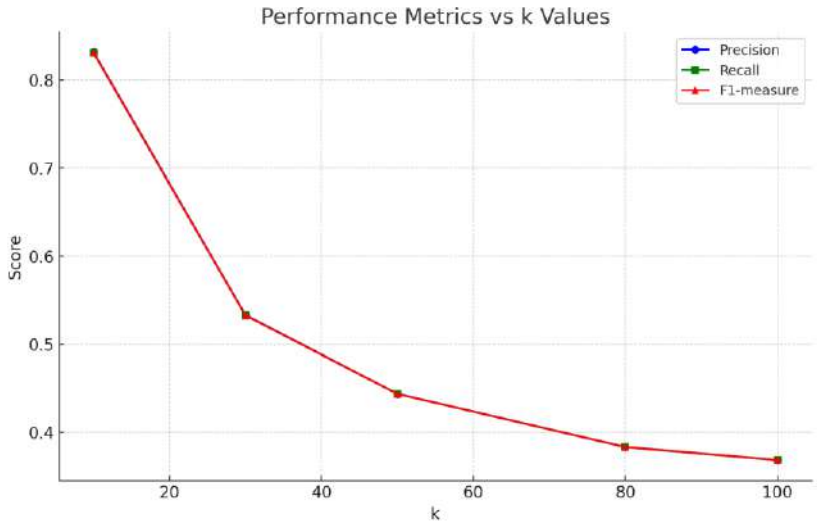

Figure 6. Graph of Collaborative Filtering Evaluation Results

Figure 6 shows a graph of the model's performance based on three main metrics: Precision, Recall, and F1-measure, with variations in k k values. At k = 10 k = 10, Precision reaches 0.8319, Recall 0.8311, and F1-measure 0.8312, indicating optimal model performance. However, when k k increases to k = 30 k = 30, the values decrease to 0.5330 for Precision, 0.5326 for Recall, and 0.5325 for F1-measure. This decline continued as k increased: at k = 50 k=50, Precision, Recall, and F1-measure were all around 0.4437; at k = 80 k=80, all three metrics were around 0.3831; and at k = 100 k=100, Precision dropped to 0.3684, while Recall and F1-measure were both around 0.3683. This decrease in performance indicates that a larger k value causes the model to become less accurate and more susceptible to noise, thus reducing the overall performance of the model.

3.4 Discussion

This study successfully shows that the application of the K-Nearest Neighbor (KNN) algorithm can make a significant contribution in understanding and predicting consumer behavior in the modern retail industry. With a dataset of 10,000 transactions and 5,302 product types, we were able to process the data into 89,908 more structured transaction records for further analysis. The results of the KNN model evaluation using 5-fold cross-validation showed that the value of k = 10 k = 10 produced the best performance with a precision of 0.8319, a recall of 0.8311, and an F1-score of 0.8312. These values indicate that the KNN model is able to provide accurate and consistent predictions in the context of product recommendations. An increase in k value above 10 indicates a decrease in performance, indicating that the model is becoming less accurate and more susceptible to noise in the data. Using the KNN method, we can identify products that consumers are most likely to buy based on previous purchase patterns. For example, the analysis shows that consumers with certain profiles are more likely to buy products such as kitchenware, personal care, and baby products. This information can be used to develop more targeted marketing strategies, such as product bundling and targeted promotions. This research makes several practical contributions to the retail industry, including improving customer satisfaction, effective marketing strategies, and operational optimization. More accurate product recommendations can improve the customer shopping experience, which in turn increases customer satisfaction and loyalty. Information on product preferences can be used to create more effective and targeted marketing campaigns, while the use of AI and big data allows retailers to optimize operations and reduce inefficiencies in inventory management and product offerings. Although this study shows promising results, there are some challenges and limitations that need to be considered. The quality and quantity of data greatly affect the performance of the model; Incomplete or unrepresentative data can reduce the accuracy of predictions. The implementation of the KNN algorithm also requires quite complex data processing and significant computing resources. In addition, models need to be constantly adjusted and updated based on changes in consumer behavior and dynamic market trends. This study

Volume 11, Issue 2, October 2024, pp. 207-215
ISSN 2355-5068 ; e-ISSN 2622-4852
DOI: 10.33019/jurnalecotipe.v11i2.4514

provides evidence that the KNN algorithm can be effectively implemented to identify consumer behavior and product personalization in the retail industry. Thus, the use of AI and big data not only increases customer satisfaction but also provides a competitive advantage for retailers in facing the challenges of the digital era.

4. CONCLUSION

This study successfully shows that the use of the K-Nearest Neighbor (KNN) algorithm can effectively identify consumer behavior and provide product personalization in the modern retail industry. Using a dataset of 10,000 transactions and 5,302 product types, we processed the data into 89,908 more structured transaction records and found that a value of k = 10 k = 10 provided optimal performance with a precision of 0.8319, a recall of 0.8311, and an F1-score of 0.8312. These results show that KNN is able to provide accurate and relevant predictions in the context of product recommendations, which in turn can increase customer satisfaction and loyalty. The research also provides important insights for retailers on how to leverage AI and big data to optimize their marketing and operational strategies. However, the study also reveals several challenges, such as the need for quality and representative data, as well as the complexity in data processing and the computing resources required. Therefore, continuous adjustment and update of the model is essential to ensure the accuracy of predictions and relevance to changes in consumer behavior and market trends. Overall, this study proves that the application of KNN in big data analysis can provide practical and strategic solutions for the retail industry to remain competitive in the digital era. The use of this technology allows retailers to be more responsive to consumer needs and preferences, as well as improve a more personalized and satisfying shopping experience.

ACKNOWLEDGMENTS

The author would like to express his deepest gratitude to the Directorate of Research and Community Service (DRPTM) and the Institute for Research and Community Service (LPPM) of Taman Siswa University for the financial support and facilities provided during the implementation of this research. The support provided by DRPTM and LPPM is very meaningful in providing the necessary resources to carry out this research, from data collection to analysis and preparation of reports. We would also like to express our appreciation to our colleagues at Taman Siswa University who have provided valuable input and technical assistance during the research process. Not to forget, thank you to the respondents who have participated in this study, providing data and information that is very important for the success of this study. The support and collaboration from various parties is very important in achieving the expected research results, and we hope that the results of this research can make a positive contribution to the development of science and the retail industry in Indonesia.

REFERENCES

[1] N. A. Hamdani, R. Muladi, dan G. A. F. Maulani, “Digital Marketing Impact on Consumer Decision-Making Process:,” dipresentasikan pada 6th Global Conference on Business, Management, and Entrepreneurship (GCBME 2021), Bandung, Indonesia, 2022. doi: 10.2991/aebmr.k.220701.031.

[2] Y. Xiong, “The Impact of Artificial Intelligence and Digital Economy Consumer Online Shopping Behavior on Market Changes,” *Discrete Dyn. Nat. Soc.*, vol. 2022, no. 1, hlm. 9772416, Jan 2022, doi: 10.1155/2022/9772416.

[3] D. Zulianti, S. K. Dewi, V. N. Izza, dan Suhairi, “THE EFFECT OF THE DIGITAL REVOLUTION ON GLOBAL MARKETING IN ERA 4.0 AND CONSUMER BEHAVIOR,” *J. Soc. Res.*, vol. 1, no. 2, hlm. 128–131, Jan 2022, doi: 10.55324/josr.v1i2.18.

[4] N. Nurjanah, “Coffee Shop New Retail Business Model,” *Int. J. Entrep. Bus. Creat. Econ.*, vol. 2, no. 2, hlm. 1–7, Jul 2022, doi: 10.31098/ijebce.v2i2.786.

[5] K. S. Golovacheva, M. M. Gogua, M. M. Smirnova, dan O. N. Alkanova, “Treating customers as individuals in online retail,” *Russ. Manag. J.*, vol. 20, no. 2, hlm. 224–246, 2022, doi: 10.21638/spbu18.2022.204.

Volume 11, Issue 2, October 2024, pp. 207-215
ISSN 2355-5068 ; e-ISSN 2622-4852
DOI: 10.33019/jurnalecotipe.v11i2.4514

[6] A. Sharma, "Analyzing the Role of Artificial Intelligence in Predicting Customer Behavior and Personalizing the Shopping Experience in Ecommerce," *INTERANTIONAL J. Sci. Res. Eng. Manag.*, vol. 07, no. 02, Feb 2023, doi: 10.55041/IJSREM17839.

[7] H. Abbu dan P. Gopalakrishna, "Digital Transformation Powered by Big Data Analytics: The Case of Retail Grocery Business," dipresentasikan pada Hawaii International Conference on System Sciences, 2022. doi: 10.24251/HICSS.2022.231.

[8] M. Tiutiu dan D.-C. Dabija, "Improving Customer Experience Using Artificial Intelligence in Online Retail," *Proc. Int. Conf. Bus. Excell.*, vol. 17, no. 1, hlm. 1139–1147, Jul 2023, doi: 10.2478/picbe-2023-0102.

[9] V. Panda, A. Mishra, dan M. Sharma, "Turning Data Into Insights: Leveraging Artificial Intelligence for Better Understanding of Social Media Consumer Behaviour," dalam *2023 International Conference on Sustainable Emerging Innovations in Engineering and Technology (ICSEIET)*, Ghaziabad, India: IEEE, Sep 2023, hlm. 271–275. doi: 10.1109/ICSEIET58677.2023.10303309.

[10] Prakash, S. M. Babu, P. P. Kumar, S. Devi, K. P. Reddy, dan M. Satish, "Predicting Consumer Behaviour with Artificial Intelligence," dalam *2023 IEEE 5th International Conference on Cybernetics, Cognition and Machine Learning Applications (ICCCMLA)*, Hamburg, Germany: IEEE, Okt 2023, hlm. 698–703. doi: 10.1109/ICCCMLA58983.2023.10346660.

[11] A. V. Calvo, A. D. Franco, dan M. Frasquet, "The role of artificial intelligence in improving the omnichannel customer experience," *Int. J. Retail Distrib. Manag.*, vol. 51, no. 9/10, hlm. 1174–1194, Nov 2023, doi: 10.1108/IJRDM-12-2022-0493.

[12] R. Kumar Kaushal, K. K. B. Giri, H. S. Kumar, K. Raina, D. Choudhury, dan K. Naikade, "AI-Based Approach for Retail Sale Forecasting," dalam *2023 International Conference on Self Sustainable Artificial Intelligence Systems (ICSSAS)*, Erode, India: IEEE, Okt 2023, hlm. 111–116. doi: 10.1109/ICSSAS57918.2023.10331651.

[13] A. Voelz, P. Hafner, dan C. Strauss, "Expert Opinions on Smart Retailing Technologies and Their Impacts," *J. Data Intell.*, vol. 3, no. 2, hlm. 278–296, Mei 2022, doi: 10.26421/JDI3.2-5.

[14] S. S, A. C, C. S, C. H C, dan A. G L, "BIG MART SALES PREDICTION USING MACHINE LEARNING," *IJARCCE*, vol. 12, no. 4, Apr 2023, doi: 10.17148/IJARCCE.2023.124112.

[15] K. Krishnareddy, T. V. Aravinda, K. Nair, U. K. Patel, G. Sadvokasova, dan V. S. Susan, "AI-based Fuzzy Clustering System for Improving Customer Relationship Management," dalam *2022 Sixth International Conference on I-SMAC (IoT in Social, Mobile, Analytics and Cloud) (I-SMAC)*, Dharan, Nepal: IEEE, Nov 2022, hlm. 673–677. doi: 10.1109/I-SMAC55078.2022.9987262.

JURNAL ECOTIPE
Electronic, Control, Telecommunication, Information, and Power Engineering

Volume 11, Issue 2, October 2024, pp. 216-226
ISSN 2355-5068 ; e-ISSN 2622-4852
DOI: 10.33019/jurnalecotipe.v11i2.4507

Design of a Rectangular Patch Microstrip Array Antenna with Proximity Coupled on ADS-B Receiver

Muhammad Fauzi Manalu[1], Muh. Wildan[2], M. Faisal Yoga Dewantara[3], Priyo Wibowo[4]
[1,2,3]Air Navigation Engineering, Curug Indonesian Aviation Polytechnic, Jl. PLP Curug, Tangerang, Banten, 15820 Indonesia
[4]National Research and Inovation Agency, Jl. M.H. Thamrin No. 8, Central Jakarta 10340 Indonesia

ARTICLE INFO

Article historys:

Received : …/…/…
Revised : …/…/…
Accepted : …/…/…

Keywords:

ADS-B; Array; Microstrip Antenna; Proximity Coupled; Rectangular Patch

ABSTRACT

One of the observation facilities available in Indonesia is Automatic Dependent Surveillance-Broadcast (ADS-B), a surveillance technology similar to Radio Detection and Ranging for monitoring air traffic. This system only received information transmissions from aircraft, broadcast on a frequency of 1090 MHz using a monopole antenna with large dimensions, ranging from 85 centimeters to 3,5 meters, and weighing between 1,5 kilograms to 26 kilograms. As an alternative, a microstrip antenna was chosen to reduce the large size and weight of the monopole antenna. This research aimed to design a 2x1 rectangular patch microstrip array antenna with a proximity coupled feeding method at a frequency of 1090 MHz. The antenna was designed using Antenna Design Software and fabricated using Epoxy substrate material with a copper ground plane. Return Loss, VSWR, Impedance and Gain parameters meet the specifications required for ADS-B receivers. However, the polarization parameters and radiation patterns do not yet meet the linear polarization and omnidirectional radiation patterns. And also array antenna design with proximity coupled supply can produce a high gain of more than 5 dBi, namely 6,4 dBi. The resulting antenna array has a bandwidth of between 20 – 30 MHz, namely 28 MHz. The test results demonstrated that the antenna successfully received signals from 32 aircraft, with the longest reception distance reaching 172,5 Nautical Miles (319,4 kilometer) at a maximum altitude of 36,950 feet.

Corresponding Author:

Muh. Wildan
Curug Indonesian Aviation Polytechnic, Jl. PLP Curug, Tangerang, Banten, 15820 Indonesia
Email: muh.wildan@ppicurug.ac.id

1. INTRODUCTION

As technology develops, facilities that support flight navigation services have also increased. Automatic Dependent Surveillance-Broadcast (ADS-B) technology is an observation facility where each aircraft, via its transponder, sends information twice every second to ground stations and other aircraft[1]. ADS-B operates as a receiver on the 1090 MegaHertz (MHz) frequency, requiring an antenna as a receiver device for electromagnetic signals emitted by aircraft[2]. Generally, ADS-B receivers use monopole antennas with lengths ranging from 0,85 m to 3,5 m, weights between 1,5 kg and 26 kg[3].

Monopole antennas which have quite large dimensions and weight provide opportunities for research and development with the aim of creating smaller antenna innovations. The microstrip antenna was chosen as the main variable in this research because microstrip antennas tend to be easy to manufacture, and have many other advantages[4]. The advantages of microstrip antennas include smaller size, light weight, and ease of manufacturing. Microstrip antennas are formed from three key components: radiating elements (patch), ground plane, and substrate. The ground plane is attached to the bottom of the substrate, while the metal conductor (patch) is attached to the top of the substrate.

JURNAL ECOTIPE
Electronic, Control, Telecommunication, Information, and Power Engineering
Volume 11, Issue 2, October 2024, pp. 216-226
ISSN 2355-5068 ; e-ISSN 2622-4852
DOI: 10.33019/jurnalecotipe.v11i2.4507

With its compact size and light weight, microstrip antennas offer a solution that is simple and easy to implement[5].

As a state of the art in this research, the design was carried out by combining antenna design methods that have been researched by previous researchers.

Table 1. The position of research on ADS-B compared with similar research

Reference	Antenna Parameter					
	Frequency (GHz)	**VSWR**	**Bandwidth (MHz)**	**Radiation Pattern**	**Gain (dB)**	**Antenna Design**
[6]	1,09	1,11	15,48	Uni-Directional	3,7	Rectangular Patch with proximity coupled
[7]	1,09	1,08	30	Unidirectional	4,01	Microstrip Circular Patch Array 4
[8]	1,09	1,22	44	Omnidirectional	2,53	Triangular Microstrip Patch Back to Back Structure
[9]	1,09	1,02	151	Omnidirectional	4,64	Microstrip Printed Collinear Dipole Array
[10]	1,09	1,65	57,5	Omnidirectional	4,04	Mikrostrip Circular Array 4 with MIMO 2x2
[11]	1,09	1,16	41	Uni-Directional	4,4	Microstrip Array Rectangular Patch
This research	**1,09**	**< 1,5**	**20 - 30**	**Omnidirectional**	**> 5**	**Recatangular Array 2x1 Microstrip Patch with Proximity Coupled**

2. RESEARCH METHOD

In this research, a rectangular microstrip antenna array was designed using the proximity coupled feeding method for ADS-B receivers. The patch and groundplane use copper or copper material, while the substrate uses FR-4 material with a dielectric value of 4,4. The technique that will be applied in this research is ADDIE (Analysis, Design, Development, Implementation and Evaluation). This method is a scientific approach to obtain information with specific targets and benefits. ADDIE is a framework that is often used to design a product efficiently[12].

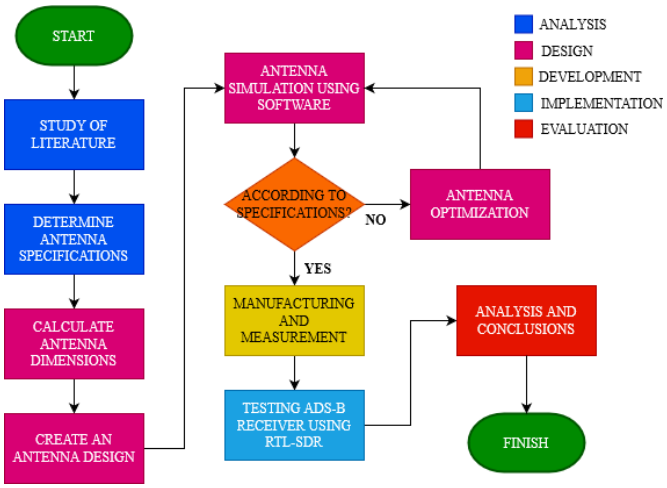

Figure 1. Flow Chart Antenna Design

Volume 11, Issue 2, October 2024, pp. 216-225
ISSN 2355-5068 ; e-ISSN 2622-4852
DOI: 10.33019/jurnalecotipe.v11i2.4507

2.1. Analysis

In this section, a literature evaluation is carried out to explore reference parameters which will be the basis for designing the antenna being planned. This reference refers to regulation KP 331 of 2016 concerning "Operational technical guidelines 171-08, Certification of ADS-B system equipment types"[13]. The following are standard parameter values that indicate good antenna performance.

Table 2. Antenna Parameter

Parameter	Value
Frequency of Work	1090 MHz
Return Loss	< -10 dB
VSWR	< 2
Bandwidth	20 – 30 MHz
Radiation Pattern	Omnidirectional

2.2. Design

At this section, This design process was carried out using the Antenna Design Software application and a simulation was carried out to evaluate the performance of the antenna created.

Table 3. Antenna Materials and Design

Parameter	Materials	Design
Patch	Copper	Array 2x1 Rectangular
Feedline	Copper	Proximity Couple Feed
Substrate	FR-4 Epoxy	Double Layer
Ground	Copper	Rectangular

Calculations are carried out to determine the length (L) and width (W) of the patch. Before calculating the length (L) and width (W), the length of the patch on the microstrip antenna must be adjusted carefully because it can impact return loss, while the width of the patch on the microstrip antenna affects the input impedance. Information regarding the material used such as dielectric thickness (h), dielectric constant (εr), and conductor thickness (t) must be known first. Therefore, With the values f = 1090 MHz, εr = 4,3, h = 1,6 mm entered into the equation, the patch dimensions can be calculated as follows:

a. Patch Width (Wp)

$$Wp = \frac{C}{2\,fo\sqrt{\frac{\varepsilon r + 1}{2}}} \tag{1}$$

Where :
C = Speed of Light (3×10^8 m/s)
fo = Frequency of Work (MHz)
ε_r = Dielectric Constant

b. Patch Length (Lp)

$$\lambda = \frac{C}{f} \tag{2}$$

$$\varepsilon_{eff} = \frac{\varepsilon_r + 1}{2} + \frac{\varepsilon_r - 1}{2}\left[\frac{1}{\sqrt{1 + 12\left(\frac{h}{w}\right)}}\right] \tag{3}$$

$$\lambda_f = \frac{\lambda}{\varepsilon_{eff}} \tag{4}$$

Where:
λ = Wave Length

JURNAL ECOTIPE
Electronic, Control, Telecommunication, Information, and Power Engineering
Volume 11, Issue 2, October 2024, pp. 216-226
ISSN 2355-5068 ; e-ISSN 2622-4852
DOI: 10.33019/jurnalecotipe.v11i2.4507

λ_f = Feedline Wave Length
C = Speed of Light (3×10^8 m/s)
f = Frequency of Work (MHz)
ε_{eff} = Effective Dielectric Constant
h = Substrate Thickness

Table 4. Calculation of Initial Parameters of Antenna Dimensions

No	Parameters	Initial Size	Information
1	*Wp*	83,74 mm	Patch Width
2	*Lp*	65,39 mm	Patch Length
3	*Wg*	138,74 mm	Groundplane Width
4	*Lg*	120,39 mm	Groundplane Length
5	*Wf*	3,05 mm	Feed Width 50 Ω
6	*Lf*	33,45 mm	Feed Length 50 Ω
7	*Wf2*	1,53 mm	T-Junction Feed Width 70 Ω
8	ε_r	4,4	Relative Permittivity
9	*h*	1,6 mm	Thick Dielectric Substrate
10	*t*	0,0335 mm	Groundplane Thickness
11	*r*	38,39 mm	Distance between patches/feed length 70Ω

2.3. Development

The next step is the development stage. At this stage, the antenna with the best parameters will be manufactured in physical form according to the equipment specifications.

2.4. Implementation

The next step is to carry out measurements and testing using a Vector Network Analyzer (VNA), Spectrum Analyzer, Signal Generator, and Antenna Tester. At this stage, the antenna will be measured in a laboratory to evaluate its physical performance after production. This measurement aims to obtain data regarding antenna parameters. This parameter data will be compared with the parameter values resulting from simulations using Antenna Design Software. Apart from that, the antenna will also be tested using an ADS-B receiver to test its ability to receive ADS-B signals at the 1090 MHz frequency and display targets or not.

2.5. Evaluation

The final step is product evaluation. By carrying out measurements in the laboratory, we can evaluate whether the parameters measured using the VNA, Spectrum Analyzer, Signal Generator, and Antenna Tester match the planned requirements or not. Next, we will analyze the causes of differences in values between simulation results and direct measurement results in the laboratory.

JURNAL ECTIPE
Electronic, Control, Telecommunication, Information, and Power Engineering
Volume 11, Issue 2, October 2024, pp. 216-225
ISSN 2355-5068 ; e-ISSN 2622-4852
DOI: 10.33019/jurnalecotipe.v11i2.4507

3. RESULTS AND DISCUSSION

3.1. Single Patch Microstrip Antenna Design

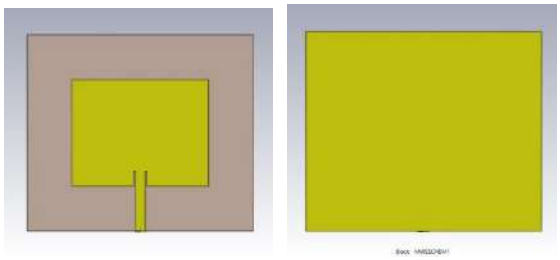

(a) (b)

Figure 2. (a) Single Patch Antenna Front View and (b) Single Patch Antenna Rear View

This antenna has been made according to the initial calculations in Table 4. The simulation results of this design do not meet the ADS-B antenna parameter values which are limited by the maximum standards for an antenna. The following are the simulation results of the single patch microstrip antenna design.

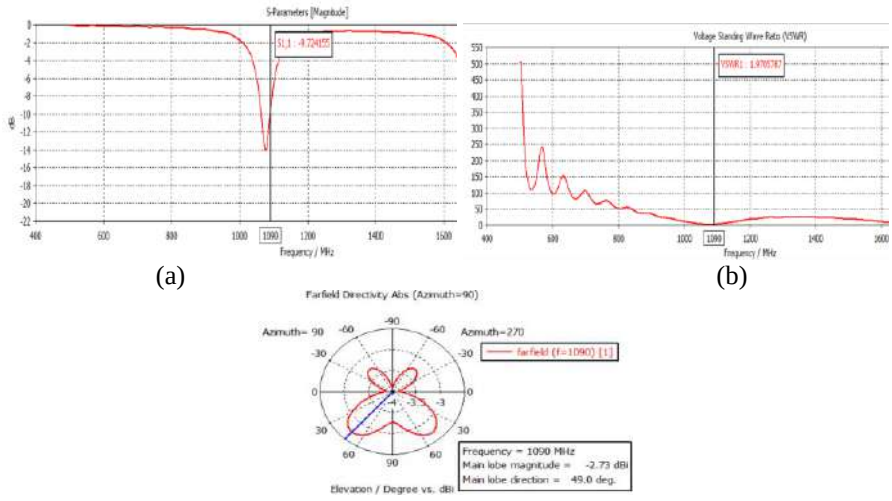

(a) (b)

(c)

Figure 3. (a) Return Loss Value of S11 (b) VSWR and (c) Radiation Pattern

The illustration of Figure 3 indicates that the antenna has not achieved optimal performance at the desired frequency, namely 1090 MHz. Apart from that, the VSWR, Return Loss and radiation pattern values of the antenna do not match the expected specifications.

3.2. Microstrip Array Antenna Design Without Proximity Couple

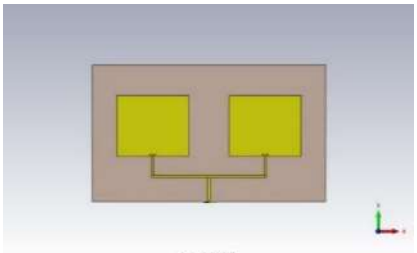

Figure 4. 2x1 Rectangular Array Antenna Design Without Proximity Couple

JURNAL ECOTIPE
Electronic, Control, Telecommunication, Information, and Power Engineering
Volume 11, Issue 2, October 2024, pp. 216-226
ISSN 2355-5068 ; e-ISSN 2622-4852
DOI: 10.33019/jurnalecotipe.v11i2.4507

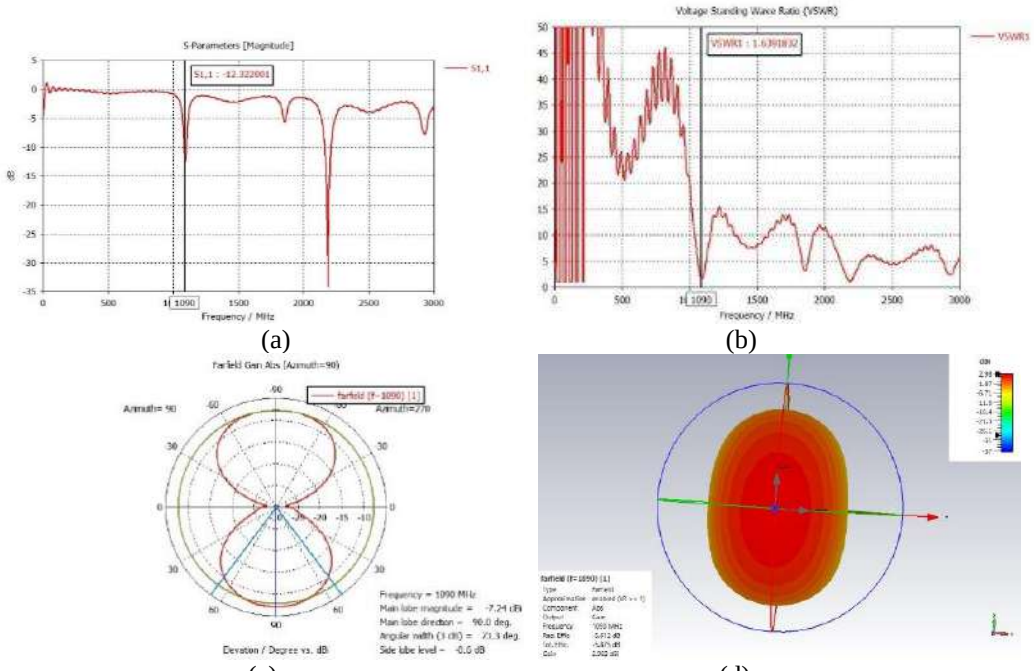

Figure 5. (a) Return Loss Value of S11 (b) VSWR (c) Radiation Pattern (d) Gain

In the picture of Figure 5, it can be seen that the return loss parameter value has reached -12,3 dB, and the VSWR value has reached 1,6, indicating that the antenna performance has improved compared to the previous design. Apart from that, the antenna radiation pattern has begun to form, although it is still bidirectional, whereas what is desired is an omnidirectional antenna radiation pattern. There is also an increase in the antenna gain value in this design, where the initial value of -2,73 dB increases to 2,98 dB

3.3. Microstrip Array Antenna Design Using the Proximity Coupled Method

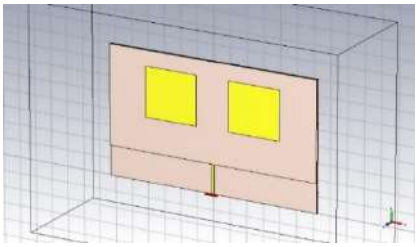

Figure 6. Microstrip array antenna design using the proximity couple method

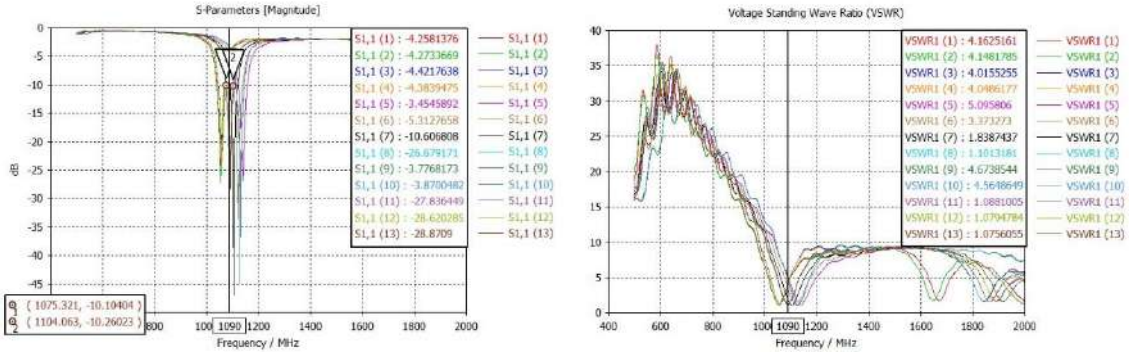

Volume 11, Issue 2, October 2024, pp. 216-225
ISSN 2355-5068 ; e-ISSN 2622-4852
DOI: 10.33019/jurnalecotipe.v11i2.4507

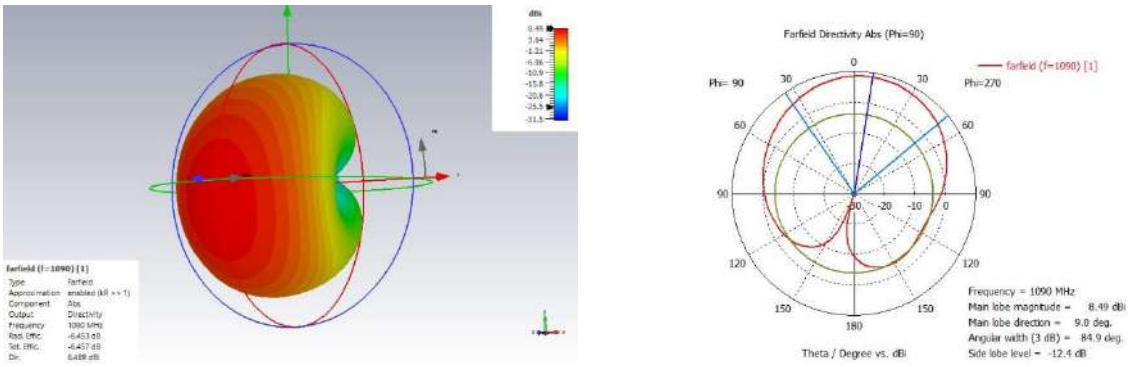

(c) (d)

Figure 7. (a) Return Loss Value of S11 (b) VSWR Optimization (c) Gain (d) Radiation Pattern

The illustration of Figure 7 shows the design and simulation results with optimization of a microstrip antenna that applies the proximity couple method and patch array configuration. By applying this technique, a return loss parameter value of -28,8 dB, a VSWR value of 1,07, a bandwidth of 28 MHz, and a gain of 8,49 dBi were obtained. This indicates that the performance of the antenna is significantly superior to previous antenna designs.

Table 5. Size Data Results After Optimization and Final Size Results for Antenna Dimensions

No	Symbol	Initial Size	Final Size	Information	Deviation
1	*Wp*	83,74 mm	62,56 mm	Patch Width	-25,28 %
2	*Lp*	65,39 mm	61,39 mm	Patch Length	-6,11%
3	*Wg*	138,74 mm	250 mm	Groundplane Width	+44,5%
4	*Lg*	120,39 mm	160 mm	Groundplane Length	+32,9%
5	*Wf*	3,05 mm	2,95 mm	Feed Width 50 Ω	-3,28%
6	*Lf*	33,45 mm	38,39 mm	Feed Length 50 Ω	+12,84%
7	*Wf2*	1,53 mm	1,53 mm	T-Junction Feed Width 70 Ω	-
8	ε_r	4,4	4,4	Relative Permittivity	-
9	*h*	1,6 mm	1,6 mm	Thick Dielectic Substrate	-
10	*t*	0,0335 mm	0,0335 mm	Groundplane Thickness	-
11	*r*	38,39 mm	38,39 mm	Distance between patches/feed length 70Ω	-

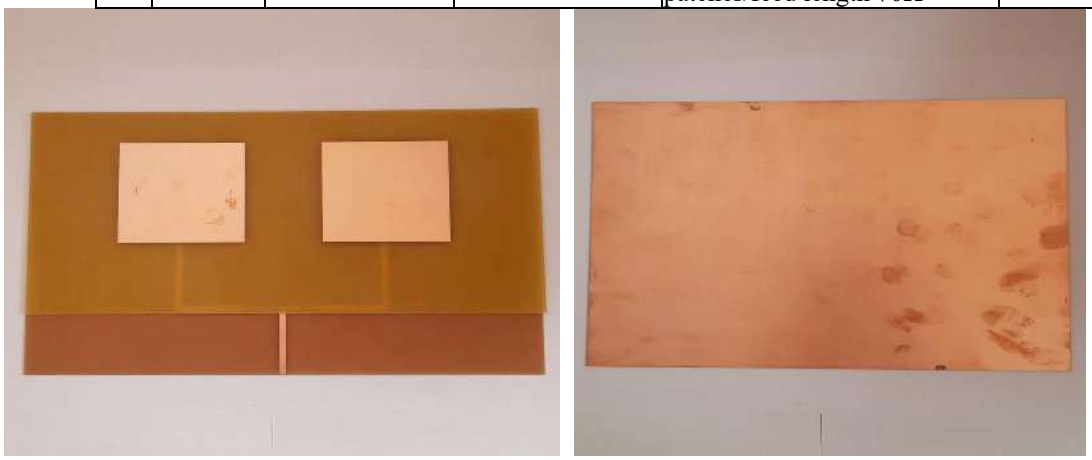

(a) (b)

Figure 8. (a) Physical Antenna Front View and (b) Physical Antenna Rear View

JURNAL ECOTIPE
Electronic, Control, Telecommunication, Information, and Power Engineering
Volume 11, Issue 2, October 2024, pp. 216-226
ISSN 2355-5068 ; e-ISSN 2622-4852
DOI: 10.33019/jurnalecotipe.v11i2.4507

3.4 Results of Direct Measurements of Antenna Parameters

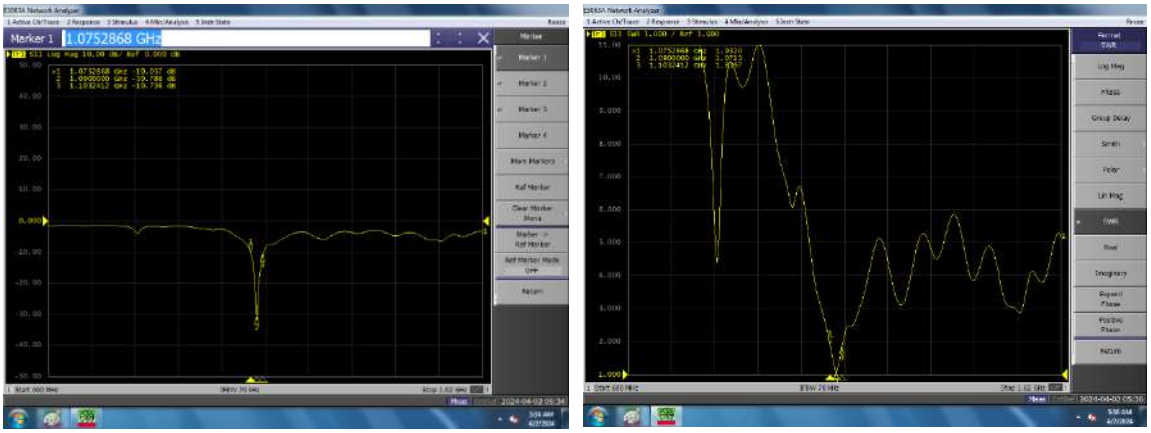

(a) (b)

Figure 9. (a) Return Loss Value on VNA and (b) VSWR on VNA

In this test, we will discuss measurements of a rectangular patch array antenna with prefabricated proximity couple supply. The aim is to verify whether the manufactured antenna has properties that correspond to the initial parameters that have been set.

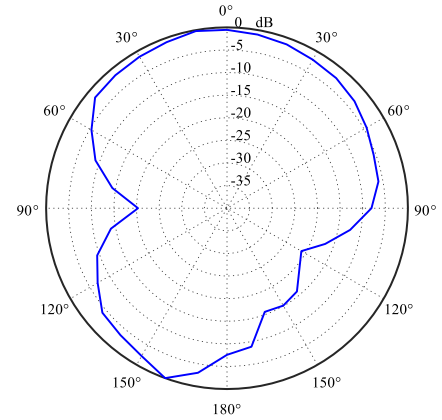

(a)

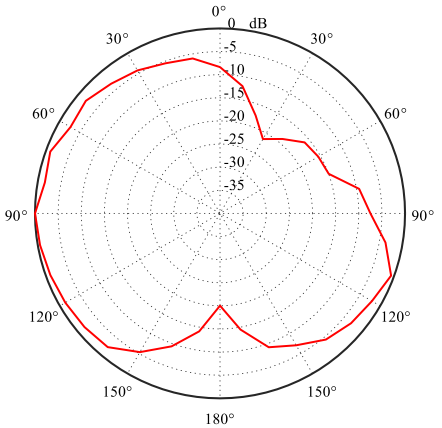

(b)

Figure 10. (a) Azimuth Radiation Pattern and (b) Elevation Radiation Pattern

JURNAL ECOTIPE
Electronic, Control, Telecommunication, Information, and Power Engineering
Volume 11, Issue 2, October 2024, pp. 216-225
ISSN 2355-5068 ; e-ISSN 2622-4852
DOI: 10.33019/jurnalecotipe.v11i2.4507

3.5 Antenna Test Results with RTL-SDR

Figure 11. Display of Antenna Test Results using RTL-SDR

Based on design testing with RTL-SDR, it shows quite good results. During testing, 32 aircraft were received, with the longest distance being 172,5 NM (319,4 km) and the maximum altitude achieved was 36,950 feet.

3.6 Comparative Evaluation of Measurement and Simulation Results

Table 6. Comparison of Parameter Values from Simulation Results and Measurement Results

Parameters	Spesification	Simulation	Measurement	Information
Return loss	≤ -10 dB	-28,87 dB	-30,78 dB	Memenuhi
VSWR	≤ 1,5	1,07	1,07	Memenuhi
Impedansi	± 50 Ω	52,4 Ω	48,91 Ω	Memenuhi
Bandwidth	≤ 30 MHz	28,7 MHz	28 MHz	Memenuhi
Gain	> 5 dBi	8,49 dBi	6,4 dBi	Memenuhi

Figure 12 shows a comparison between the graph of the measured return loss value and the simulated value resulting from the Antenna Design Software.

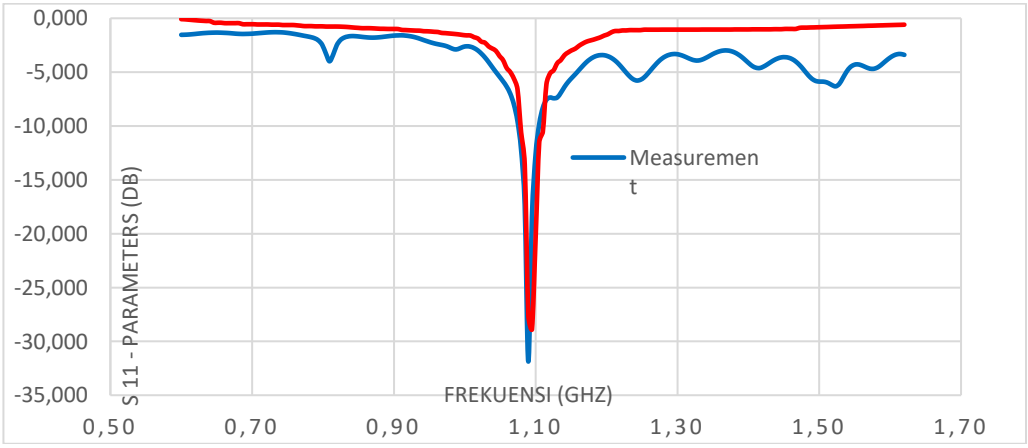

(a)

JURNAL ECTIPE
Electronic, Control, Telecommunication, Information, and Power Engineering
Volume 11, Issue 2, October 2024, pp. 216-226
ISSN 2355-5068 ; e-ISSN 2622-4852
DOI: 10.33019/jurnalecotipe.v11i2.4507

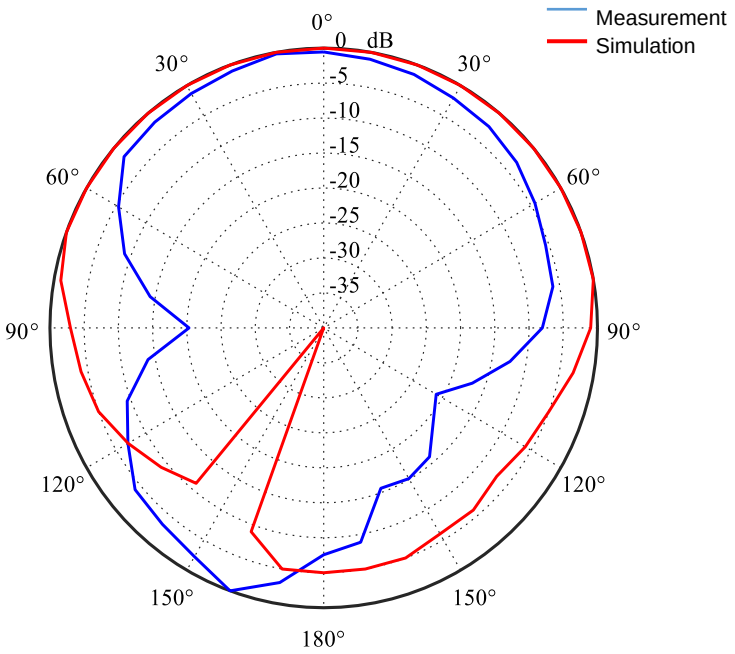

(b)

Figure 12. (a) Comparison of Return Loss Results and (b) Comparison of Radiation Pattern Results

4. CONCLUSION

Based on research from studies that have been carried out, the following conclusions can be drawn:

1. Obtaining a rectangular microstrip patch antenna array design using FR-4 Epoxy material using proximity couple feeding which operates at a frequency of 1090 MHz.
2. Return Loss, VSWR, Impedance and Gain parameters meet the specifications required for ADS-B receivers. However, the polarization parameters and radiation patterns do not yet meet the linear polarization and omnidirectional radiation patterns.
3. An array antenna design with proximity coupled supply can produce a high gain of more than 5 dBi, namely 6,4 dBi.
4. The resulting antenna array has a bandwidth of between 20 – 30 MHz, namely 28 MHz.

Based on the conclusions above, there are several recommendations for further research that can be considered in order to achieve better antenna performance, including:

1. Optimize and modify existing patch antenna designs, as well as designing antennas using other methods such as making them sectoral directional using three antennas combined into one to achieve an omnidirectional radiation pattern and linear polarization.
2. Develop research by trying various types of substrate materials which have a big influence on the results of the simulation and design, even though some materials may have a high price.
3. Carry out antenna trials in locations with minimal obstacles, to increase antenna power reception and widen the antenna coverage area.

REFERENCES

[1] Y. Nurhayati and Susanti, "Implementasi Automatic Dependent Surveillance Broadcast (ADS-B) di Indonesia," *Jurnal Perhubungan Udara*, 2014.
[2] A. B. Pradana, *Surveilance Techniques*, 1st ed, 2013.

JURNAL ECOTIPE
Electronic, Control, Telecommunication, Information, and Power Engineering
Volume 11, Issue 2, October 2024, pp. 216-225
ISSN 2355-5068 ; e-ISSN 2622-4852
DOI: 10.33019/jurnalecotipe.v11i2.4507

[3] Thales, *Thales ADS-B Training Overview*, Paris, France, 2007.
[4] H. Madiawati, A. B. Simanjuntak, E. Sulaeman, and M. S. I. Hibban, "Antena Mikrostrip Array untuk Aplikasi Radar Cuaca pada Frekuensi C-Band Menggunakan Metode Defected Ground Structure," *JTERA (Jurnal Teknologi Rekayasa)*, vol. 7, no. 2, p. 181, Dec. 2022, doi: 10.31544/jtera.v7.i2.2022.181-188.
[5] Balanis C.A., *Antenna Theory-Analysis and Design*, 3rd ed. New Jersey, 2005.
[6] A. Aditya, "Rancangan Antena Mikrostrip Rectangular Patch Dengan Pencatuan Proximity Coupled Untuk Aplikasi ADS-B Receiver," 2021.
[7] Z. Faizin, "Rancangan Antena Mikrostrip Circular Patch Array 4 Sebagai Antena Penerima Automatic Dependent Surveillance Broadcast (ADS-B)," 2022.
[8] I. Apriadi, "Rancang Bangun Antena Mikrostrip Triangular Patch Dengan Teknik Back To Back Structure Untuk Menghasilkan Pola Radiasi Omnidirectional Pada ADS-B Receiver," 2023.
[9] Y. C. Simamora, D. A. Nurmantris, and Y. P. Saputera, "Rancang Bangun Antena Mikrostrip Printed Collinear Dipole Array Untuk Aplikasi ADS-B Receiver," Dec. 2021.
[10] N. P. M. I. Pertiwi, R. P. Astuti, and B. S. Nugroho, "Antena Mikrostrip Circular Array 4 Patch 1090 MHz Dengan MIMO 2X2 Untuk Penerima ADS-B Pada Pesawat Terbang," Dec. 2022.
[11] Y. N. Perdana, "Rancangan Antena Mikrostrip Rectangular Patch Berbentuk Array Sebagai Receiver Automatic Dependent Surveillance Broadcast," 2022.
[12] N. Aldoobie, *ADDIE Model*," Dec. Florida, 2015.
[13] Direktorat Jenderal Perhubungan Udara, *KP 331 Tahun 2016 tentang "Pedoman Teknis Operasional 171-08 (Advisory Circular PART 171-08) Sertifikasi Tipe Peralatan Automatic Dependent Surveillance Broadcast (ADS-B) System*. 2016.

JURNAL ECOTIPE
Electronic, Control, Telecommunication, Information, and Power Engineering

Volume 11, Issue 2, October 2024, pp. 227-236
ISSN 2355-5068 ; e-ISSN 2622-4852
DOI: 10.33019/jurnalecotipe.v11i2.4523

Enhanced Depth Control and Stability in Submersible Pylon Inspection Robots Using IMU-Based Extended Kalman Filter and PID Control

Hendi Purnata[1] , Riyani Prima Dewi[2] , Saepul Rahmat[3] Erna Alimudin[4] , Novita Asma Ilahi[5]
[123]Mechatronics Engineering, Cilacap State of Polytechnic, Jl. Dr. Soetomo No. 1, Cilacap 53212, Indonesia

ARTICLE INFO

Article history:

Received: .../.../...
Revised: .../.../...
Accepted: .../.../...

Keywords:

IMU, EKF, PID, depth control, underwater robot, stability

ABSTRACT

This research develops a Submersible Pylon Inspection Robot (SPIR) equipped with an Inertial Measurement Unit (IMU) and Extended Kalman Filter (EKF) to improve stability and depth control in dynamic underwater environments. The implemented control system uses a customized PID algorithm to optimize the depth response. Results show that SPIR is able to maintain depth well at shallow depths, but struggles to maintain stability at deeper depths, especially when encountering strong currents. Large fluctuations in the z-axis and position deviation at deeper depths indicate the need for refinement of the PID control algorithm, including the possible use of advanced control or prediction-based control to cope with dynamic environmental conditions. In addition, the integration of IMU and EKF showed good performance in reducing noise in the sensor data, but challenges arose in the early phase of measurement, where large fluctuations in the quaternion angle indicated the initial instability of the sensor. Therefore, it is recommended to make further adjustments to the EKF parameters to accelerate convergence and reduce sensor noise. This research shows that with further refinements to the sensor control and integration, SPIR can be an effective tool for underwater inspection operations at more extreme conditions.

Corresponding Author:

Hendi Purnata
Electronics Engineering, Cilacap State of Polytechnic, Jl. Dr. Soetomo No. 1, Cilacap 53212, Indonesia
Email: hendipurnata@pnc.ac.id

1. INTRODUCTION

In recent decades, advances in marine technology have triggered a growing interest in the exploration and exploitation of marine resources, especially in maritime countries such as Indonesia with vast marine areas [1]. However, the complexity of marine robotics, including high cost, large size, and significant weight, is a major obstacle in the development of this technology. The sinking of submarine 402 in April 2021, which was caused by natural factors such as underwater currents, shows the urgency of developing underwater technology to strengthen Indonesia's marine security [2]. Rapid advances in marine science and technology over the past two decades have fueled a growing interest in the exploration and exploitation of the oceans for scientific and commercial purposes. In this context, marine robotics has emerged as a key technology to carry out increasingly complex and challenging missions at sea. Although there have been significant advances in methodologies and applications, major challenges remain, requiring further research and development to meet the requirements of the next generation of marine robots and their support systems [3-5].

Despite the progress that has been made, major challenges such as depth control and stability still hinder the development of underwater vehicles. Some research, such as the development of the

Volume 11, Issue 2, October 2024, pp. 227-236
ISSN 2355-5068; e-ISSN 2622-4852
DOI: 10.33019/jurnalecotipe.v11i2.4523

Submersible Pylon Inspection Robot (SPIR), has focused on improving automation to reduce human involvement in hazardous conditions. SPIR uses SONAR-based navigation and 3D reconstruction, but still faces difficulties in controlling depth, especially in environments with strong currents [6]. In marine environments, effective depth control on underwater vehicles faces significant challenges due to the reliance on navigation and communication systems that often suffer from limitations in range and latency. The integration of unmanned systems, such as UAVs, can offer potential solutions to improve connectivity and resource management with great flexibility, but also introduces new complexities in data management and dynamic control. Despite the progress made in the automation of underwater vehicle docking and navigation systems, there is still an urgent need to overcome these constraints, including the adaptation to non-specially designed docking systems as well as the application of new technologies in extreme environments [7-8]

Similar challenges are also encountered in the control of Remotely Operated Vehicles (ROVs), where reliance on limited sensors in a dynamic environment often leads to depth and position estimation errors [9-11].This paper highlights the importance of advanced methods and techniques for depth control in underwater Remotely Operated Vehicles (ROVs). Given the wide maritime and industrial applications, including repair, the maintenance of precise depth control is crucial. The methods proposed in this study, such as a robust H∞ depth tracking controller with an innovative event-triggering method, the use of a tether to measure hydrodynamic forces without interference, as well as a fuzzy PID strategy with dynamic compensation, all aim to improve ROV accuracy and stability under complex environmental conditions. Experimental results show that these approaches are effective in reducing depth errors, minimizing the influence of disturbances, and optimizing ROV performance, which are indispensable for meeting the requirements of practical applications in various sectors.

The use of Inertial Measurement Unit (IMU) and Extended Kalman Filter (EKF) in depth control has been an active research area, but current technologies still face limitations in terms of accuracy and stability. In an effort to improve accuracy, several studies have proposed multi-sensor fusion systems that combine data from IMUs, pressure sensors, optical flow, and ArUco markers to obtain more precise positions and reduce location drift over time. In addition, techniques such as the combination of short baseline (SBL) and inverted ultrashort baseline (iUSBL) measurements using EKF have been applied in underwater mining scenarios to overcome localization challenges in confined environments. Orientation estimation with EKF is also used in Autonomous Underwater Vehicles (AUVs) to update position estimation under magnetic disturbance conditions, by combining data from GPS, Doppler Velocity Log (DVL), and Fiber Optic Gyroscope (FOG). Although these approaches show promising results, further development is needed to achieve more accurate and stable depth control in various environmental conditions [12-13]. However, these methods still have limitations in terms of accuracy and adaptability under rapidly changing environmental conditions.

The use of MEMS-based nine-axis Inertial Measurement Units (IMUs) has been widely applied in various fields, such as underwater vehicles, unmanned aerial vehicles, and bionic robots. However, due to the noise in gyroscope sensors and errors in the solution process, the rotation angle estimated with only angular velocity data usually contains large accumulated errors and must be corrected by acceleration and geomagnetic measurements. A serious problem arises if there are strong magnetic field anomalies in the environment, which can degrade the performance of geomagnetic field correction and add errors. To improve the heading and attitude estimation accuracy of the nine-axis MEMS IMU in magnetic field anomalies, this study proposes the use of a partially adaptive Extended Kalman Filter (EKF) (PADEKF) with dual quaternions. To reduce the connected influence of magnetic measurement noise on attitude estimation in one quaternion, the heading angle and attitude are represented with two independent quaternions in the state vector. A self-adaptability design is adopted in EKF to improve robustness to spatially varying magnetic anomaly data. In the case of strong and fast-varying magnetic anomaly fields that cannot be well modeled by PADEKF, a combination algorithm of LSTM neural network and Runge-Kutta method is given to obtain a good heading estimation. Field experiments in various scenarios are conducted and verify the effectiveness of the proposed approach [14].

PID control methods are frequently used in autonomous underwater vehicle (AUV) depth control, but they are often unable to cope with significant depth fluctuations or adapt to dynamic changes in the underwater environment. For example, in the proposed study, PID control is used to regulate the

Volume 11, Issue 2, October 2024, pp. 227-236
ISSN 2355-5068 ; e-ISSN 2622-4852
DOI: 10.33019/jurnalecotipe.v11i2.4523

propeller rotation of a fast-moving AUV in a horizontal orientation and then rotate downward to float at the desired water depth. Although PID control can execute depth control maneuvers, this approach is not always effective in dealing with rapidly changing and dynamic conditions underwater. The optimization of inertia, propeller, battery capacity, and PID control characteristics proposed in this study shows that, although useful, PID control requires further adjustments to work efficiently under extreme environmental fluctuations. The numerical simulations performed also show that the AUV propeller often works in turbine mode, which requires additional protection for the AUV's electrical/electronic components, highlighting the need for more adaptive and robust control methods in underwater environments [15]

Previous research shows that advanced methods such as PID, EKF, and IMU control can improve depth control, but are often not fully effective under complex and dynamic environmental conditions [9-11]. Recent advances in the application of Lie Groups to robotic localization, such as the use of the Invariant Extended Kalman Filter (InEKF), have significantly improved the accuracy of estimation and characterization of uncertainty in underwater navigation. InEKF, which utilizes the dynamic error in the Lie Groups matrix, offers linearity with minimal approximation error and excellent convergence, enabling more effective integration of sensors such as IMU and DVL in navigation systems. Recent research integrating IMUs with sensor fusion systems and Invariant Extended Kalman Filter (InEKF)-based navigation techniques has shown improvements in stability and position estimation accuracy [16-17].

Although many solutions have been proposed for depth control, there is still an urgent need to develop a more adaptive and robust system in the face of uncertain environmental conditions, especially in underwater robotic applications such as SPIR. This research aims to integrate IMU with EKF to improve depth estimation accuracy and stability, and apply more adaptive PID control to deal with depth fluctuations more effectively. With this technology, it is expected that SPIR can achieve better stability, making a significant contribution to the safety and efficiency of underwater missions.

2. RESEARCH METHOD

To control the motor as the movement of SPIR, this research uses sensor stages such as Inertial Measurement Unit (IMU) and Extended Kalman Filter (EKF). The IMU is used to measure the linear acceleration and angular velocity of the robot, which provides information about the robot's position and orientation in space. The data obtained from the IMU is then processed using the EKF, which is a probability-based estimation technique to reduce noise and produce more accurate estimates of the robot's position and orientation. Controlling the estimation and movement of the robot is assisted by the PID method so that SPIR can move by adjusting the actuators used.

2.1. SPIR

SPIR (Submersible Pylon Inspection Robot) is an advanced technology specifically designed to facilitate movement and inspection below the water surface, especially in conditions that are difficult to reach by humans. The main focus of SPIR is its ability to maneuver in the underwater environment, using a series of thrusters and sensors. Movement on the SPIR (Submersible Pylon Inspection Robot) uses a configuration of four DC motors. Each motor has a specific role in controlling the horizontal and vertical motion of the robot, with the aim of improving stability and precision during underwater operations.

Motor 1 and Motor 2 (Horizontal Movement): The motors are placed at the back of the robot and configured to control forward and backward movements. The two motors work together to push the robot in a forward or backward direction, and differentially to perform turning maneuvers. Motor 3 and Motor 4 (Vertical Movement): The motors are mounted vertically and work to control the up and down motion of the robot. By varying the rotation speed of these two motors, SPIR can adjust its depth in the water.

2.1. IMU

The positioning designer of the SPIR uses control principles on the x, y, and z axes. The x-axis determines the position or motion of the SPIR to the right and left, called surge motion, as well as

JURNAL ECTIPE
Electronic, Control, Telecommunication, Information, and Power Engineering
Volume 11, Issue 2, October 2024, pp. 227-236
ISSN 2355-5068; e-ISSN 2622-4852
DOI: 10.33019/jurnalecotipe.v11i2.4523

rotation about the x-axis known as roll. On the y-axis, there is forward and backward movement called sway, and rotation about the y-axis called pitch motion. While in the z-axis, the SPIR position will form heave motion, which is the movement up and down in the z-axis direction, as well as rotation about the z-axis which determines the yaw position.

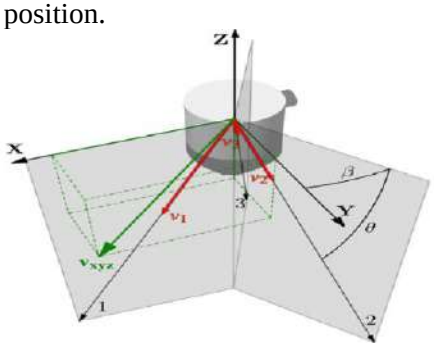

Figure 1. Axis of the IMU sensor

The propagation is described by a unit vector referenced to the sensor body frame and aligned with the transducer axis. The unit vector defines the relationship between these two velocities as

$$v_i = e_i \cdot v_{xyz} \tag{1}$$

Where *vi* is a scalar value representing the speed measured by transducer I, **ei** is the unit vector corresponding to the same transducer and **vxyz** represents the vehicle speed in the sensor body frame:

$$v_{xyz} = \begin{bmatrix} v_x & v_y & v_z \end{bmatrix} \tag{2}$$

In a three-transducer configuration, the unit vector is defined as

$$\begin{aligned} e_1 &= [cos\ cos\ \theta \quad -sin\theta\ ] \\ e_2 &= [-cos\ cos\ \theta \quad sin\ sin\ \beta \quad cos\ cos\ \theta\ cos\ cos\ \beta \quad -sin\ sin\ \theta\ ] \\ e_3 &= [-cos\ cos\ \theta \quad sin\ sin\ \beta \quad \theta\ cos\ cos\ \beta \quad -sin\ sin\ \theta\ ] \end{aligned} \tag{3}$$

Then, the velocity measured on each beam can be obtained by substituting the unit vector:

$$\begin{aligned} v_1 &= v_x\ cos\ cos\ \theta \quad - v_z\ sin\ sin\ \theta \quad v_2 \\ &= -v_x\ cos\ cos\ \theta \quad sin\ sin\ \beta \quad + v_y\ cos\ cos\ \theta \quad sin\ sin\ \beta \quad - v_z\ sin\ sin\ \theta \quad v_3 \\ &= \ -v_x\ cos\ cos\ \theta \quad sin\ sin\ \beta \quad - v_y\ cos\ cos\ \theta \quad cos\ cos\ \beta \quad - v_z\ sin\ sin\ \theta \end{aligned} \tag{4}$$

Finally, these three equations can be used to determine the three unknown components of vehicle speed

$$\begin{aligned} v_x &= \frac{v_1}{cos\ cos\ \theta} + \frac{v_3 + v_2 + 2v_1\ sin\ sin\ \beta}{-2\ cos\ cos\ \theta \quad - 2\ cos\ cos\ \theta \quad sin\ sin\ \beta} \quad v_y = \frac{v_2 - v_3}{2\ cos\ cos\ \theta\ cos\ cos\ \beta} \quad v_z \\ &= \frac{v_3 + v_2 + 2v_1\ sin\ sin\ \beta}{-2\ sin\ sin\ \theta \quad - 2\ sin\ sin\ \theta\ sin\ sin\ \beta} \end{aligned} \tag{5}$$

The navigator aims to estimate the position of the robot. To achieve this goal, an interface known as the Navigation Sensor of the IMU is used. This interface provides various methods to return position, velocity, and acceleration in 6 DOF (Degree of Freedom) as well as an estimation of the quality of its measurements.

2.2. EKF

Extended Kalman Filter (EKF) is used to estimate the position, velocity, and orientation of SPIR by combining data from IMU and other sensors. EKF is a method capable of handling non-linear systems, which are often encountered in underwater navigation. The state equation describes the evolution of the system over time.

Extended Kalman Filter (EKF) is used to estimate the position, velocity, and orientation of an underwater vehicle (ROV) by combining data from IMU and other sensors. EKF is a method capable of handling non-linear systems, which are often encountered in underwater navigation. The state equations describe the evolution of the system over time:

$$x_{k+1} = f(x_k, u_k) + w_k \tag{6}$$

Where x_k is the state vector, u_k is the input vector and w_k is the process noise.

The observation equation describes how sensor measurements relate to the system state:

$$z_k = h(x_k) + v_k \tag{7}$$

JURNAL ECOTIPE
Electronic, Control, Telecommunication, Information, and Power Engineering
Volume 11, Issue 2, October 2024, pp. 227-236
ISSN 2355-5068 ; e-ISSN 2622-4852
DOI: 10.33019/jurnalecotipe.v11i2.4523

Where z_k is the measurement vector and v_k is the measurement noise which is the algorithm of EKF with initialization

$$\hat{x}_0 = x_0, P_0 = P_0 \tag{8}$$

Where $\hat{x}_0$ is the initial estimate of the state and P_0 is the initial error covariance matrix, with prediction

$$\begin{aligned} \hat{x}_{k|k-1} &= f\left(\hat{x}_{k-1|k-1}, u_{k-1}\right) \\ P_{k|k-1} &= F_k P_{k-1|k-1} F_k^T + Q_k \end{aligned} \tag{9}$$

Where F_k is the Jacobian matrix of **f** with respect to x_k, and Q_k is the process noise covariance matrix. Update equations such as

$$\begin{aligned} K_k &= P_{k|k-1} H_k^T \left(H_k P_{k|k-1} H_k^T + R_k\right)^{-1} \\ \hat{x}_k &= \hat{x}_{k|k-1} + K_k \left(z_k - h\left(\hat{x}_{k|k-1}\right)\right) \\ P_{k|k-1} &= (I - K_k H_k) P_{k|k-1} \end{aligned} \tag{10}$$

Where H_k is the Jacobian matrix of **h** exposed x_k and R_k is the measurement noise covariance matrix.

2.3. Control System

Movement control is performed according to the desired direction. Once the data from the IMU and EKF is processed to estimate the position and orientation of the SPIR, the next step is to drive the motor or actuator to achieve the set goal. A PID (Proportional-Integral-Derivative) controller is used to generate the control signals required to drive the SPIR.

In this section, we define the basic parameters of SPIR (Submersible Pylon Inspection Robot) and the PID controller used in the simulation using MATLAB. The mass used is 10 Kg and with a damping coefficient that controls how fast the speed decreases due to friction or resistance of 0.5. The setpoint in this study is a depth of 5 meters. The simulation process is carried out in a loop with the following steps:

Calculating error

$$e(t) = depth - position\ (i-1) \tag{11}$$

Calculating integral and derivative errors

$$\begin{aligned} \text{Integral Error} &= \int_0^t e(\tau) d\tau \\ \text{Derivative Error} &= \frac{de(t)}{dt} \end{aligned} \tag{12}$$

Calculating the PID Control Signal

$$u(t) = K_p \cdot e(t) + K_i \cdot \int_0^t e(\tau) d\tau + K_d \cdot \frac{de(t)}{dt} \tag{13}$$

SPIR Dynamics Model

$$a\ (i) = \frac{u\ (i) - c \cdot v(i-1)}{m} \tag{14}$$

$$v\ (i) = v(i-1) + a\ (i).\Delta t \tag{15}$$

$$x(i) = x\ (i-1) + v(i).dt \tag{16}$$

The output of the controller is an 8 bit PWM signal with $[0,255]$ or as $pwmrange$ with scale

$$scaledoutputController = \frac{controlSignal - \min\ (controlSignal)}{\max(controlSignal) - \min(controlSignal)} \tag{17}$$

To make the duty cycle to signal the motor then

$$Duty\ Cycle = \frac{scaledoutputController}{pwmrange} \tag{18}$$

JURNAL ECTIPE
Electronic, Control, Telecommunication, Information, and Power Engineering
Volume 11, Issue 2, October 2024, pp. 227-236
ISSN 2355-5068; e-ISSN 2622-4852
DOI: 10.33019/jurnalecotipe.v11i2.4523

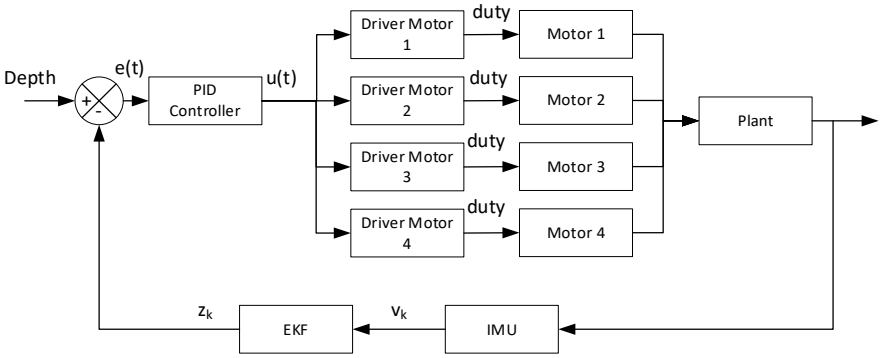

Figure 2. Overall Block Diagram

3. RESULTS AND DISCUSSION

In this chapter, we discuss the results of the analysis and implementation of controls for the Submersible Pylon Inspection Robot (SPIR) based on data obtained from various measurements and the mathematical equations used in the system. This discussion begins with an assessment of the system's accuracy in position estimation, continues with orientation and depth analysis, and concludes with an evaluation of the motor control.

3.1 Z Axis Position Error

Graph the position error on the Z-axis to evaluate the accuracy of the system in maintaining the desired depth. The equations used to calculate the velocity of the IMU, and the estimation results using the Extended Kalman Filter (EKF), will form the basis for understanding how this position error evolves over time.

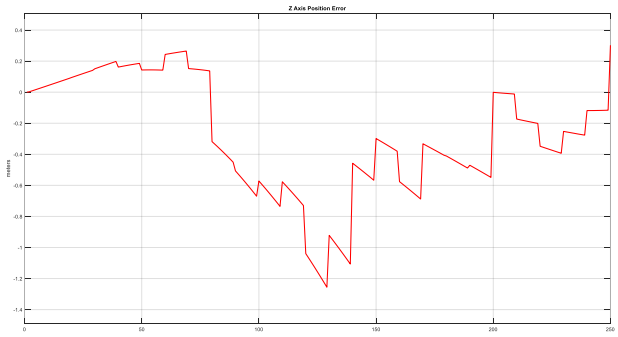

Figure 3. Error on the Z-axis

This figure illustrates the position error in the z-axis. At the beginning of the measurement, the position error starts from a value close to 0.5 meters and shows a significant decrease with some large fluctuations. The position error reaches its lowest value of about -1.5 meters at the 100th step, indicating a large error in position estimation at that phase. After reaching the lowest point, the position error starts to increase again, albeit with smaller fluctuations. The figure above shows that the system experiences large fluctuations in the early stages of measurement, both in quaternion angle and in position estimation. The correlation between quaternion angle fluctuations and position error may indicate that the stability of the quaternion angle contributes to the reduction of position error over time.

3.2 Quaternion distance

Furthermore, the quaternion angle graph is displayed to check the stability of the SPIR orientation. The quaternion angle provides information about the rotation and orientation of the SPIR during the simulation, which is a key factor in ensuring that the position and depth estimates are accurate. This data is important for understanding the effect of orientation on position error and how orientation stability contributes to depth control.

JURNAL ECTIPE
Electronic, Control, Telecommunication, Information, and Power Engineering
Volume 11, Issue 2, October 2024, pp. 227-236
ISSN 2355-5068 ; e-ISSN 2622-4852
DOI: 10.33019/jurnalecotipe.v11i2.4523

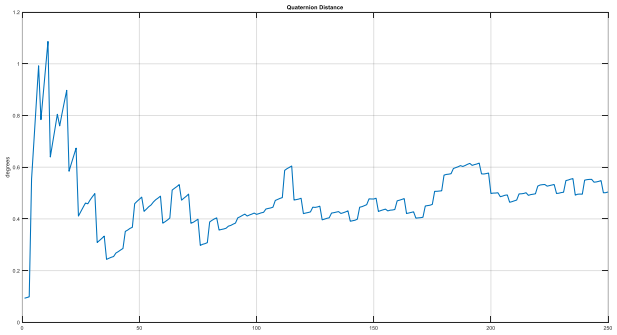

Figure 4. Quaternion distance

In the analysis of the resulting data, it shows significant variations at the start of the measurement. The large fluctuations seen in this plot, with peaks reaching about 1.1 degrees, are due to the initial instability of the sensor. After the initial fluctuation period, the quaternion angle shows a tendency to stabilize with small fluctuations that persist until the end of the measurement.

3.3 Depth Position

The depth position graph shows the change in SPIR depth over time. This graph provides immediate context on how the system responds to depth control and relates it to previously identified position errors. The depth position analysis allows us to assess the effectiveness of the control in practice and see how the desired depth is achieved or maintained.

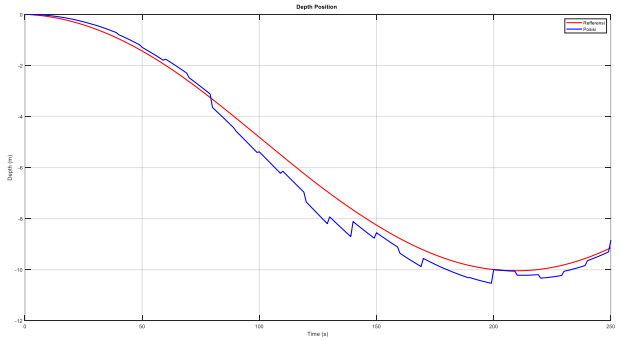

Figure 5. Depth position

In the initial phase of measurement (0 to 50 seconds), the actual depth generally follows the reference depth accurately, although there is a slight deviation. However, after 50 seconds, the deviation between the actual and reference depths began to increase, with the actual depth showing greater fluctuations than the reference. At a depth of about -6 meters, the deviation becomes more significant, and at a maximum depth of about -10 meters, there is the greatest deviation, with the actual depth far below the reference line. This shows the difficulty of the system in maintaining the desired depth at deeper depths.

After reaching the deepest depth, both the actual and reference depths started to return to shallower depths, with the actual depth still showing fluctuations but getting closer to the reference depth. Overall, while SLAM can follow the reference depth at shallower depths quite well, the system shows limitations in maintaining a stable depth at deeper depths.

In addition, the performance of the system combining the Inertial Measurement Unit (IMU) and Extended Kalman Filter (EKF) is shown to improve the accuracy of depth and position estimation. In the Z-axis position error graph, it can be seen that the large fluctuations in the initial phase of measurement are minimized over time thanks to better system calibration. The IMU is able to provide fairly accurate data on acceleration and angular velocity, while the EKF is effective in filtering out noise and integrating data from multiple sensors to provide more stable position estimation. Even so, challenges remain at deeper depths, where the deviation from the reference depth becomes larger. This

JURNAL ECTIPE
Electronic, Control, Telecommunication, Information, and Power Engineering
Volume 11, Issue 2, October 2024, pp. 227-236
ISSN 2355-5068; e-ISSN 2622-4852
DOI: 10.33019/jurnalecotipe.v11i2.4523

signals the need for further customization of the system to deal with more extreme environmental conditions.

3.4 SPIR Robot Movement Depth

This motor is for depth regulation, and this graph shows how the PID control signal is translated into motor motion. This evaluation helps in assessing how well the depth control is controlled by the motor.

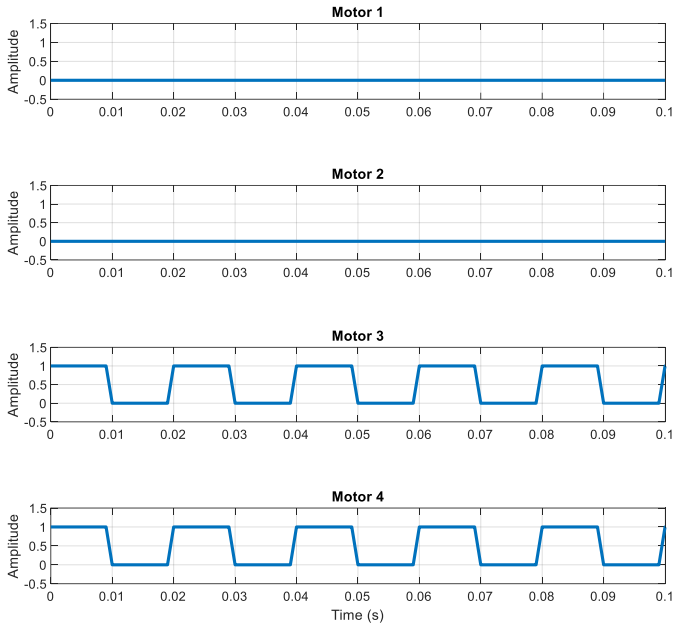

Figure 6. Depth movement of the SPIR robot

The figure above shows the activity of the four motors depicted through the change in amplitude against time. In the first and second subplots, it can be seen that motor 1 and motor 2 show no significant change in amplitude, remaining around zero all the time. This indicates that motor 1 and motor 2 are inactive or stopped, with no PWM (Pulse Width Modulation) applied to them.

In contrast, in the third and fourth subplots, there is a clear and oscillating change in amplitude, indicating that motor 3 and motor 4 are active. This changing amplitude indicates that the presence of PWM indicates that motors 3 and 4 are rotating. The activity of motors 3 and 4 indicates that they are operating to reach a certain depth according to the given PWM pattern, while motors 1 and 2 remain inactive.

The motor activity in SPIR shows specific coordination for the stabilization and depth regulation tasks. Motor 1 and Motor 2 remain inactive during depth setting operations, as these motors function to maintain horizontal stability (roll and pitch). Meanwhile, Motor 3 and Motor 4 are active in controlling the vertical movement, which allows SPIR to achieve and maintain the desired depth. This pattern shows the logic behind the motor assignment, where the depth drive motors are focused on setting the vertical position, while the stabilization motors function in maintaining balance when there is no significant depth change.

3.5 SPIR Robot Motion to Maintain Special Stability of Motors 1 and 2

Analyze the motion graphs of motors 1 and 2 that stabilize the SPIR. This graph illustrates how these motors operate to stabilize the SPIR and maintain balance, as well as ensuring that the system can cope effectively with changes in position and depth. This evaluation provides a complete view of how position stabilization is maintained and how the overall control is implemented.

JURNAL ECTIPE
Electronic, Control, Telecommunication, Information, and Power Engineering
Volume 11, Issue 2, October 2024, pp. 227-236
ISSN 2355-5068 ; e-ISSN 2622-4852
DOI: 10.33019/jurnalecotipe.v11i2.4523

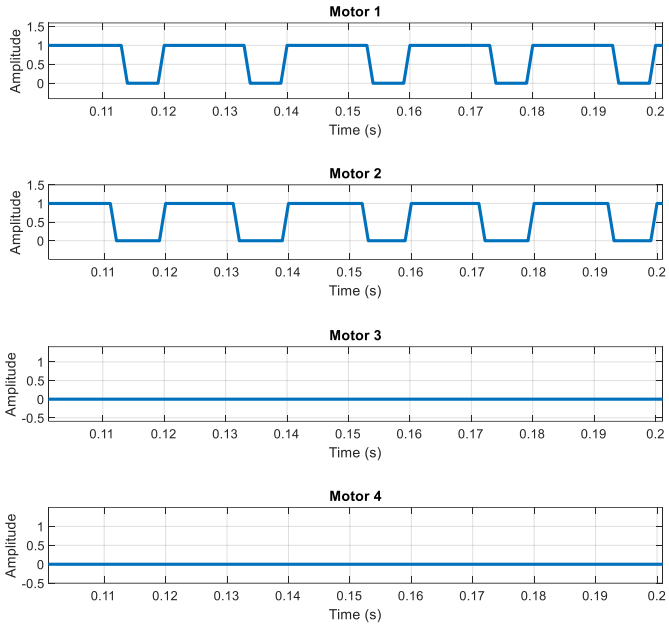

Figure 7: Movement to maintain depth position

This figure shows the activity of four motors in an attempt to maintain a certain depth, focusing on motor 1 and motor 2. In the first and second subplots, it can be seen that motor 1 and motor 2 experience significant amplitude changes and oscillate between certain values. This pattern indicates that motor 1 and motor 2 are active and rotating, following the given PWM (*Pulse Width Modulation*) signal. This activity of motors 1 and 2 indicates that they are functioning to maintain the desired depth by regulating their rotation speed and direction based on the PWM pattern.

In contrast, the third and fourth subplots show that motor 3 and motor 4 were not active during this observation period, as the amplitude remained around zero all the time. The absence of amplitude change in motor 3 and motor 4 indicates that no PWM signal was applied.

4. CONCLUSION

This research has shown that the integration of Inertial Measurement Unit (IMU) and Extended Kalman Filter (EKF) as well as the use of customized PID control provide improvements in the depth control of the Submersible Pylon Inspection Robot (SPIR). However, test results show that large fluctuations at deeper depths, especially around 6 to 10 meters, require more specific refinement of the control algorithm. To improve stability and accuracy at more extreme conditions, refinements to the PID control algorithm are required. These enhancements could be the application of advanced control or even predictive model-based control to adapt the system response to rapid changes in underwater current and depth fluctuations. In addition, the performance of the IMU and EKF in this system shows good results under normal conditions, but significant challenges arise when the system encounters sensor noise, especially in the early phase of measurement. Large fluctuations in the quaternion angle due to the initial instability of the sensor contribute to the initial estimation error. To address this issue, it is recommended to make adjustments to the EKF parameters and consider the use of additional filters that can accelerate convergence and reduce noise in the sensor data. Overall, this research has contributed to developing more accurate depth control in SPIR. However, the next step involves improving the PID control algorithm as well as refining the integration of IMU and EKF, especially to deal with dynamic and fluctuating underwater environmental conditions at greater depths.

ACKNOWLEDGMENTS

This research is supported by funding from the Academic Directorate of Vocational Education and the Research and Service Center (P3M) of Cilacap State Polytechnic. We would like to thank all parties

Volume 11, Issue 2, October 2024, pp. 227-236
ISSN 2355-5068; e-ISSN 2622-4852
DOI: 10.33019/jurnalecotipe.v11i2.4523

who have provided support and contributions in the implementation of this research. The support we receive is very meaningful in realizing the development of the technology we study.

REFERENCES

[1] E. Zereik, M. Bibuli, N. Mišković, P. Ridao, and A. Pascoal, "Challenges and future trends in marine robotics," *Annu Rev Control*, vol. 46, no. October, pp. 350–368, 2018, doi: 10.1016/j.arcontrol.2018.10.002.

[2] scmidt iotc 2021, *Membaca Pesan Komandan KRI Nanggala-402*. 2021, p. 6.

[3] J. Collins, S. Chand, A. Vanderkop, and D. Howard, "A Review of Physics Simulators for Robotic Applications," *IEEE Access*, vol. 9, pp. 51416–51431, 2021, doi: 10.1109/ACCESS.2021.3068769.

[4] C. Li *et al.*, "An Underwater Image Enhancement Benchmark Dataset and Beyond," *IEEE Transactions on Image Processing*, vol. 29, pp. 4376–4389, 2020, doi: 10.1109/TIP.2019.2955241.

[5] M. J. Islam, Y. Xia, and J. Sattar, "Fast Underwater Image Enhancement for Improved Visual Perception," *IEEE Robot Autom Lett*, vol. 5, no. 2, pp. 3227–3234, 2020, doi: 10.1109/LRA.2020.2974710.

[6] K. Le, A. To, B. Leighton, M. Hassan, and D. Liu, "" The SPIR: An Autonomous Underwater Robot for Bridge Pile Cleaning and Condition Assessment," 2021. [Online]. Available: https://www.youtube.com/watch?v=uz1ZXV5Oths

[7] N. Nomikos, P. K. Gkonis, P. S. Bithas, and P. Trakadas, "A Survey on UAV-Aided Maritime Communications: Deployment Considerations, Applications, and Future Challenges," *IEEE Open Journal of the Communications Society*, vol. 4, pp. 56–78, 2023, doi: 10.1109/OJCOMS.2022.3225590.

[8] P. Trslic *et al.*, "Vision based autonomous docking for work class ROVs," *Ocean Engineering*, vol. 196, p. 106840, 2020, doi: https://doi.org/10.1016/j.oceaneng.2019.106840.

[9] Y. Batmani and S. Najafi, "Event-Triggered H∞ Depth Control of Remotely Operated Underwater Vehicles," *IEEE Trans Syst Man Cybern Syst*, vol. 51, no. 2, pp. 1224–1232, 2021, doi: 10.1109/TSMC.2019.2896382.

[10] R. Gabl *et al.*, "Hydrodynamic loads on a restrained ROV under waves and current," *Ocean Engineering*, vol. 234, p. 109279, 2021, doi: https://doi.org/10.1016/j.oceaneng.2021.109279.

[11] M. Dong, J. Li, and W. Chou, "Depth control of ROV in nuclear power plant based on fuzzy PID and dynamics compensation," *Microsystem Technologies*, vol. 26, no. 3, pp. 811–821, 2020, doi: 10.1007/s00542-019-04605-x.

[12] A. Bucci, L. Zacchini, and A. Ridolfi, "EKF on Lie Groups for Autonomous Underwater Vehicles orientation initialization in presence of magnetic disturbances," in *2022 IEEE/OES Autonomous Underwater Vehicles Symposium (AUV)*, 2022, pp. 1–6. doi: 10.1109/AUV53081.2022.9965905.

[13] H. Xing *et al.*, "A Multi-Sensor Fusion Self-Localization System of a Miniature Underwater Robot in Structured and GPS-Denied Environments," *IEEE Sens J*, vol. 21, no. 23, pp. 27136–27146, 2021, doi: 10.1109/JSEN.2021.3120663.

[14] H. Li, S. Chang, Q. Yao, C. Wan, G.-J. Zou, and D.-L. Zhang, "Robust Heading and Attitude Estimation of MEMS IMU in Magnetic Anomaly Field Using a Partially Adaptive Decoupled Extended Kalman Filter and LSTM Algorithm," *IEEE Trans Instrum Meas*, vol. 73, pp. 1–13, 2024, doi: 10.1109/TIM.2024.3381659.

[15] P. V. Patil, M. K. Khan, M. Korulla, V. Nagarajan, and O. P. Sha, "Design optimization of an AUV for performing depth control maneuver," *Ocean Engineering*, vol. 266, p. 112929, 2022, doi: https://doi.org/10.1016/j.oceaneng.2022.112929.

[16] E. R. Potokar, K. Norman, and J. G. Mangelson, "Invariant Extended Kalman Filtering for Underwater Navigation," *IEEE Robot Autom Lett*, vol. 6, no. 3, pp. 5792–5799, 2021, doi: 10.1109/LRA.2021.3085167.

[17] P. Trslic *et al.*, "Vision based autonomous docking for work class ROVs," *Ocean Engineering*, vol. 196, p. 106840, 2020, doi: https://doi.org/10.1016/j.oceaneng.2019.106840.

JURNAL ECOTIPE
Electronic, Control, Telecommunication, Information, and Power Engineering

Volume 11, Issue 2, October 2024, pp. 237-247
ISSN 2355-5068 ; e-ISSN 2622-4852
DOI: 10.33019/jurnalecotipe.v11i2.4528

Control of Multi-Robot Arms in Object Retrieval Based on Human-Machine Interface

Rendyansyah[1], Hera Hikmarika[2], Melia Sari[3], M. Al Furqon Syaidin Fikri[4], Ichlasul Akmali Rizky[5]

[1,2,3,4,5]Departement of Electrical Engineering, Universitas Sriwijaya, Palembang-Prabumulih street KM. 32, Inderalaya, Ogan Ilir 30662, Indonesia

ARTICLE INFO

Article historys:

Received : …/…/…
Revised : …/…/…
Accepted : …/…/…

Keywords:

Multi-Robot Arm; Human Machine Interface; Trajectory Planning

ABSTRACT

Multi-robot arm control is the result of the development of advanced robotics technology. With the advancement in the field of human-machine interface, controlling robot arms has become more efficient and can be done intuitively by humans. In this study, we designed three robot arms of 4-DoF, each controlled by a computer in a visual program interface. This research aims to develop a human-machine interface-based multi-robot arm control system that allows humans to interact with the robots directly. The movement method of each robot uses Trajectory Planning, which works when the operator gives motion commands through the interface display. Multi-robot communication with a computer using USB hub serial format. The computer is the master, and each Arduino on the robot is the enslaved. The HMI computer has tested and controlled three robot arms, and all move according to the operator's commands. The time required by each robot to complete its mission is ± 10 seconds. The results of this study are expected to open new opportunities in the application of robotics in various fields, such as the manufacturing industry, health services, and transportation.

Corresponding Author:

Rendyansyah
Departement of Electrical Engineering, Universitas Sriwijaya, Palembang, Indonesia
Email: rendyansyah.unsri@gmail.com

1. INTRODUCTION

The development of robotics technology in the industrial field has experienced rapid growth over the past few decades. Robotics has significantly increased production efficiency, reduced labor costs, and improved work safety in various industrial fields. One example of robotics technology development in the industrial field is using robots in automated manufacturing processes [1]. Industrial robots can perform repetitive and dangerous tasks quickly and accurately, which is impossible for human labor. This robot technology has helped companies to increase their productivity and reduce the risk of workplace accidents. Robotics technology development has also enabled the creation of more intelligent and adaptive robots [2]. Cognitive and collaborative robots can work with humans in complex work environments [3, 4]. They can learn and adapt quickly to changes in the work environment, thereby increasing production flexibility and productivity.

On the other hand, developing human-machine interaction is essential to developing robotics systems. In this context, human-machine interface (HMI) is a field that studies how humans and machines interact effectively and efficiently [5]. With the rapid development of technology in robotics, robotics system developers need to understand how humans can work together with robots to achieve desired goals. One of the main goals of HMI in robotics systems is to create an interface that is intuitive and easy for the user to understand. Using a good interface, humans can give instructions to the robot

Volume 11, Issue 2, October 2024, pp. 237-247
ISSN 2355-5068 ; e-ISSN 2622-4852
DOI: 10.33019/jurnalecotipe.v11i2.4528

clearly, and the robot can respond appropriately. For example, in robots used in industrial environments, human and machine interaction can be done through a graphical interface that allows the operator to control the robot easily through a control panel [6]. However, despite the importance of HMI in the development of robotics systems, some challenges still need to be overcome. One of the main challenges is the compatibility between the provided interface and the user's needs. Robotics system developers need to understand the needs and preferences of users well so that the interface provided can meet user's expectations.

Some research related to robot arms has been carried out by Rokhim et al. (2021), discussing end effector control on robot arms for pick and place applications using the line equation method. The goal is to increase object retrieval accuracy by effectively detecting objects' position and orientation [7]. Ayega et al. (2023) also discussed the design of a prototype robotic arm manipulator with three degrees of freedom. This research includes several stages: mathematical modelling of motion kinematics, design and simulation using Matlab/Simulink and SolidWorks software, and hardware construction using 3D printing technology [8]. These papers have yet to present information about the user interface used in the robot arm system. Although there are physical control elements such as buttons and indicators, no explanation or illustration shows how the user interacts with the system visually. This situation can reduce understanding of the user experience and how data from the system is presented to the operator, an essential aspect of operating the robot effectively.

In this study, we designed a visual display-based system to control multiple robot arms, each with 4-DoF. This system develops our previous research on motion control of computer-based robot arms [9, 10]. This research aims to facilitate the operator in controlling the motion of three 4-DoF robot arms based on the Human Machine Interface. This robot arm is in the form of a prototype on an educational laboratory scale. This HMI system consists of forward kinematics and cubic trajectory. Cubic trajectory makes it easy for the robot arm to move from one position to another [11]. This HMI also has an animation display that moves three robot arms. The motivation for making this system is based on the ease of an operator in monitoring multiple robots simultaneously for semi-automatic systems in industry.

Figure 1. 4-DoF multi-robot arm (red, orange, and blue colors).

2. RESEARCH METHOD

2.1. Robotic Arm

In this study, three 4-dof robot arms are used. Robot_1 with red color, robot_2 orange color, and robot_3 blue color. This study is a development of our previous research, namely the control of robot arms using visual computer programs. The physical form of the multi-robots is shown in Figure 1. These robots each have a length of d_1 = 5 cm, a_2 = 10 cm, a_3 = 10 cm, and griper a_4 = 5 cm. There are four servo motors placed for the movement of each joint. The servo motor used is a standard type that can rotate from an angle of 0º to 180º. This robot arm is also linked to the computer program using an Arduino microcontroller. An IO board has also been added to connect several servo motors and their power supply terminals. Figure 2 shows the schematic diagram of controlling multi-robot arms using a human-machine interface. HMI runs in the computer as a control center for three 4-dof robot arms.

JURNAL ECOTIPE
Electronic, Control, Telecommunication, Information, and Power Engineering
Volume 11, Issue 2, October 2024, pp. 237-247
ISSN 2355-5068 ; e-ISSN 2622-4852
DOI: 10.33019/jurnalecotipe.v11i2.4528

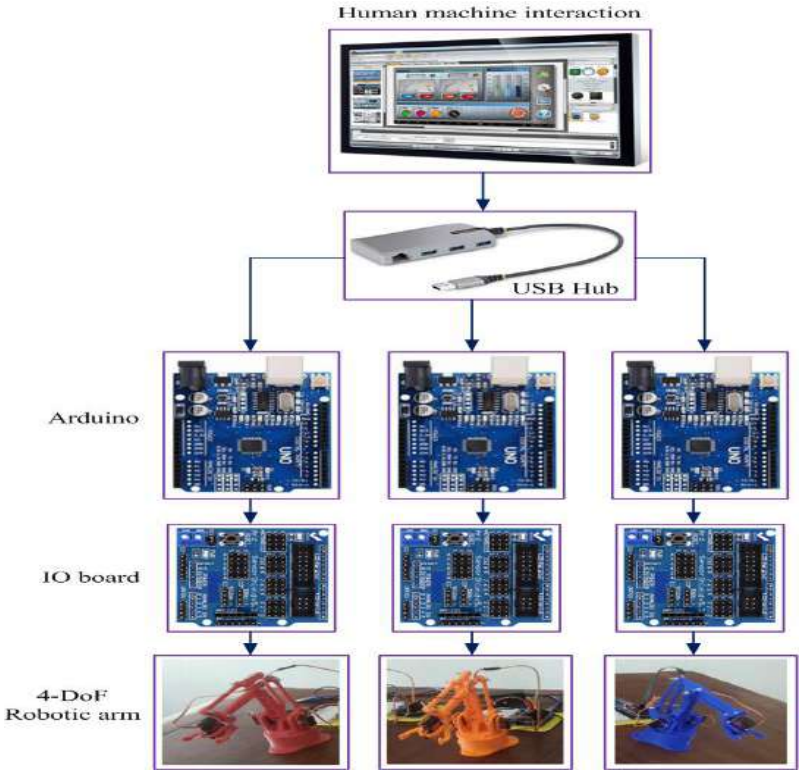

Figure 2. Schematic diagram of the 4-DoF multi-robot arm based on human-machine interface.

2.2. Human-Machine Interface

Three robot arms are connected to the computer using different ports, and the connection is done in a separate group for each robot connection. The robot moves based on commands from the computer either manually or automatically (see illustration Figure 2). The computer program, in the form of a visual display, is designed to adjust the sequence of robot movements, especially with servo motors. Interface forms are made separately for each robot, and this study used three forms for each robot. The robot arm in this HMI display applies the forward kinematic formula derived from the DH-parameter method [12, 13]. Figure 3 shows a trigonometric illustration of the angular direction in the movement of the robot arm. The joint_1 angle is formed from the total length of links a_2, a_3, and a_4 concerning the x-axis. Joint_2 angles from link a_2 to the horizontal position. Joint_3 from link a3 against the directional position of link a_2. At joint_4 is the open and close position for the gripper; the smaller the angle value, the gripper closes to take the object, while the more significant the angle, the gripper opens to release the object.

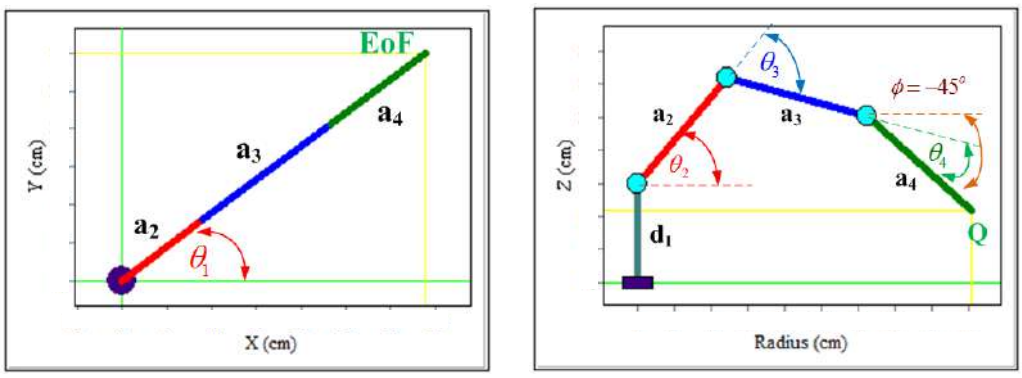

(a) (b)

Figure 3. Joint angles of the 4-dof robot arm, (a) top view, and (b) side view.

JURNAL ECTIPE
Electronic, Control, Telecommunication, Information, and Power Engineering
Volume 11, Issue 2, October 2024, pp. 237-247
ISSN 2355-5068 ; e-ISSN 2622-4852
DOI: 10.33019/jurnalecotipe.v11i2.4528

$$
\begin{aligned}
x &= \left(a_2 \cos\theta_2 + a_3 \cos\left(\theta_2 + \theta_3\right) + a_4 \cos\left(\theta_2 + \theta_3 + \theta_4\right)\right)\cos\theta_1 \\
y &= \left(a_2 \cos\theta_2 + a_3 \cos\left(\theta_2 + \theta_3\right) + a_4 \cos\left(\theta_2 + \theta_3 + \theta_4\right)\right)\sin\theta_1 \\
z &= d_1 + a_2 \sin\theta_2 + a_3 \sin\left(\theta_2 + \theta_3\right) + a_4 \sin\left(\theta_2 + \theta_3 + \theta_4\right)
\end{aligned} \tag{1}
$$

In Equation (1), forward kinematics receive input values as joint angles and produce output values in Cartesian. The x and y values illustrate the horizontal movement of the robot (Figure 3. a), and the z value on the vertical movement of the robot (Figure 3. b). These joint angle values are based on data provided by the HMI operator. The robot display in the HMI adjusts the movement route of the robot arm. The HMI sends data in 8-bit format for each robot. The data is in the form of angle values arranged in order from joint_1 to joint_4, and the data ends with a "#" sign as a tail. When sending data for three-robot arms, the HMI activates the trajectory command for all robots.

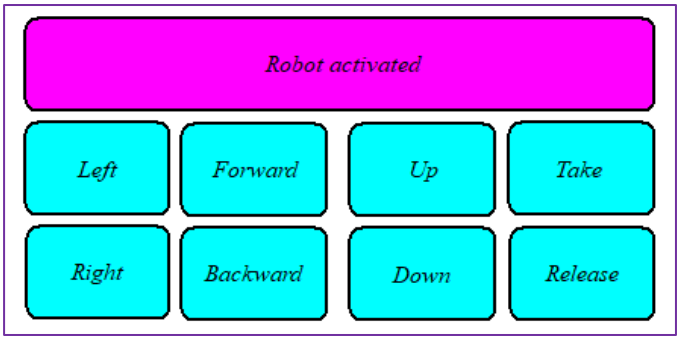

Figure 4. Motion command button for the robot arm.

Visualization forms have been designed for each robot arm. Each form has eight buttons as motion commands: movement to the left, right, forward, backward, up, down, take an object, and release. Figure 4 shows the command buttons to move the robot arm. Before giving commands to the robot, the robot must be activated by clicking the "Robot activated" button, and a visual simulation of the robot is displayed on the HMI. This button contains data as commands sent to the Arduino micro via USB serial communication. "Left" and "Right" commands to move the joint_1 angle. "Forward" and "Backward" commands to move the angle of joint_2 and joint_3. "Up" and "Down" commands to move the angle of joint_3. "Take an object" and "Release an object" commands to move the angle of joint_4 (gripper). The purpose of this button is to determine the robot's response and whether the robot's movement is by the user's wishes, including the direction of movement of both the display and the robot.

2.3. Trajectory Planning

This HMI has a feature for recording joint angle data and can be run for automatic movement using the cubic trajectory method. Cubic trajectory is one of the trajectory planning methods in path planning to move automatically from one position to another [14 - 16]. The cubic trajectory is obtained by solving the third-order polynomial formula, and the result is Equation (2). The variable *qs* is the initial position, and *qf* is the final position. The variable *tf* is the time duration for the robot to move from the initial to the final position.

$$
q(t) = q_s + 3\left(\frac{q_f - q_s}{t_f^2}\right)t^2 - 2\left(\frac{q_f - q_s}{t_f^3}\right)t^3 \tag{2}
$$

JURNAL ECTIPE
Electronic, Control, Telecommunication, Information, and Power Engineering
Volume 11, Issue 2, October 2024, pp. 237-247
ISSN 2355-5068 ; e-ISSN 2622-4852
DOI: 10.33019/jurnalecotipe.v11i2.4528

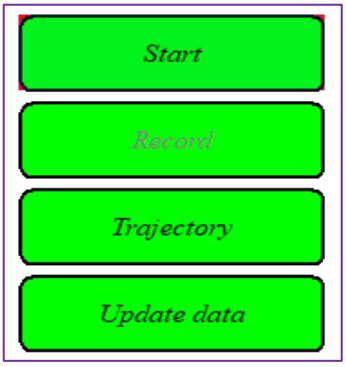

Figure 5. Visual form for running the trajectory function.

Equation (2) is applied to the robot arm's automatic movement of the four corner joints. The cubic trajectory is activated when the operator clicks the "Trajectory" button, which reads the data from the record results. Figure 5 shows the visual form of the robot arm undergoing trajectory functions. There are four buttons: the start button for the Arduino micro connection and the record button functions to record joint angle data according to the user's wishes. The "Trajectory" button functions when running the robot arm based on the recorded joint angle path. The "Update data" button calls a text file, and the operator can update it manually. In this study, the Human Machine Interface is designed to manually and automatically control multiple robot arms.

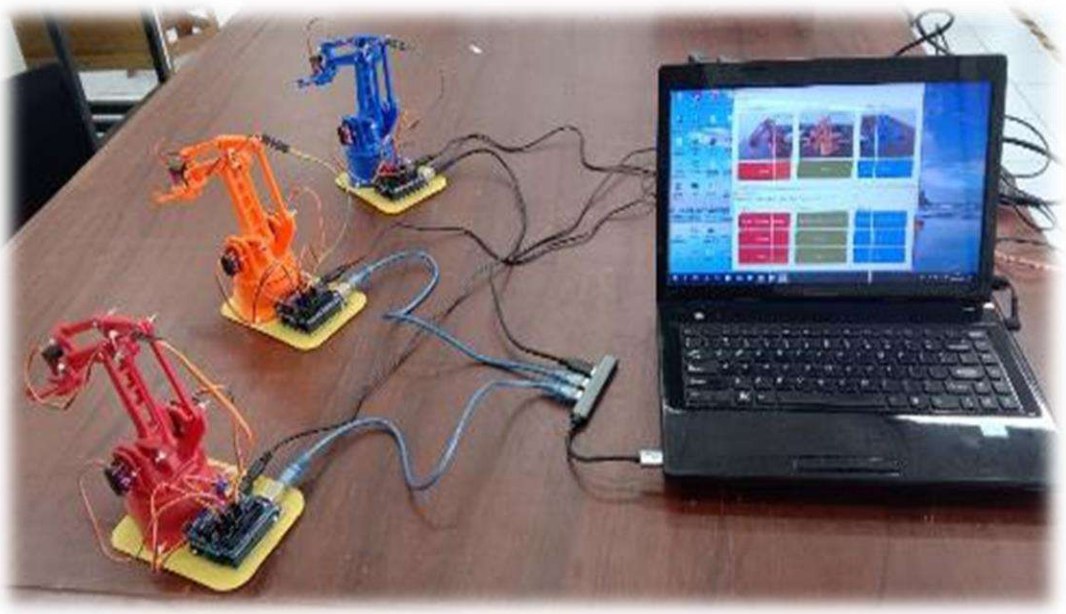

Figure 6. Experimental setup of the 4-DoF multi-robot arm.

3. RESULTS AND DISCUSSION

Three 4-dof robot arms have been designed in this study, robots in prototype form to be applied in picking up and moving objects. Experiments were conducted in the Control Engineering and Robotics Laboratory, Department of Electrical Engineering, UNSRI. First, three robotic arms were supplied through their respective adapters. The robot is connected to a computer via a USB hub, and the respective port settings detected by the system are Com5, Com6, and Com7. Figure 6 shows the setup of the multi-robot arm experiment connected to the computer. The human-machine interface program is embedded in the computer. Each robot's interface is designed separately, and a connection management system includes data transmission. Figure 7 shows the human-machine interface to control the movement of the 4-DoF multi-robot arm.

JURNAL ECTIPE
Electronic, Control, Telecommunication, Information, and Power Engineering
Volume 11, Issue 2, October 2024, pp. 237-247
ISSN 2355-5068 ; e-ISSN 2622-4852
DOI: 10.33019/jurnalecotipe.v11i2.4528

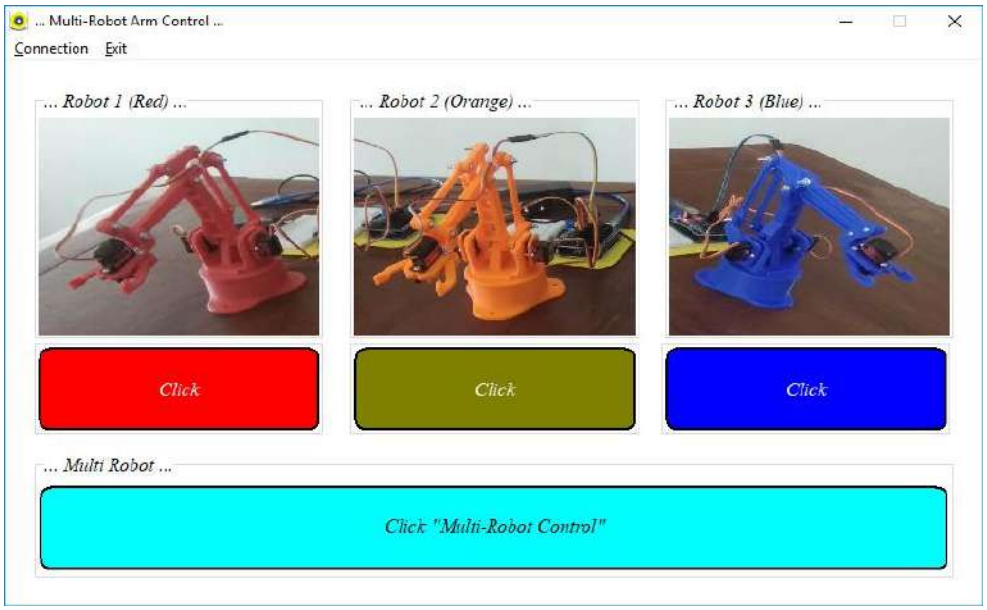

Figure 7. Human-machine interface for multi-robot arm control..

In Figure 7, an operator can choose which robot arm to activate and control; robot_1 is red, robot_2 is orange, and robot_3 is blue. The visualization of the robot arm is activated when the operator presses the "Robot activated" button. By default, the original position of each joint angle is set at 90º. Figure 8 visually shows the original position of each robot arm. The angle is chosen at 90º because the center position of the standard servo motor has an angle from 0º to 180º. This position allows the robot joints to move left or right, forward or backwards, and up or down. This HMI is designed to adjust the movement pattern of each robot arm.

Experiment on the red robot arm; the robot is activated and runs to move left, right, forward, and backwards, take the object, and release the object. This experiment also applies to orange and blue robots. Table 1 shows the movement experiments of three robot arms controlled from the human-machine interface. The HMI sends servo angle data to each robot arm. The robot arm moves to the left, activating joint_1, increasing its angle value, and moving right to decrease the value of joint_1. The robot moves forward, the value of joint_2 decreases, and joint_3 increases. The robot moves backwards, the value of joint_2 increases, and joint_3 decreases. In the robot, when the end-effector rises upwards, the value of joint_3 increases; when it goes down, joint_3 decreases. The robot picks up the object, and the value of joint_4 decreases. The robot releases the object, that is, joint_4 increases. This activity is the same as the movement and HMI on robot_2 (orange) and robot_3 (blue). The HMI can run and become a remote control in moving each robot. This HMI successfully controls the movement of robots based on commands given by the operator through the interface by pressing the command button.

JURNAL ECTIPE
Electronic, Control, Telecommunication, Information, and Power Engineering
Volume 11, Issue 2, October 2024, pp. 237-247
ISSN 2355-5068 ; e-ISSN 2622-4852
DOI: 10.33019/jurnalecotipe.v11i2.4528

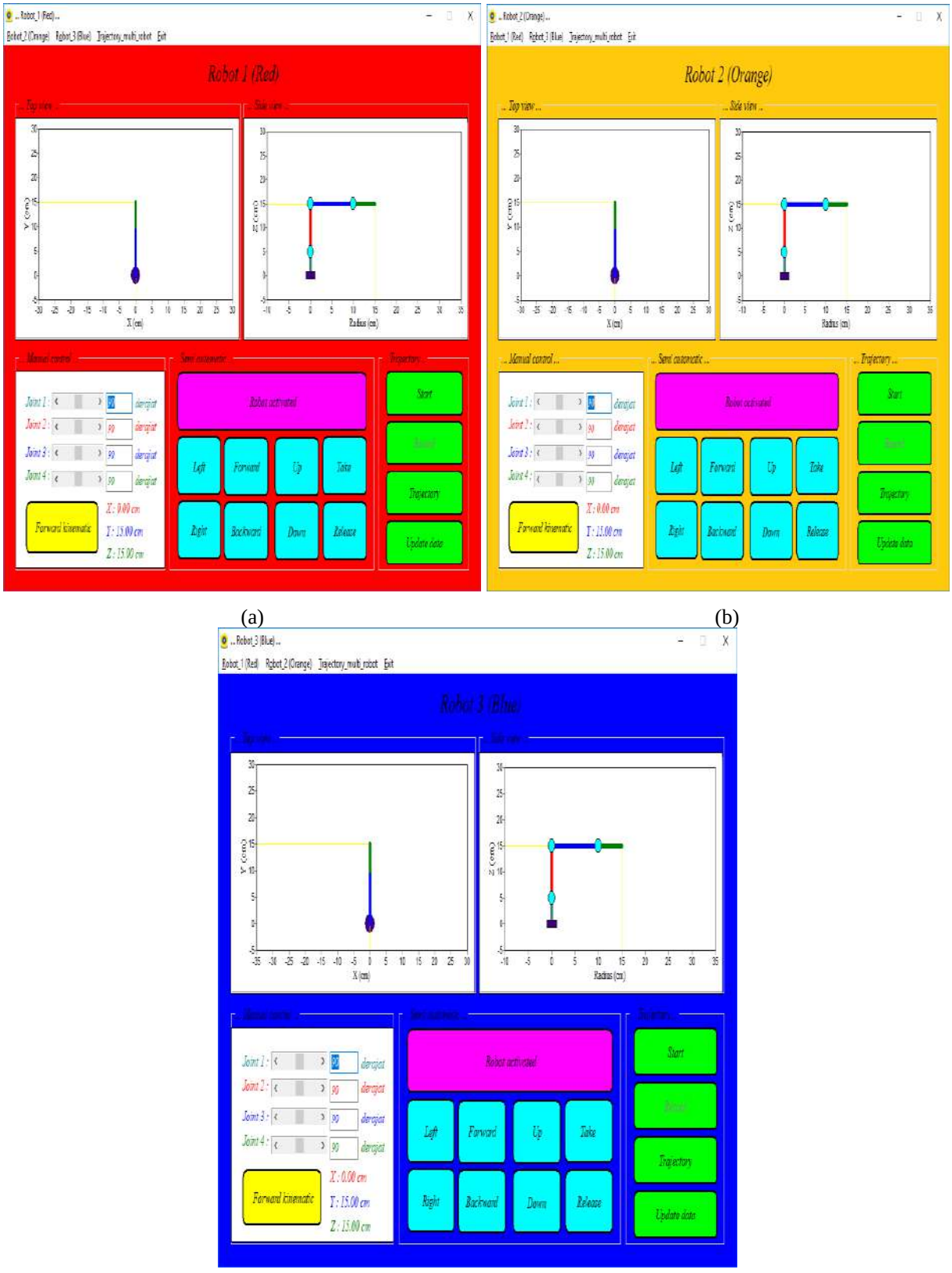

(a) (b)

(c)

Figure 8. Interface for each robot arm: (a) Robot_1 (Red), (b) Robot_2 (Orange), and (c). Robot_3 (Blue).

JURNAL ECTIPE
Electronic, Control, Telecommunication, Information, and Power Engineering
Volume 11, Issue 2, October 2024, pp. 237-247
ISSN 2355-5068 ; e-ISSN 2622-4852
DOI: 10.33019/jurnalecotipe.v11i2.4528

Table 1. Table 1. Movement trials of three robot arms.

Commands	Robot_1 (Red)	Robot_2 (Orange)	Robot_3 (Blue)	Information
Left			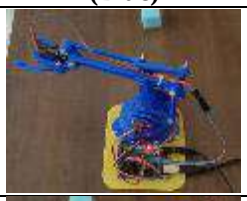	Movement ranging from joint_1 angle 90º to 170º
Right				Movement ranging from joint_1 angle 90º to 10º
Forward				Angle of joint_2 (90º to 10º) and joint_3 (90º to 170º)
Backward				Angle of joint_2 (90º to 170º) and joint_3 (90º to 10º)
Up				Joint_3 angle ranging from 90º to 170º
Down			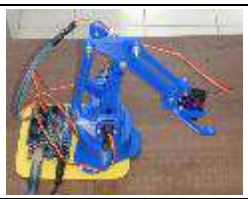	Joint_3 angle ranging from 90º to 10º
Take an object				Joint_4 angle ranging from 90º to 10º
Release an object	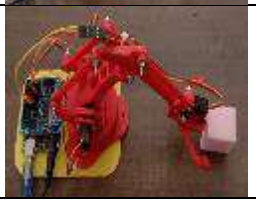	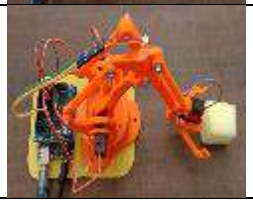		Joint_4 angle ranging from 90º to 170º

In the next experiment, three robots were given the same joint angle movement command for each robot. The three robots have determined the joint angle value for each route in picking up and moving objects. Figure 9 shows the original position of each robot arm. The robot arm is activated to follow the trajectory recorded by this HMI system, as shown in Table 2. This trajectory data is given to each robot arm.

JURNAL ECTIPE
Electronic, Control, Telecommunication, Information, and Power Engineering
Volume 11, Issue 2, October 2024, pp. 237-247
ISSN 2355-5068 ; e-ISSN 2622-4852
DOI: 10.33019/jurnalecotipe.v11i2.4528

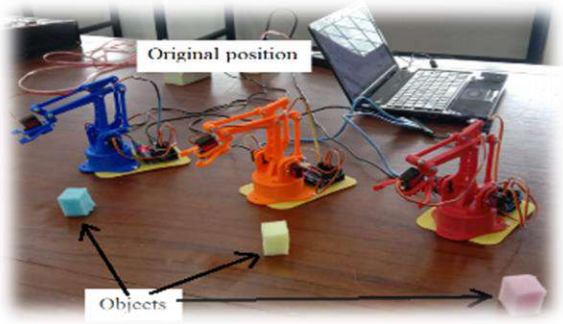

Figure 9. The original position of the 4-DoF multi-robot arm.

Table 2. Trajectory of the robot in picking up and moving the object.

Joint_1	Joint_2	Joint_3	Joint_4	Description
90º	90º	110º	90º	The robot is active, heading toward the object.
165º	90º	110º	90º	
165º	41º	63º	90º	
165º	41º	63º	28º	The robot picks up and moves objects.
165º	88º	106º	28º	
37º	88º	106º	28º	
37º	53º	47º	28º	The robot places and releases objects.
37º	53º	47º	78º	
37º	86º	114º	78º	
90º	97º	115º	78º	

When the operator clicks the "Multi Robot Control" button (interface in Figure 7), the red robot arm activates and moves according to the route in Table 2. The red robot moves to the left towards the object and picks up the object. The robot moves the object to the right, places the object, and releases the object. After completing its task, the red robot returns to its original position. An illustration of the movement of the red robot can be seen in Figure 10. The red robot arm succeeds in carrying out the task of taking objects with the required time of ± 10 seconds. Then, the HMI system activates the orange robot arm to move towards the target, pick up and move the object, and return to the original position. Figure 11 shows an illustration of the movement of the orange robot in picking up the object. Then, the blue robot arm moves towards the target, picks up and moves the object, and returns to its original position. Figure 12 shows an illustration of the movement of the blue robot in picking up the object. The orange and blue robot arms also performed the task with the required time of ± 10 seconds. From the experiment, the robot runs and completes the task alternately due to communication via USB hub serially with sequential Comport. The HMI system on multiple robots can run well, and the robot's movement is by the predetermined route.

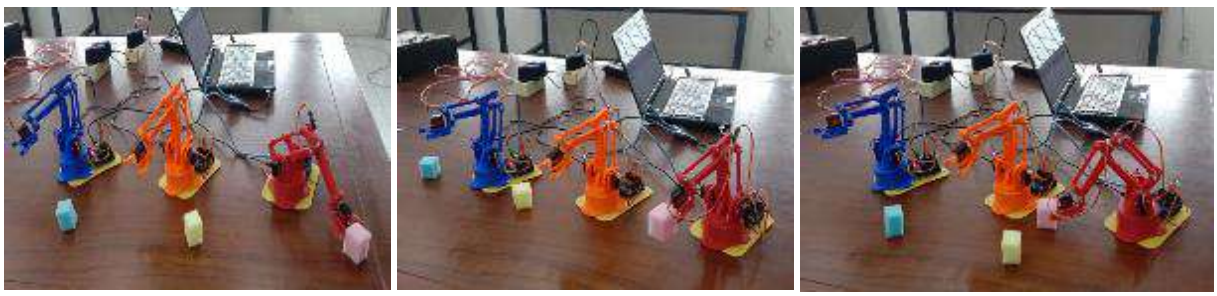

(a) (b) (c)

Figure 10. The movement of the red robot in picking up objects, (a) the robot picks up an object, (b) moves the object, and (c) places and releases the object.

Volume 11, Issue 2, October 2024, pp. 237-247
ISSN 2355-5068 ; e-ISSN 2622-4852
DOI: 10.33019/jurnalecotipe.v11i2.4528

(a) (b) (c)

Figure 11. The movement of the orange robot in picking up objects, (a) the robot picks up an object, (b) moves the object, and (c) places and releases the object.

(a) (b) (c)

Figure 12. The movement of the orange robot in picking up objects, (a) the robot picks up an object, (b) moves the object, and (c) places and releases the object.

This study offers an intuitive Human-Machine Interface (HMI), making it easier for operators to control multiple robots simultaneously, while the previous study used a scrollbar for individual joint control. This study handles three robotic arms, making coordination more complex than the earlier study, which only dealt with a single robotic arm performing more straightforward tasks. In terms of performance, this robotic system completes tasks more quickly, taking 10 seconds per task, while the previous study required 100 seconds. The earlier study emphasized motion recording for playback, whereas this study focuses on real-time multi-robot control through HMI [10].

4. CONCLUSION

Three robot arms were built in this study: robot_1 in red, robot_2 in orange, and robot_3 in blue, each with four degrees of freedom. The robots are connected to a computer via a serial USB hub. The computer's human-machine interface is designed according to the robot arm prototype. There are command buttons such as "Left", "Right", "Forward", "Backward", "Up", "Down", "Take an object", and "Release an object". The operator uses these commands to move the robot arm. The operator can also give automatic commands by recording robot movements and running them through the "Trajectory" command. The robot experiment went well; the robot moved according to the operator's commands. The robot also completes picking up and moving objects based on the route recorded in the HMI. The time required for the robot to complete the task is ± 10 seconds. In future research development, we will apply computer vision for object detection and recognition and provide information to the robot assigned to retrieve the object.

ACKNOWLEDGMENTS

The research/publication of this article was funded by DIPA of Public Service Agency of Universitas Sriwijaya 2024. Nomor SP DIPA 023.17.2.677515/2024, On November 24, 2023. In accordance with the Rector’s Decree Number: 0013/UN9/LP2M.PT/2024, On May 20, 2024.

JURNAL ECOTIPE
Electronic, Control, Telecommunication, Information, and Power Engineering
Volume 11, Issue 2, October 2024, pp. 237-247
ISSN 2355-5068 ; e-ISSN 2622-4852
DOI: 10.33019/jurnalecotipe.v11i2.4528

REFERENCES

[1] L. Pérez, S. Rodríguez-Jiménez, N. Rodríguez, R. Usamentiaga, and D. F. García, "Digital Twin and Virtual Reality Based Methodology for Multi-Robot Manufacturing Cell Commissioning," *Appl. Sci.*, vol. 10, no. 10, pp. 1–18, 2020.

[2] A. Bolu and O. Korcak, "Adaptive task planning for multi-robot smart warehouse," *IEEE Access*, vol. 9, pp. 27346–27358, 2021.

[3] A. Grau, M. Indri, L. Lo Bello, and T. Sauter, "Robots in industry: The past, present, and future of a growing collaboration with humans," *IEEE Industrial Electronics Magazine*, pp. 50–61, 2020.

[4] M. L. Nicora, R. Ambrosetti, G. J. Wiens, and I. Fassi, "Human–Robot Collaboration in Smart Manufacturing: Robot Reactive Behavior Intelligence," *J. Manuf. Sci. Eng.*, vol. 143, no. 3, pp. 1–9, 2021.

[5] D. Mourtzis, J. Angelopoulos, and N. Panopoulos, "The future of the human–machine interface (HMI) in society 5.0.," *Futur. Internet*, vol. 15, no. 162, pp. 1–25, 2023.

[6] H. Roibu, L.-C. Bazavan, S.-I. Cismaru, and N. G. Bizdoaca, "HMI for cooperative robot Kuka youBot based on Electromyography technique," in *11th International Conference on Modern Circuits and Systems Technologies (MOCAST)*, 2022, pp. 1–4.

[7] I. Rokhim, P. Anggraeni, H. Khoirunnisa, and H. M. Purnama, "Pengendalian End Effector Robot Lengan untuk Aplikasi Pick and Place dengan Metode Persamaan Garis," *J. Teknol. Rekayasa*, vol. 6, no. 1, pp. 7–14, 2021.

[8] I. H. Ayega, T. A. Tamba, and B. M. Arthaya, "Rancang Bangun Purwarupa Manipulator Lengan Robot Dengan Tiga Derajat Kebebasan," *ELKOMIKA J. Tek. Energi Elektr. Tek. Telekomun. Tek. Elektron.*, vol. 11, no. 3, pp. 796–810, 2023.

[9] Rendyansyah *et al.*, "Pengendalian Robot Manipulator 4 DOF Berbasis Tampilan Visual pada Komputer," in *Annual Research Seminar (ARS)*, 2020, pp. 105–109.

[10] Rendyansyah, A. P. P. Prasetyo, K. Exaudi, and S. Sembiring, "Pergerakan Robot Lengan Pengambil Objek Dengan Sistem Perekam Gerak Berbasis Komputer," *JTEV (Jurnal Tek. Elektro dan Vokasional)*, vol. 8, no. 2, pp. 230–240, 2022.

[11] T. F. Abbas, A. A. Khleif, and M. Q. Abbood, "Velocity Kinematics Analysis and Trajectory Planning of 5 DOF Robotic Arm," *Eng. Technol. J.*, vol. 38, no. 5, pp. 738–747, 2020.

[12] M. F. W. Satriatama and L. Halim, "Perancangan Awal dan Simulasi Lengan Robot 3 Derajat Kebebasan Berbasis Arduino yang Dikontrol dengan Aplikasi," *J. Tek. Mesin dan Mekatronika*, vol. 7, no. 2, pp. 118–130, 2022.

[13] Z. Nurkholik, F. Alif, and D. Arie, "Rancangan Bangun Lengan Robot Arm Untuk Menggambar Menggunakan Invers Kinematik," *J. Ilm. Sist. Inf.*, vol. 1, no. 3, pp. 59–68, 2022.

[14] H. Afrisal, B. Setiyono, M. F. Yusuf, R. M. Suin, and O. Toirov, "Trajectory Planning with Obstacle Avoidance of 3 DoF Robotic Arm for Test Tube Handling System," in *In 2020 7th International Conference on Information Technology, Computer, and Electrical Engineering (ICITACEE)*, 2020, pp. 41–46.

[15] P. A. Parikh, R. Trivedi, and J. Dave, "Trajectory planning for the five degree of freedom feeding robot using septic and nonic functions," *Int. J. Mech. Eng. Robot. Res.*, vol. 9, no. 7, pp. 1043–1050, 2020.

[16] Rendyansyah, B. Y. Suprapto, H. Hikmarika, and Irmawan, "Application of Learning Vector Quantization and Trajectory Planning On a 4-DoF Robotic Arm to Move the Object," *J. Ecotipe (Electronic, Control. Telecommun. Information, Power Eng.*, vol. 10, no. 2, pp. 268–276, 2023.

Volume 11, Issue 2, October 2024
ISSN 2355-5068
e-ISSN 2622-4852

Publisher Address :

Electrical Engineering Department
Faculty of Science and Engineering - Bangka Belitung University
Balunijuk, Kab. Bangka, Prov. Kep. Bangka Belitung
University Phone : (0717) 422145, 422965 Fax. (0717) 421303
Faculty Phone : (0717) 4260033 ext. 2122, 2124
Website : https://ecotipe.ubb.ac.id/index.php/ecotipe
E-mail : jurnalecotipe@ubb.ac.id / jurnal.ecotipe@yahoo.com